

International Journal of Computational and Engineering

SEPTEMBER 2018 VOLUME3 NUMBER3

Publisher: ACADEMIC PUBLISHING HOUSE
Address: Quastisky Building, Road Town, Tortola, British Virgin Islands
UK Postal Code: VG1110

E-mail: editorial@ij-ce.com
www.ij-ce.com



ACADEMIC PUBLISHING HOUSE

CONTENTS

DESIGN AND IMPLEMENTATION OF SECURE PRODUCTION GRID SYSTEM BASED ON MOBILE INTERNET	1
ANALYSIS ON THE INFLUENCING FACTORS OF ENVIRONMENTAL INFORMATION DISCLOSURE IN CHEMICAL INDUSTRY	6
PROFIT MODEL OF BUS MOBILE PAYMENT.....	9
ANTI-COLLISION SYSTEM BASED ON CAR NETWORK	14
APPLICATION OF BIM TECHNOLOGY IN CONSTRUCTION OF METRO STATIONS.....	17
TRAINING COURSE TIMES OPTIMIZATION METHOD BASED ON SVR-GA.....	21
CLOUD COMPUTING BASED REMOTE MONITORING SYSTEM FOR MINING EQUIPMENT	26
EVALUATION OF SERVICE CAPACITY OF CHINA'S MEMBRANE SEPARATION INDUSTRY CLUSTER BASED ON ANP THEORY	33
EFFECT ANALYSIS AND DESIGN METHOD IMPROVEMENT OF EXPANSION TANK IN HEATING SYSTEM BY HEAT TRANSFER FLUIDS.....	38
A COMPARISON OF EPIDURAL ANESTHESIA WITH CHLOROPROCAINE AND LIDOCAINE FOR OUTPATIENT KNEE ARTHROSCOPY.....	43
FAST CONVERGENT VHGMRES(M) ITERATION ALGORITHM.....	47
COLOR AND MATTER CONCENTRATION IDENTIFICATION BASED ON MULTIPLE LINEAR REGRESSION	51
PROTECTIVE CLOTHING PROBLEM BASED ON BIDIRECTIONAL UNSTEADY HEAT CONDUCTION.....	54
ACCURATE TREATMENT OF DIABETES BASED ON BIG DATA	58
DISCUSSION ON THE RELATIONSHIP BETWEEN SUBSTANCE CONCENTRATION AND COLOR READING.....	61
TALKING ABOUT ARTIFICIAL INTELLIGENCE	64
BEST DESIGN FOR HIGH TEMPERATURE PROFESSIONAL CLOTHING	68
HUMAN BODY TEMPERATURE SIMULATION OF MULTI-LAYER THERMAL PROTECTIVE CLOTHING UNDER CONSTANT TEMPERATURE ENVIRONMENT	73
DESIGN OF HIGH RESOLUTION NUCLEAR MAGNETIC RESONANCE MAGNET.....	77
QUAD-ROTOR AIRCRAFT CONTROL BASED ON FRACTIONAL ORDER PID.....	82
THERMAL ANALYSIS AND RESEARCH OF ELECTRONIC PUMP FOR PASSENGER VEHICLES	89
SOFTWARE ENGINEERING COURSE PRACTICE TEACHING	92
HYPERSPECTRAL IMAGES CLASSIFICATION BASED ON MULTIFRACTAL SPECTRUM	95
RESEARCH ON THE MAINTENANCE SPARE PARTS SUPPORT RISK MODEL OF INSUFFICIENT RESERVE STARTING POINT	100
PRACTICAL TEACHING REFORM OF GRADUATION DESIGN IN CIVIL ENGINEERING.....	102

IS SELF-ENHANCEMENT RESTRICTED TO INDIVIDUALISTIC CULTURES?—THE EVIDENCE FROM RISK DECISION MAKING.....	106
STUDY AND EVALUATION OF CONCRETE DURABILITY OF PLASTIC IMPERVIOUS WALL.....	112
STUDY ON ULTRA-HIGH STRENGTH AND IMPACT ABRASION CONCRETE OF IRON ORE AGGREGATE.....	116
RESEARCH ON THE SELECTION OF DIODE BASED ON ESD SIMULATION	120
DESIGN OF INTELLIGENT STEELMAKING SYSTEM.....	124
STUDY ON CONTROL OF POSTHARVEST DISEASES OF FRUITS AND VEGETABLES AND STORAGE PERFORMANCE OF YEAST	128
RESEARCH ON LOGISTICS DEMAND FORECASTING MODEL COMBINING TIME SERIES AND NEURAL NETWORK	134
META-ANALYSIS OF RELATIONSHIP BETWEEN IONIZING RADIATION AND CHROMOSOME ABERRATION RATE OF THE RADIATION WORKERS.....	139
OPTICAL CHARACTER RECOGNITION.....	141
CLOTHING DESIGN FOR HIGH TEMPERATURE OPERATION	144
ANALYSIS BASED ON COLOR AND SUBSTANCE CONCENTRATION IDENTIFICATION.....	147
IMAGE RESTORATION USING RADON TRANSFORM.....	149
ORBIT DESIGN AND CONTROL STRATEGY FOR CHANG'E-3 SOFT LANDING.....	152
PREDICTION OF COKE QUALITY BY COAL ROCK METHOD	156
ANALYSIS AND APPLICATION OF NETWORK HOT VIDEO SERVICE CHARACTERISTICS BASED ON BIG DATA.....	160

Design and Implementation of Secure Production Grid System based on mobile Internet

Huang He

Wenzhou Vocational & Technical College, Wenzhou. 325035, China

Huanghe@sohu.com

Abstract: This is designed to further standardize the production safety management, carry out hidden perils in safety in production accident management, the implementation of the production and business operation entities safety production main body responsibility, improve the pertinence and effectiveness of the work of production safety, build efficient and orderly mode of production safety supervision, strengthen safety in production foundation structure, make the present situation of the production and business operation entity digital, classification management, dynamic.

Key words: Mobile Internet; Safety; Production grid; Screening system

1. INTRODUCTION

The function modules of safety production grid screening system based on mobile Internet include: enterprise management, self-report, grid check, statistical analysis, user and grid management.

In terms of user role type, there are four types of users: county, large grid (area), medium grid, small grid and enterprise. The functional permissions of each role will be different.

In the form of use, there are WEB client and mobile client, and the mobile client is divided into iOS (apple) and Android (Android) versions. Its main purpose is to enable users at all levels (including grid managers at all levels, business owners, inspection teams and supervision squadrons) to check the enterprise status at any time through the "safety supervision and communication" site, and conduct on-site law enforcement, and submit on-site inspection of hidden dangers of production safety accidents.

2. TECHNICAL ROUTE

(1) Software Structure

This system takes domain driven design (DDD) as the core idea. In terms of specific technologies, Microsoft Entity Framework is adopted as a domain-oriented implementation Framework. The system is divided into model layer, business service layer, interface layer and page layer. Technically, EasyUI is used as the page-layer framework to exchange data with the interface layer through JSON format, and mobile APP in the system will also interact with the interface layer

through JSON format.

(2) domain driven design (DDD)

In 2004, renowned modeling expert Eric Evans published his most influential book: "Domain Driven Design", or Domain Driven Design architecture [Evans DDD].

DDD is telling us how to do well at the business level! And with domain - driven design ideas to select and appropriate framework.

Software generation process is: analysis, design, programming, testing, deployment. In the past, the analysis domain and software design were fragmented, with analysts gathering basic concepts from the domain; The design must specify a set of components that can be adapted to the construction of programming tools in the project, that can be executed effectively in the target environment, and that can properly solve problems that arise in the application. Model-driven Design abandons the approach of split analysis Model and Design, and USES a single Model to meet the requirements of these two aspects. This is the domain model.

Model-driven design abandons the split analysis Model and design practice and USES a single Model to meet the requirements of these two aspects. This is the domain model. A single domain model satisfies both the analysis prototype and the software design. If a model is not practical to implement, a new model must be found. If the model does not faithfully represent the domain key concepts, it must also look for new models. Modeling and design becomes a single iteration loop. Tie the domain model closely to the design. Therefore, modeling experts must have the knowledge of design and program.

According to Eric's theory, the business layer will be subdivided into two layers. That is, application layer and domain layer. Application layer: define the work that the software can accomplish, and command the domain object with rich meaning to solve the problem and keep it concise; State of no business condition excluding business rules or knowledge. Domain layer: information and business rules that represent business concepts and business states are the core of business software. The layers must be clearly separated, and each layer is cohesive and depends only on its lower

layer.

Eric points out in particular that the fast UI approach that leaves business logic to the business interface is a sideshow. Software development that you want to visualize drag-and-drop graphics as a C/S structure is the wrong direction. development is fast and difficult to maintain and extend, although using J2EE technology is a pseudo-multi-tier technology. Development is fast, but difficult to maintain and extend. Although using J2EE technology, it is actually a pseudo-multi-tier technology

In the lifetime of domain objects, there are three patterns to maintain object integrity. Clearly defined ownership and boundaries of the Aggregate make the

model more compact and avoid a dense network of objects. At the beginning of an object's life cycle, an aggregate model is built using factories and combinations that provide access and control over the model objects and incorporate the factories and combinations into the design to systematically manage the model objects. The aggregation loops out a scope in which the object remains invariant regardless of its lifetime.

3. SOFTWARE LAYERED ARCHITECTURE DESCRIPTION

(1) Solid model layer

The system contains the following main entities:

Entity name	Description
Area set	County and city information
Big grid set	Big grid information under county and city
Middle grid set	Middle grid information under large grid
Small grid set	Small grid information under the middle grid
Staff table set	Personnel account information
District master set	Management relationship between personnel and urban areas
Large grid master set	Management relationship between people and large grid
Middle grid master set	Manage the relationship between people and the grid
Small grid master set	Management relationships between people and small grids
Enterprise basic information set	Basic information of the enterprise
Hidden dangers in library collection	Hazard information to be checked during inspection
Inspect table set	Basic information such as inspection time, inspectors, etc.
Hidden danger patrol set	Check out the hidden danger information
Patrol file set	Photo information submitted during the inspection
Pull down data set	Some basic pull-down data in the system
Information bulletin set	Information bulletin issued by administrators at all levels
Collection of laws and regulations	Information on laws and regulations issued by administrators at all levels
Information announcement annex set	Attached to the information bulletin
Annex set of laws and regulations	Annex to laws and regulations
Safety production basic information set	Information related to enterprise safety production
Set of security managers	Information of enterprise security management personnel
Hazardous chemicals set	Information on hazardous chemicals in enterprises
Information set for special operators	Information of special operators in enterprises
System construction situation set	Construction of enterprise safety production system
Register of fire equipment	Enterprise's fire equipment registration
Special equipment registration information set	Special equipment registration of the enterprise
hazardous chemical substance collection	Basic data on hazardous chemicals
Self-report hidden danger pool set	Different types of enterprises need to self-report the underlying hidden risks
Self-report hidden danger result set	Enterprise self-reported hidden consequences
Report your hidden danger list	The basic data of enterprise self-report
Self-report hidden trouble file set	Relevant attachments uploaded by enterprises when self-reporting
Listing remediation set	Risk listing remediation data
No license or license set	Unlicensed enterprise data

(2) Entity service layer

During the development process, the interface oriented programming principle is followed. The specific structure is as follows:

Each entity service class provides data manipulation methods for that entity (including add, delete, change, and so on). For concrete entity query operations,

query conditions are defined using Lamda expressions with Specification objects (Specification), which can be combined to achieve standardized complex condition data acquisition.

(3) Controller layer

The controller layer implementation provides complete business functions, so the client is shielded

Serial number	List of names	data type	length	Decimal	Identification	Primary key	foreign key	Allowable empty	Default value	Explanation
1	ID	uniqueidentifier		0	Yes	Yes		No		
2	Name	nvarchar	1000					No		
3	Description	nvarchar	100					No		grid number

(7) large grid set

Serial number	List of names	data type	length	Decimal	Identification	Primary key	foreign key	Allowable empty	Default value	Explanation
1	ID	uniqueidentifier		0	Yes	Yes		No		
2	Name	nvarchar	1000					No		
3	Description	nvarchar	100					Yes		Grid number
4	Zone_ID	uniqueidentifier					Area set			

(8) Medium Grid Set

Serial number	List of names	data type	length	Decimal	Identification	Primary key	foreign key	Allowable empty	Default value	Explanation
1	ID	uniqueidentifier		0	Yes	Yes		No		
2	Name	nvarchar	1000					No		
3	Description	nvarchar	100					Yes		Grid number
4	Large grid_ID	uniqueidentifier					Big grid ID			

4. EPILOGUE

Through the implementation of system projects, the safety supervision bureau can achieve scientific and efficient management of enterprise safety production. We also provide functions and information that meet the needs of government departments and enterprises, leading to corresponding social benefit and economic benefit.

ACKNOWLEDGEMENT

The paper was supported by Wenzhou science and technology project (G20140010).

REFERENCES

[1] Benjamin Turnbull, Suneel Randhawa. Automated event and social network extraction from digital evidence sources with ontological mapping. *Digital Investigation*, 2015, 13.
 [2] Danilo F.S. Santos, Hyggo O. Almeida, Angelo Perkusich. A personal connected health system for the Internet of Things based on the Constrained Application Protocol. *Computers and Electrical Engineering*, 2015, 44.

[3] Soohong Park, Jaehoon (Paul) Jeong, Choong Seon Hong. QoS-guaranteed Mobile IPTV service in heterogeneous access networks. *Computer Networks*, 2014, 69.

[4] A. Urbietta, A. González-Beltrán, S. Ben Mokhtar, M. Anwar Hossain, L. Capra. Adaptive and context-aware service composition for IoT-based smart cities. *Future Generation Computer Systems*, 2016.

[5] Shu-Lin Wang, Young Long Chen, Alex Mu-Hsing Kuo, Hung-Ming Chen, Yi Shiang Shiu. Design and evaluation of a cloud-based Mobile Health Information Recommendation system on wireless sensor networks. *Computers and Electrical Engineering*, 2016, 49.

[6] T. Frantti, M. Majanen. An expert system for real-time traffic management in wireless local area networks. *Expert Systems With Applications*, 2014, 41(10).

[7] J. López, Diego Pérez, Enrique Paz, Alejandro Santana. WatchBot: A building maintenance and surveillance system based on autonomous robots. *Robotics and Autonomous Systems*, 2013, 61(12).

- [8]Seung-Ho Lim,Seongwoo Lee,Woo Hyun Ahn. Applications IO profiling and analysis for smart devices. *Journal of Systems Architecture*, 2013, 59(9).
- [9]Nikhil Bassi, Ilya Karagodin, Serena Wang, Patricia Vassallo, Aparna Priyanath, Elaine Massaro, Neil J. Stone. Lifestyle Modification for Metabolic Syndrome: A Systematic Review. *The American Journal of Medicine*, 2014, 127(12).
- [10]Julien Montavont, Damien Roth, Thomas Noël. Mobile IPv6 in Internet of Things: Analysis, experimentations and optimizations. *Ad Hoc Networks*, 2014, 14.
- [11]YangSun Lee, Junho Jeong, Yunsik Son. Design and implementation of the secure compiler and virtual machine for developing secure IoT services. *Future Generation Computer Systems*, 2016.
- [12]Erik Nordström, Christian Rohner, Per Gunningberg. Haggel: Opportunistic mobile content sharing using search. *Computer Communications*, 2014, 48.
- [13]Awais Ahmad, Anand Paul,M. Mazhar Rathore, Hangbae Chang. Smart cyber society: Integration of capillary devices with high usability based on Cyber - Physical System. *Future Generation Computer Systems*, 2016, 56.
- [14]J. Ignacio Hidalgo, Esther Maqueda, José L. Risco-Martín, Alfredo Cuesta-Infante, J. Manuel Colmenar, Javier Nobel. glUCModel: A monitoring and modeling system for chronic diseases applied to diabetes. *Journal of Biomedical Informatics*, 2014, 48.
- [15]Hae-Duck J. Jeong,Woojin Lee,Jiyoung Lim,WooSeok Hyun. Utilizing a Bluetooth remote lock system for a smartphone. *Pervasive and Mobile Computing*, 2015, 24.
- [16]Li Yang, Jianfeng Ma, Wenjing Lou, Qi Jiang. A delegation based cross trusted domain direct anonymous attestation scheme. *Computer Networks*,2015, 81.
- [17]Jidong Chen, Ye Tao, Haoran Wang, Tao Chen. Big data based fraud risk management at Alibaba. *The Journal of Finance and Data Science*, 2015, 1(1).
- [18]Takayuki Matsumoto, Kazuyoshi Hidaka. Evaluation the effect of mobile information services for public transportation through the empirical research on commuter trains. *Technology in Society*, 2015, 43.

Analysis on the Influencing Factors of Environmental Information Disclosure in Chemical Industry

Zhao Haiyan^{1*}, Zhang Shan²

¹Business College, Lingnan Normal University, Zhanjiang in Guangdong Province, China

²College of Accounting, Heilongjiang Bayi Agricultural University, Daqing in Heilongjiang Province, China

Abstract: In this paper, the social responsibility report of A-share listed companies in Shanghai and Shenzhen chemicals industry in 2013 to 2015 is taken as the research sample, the content of environmental information disclosure is quantitatively analyzed, at the same time, the relationship between influencing factors and environmental information disclosure was analyzed by multiple regression model.

Keywords: Chemical industry; Environmental information disclosure; Social responsibility report

1. INTRODUCTION

Based on the social responsibility report of A-share listed companies in chemical industry in Shanghai and Shenzhen from 2013 to 2015, this paper establishes a multiple regression model to analyze the relationship between environmental factors and environmental information disclosure, and explores the correlation between variables.

2. LITERATURE REVIEW

Lynn (1992) through the study of relevant enterprises that H shares, scale effect and reliability on independent [1]; Hackston, Milne (1996) analysis of the company's operation mode and efficiency, that corporate profits and environmental information disclosure two poor correlation [2]; Tang Jiufang et al. (2010) based on the relevant data of listed companies, we concluded that the operation efficiency and the size of enterprises directly affect the disclosure of corporate environmental information.

3

3.1 The relationship between listed websites and environmental information disclosure

The different directions and scopes considered by the makers of different systems will also affect the standardization of corporate environmental information disclosure in different places. According to the following assumptions:

Hypothesis 1: For the chemical products industry, the Shanghai stock market regulation is more binding than the Shenzhen stock market speculation.

3.2 The nature of the company and the relationship between environmental information disclosure

Table 1 corporate environmental information disclosure

For an enterprise, it is generally considered that a higher proportion of state-owned shares will be more likely to consider the overall consideration and pay attention to the overall economic and social benefits. According to the following assumptions:

Hypothesis 2: For chemical products industry, the type of state-controlled shares is more conducive to improving the disclosure level of environmental information.

3.3 The relationship between company's organizational form and environmental information disclosure

Generally listed the size of the board of directors will improve the quality of decision-making. According to the following assumptions:

Hypothesis 3: The larger the board of chemical companies, the better the quality of environmental disclosure.

3.4 The relationship between company size and environmental information disclosure

The larger the company, the greater the demand for capital, and the greater the demand for raw materials and other resources. According to the following assumptions:

Hypothesis 4: In the chemical industry, the larger the company, the higher the reliability of corporate environmental information.

3.5 Company profitability and environmental information disclosure

In the process of making relevant decisions, the enterprise stakeholders will focus on the profitability. According to the following assumptions:

Hypothesis 5: The profitability of enterprises can promote the improvement of environmental accounting information disclosure.

4. RESEARCH DESIGN

4.1 Sample selection and data sources

Due to the late start of the restriction on the related social responsibilities in our country, there is no explicit regulation on the disclosure of environmental information and norms and their unification on the form and index. Table 1 reflects the chemical industry environment information disclosure methods:

	Disclosure of the number of enterprises	The proportion(%)
Prospectus	102	46.58
annual report	102	46.58

social responsibility Report	42	19.18
As can be seen from Table 1, the number of enterprises disclosed in the annual report and prospectus are the same, accounting for 46.58% of the total number of enterprises in the industry. Compared with the 42 enterprises disclosed through the social responsibility report, 19.18% of the share was significantly lower.	4.2.1 Environmental information disclosure index (EDI). Quantitative description of 3 points, the specific qualitative description of 2 points, the general description of a score of 1, did not disclose 0 points. Specific calculation of the score as shown in the following table:	

Table 2 ED calculation table

Serial number	Disclosure items	Score
1	Corporate environmental philosophy, behavior and goals of success	1
2	Corporate environmental investment and environmental technology development	3
3	Enterprise environmental protection facilities construction and operation	3
4	Disposal of enterprise waste, recycling of waste products	3
5	Corporate honor of environmental protection	2
6	Specific pollutant emissions of enterprises	3
7	Environmental policy implementations	1
8	Environmental performance of enterprises	3
9	Other environmental information voluntarily disclosed by the enterprise	3

4.2.2 Empirical model

$$EDI = \beta_0 + \beta_1 LIST + \beta_2 NATURE + \beta_3 SCALE + \beta_4 SIZE + \beta_5 ROA + \varepsilon$$

4.2.3 Variable definition

Define EDI as an explanatory variable and set 5 variables as LIST, NATURE, SCALE, SIZE and ROA of the enterprise as Explanatory variables.

Variable definitions as shown in Table 3:

5. EMPIRICAL RESULTS ANALYSIS

5.1 Descriptive analysis

From the difference between the maximum and

Table 3 variable definition table

Variable type	Variable sign	Variable explanation
Explained variable	EDI	Calculated from Table 1 and Equation 1.
	LIST	Place of listing, the Shanghai Stock Exchange is 1, Shenzhen Stock Exchange is 0.
Explanatory variables	NATURE	Type of holding, State holding is 1, Non-state holding is 0.
	SCALE	Board size and number.
	SIZE	Enterprise size, the absolute value of total assets.
	ROA	Profitability, Total Return on Assets.

Table 4 descriptive statistical analysis table

variable	maximum	Minima	Mean	Standard deviation
EDI	1.00	0.23	0.6038	0.18922
LIST	1.00	0.00	0.4524	0.50376
NATURE	1.00	0.00	0.4524	0.50376
SCALE	16.00	5.00	9.8571	2.04309
SIZE	8071321.00	88786.00	1.3173E6	1.85596E6
ROA	1.09	0.02	0.2693	0.21390

Table 5 correlation analysis matrix

variable	EDI	LIST	NATURE	SCALE	SIZE	ROA
EDI	1					

LIST	-.167	1				
NATURE	.204	.135	1			
SCALE	.171	.278	.372*	1		
SIZE	.322*	.176	.466**	.372*	1	
ROA	-.018	.162	.098	-.066	-.230	1

Table 6 colinearity test situation table

Model 1		Collinearity statistics	
		Tolerance	VIF
5	LIST	.874	1.145
	NATURE	.692	1.444
	SCALE	.764	1.308
	SIZE	.659	1.517
	ROA	.850	1.177

5.3 Test assumptions

Table 7 shows: Adjusting R 0.663, confirming that the explanatory power of EID in this model is 66.3%, the other influencing factors are not clear and need further tests.

As shown in Table 8: Analyze the overall regression results and explain that the impact of variables on environmental information disclosure passed the test at 1% level.

Table 7 regression model overall parameter table

model	R	R side	Adjust R side	Standard estimation error	df	F	Sig.
1	.848a	.719	.663	.37622	6	12.813	.000a

Table 8 model regression coefficient analysis of results table

Model 1	Non-standard coefficient		Standard factor			
	B	Standard error	Beta	t	Sig.	
5	LIST	-.113	.033	-.643	-3.406	.002
	NATURE	-.001	.046	-.006	-.023	.982
	SCALE	.034	.007	.609	4.748	.000
	SIZE	3.070E-8	.000	.415	3.076	.004
	ROA	.123	.076	.216	1.612	.118

6. CONCLUSION AND RECOMMENDATIONS

6.1 Conclusion

(1) complicated disclosure methods, norms can not be unified

For the chemical industry, the disclosure form is mainly the prospectus, financial reports and social responsibility reports.

The disclosure reliability of EID in chemical products industry is relatively low

EDI score maximum 1, minimum 0.23, mean 0.6038. Based on the overall view, the industry is at a low level and there is no uniform requirement for disclosure.

6.2 Suggestions for improving environmental accounting information disclosure

(1) The establishment and improvement of relevant laws and regulations system

The state should give full play to the formulation and modification of the law of this function, and accelerate the establishment of environmental

accounting information disclosure laws and regulations, to provide an important basis for corporate disclosure.

Improve the environmental awareness of enterprises, and guide enterprises to voluntarily conduct environmental information disclosure

In order to promote the sustainable development of social ecological civilization, enterprises should proactively implement the social responsibility and environmental protection concepts in daily business activities.

REFERENCES

- [1]M. Lynn, A Note on Corporate Social Disclosure in Hong Kong. *The British Accounting Review*, 1992, 2(2):105-110.
- [2]D. Hackston, and M.J. Milne, Some Determinants of Social and Environmental Disclosures in New Zealand Companies. *Accounting Auditing and Accountability Journal*, 1996, 9(1):77-108.

Profit Model of Bus Mobile Payment

Zhijiang Lin¹, Yujie Zeng¹, Shengli Wang², Changjiang Liu^{3,4,*}

¹ School of Automation and Information Engineering, Sichuan University of Science and Engineering, Sichuan, China

² School of Chemical Engineering, Sichuan University of Science and Engineering, Sichuan, China

³ Key Lab of Enterprise Informationization and Internet of Things of Sichuan Province, Sichuan, China

⁴ School of Mathematics and Statics, Sichuan University of Science and Engineering, Sichuan, China

*liuchangjiang@189.cn

Abstract: Mobile payment plays a vital role in modern daily life. This paper studies the related issues of mobile payment in public transportation under the condition of known experimental data. Experimental data was preprocessed with cleaning and excavation procedures to guarantee to exclude the abnormal or error data. Under reasonable assumptions, the user's trip payment method was proposed. In detail, multivariate nonlinear regression fitting and Fourier fitting were used to establish a mobile payment based on the bus profit model. Furthermore, the Bass diffusion model was then used to improve the model, which makes the proposed profit model fit for large-scale bus mobile payments. Results on experimental data available on MathorCup official website prove the availability and reasonability.

Keywords: Multiple nonlinear regression; Fourier fitting; Profit model; Bass diffusion model

1. INTRODUCTION

With the popularization of smart phones and the improvement of mobile payment technologies, more and more payment methods have been transferred to mobile phones [1, 2]. There are many shortcomings in cash payment and physical bus card payment. For example, in the course of using the bus card, there are problems such as inconvenient to recharge, unable to return change, difficult to view purchase history, and restricted for use in specific regions. Cash payment brings a lot of inconveniences and increasing labor costs, etc. . However, bus mobile payment can be a good solution to these problems [3]. With the widespread popularity of public mobile payment, it is particularly important for bus companies and third-party platforms.

The most typical way to represent the profitability of a company is to use the difference between income and expenses, namely, the more the difference is, the more profitable the company is. The main income items of the third-party payment platform are composed of fee, advertising fee, deposit fund revenue, service fee, and etc [4]. The main expenditure items include platform development and routine maintenance costs and bank fees.

The concept of mobile payment has long been widely studied by many scholars. Alexandrou [5] gave an example method which includes a customer accepting a merchant's offer for sale of a product, the customer

paying a third party for the product, and the third party facilitating the payment for the product to the merchants. Sada and Mikal [6] mentioned a system and method for enabling a debtor to charge a payment to a credit card when a creditor does not accept credit card payments is provided. Bishop and Saunders [7] researched on payment authorization. The Bass diffusion model has a good value for the adoption and diffusion of innovative products and technologies. Dragan Jukić [8] proved the rationality of Bass diffusion model. Sood and James [9] also analyzed the feasibility of regression analysis to solve Bass diffusion model.

In this paper, payment characteristics of people's travel are obtained. And on this basis, the profitability of third-party payment platforms is studied. A reasonable analysis of people's travel modes and payment methods is performed based on existing data of a specific city. Assuming mobile payment equipments install in one fourth of the public transportation systems in the first phase, then they will extend to all public transport systems. The changes are a diffusion process in line with the Logistic curve. Therefore, the Bass diffusion model is established under reasonable assumptions. Thus, the profit of the third-party payment platform is calculated, followed by multiple linear regression analysis and Fourier fitting analysis of experimental city data. Then, the Bass diffusion model is employed to derive the equation. The model aforementioned easily to generalize to all public transport and also achieve profitability after third-party mobile payment.

The main contributions of our paper are:

1. This paper digs deeply into the data and basically eliminates the influence of abnormal data on the calculation process, making the calculation process easier and more accurate.
2. In establishing the profit model of the third-party payment platform, the Bass diffusion model is used in this paper. The development status of the third-party payment platform fully complies with the requirements of the model, making the results more convincing.

2. ESTABLISHMENT OF A PROFIT MODEL

We first analyze locally wide profit model, then generalize it to globally wide profit model.

2.1 Locally wide profit model

The profitable methods of third-party payment mainly comprise handling fees, advertising fees, interest

income from deposit funds, service fees, and customer data income. Combined with relevant information, this paper mainly discusses the main profit-making methods of third-party payment platforms, including fees, advertising fees, deposit fund revenues, service

fees, and other income expenses. Meanwhile, the main expenditure items are platform development, routine maintenance costs and bank charges. The main items of the third party platform revenue and expenditure are listed, as shown in Figure 1.

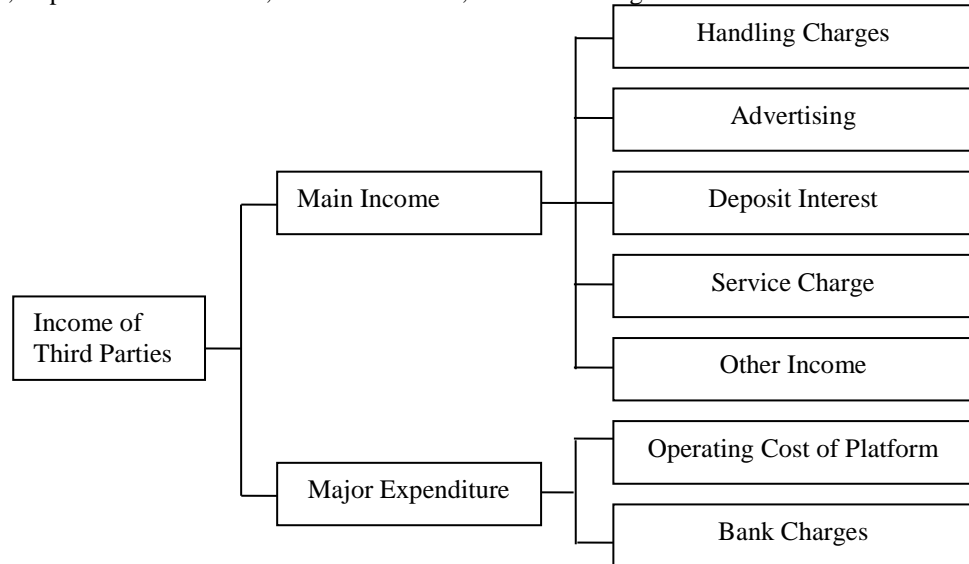


Figure 1 The main items of the third party platform revenue and expenditure

2.1.1 Handling charges

In the profit-making method of the third-party payment platform, using handling charges incurred by the merchant is a relatively mature profit-making method. Third-party payment platforms have developed rapidly. As a traditional and mature means of profit, handling charges from processing fees have been limited. Henceforth, this proportion of profits has become less and less. In public mobile payment, the third-party payment platform charges the bus company as to make profit.

The income from the handling charges and the unit price of the user’s expenses and the total amount charged by the merchant are presented as follows:

$$A = y * a\% + y(1 - a\%)b\% \quad (1)$$

where A represents the total fee income, y single ride cost, a represents the proportion of fees charged to individuals, generally taking 1% of the amount of user expenditure; b denotes the proportion of fees charged to the bus company, generally taking 1.5% of the amount charged by the merchant.

2.1.2 Advertising fee income

In the mobile payment of public transportation, the advertising fee income of the third-party payment platform is similar to that of other online platforms. The advertising fee income of the online platform is directly related to the scale of development and the scale of users. Based on relevant literature report, the specific relationship between advertising fee income and platform development scale and user scale is given below:

$$\lg(b) = 0.2319051\lg(Y) \pm e^{0.2319051\lg(Y)} \quad (2)$$

Where b represents the amount of pre-tax advertising expenses, Y is the total number of rides by the user

and e is the symbol of the base of the natural logarithm. Advertising expenses are sales expenses and are included in the profit and loss amount. The tax department will charge a certain amount of advertising tax based on the amount of advertising fees. Generally speaking, the tax rate charged by the taxation department is 5% of the advertising cost, and the after-tax income of the advertising fee is presented as:

$$B = b * 95\% \quad (3)$$

Among them, B represents the amount of post-tax advertising expense income.

2.1.3 Income from precipitation funds

In the third party payment, it is often the user who prepays the funds to the third party payment platform. After the user receives the corresponding goods or achieves the purpose of the transaction, the third party payment platform will assign the money to the seller’s account. Because there is a time difference between the collection and payment of the third-party payment platform, there will be a large amount of in-transit funds, i.e. deposit funds. The third-party payment platform can, with the permission of relevant policies and management measures, keep sufficient funds to run the daily operation of the platform, and deposit the overflowed deposit funds into the bank in the form of fixed-term deposits to receive the fairly preferable interest income. This paper concludes that the relationship between the general third-party payment platform and the front-end third-party payment platform is as follows:

General third-party payment platform:

$$C = \frac{1}{4} y * c_1\% * 1.1\% \quad (4)$$

Front-end third-party payment platform:

$$C = y * c_2 \% * (4\% - 0.78\%) \quad (5)$$

Here, C represents the amount of income from deposits, c_1 represents the deposited funds of the general third party payment platform; c_2 represents the deposit funds of the front-end third-party payment platform.

2.1.4 User service fee income

Service fee refers to a series of fees by a third-party payment platform for providing customers with payment solutions, payment systems, and various value-added services. It is calculated as follows:

$$D = 0.2\% * y \quad (6)$$

2.1.5 Other income

Other income is composed of the potential value of customer information, the company's development potential, etc. Because it is difficult to quantify, other income is not considered in this paper.

2.1.6 Platform's expenditure items and calculation methods

The expenditure items of the platform in this paper include platform development and routine maintenance costs and bank charges.

When the third-party payment platform pays the goods to the merchant authorized bank, the bank will pay a certain amount of fees to the third-party platform. It is expressed as follows:

$$E = y * 1.25\% \quad (7)$$

Generally, the processing fee charged by the bank to the third-party payment platform is 1% to 1.5% of the purchase price. To simplify calculation, the median value 1.25% is taken in this paper.

2.1.7 Third party platform profit calculation

Through the above analysis, we have obtained the calculation methods for various revenues and expenditures of third-party payment platforms. The profit of third-party platforms is the difference between various revenues and various expenditures. The specific expression of the profitability of third-party platforms is seen in followed sections.

2.1.8 Calculation of the total number of bus mobile payments

With the maturity of mobile payment technology, the use of public mobile payment users will gradually increase. As a result, the total number of mobile bus transactions is a function of time.

Segmenting the time of one day into seven parts, the total number of public transportation payments on a particular day can be expressed as:

$$Y = \sum_{i=1}^7 y_i * N \quad (8)$$

where y_i indicates the ratio of mobile payment to all payment methods in the i -th period; N indicates the number of users of all payment methods.

In formula (8) above, the ratio of mobile payment to total payment method during a period of time, the ratio of daily bus mobile payment to all payment methods, and the proportion of monthly bus mobile payment to

all payment methods can be depicted as a nonlinear function f .

Setting the proportion of mobile payment in each period to all payment methods x_1 , the ratio of daily bus mobile payment to all payment methods in one day x_2 , and the proportion of monthly bus payment in all payment methods in one month x_3 , the functional relationship can be expressed as:

$$y_i = f(x_1) * f(x_2) * f(x_3) \quad (9)$$

2.1.9 Total profit calculation of third-party platforms

According to the analysis of the background of the topic and repeated trials, this paper concludes that the total profit of the third-party payment platform is proportional to the single ride profits and the total number of rides. Total profit can be expressed as:

$$\Pi = \pi Y \quad (10)$$

where π represents single ride profits, Y indicates the total number of mobile bus payments in a month.

2.2 globally wide profit model

The Bass diffusion model was proposed by Frank M. Bass for the adoption and diffusion of innovative products and technologies. Its use of differential equation method to describe the diffusion process and mechanism of new products, has a good ability to explain the general rules of the new trend of proliferation. This model can provide a dynamic description of the law, which is widely used in market prediction of new products or new technologies. In the prediction of network products normally have a good effect.

The Bass diffusion model is only applicable to the market forecast of new products that have existed in the market for a certain period of time, and does not apply to products that have not been listed on a large number of user bases. Supposed one-quarter of subways and buses have installed mobile payment devices and conducted trials, which has a certain customer base and satisfies the conditions of the Bass model.

Bass's basic model equation is as follows:

$$\frac{dN(t)}{dt} = p(M - N(t)) + q \frac{N(t)}{M} (M - N(t)) \quad (11)$$

where $N(t)$ is the number of people who purchase the product at time t , M is the market's greatest potential, and p is the coefficient of innovation which is related to the number of potential users of the product. The imitation coefficient q is related to the number of potential users and the number of used products.

The Bass diffusion model is based on conditional probability and represents the conditional probability of consumer transactions at time t as a linear function of the cumulative probability at time t . Henceforth, the conditional probability of trading at time t is given by:

$$\frac{f(T)}{1 - f(T)} = P(T) = p + \frac{q}{M} Y(T) = p + qF(T) \quad (12)$$

In equation (12), the probability $\frac{f(T)}{1 - f(T)}$ depends on

$F(T)$, the cumulative probability function. And p

variable represents innovative user's role in diffusion dissemination, q represents the role of the imitator. From analytical framework we built above, it can be seen that the relationship between the transaction volume and the total transaction volume at time t is:

$$N(T) = pM + (q - p)Y(T) - \frac{q}{M}[Y(T)]^2 \quad (13)$$

At time T , the third-party mobile payment transaction scale is $N(T)$, the third-party mobile payment cumulative transaction size is $Y(T)$, and the square of the third-party mobile payment cumulative transaction size is $[Y(T)]^2$. Let $N(0) = 0$, integrate equation (13) and obtain another formation:

$$N(T) = \left(\frac{M(p+q)^2}{p} \right) \left[\frac{e^{-(p+q)T}}{(q/pe^{-(p+q)T} + 1)^2} \right] \quad (14)$$

However, in the actual analysis and calculation, the calculation of equation (14) is too difficult and almost impossible to implement. Instead, the common formula (13) is used to calculate the result.

In numerical calculation we can set

$$f(x_1) = 0.0002x_1^6 - 0.0049x_1^5 + 0.0479x_1^4 - 0.2291x_1^3 + 0.5659x_1^2 - 0.6702x_1 + 0.7766$$

$$f(x_2) = 0.00002x_2^6 - 0.0006x_2^5 + 0.0057x_2^4 - 0.0256x_2^3 + 0.0589x_2^2 - 0.06486x_2 + 0.4879$$

By Fourier fitting, the expression is obtained

$$f(x_3) = 0.03933 \cos(0.1944x_3) + 0.0702 \sin(0.1944x_3) + 0.4461$$

Henceforth, we can compute $y_i = f(x_1) * f(x_2) * f(x_3)$. In combination with other known parameters, it is possible to obtain a partial total profit.

3.2 Diffusion model solution

Using the same solution as the local interest model, the expression is obtained by fitting the toolbox with a multiple nonlinear regression equation:

$$f(x_1) = 0.0005x_1^2 + 0.0026x_1 + 0.4765 \quad (17)$$

$$f(x_2) = -0.0001x_2^2 + 0.0012x_2 + 0.5892 \quad (18)$$

$$f(x_3) = -0.0009x_3^2 + 0.0222x_3 + 0.4939 \quad (19)$$

The dynamic relationship between the total number of times of public mobile payment over time is:

$$Y(T) = f(x_1)f(x_2)f(x_3) \quad (20)$$

From the above relationship, the coefficient parameter value matrix in the relationship is:

$$\alpha_i = [0.4756 \quad 0.5892 \quad 0.4939] \quad (21)$$

Therefore, we have

$$\alpha = 0.4756 \times 0.5892 \times 0.4939 = 0.1384 \quad (22)$$

Similarly,

$$\beta_i = [0.0026 \quad 0.0012 \quad 0.0222] \quad (23)$$

$$\beta = 0.0026 \times 0.0012 \times 0.0222 = 6.9624 \times 10^{-8} \quad (24)$$

$$\gamma_i = [0.0005 \quad -0.0001 \quad -0.0009] \quad (25)$$

$$\gamma = 0.0005 \times (-0.0001) \times (-0.0009) = 4.5 \times 10^{-11} \quad (26)$$

Putting equations above into (15), the p and q can be calculated:

$$p = 9.2443 \times 10^{-7}, q = 2.7000 \times 10^{-5} \quad (27)$$

$$\alpha = pM, \beta = q - p, \gamma = | -q/M | \quad (15)$$

Thus equation (12) can be simplified as:

$$N(T) = \alpha + \beta Y(T) + \gamma [Y(T)]^2 \quad (16)$$

The relationship between $N(T)$, $Y(T)$ in equation (16) obviously accords with the quadratic function relationship. Once data is predefined, coefficients α , β , γ can be calculated by fitting the quadratic function.

3 SOLUTION OF THE MODEL

In this paper, we focused on experimental data [10] to validate our proposed method. The model was implemented using the Matlab R2014a.

3.1 The solution of local profit

Without considering the large-scale use, only the existing data is analyzed and the expression is obtained by fitting a toolbox with a multiple nonlinear regression equation:

In conclusion, the relationship between $N(T)$, $Y(T)$ is described as follows:

$$N(T) = 0.1390 + 6.9624 \times 10^{-8} Y(T) + 4.5 \times 10^{-11} [Y(T)]^2 \quad (28)$$

4. CONCLUSION

Based on the Bass diffusion model established in this paper, it is clear that there are a large number of potential users on the third-party payment platform. This happens to coincide with the status of the third-party payment platform in initial step. It is strongly recommended that the platform augments investment in publicity to increase awareness and converts potential customer groups into using customer groups.

There are numerous profit models for Internet products, but advertising costs and service fees still account for a large proportion of profit. Therefore, as the platform itself increases its advertising efforts, it must also strengthen the function of the platform's web pages to attract more merchants to participate in advertising. Developing more loyal users and increasing economic resources is a good way out.

As a huge social resource, deposited funds can be used as a huge social resource if they can be reasonably openly operated. It is also a stable profit support point constructed by third-party payment agencies. If you find a suitable partner, you can ensure that you can provide them with quality services and accumulate large amounts of deposited funds, which will bring a lot of profits to the platform.

In this paper, the data of each column was analyzed in depth, i.e. the abnormal data was effectively cleaned, the error data was corrected effectively, and the

correctness of the calculation result was effectively guaranteed.

In addition, this article can be used to promote mobile payment to a wider relevant payment fields, such as campus electronic card payment and debit card electronic payment. The model adopted in this paper has a certain guiding role in the future development of emerging network products.

5. ACKNOWLEDGEMENTS

This work was supported in part by the Open Project of Key Lab of Enterprise Informationization and Internet of Things of Sichuan Province under Grant No. 2017WZY01, the open Project of the Artificial Intelligence Key Laboratory of Sichuan Province under Grant No. 2014RZY02 and 2017RZJ03, the Open Project of Sichuan Province University Key Laboratory of Bridge Non-destruction Detecting and Engineering Computing under Grant No. 2014QZY01, Natural Science Foundation of Sichuan University of Science and Engineering (SUSE) under Grant No.2015RC08, 2017RCL54 and 2017RCL23, and Educational reform project of SUSE under Grant No. JG-1707. The work was also supported in part by the The Challenge Cup of Undergraduates.

REFERENCES

- [1] S. Karnouskos, "Mobile payment: A journey through existing procedures and standardization initiatives", *IEEE Communications Surveys & Tutorials*, 2004, 6(4): 44-66.
- [2] Seaborn, Catherine, J. Attanucci, and N. H. M. Wilson, "Analyzing Multimodal Public Transport Journeys in London with Smart Card Fare Payment Data", *Transportation Research Record Journal of the Transportation Research Board*, 2009, 2121: 55-62.
- [3] Michael John M. Belda, Girlie M. Enero, Rhendell John M. Pariño, XyriLMaicah F. Saul, Mariel Ruth S. Villegas, Rhowel M. Dellosa and Rionel B. Caldo, "Enhancing the bus payment method using Android and RFID Technology", *LPU-Laguna Journal of Engineering and Computer Studies*, 2015, 3(1): 20-28.
- [4] Ma, Z., Dong, X., Zhang, R., Yang, H., and Song, C, "Analyzing the factors that influence development of Chinese mobile third-party payment platform: the customers perspective", *Applied Mathematics & Information Sciences*, 2016, 10(2): 729-737.
- [5] AP Alexandrou, "Third party transaction payment processing", US, US20110264558A1. 2011.10.27.
- [6] Sada, A. and Mikal, P. J, "System and method for third party payment processing of credit cards", US, US20090248555A1. 2008.03.06.
- [7] Bishop, F. A. and Saunders, P. D., "Methods for a third party biller to receive an allocated payment authorization request", US, US20090164324A1. 2014. 09. 02.
- [8] Jukić, D., "On nonlinear weighted least squares estimation of bass diffusion model", *Applied Mathematics & Computation*, 2013, 219(14): 7891-7900
- [9] Sood, A., James, G. M., and Tellis, G. J., "Functional Regression: A New Model for Predicting Market Penetration of New Products", 2009.
- [10] MathorCup Mathematics Model Challenge For Undergraduates.<http://www.mathorcup.org/>

Anti-collision System based on Car Network

Xiong Xin, Zhang Shang*, Chen Xiaohui, Du Jiangwei, Wang Chen

College of Computer and Information Technology, China Three Gorges University, YiChang, China

*E-mail: wetoo@163.com

Abstract: With the rapid growth of car ownership in China, road congestion and traffic accidents are becoming more and more critical. The Internet of Vehicles is the specific solution as an important part of the future intelligent transportation, At the same time the concept of the Internet of Things in urban transportation is emerging. This paper proposes a Zigbee-based car network assisted driving platform design, which can exchange information among vehicles, with the functions of abnormal vehicle behavior reminding, anti-collision, path planning combined with road conditions, which would improve the convenience of driving and increase the safety of driving among vehicles. The design has strong practicability, low cost with scale-ability, and certain reference value for the development and planning of intelligent transportation.

Keywords: Zigbee; vehicle networking; radio frequency communication; intelligent transportation; anti-collision

1. INTRODUCTION

In recent years, with the rapid growth of China's car ownership, road traffic problems have been becoming increasingly severe. Many cities were heavily congested. On the other hand, road traffic accidents occurred frequently.

It can be seen that the current problem of driving and the safety of driving among vehicles are becoming more and more prominent and needed to be improved. As an important part of the future intelligent transportation, the Internet of Things (IoT) is the specific solution in urban transportation. This paper proposes a Zigbee-based vehicle-network assisted driving platform design, which can exchange information among vehicles and roads, which imply the functions of vehicle abnormal behavior reminding, anti-collision, path planning combined with road conditions.

2. SYSTEM COMPOSITION

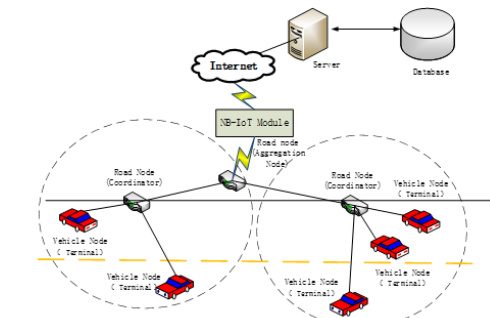


Figure 1 Network structure

The system is divided into three parts: vehicle nodes installed inside the vehicle, road nodes installed on both sides of the road, and servers. All vehicle nodes are used as terminals, and road nodes are divided into ordinary routers and aggregation node routers. The traffic information collected by the road node [6] will be collected by the ordinary router to the aggregation node router, and the NB-IoT module connected by the router will be sent to the server via the 5G network, and the data processing will be feed back to the vehicle node for information interaction and collision detection through the server.

(1) Vehicle node

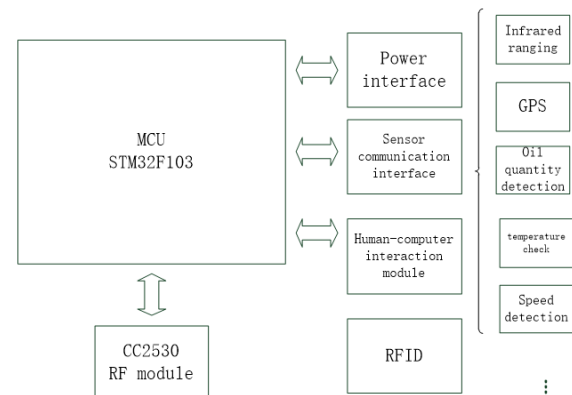


Figure 2 Vehicle node structure

The main controller of the system is the STM32F103 which apply ARM architecture. It is a 32-bit enhanced microcontroller designed by ST for the Cortex-M3 core. The chip has a maximum operating frequency of 72MHz and has a variety of low-power modes. The on-chip resources are abundant [7], which greatly facilitates embedded program development. The system's RF unit uses TI's SoC chip CC2530. The CC2530 integrates a high-performance RF module and an enhanced low-power 8051 microprocessor [8] for easy RF communication through the program. The vehicle node further would include infrared ranging module, and RFID tag that records its own information, a power interface, and a human-machine interaction device. Vehicle nodes are connected to devices such as fuel gauges, satellite navigation receivers, and inertial measurement units to obtain information about the vehicle itself; infrared ranging sensors are installed in the front, rear, left and right directions to detect distances from other vehicles or obstacles. Since the vehicle most concerned about the traveling vehicle is an adjacent vehicle, the vehicle node is configured with infrared ranging modules in front, rear, left, and right

directions for ranging with adjacent vehicles. When the 2 cars are in relative position, they will transmit their own network identification numbers. In this way, the vehicle node will use the received ID to form a wireless network with only neighboring vehicles and obtain its information in real time. The STM32 will use the position information of the other vehicle relative to its own position and the infrared distance measuring sensor to measure the distance information, combined with the state information of the neighboring vehicles obtained from the wireless network, through the analysis and processing of the application layer program, some judgments are provided and provided to the driver for reference.

(2) Road node

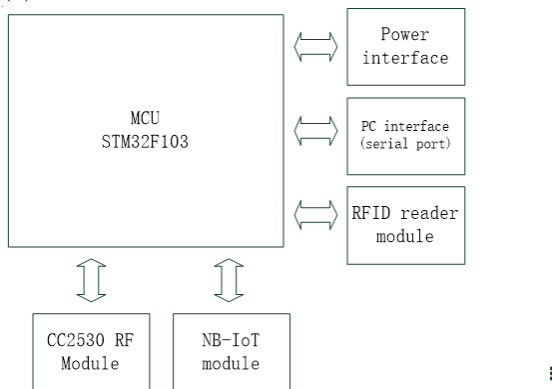


Figure 3 Road node structure

The hardware structure of the road node is shown in Figure 3. The main control device is MCU STM32F103, and the RF communication unit is CC2530. It is equipped with RFID reader module, power interface and serial port for communication with PC. If the road node is a Sink node, it also includes an NB-IoT Internet access module for transmitting data to the server through the 5G network.

The road node senses the passing of the vehicle through RFID, records the number of passing vehicles in real time, and can also communicate wirelessly with the surrounding vehicle nodes. Based on such a network platform, the road node can provide multiple services for passing vehicles. The proposed path planning service is combined with road conditions: road junctions and important locations of each road are arranged with road nodes. The road nodes obtain the passing traffic information through RFID and upload the information to the server via the road Sink router. At the same time, if the vehicle node in the area issues a path planning request, the road node will upload the request to the server after receiving the request, and the server calculates the optimal path back to the road node in combination with the road condition information, and then returns the road node to the vehicle node, so that the road node returns to the vehicle node, so that Drivers get a path planning solution that combines road conditions to avoid congestion or roads under construction.

3. SOFTWARE DESIGN

The system programming includes the programming of vehicle nodes and road nodes. Both nodes include STM32 and CC2530 program design. Among them, STM32 and CC2530 rely on SPI communication. Communication between STM32 and other sensor modules is mainly done through UART and I2C. STM32 programming uses the ST library officially created for the STM32F1 series (STM32F10x_StdPeriph_Lib_V3.5.0). The CC2530 programming uses the Z-Stack protocol stack from TI's ZigBee specification [9].

(1) Vehicle node

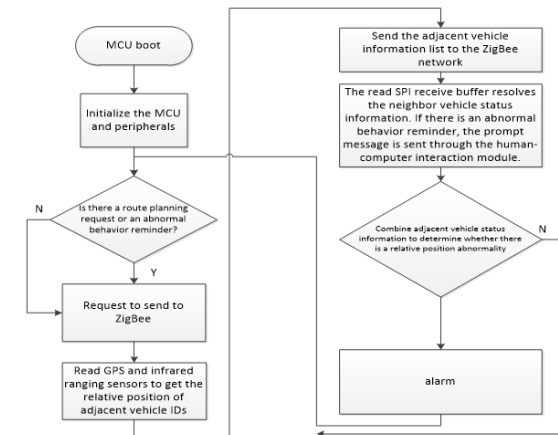


Figure 4 Vehicle node flow

The control flow of the STM32 of the vehicle node is shown in Figure 4. During each execution cycle, the STM32 will check for any abnormal behavior reminders that need to be sent to the CC2530, and then send it; at the same time, the list of neighboring vehicles will be sent to the CC2530. It will then check if the SPI Receive Buffer receives the CC2530 information, if it is, analyze it and send it back to the driver via the human-machine interaction device (touch screen and buzzer).

The CC2530 program is based on Z-Stack design. When the SPI receive data event SPI_INCOMING_ZAPP_DATA is generated in the Z-Stack, the program will analyze the packet type: if it is updating the adjacent vehicle list, it will be updated immediately; If it is an abnormal behavior reminder, the RF sending function is called to send a reminder to the preceding vehicle node. When the RF receive data event AF_INCOMING_MSG_CMD is generated in the Z-Stack, the program parses the data packet and sends the analysis result to the STM32 for further processing. At the same time, the CC2530 will periodically refresh the adjacent vehicle network in conjunction with the list of adjacent vehicle IDs received from the STM32.

(2). Road node

The STM32 of the road node mainly has three tasks: (1) recording through the vehicle through RFID; (2) communicating with the CC2530, and forwarding the vehicle node data packet in the area; (3) The Sink road node periodically exchanges the aggregated data packets with the server through 3G. The STM32 is equipped with the μ C-OSII operating system and

will handle task 1 and task 2 [10] in parallel. Task 3 will be executed once every 1 s through the timer interrupt.

4. APPLICATION

The vehicle networking integration platform adopts LBS Baidu open platform to realize the application system. The map interface based on WebGIS design can combine the GPS location information and the information provided by the server to provide users with path planning services including busy road marking and integrated road conditions.

The interface of the vehicle node is shown in the figure. The current vehicle location and busy road are marked in the map. Green indicates smoothness, yellow indicates congestion, and red indicates severe congestion. If the vehicle node issues a route planning request and receives planning information, it will be marked with a green line on the map. The picture shows vehicle condition monitoring, which is used to show whether the surrounding vehicles are in danger. In the figure, since there is a high-speed car in front of the vehicle but the distance is long, there is no danger, so there is a hint of distance speed and danger on the display interface. In the same interface, when the vehicle node receives abnormal behaviors such as lane change and sudden braking of surrounding vehicles, it will also be represented by a similar animation, and display different colors depending on the degree of danger.

5. CONCLUSION

As the core foundation of the new generation of intelligent transportation systems, the Internet of Vehicles has a very broad prospect. At present, there are still many problems in the car network that have not been solved. One of them is that the implemented applications are still independent of each other, and there is no platform for unified resource allocation and scheduling. A design framework was proposed and a variety of application designs were proposed based on it. It can also carry more applications, such as special vehicle identification and reminders, overnight network monitoring of vehicles. However, there are some technical details that need to be optimized. At the same time, security issues such as error messages and user privacy issues cannot be ignored. It is necessary to find a balance between

security issues and privacy issues [10].

ACKNOWLEDGEMENTS

This paper is supported by the CERNET through Project "NGII20161210".

REFERENCES

- [1] Burange A W, Misalkar H D. Review of Internet of Things in development of smart cities with data management & privacy[C]. Computer Engineering and Applications (ICACEA), 2015 International Conference on Advances in. IEEE, 2015: 189-195.
- [2] Pakanati C, Padmavathamma M, Reddy N R. Performance Comparison of TCP, UDP, and TFRC in Wired Networks[C]. Computational Intelligence & Communication Technology (CICT), 2015 IEEE International Conference on. IEEE, 2015: 257-263.
- [3] G. Kim, S. Lee, H. Park, D. Kim. A request based adaptive beacon rate control scheme for vehicular ad-hoc networks[C]// International Conference on Ubiquitous and Future Networks (ICUFN). July 2016:67-69.
- [4] M.M. Alotaibi, H.T. Mouftah. Adaptive expiration time for dynamic beacon scheduling in vehicular ad-hoc networks[C]// IEEE Vehicular Technology Conference (VTC2015-Fall). Sept.2015:1-6.
- [5] M. A. Nadeem and M. A. Saeed, "Fog computing: An emerging paradigm," 2016 Sixth International Conference on Innovative Computing Technology (INTECH), Dublin, Ireland, 2016, pp.83—86.
- [6] Luan TH, Gao L, Li Z, et al. Fog Computing: Focusing on Mobile Users at the Edge. Computer Science, 2016.
- [7] S. Yi, Z. Hao, Z. Qin, et al. Fog Computing: Platform and Applications, 2015 Third IEEE Workshop on Hot Topics in Web Systems and Technologies (HotWeb), Washington, DC, 2015, pp.73-78.
- [8] Protocols and architectures for wireless sensor networks. Karl H, Willig A. 2007
- [9] Wireless sensor networks: an information processing approach. ZHAO F, GUIBAS L J. . 2004
- [10] Overview of sensor network. D. Cullar, D. Estrin, M. Strvastava. Computer. 2004

Application of BIM Technology in Construction of Metro Stations

Dongyang Geng^{1,2,*}, Karel Vojtasik¹

¹ VŠB-Technical University of Ostrava Faculty of Civil Engineering

² School of management science and engineering Hebei GEO Unibersity shijiazhuang, china

*Email: 15200012621@139.com

Abstract: In view of the narrow, difficult, tight schedule and high requirements of the construction site of Beijing Dahongmen Bridge Subway Station, this paper combines the Revit series of software architecture BIM program to give full play to the Revit series software's functions of fine modeling and good display. He also conducted in-depth research and practice in aspects such as three-dimensional rendering, collision checking, quota picking, and quality assurance in mobile tracking.

Index Terms: BIM technology, subway station, construction

1. INTRODUCTION

BIM technology has been widely used in the field of civil engineering engineering at home and abroad, and foreign countries are relatively advanced in BIM technology theory and practice research. This project differs from other subway BIM projects in that it aims at the construction of the Dahongmen Bridge subway station in Beijing. It uses Revit software to build the BIM model of the Dahongmen Bridge Subway Station in Beijing, and uses BIM technology to perform three-dimensional bottoming, collision checking, and quota picking. In-depth research and practice in aspects such as mobile tracking quality and safety issues.

2. ENGINEERING APPLICATION BACKGROUND

Beijing Metro Line 16 is a north-south backbone line under construction of the Beijing Subway. It uses the 8-car formation A-type train for the first time and has a maximum capacity of 3560 passengers^[1]. The Daohuhu Road Station of the Beijing Metro Line 16 and the Zhongguancun Innovation Park The A-Plant Integration Project is located in the planned green area north of Daoxianghu Road Station of Beiqing Road and Metro Line No. 16, and is an integrated development project with the Daoxianghu Road Station of the Metro^[2]. "Figure 1" The south side is the Daoxianghu Road Station and the urban main road Beiqing Road, the west side is the Daoxianghu Road, the city's main road, the east side crosses the Xinyuantou Flood Drainage Channel via the No. 6 Innovation Park, and the north is a city slip road^[3].



Figure 1 3D site layout

The Dahongmen Bridge subway station project in Beijing is difficult to construct and has high quality requirements. BIM technology is an important means to improve the level of construction management and implement refined manpower machine control. The specific reasons for using BIM technology in this project include the following four aspects^[4]:

(1) Solve drawing problems in advance and avoid work. The traditional two-dimensional design drawings have a lot of mistakes. Through modeling, collision checking, and virtual construction^[5], errors can be discovered in advance, and changes can be organized in advance so as to avoid labor caused by changing the design in the construction process, thereby improving construction work efficiency^[6].

(2) Three-dimensional visualization gives a precise understanding of design intent and avoids construction errors.

(3) Fine management of materials, implementation of quotas, reduction of waste, rapid calculation of current project quantities, timely application of progress payments to owners, quick review of subcontracted teams, and accurate accounting of project volumes.

(4) Coordinate quality and safety management, and establish a rapid response mechanism to ensure that there are no safety and quality accidents in the construction process.

3. BIM APPLICATION IMPLEMENTATION CORE CONCEPT

Focusing on the BIM model of the Dahongmen Bridge Subway Station in Beijing, BIM technology is used to rapidly provide accurate, comprehensive, and detailed basic project data for all parties involved in the construction process. This enables owners, design institutes, construction agencies, supervision organizations, and third-party inspections. Units and BIM consulting units can work together in the same

BIM model and system platform to improve the efficiency of collaborative work among all parties, and help clear the respective responsibilities and obligations of various departments and units, and reduce the delays caused by poor communication between units. Wrangling, accelerating the construction progress of the entire project. The BIM co-operation of the Metro means in short, that the parties participating in the metro can realize the same subway BIM model on the same platform and use it to perform their own work. The BIM modeler builds a three-dimensional information model of the metro in accordance with the norms and standards, and uploads it to the Luban software for unified management in the background. The BIM resident manager is responsible for organizing the application of BIM technology on the site to guide the construction of the subway. The BIM model is constantly maintained, modified, and modified according to actual project changes. The modified BIM model information is saved in the cloud so that everyone can see the updated BIM in time. model. The professional design staff of the design unit can also conduct professional design in the same subway BIM model, and upload the design results to the cloud in time, which is beneficial to the collaborative design between the various professions. The construction unit applies the same subway BIM model to provide layered technical disclosures, conveys BIM 3D information, and organizes workers to strictly follow BIM model construction. The supervision unit and the third-party testing unit compared the BIM model to check whether the size of the subway structure at the site and the spacing of the Steel Bar type are consistent with the design requirements, so as to ensure the construction of a high-quality project. The owner reviews the design, construction, and delivery processes according to the BIM model to ensure that the actual project delivery fully complies with the BIM model requirements for the subway. Senior managers of construction companies can remotely view the cloud platform to control the progress and quality of the project and realize the goals of strategic management and remote management.

4. METRO STATION BIM 3D MODELING

Beijing Bahrain Bridge Subway Station BIM model has the following characteristics:

(1) Targeted. For different functional structures and specific requirements, different software is used to establish the model. For example, for the three-dimensional joints of the complex node of the reinforcement model, the Steel Bars of the local node's complex Steel Bar are displayed with good display effect, and the modelling speed is faster for the Guanglianda software Steel Bar reinforcement model for the computational needs.

(2) Intelligent. Guanglianda software civil engineering can directly identify the two-dimensional flat construction drawings. Guanglianda

steel automatically calculates the length of the reinforcement laps. Therefore, the Guanglianda company series software is more intelligent, the modeling speed is faster, and the modeling efficiency is higher. The calculation results are closer to the actual construction and more scientific and reasonable.

(3) According to the construction process and structural characteristics, build a BIM model that meets the application needs, summarize the modeling method, and meet the fine modeling requirements for subway construction.

5. APPLICATION OF BIM TECHNOLOGY IN PRACTICAL PROJECT MANAGEMENT

(1) Model-Based Drawing Deepening Design

The process of establishing a three-dimensional model is a process of reviewing a drawing. If there are problems, communication with related parties will be carried out before construction to reduce secondary construction, save time, and save costs. Based on the accurate construction of the BIM model at the Dahongmen Bridge Subway Station in Beijing, the three-dimensional visualized dynamic technology was used to provide insights and collision detections to identify deviations and errors in drawings, implement quotas, materials "Figure 2", and cost management for in-depth research and practice. The visualization of 2D drawings through 3D models greatly improves the ability of the relevant personnel to read maps and improve the efficiency of drawing and communication. In the initial modeling process, a total of 112 construction drawing problems were discovered and adjusted through the model in advance. It is expected that the cost of the rework-related rework will increase by nearly 10 million, and the model-based drawing review work will be completed 15 times.

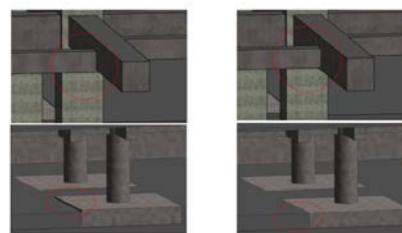


Figure 2 The contrast chart before and after the model rectification

(2) Proof of project demonstration and construction technology based on BIM model

According to the difference in the demand of construction time nodes, the three-dimensional bottom follows from the whole to the local, from the local to the nodes, from coarse to fine, hierarchical, and orderly. Before the start of the construction, the 3D dynamic roaming for the overall structure of the subway station was completed. During the construction process, three-dimensional details were displayed for specific construction details, especially the joints of slabs, beams and columns with complex structure and complex steel bars. With the help of the

three-dimensional technology, the understanding of the drawings by the construction technicians can be deepened, a vivid three-dimensional image can be created, and mistakes can be avoided during the construction process.

(3) Collision detection fine offset drawing error

The essence of collision inspection is to integrate the professional design of Dahongmen Bridge Subway Station in Beijing, that is, to integrate the civil structure, steel structure, water heating pipe, cable tray bridge, elevator installation and other information according to the position and elevation of the design requirements, and then import the model. The BIM software sets collision boundary conditions, performs collision checking, and accurately finds the position and elevation of the axis network where the conflict point is located, that is, obtains its three-dimensional coordinate point. Through collision inspection, drawing problems can be found out in advance and integrated pipeline optimization can be carried out to achieve rational design of the space location of the subway, improve the design clearance height, and avoid rework and missed work due to position collision.

For the collision inspection of large-scale components, such as the conflict between elevator shafts, stairs, and structural beams "Figure 3", it is essentially a low-level error caused by two-dimensional design defects. The irrationality of its spatial position can be directly Look through the Revit model carefully. For specific detailed structural conflicts, downstream BIM software needs to be imported to accurately find and determine the location and to compare the specific information of the drawings with the BIM model.

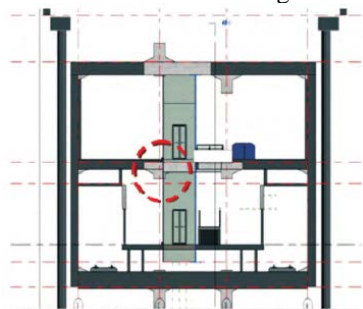


Figure 3 Collision between the elevator shaft and the structure beam of the station hall

(4) 5D Construction Schedule Dynamic Control

The influence factors of construction progress of Dahongmenqiao subway station in Beijing include narrow construction sites, inconvenient urban traffic congestion, poor supply of materials and mechanical equipment. Therefore, the planned progress and actual progress are related to the 3D model in the Guanglida BIM5D (3D entity, time, process) system to realize 5D construction dynamic simulation.

The lagging construction tasks can be analyzed in a timely manner to remind the chief engineer or manager of the project department to make targeted

adjustments to the progress of key construction nodes to ensure the contract duration.

(5) 5D Construction Process Data Management

The implementation of 5D construction process data management using Guanglida Cloud Management Platform refers to the dynamic management of series of construction process data such as technical disclosure, construction plans, test data, quality inspection, and completion acceptance. The basic principle is to follow the occurrence of construction process data. The natural order of the data is associated with the BIM model and uploaded to the cloud platform for storage management so that the decision-making layer can call and view it at any time and at any place. This is equivalent to establishing the historical archives of the construction process of the Dahongmen Bridge subway station in Beijing. BIM technology can realize long-term preservation and inspection, and records the construction process information of subway construction in detail as a basis for inspection, improvement and responsibility traceability.

6. CONCLUSION

The application of BIM technology in the Dahongmenqiao subway station in Beijing is very good. The specific BIM application value includes the following four aspects:

(1) For the current metro design drawings, only the objective conditions of the total amount of main materials such as reinforced concrete, BIM technology can be used to divide the BIM model according to the actual construction section to achieve rapid and accurate extraction of the sub-components of the project, saving the Ministry of Planning and Contract Human resources, improve the work efficiency of engineering statistics;

(2) By collecting construction safety and quality problems on-site, the on-site information can be transmitted to the decision-making level of the project department through the cloud platform at the first time, which is conducive to timely detection and timely solution of problems and guarantees the construction safety and quality of the Dahongmen Bridge Subway Station in Beijing. .

(3) Data sharing and centralized analysis through BIM5D Cloud to achieve on-site construction quality, safety issue tracking management, component tracking management and progress tracking management, leaving records of work, responsibility to people, and communication of work The implementation is smoother and more efficient, the communication time is saved by 20%, the production time of the report material is saved by half an hour, and the work efficiency is increased by 10%. This kind of information and scientific construction management means and tools are used to innovate on-site construction management.

(4) Through the dynamic management of construction data, the historical archives of the construction

process of the Dahongmen Bridge subway station in Beijing are preserved, and the Guanglian Cloud Platform is also provided for the data management in the later operation and maintenance phases.

ACKNOWLEDGMENTS

The authors acknowledge the Social Science Fund Project in Hebei Provincial of China (HB18YJ015)

REFERENCES

- [1]Qiang Meng,Zhiyuan Liu. "Mathematical models and computational algorithms for probit-based asymmetric stochastic user equilibrium problem with elastic demand". *Transportmetrica* 2013(8). pp. 20-23
- [2]Zhong Zhou,Anthony Chen,Shlomo Bekhor. "C-logit stochastic user equilibrium model: formulations and solution algorithm". *Transportmetrica* . 2012 (1) . pp. 49-81
- [3]Qiang Meng,William H. K. Lam,Liu Yang. "General stochastic user equilibrium traffic assignment problem with link capacity constraints". *J. Adv. Transp.* 2008 (4) . pp.30-35
- [4]Shlomo Bekhor,Tomer Toledo. "Investigating path-based solution algorithms to the stochastic user equilibrium problem". *Transportation Research Part B* . 2004 (3) . pp. 27-34
- [5]Francesco Russo,Antonino Vitetta. "An assignment

model with modified Logit, which obviates enumeration and overlapping problems". *Transportation* . 2003 (2) . pp. 51-56

[6]Qiang Meng,Zhiyuan Liu. Mathematical models and computational algorithms for probit-based asymmetric stochastic user equilibrium problem with elastic demand. *Transportmetrica* . 2012 (4) . pp. 62-67

Dongyang Geng, Birthdate:Dec.1982, Mar. 2008-Jan. 2013 studied for doctor's degree in Engineering Mechanics in NEU,Sep.2006-Mar.2008 studied for MS in Rock Engineering in NEU , Research areas include: subway station construction, tunnel settlement and stability analysis. Currently studying for Ph.D. degree at VŠB-Technical University of Ostrava.

Karel Vojtasik, Associate Professor, Engineer, CSc. (Ph.D.), 1999 Habilitation in the field of "Mining geotechnics and underground construction"Main research areas: Geotechnical engineering, Geotechnical construction and structures, Underground construction and structures, Soil and rock improvement engineering, Environmental geotechnical engineering

Training Course Times Optimization Method based on SVR-GA

MA Zhi-xin^{1*}, LU Xing-hua², Song Xing¹, MA Quanyue¹

¹Army Engineering University Shijiazhuang campus Equipment Command and Management Department, Hebei Shijiazhuang, 050003

²Army Engineering University Shijiazhuang campus Teaching evaluation center, Hebei Shijiazhuang, 050003

*E-mail: 907229834@qq.com

Abstract: The basic methods of teaching and training course design was studied in the paper, and the specific ideas for the course optimization was put forward. It is difficult to quantitatively describe the ability training and curriculum design in the actual work, and for the absence of the necessary tools for curriculum optimization, a SVR-GA-based curriculum times optimization method was proposed. The AHP analysis of the flight students' ability evaluation in the past three years and the SVR regression prediction model was used, then simulation and calculation was carried out by MATLAB, which can provide technical reference and research direction for teaching training reform.

Keywords: support vector machine for regression; genetic algorithm; Course optimization

1. INTRODUCTION

The ability of pilots determines the combat effectiveness of future aviation operations. The pilots are the reserve force of aviation operations. The resources of training pilots are scarce and the cost is high. There is an urgent need for front-line flight personnel. Therefore, it is of great significance to study the law of ability generation of pilots and the quality and efficiency of training.

The training of flight cadets is a complex process, and the training content and training volume are the key factors to determine the ability of flight cadets. The difference between the training course and times will have a direct impact on the training effect of the flying cadets. One of the important contents of studying the training law of the flying cadets is how to set up the flying training course so as to turn the problem into optimizing the training times of the flying cadets. Traditionally, experience-based flight training syllabus settings are suitable for the improvement or replacement of mature aircraft training syllabus. However, there is no effective

guidance for new training content and new aircraft types. The training times and sorties are usually increased so that the trainees can get adequate adaptation time and air traffic. To ensure flight safety, the training cycle will inevitably be extended. Due to the lack of quantitative prediction of the training effect, it is difficult to form a scientific guidance for the formulation of personnel training programs.

At present, the research mainly concentrates on the military and civil aviation fields. The research focuses on the construction of flight ability system, teaching system and flight training mode. To some extent, the training process of pilots is explored[1-8]. However, quantitative research on the relationship between flight ability and training subjects, and capacity building process is very limited.

Flight training management is aimed at the available resources and students' learning basis, and following the law of students' ability growth, to develop an effective training plan. The influence of teaching and training courses and times on the training effect of flying cadets can be obtained by evaluating the comprehensive ability of flying cadets at different stages. The training courses and times in the existing training data are taken as input and the comprehensive ability of flying cadets as output. That is to say, the internal relationship can be modeled and analyzed, and the mapping model of training content and flight capability can be constructed. On the basis of this model, exhaustive method is used to find out the optimal combination of curriculum design when the target ability is reached, so as to provide quantitative auxiliary method for curriculum design. In this paper, regression support vector machine (SVR) method is used to construct the quantitative model of content-flight capability, and then genetic algorithm (GA) is used to realize the optimization process. The basic idea is shown in Figure 1.

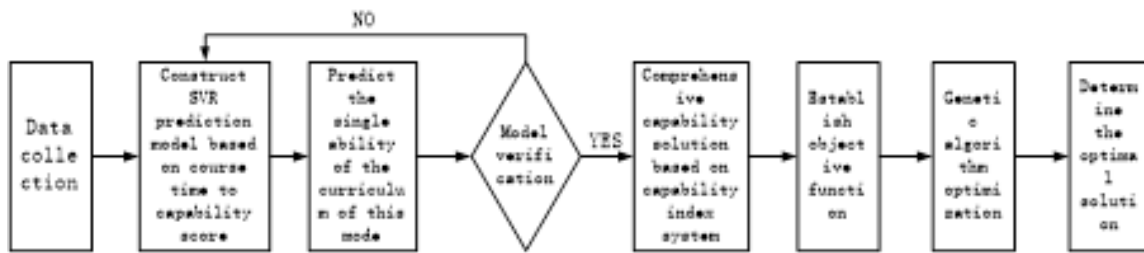


Figure 1 The basic idea of optimizing curriculum hours In the article of "Simulation Research on Predicting the Training Effect of Flight Cadets Based on SVR", the author constructs the prediction model of flying Cadet's ability and realizes the mapping between ability and course. On this basis, genetic algorithm was used to optimize the course schedule, which provides verification method for scientific training scheme of design personnel.

2. TRAINING CONTENT TIMES SETTING PROCESS

The process of training follows the principle of "from easy to difficult, from simple to complex, take first and then single". The mode is basically fixed. The effect of training courses on training effect is mainly reflected in the different times combination of courses on the training efficiency of students. The combination of different training courses and the adjustment of times will lead to the difference of training effect. For example, the result of 50 visual flight courses, 20 visual flight training will be different from instrument flight training, formation flight training and navigation flight training. There are great differences in the quality of training, so the influence of training courses on the training of flying cadets will be translated into the mapping relationship between the students' ability score and the combination of class hours.

The process of determining the training outline is a dynamic adjustment process. For the newly added training tasks, due to lack of experience guidance, we can only draw lessons from the similar training contents for analogical training. While determining the prefabricated training outline, we should predict the training effect of the outline, which can be used to evaluate the training effect of the trainees in the future. The training process evaluates the training results of the trainees at various stages, evaluates the training effect with the progress of the courses, judges whether the training meets the expectations, updates the reference data at any time, constantly revises the training content, and optimizes the curriculum. After completing the class training, the reference data are updated again to further optimize the curriculum until the final outline is determined. The setup process is shown in Figure 2.

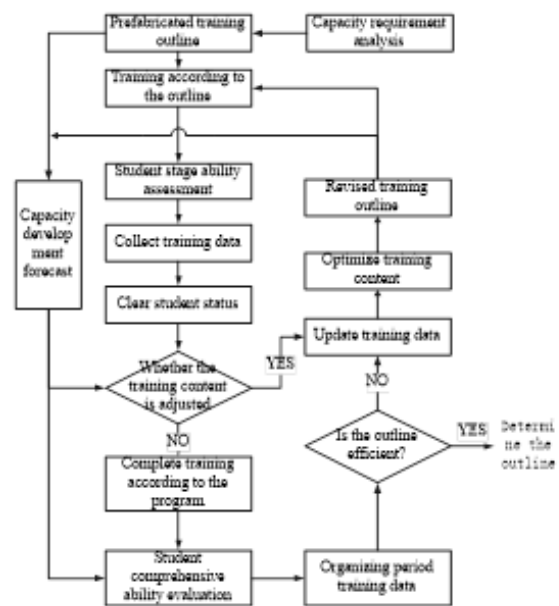


Figure 2 Teaching training course times optimization process

3. TRAINING COURSE OPTIMIZATION DESIGN METHOD BASED ON SVR-GA

Support Vector Machine (SVM) is proposed by mathematician Vladimir N. Vapnik and others through more than 30 years of rigorous mathematical theory research. This method has been paid attention by international data mining academia and has been successfully applied in speech recognition, character recognition, drug design, combinatorial chemistry, times series prediction and other research fields. Different from the classification idea, when SVM is applied to regression fitting analysis, it is no longer simply to find an optimal classification surface for sample classification, but to find an optimal classification is to minimize the error of all samples from the optimal classification surface. This method is called regression support vector machine. It has good results on predicting small samples.

The principle of genetic algorithm originates from the inspiration of genetic mechanism and natural selection in Darwin's principle of biological evolution. It is a global search algorithm which iterates repeatedly by setting the initial population. The basic idea is to express the problem variables to be solved as "chromosomes" and to simulate a set of variables as a set of chromosomes. Several different

"chromosome" variables are put into the problem of constraints, and the fitness is used to express the solution. According to the evolutionary principle of survival of the fittest, the "chromosome" with higher fitness is selected for replication, and then a new generation of "chromosome" is produced by crossover and mutation. This generation of "chromosomes" has higher fitness; so repeated cycles, after several iterations, eventually converge to a maximum fitness of the individual or solution, the corresponding solution is the optimal solution [7-8]. In this paper, SVM is used to build the curriculum-capability model, and exhaustive method is used to optimize the 1-100 hours of the curriculum. The optimization process is solved with the aid of genetic algorithm. The process is shown in Figure 3.

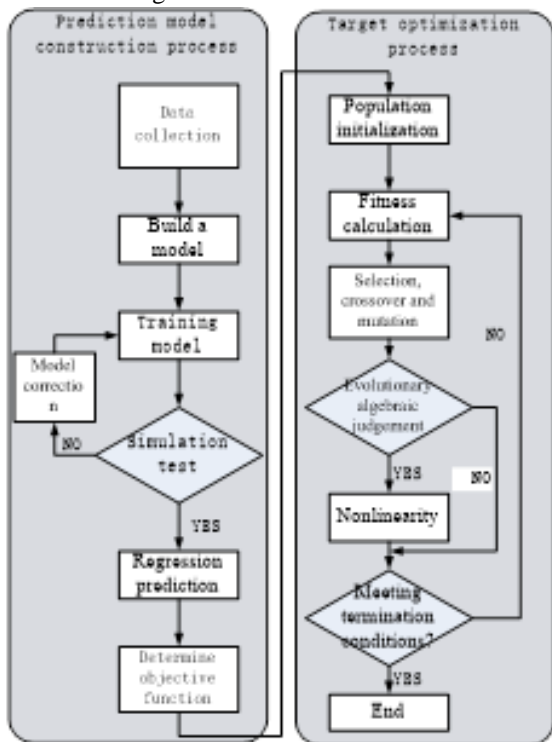


Figure 3 Training course optimization design process based on SVR—GA

(1) SVR regression function construction

The form of SVR regression function is similar to that of neural network. The output of intermediate nodes can be obtained by linear combination. Each intermediate node corresponds to a test vector. Its basic structure is shown in Figure 4.

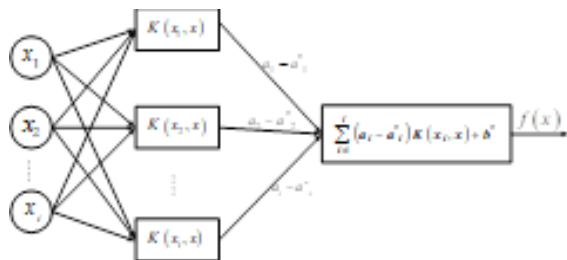


Figure 4 Basic structure of SVM regression prediction

A training set sample pair of l training sample is $\{(x_i, y_i), i=1, 2, \dots, l\}$, of which $x_i (x_i \in R^d)$ is the input column vector of the i training sample, $x_i = [x_i^1, x_i^2, \dots, x_i^d]^T$, x is the training course set in

the flight Cadet ability prediction model, $y_i \in R$ is the corresponding output, that is, the ability evaluation score reflecting the training effect of the flight cadet. Let x and y correspond to the corresponding functions in the high-dimensional feature space.

$$f(x) = w\phi(x) + b \tag{1}$$

The following regression functions can be obtained from the support vector machine process. The reasoning process is described in detail in the "Simulation Research on Training Effect Prediction of Flight Cadets Based on SVR" and will not be repeated here.

$$\begin{aligned} f(x) &= w^* \phi(x) + b^* \\ &= \sum_{i=1}^l (a_i - a_i^*) \phi(x_i) \phi(x) + b^* \\ &= \sum_{i=1}^l (a_i - a_i^*) K(x_i, x) + b^* \end{aligned} \tag{2}$$

Among them, $K(x_i, x_j)$ is kernel function, $a_i = [a_1, a_2, \dots, a_l]$ and $a_i^* = [a_1^*, a_2^*, \dots, a_l^*]$ is the optimal solution of Lagrange operator in the calculation process.

(2) Genetic algorithm optimization process

Competence-oriented curriculum optimization is a multi-objective optimization problem. The objective function is contradictory to each other, which requires the least curriculum and the highest ability. Therefore, the solution is either non-inferior or satisfactory. Among them, the objective function is determined as follows:

$$\begin{cases} \min \sum x_{i,1}/Y, 1/C_{ij} \\ C_{ij} = f_i(x) \\ Y = \sum w_{ij} C_{ij}, x_i \in [1, 100] \\ 5 \geq Y \geq 4.5 \\ 5 \geq C_{ij} \geq 4 \end{cases} \tag{3}$$

It can be seen that this problem solves a multi-objective optimization problem with the largest capacity and the shortest class hour on the basis of satisfying the constraints. Since the class hours are all integer, the original problem is transformed into an integer programming problem. The basic process of using genetic algorithm to solve this problem is as follows:

Step1: population initialization process

In this paper, real coding is used, so the numerical transformation process can be cancelled and the algorithm can be operated directly on the phenotype of the solution. The real vector corresponding to the SVR model is calculated as a chromosome.

Step2: Determination of fitness function

Fitness function is the basic basis for selection, which is used to reflect the results of individual evaluation in the group. In this paper, we want to minimize the objective function, so we take the reciprocal of the objective function. Thus, the smaller the function value is, the larger the fitness value can be, and the closer the corresponding individual is to the optimal value.

Step3: selection, crossover and mutation process

Selection process refers to a probability from the original population to select a better individual into a new group, as the reproduction of the next generation of individual population, this probability depends on fitness, fitness value of the higher probability of being selected. The crossover process is to pass on the excellent characteristics of the original chromosome to the next generation by two selected real-valued vectors, i.e. chromosome exchange combinations, so as to obtain better individuals. The process of variation refers to the variation of an individual's chromosome. After variation, the individual's fitness is higher, and the process of variation ensures the diversity of the population.

Step4: optimization process

Repeated iteration loop step 3, after several iterations, the result will converge to an optimal individual, at this time the corresponding fitness is the highest, that is, the optimal solution of the problem. The core code is as Figure 5:

```
warning off;
delete('*.mat');
global dataCourse dataAbility weight;
dataCourseRaw = xlsread('x.xls','Course');
dataCourse = dataCourseRaw';
dataAbilityRaw = xlsread('x.xls','Ability score');
dataAbility = dataAbilityRaw(1:16,2:end)';
weight = dataAbilityRaw(1:16,1);
for i=1:16
    trainSingleAbility(i);
end
lb = ones(20,1);
ub = ones(20,1)*100;
rng default;
options = optimoptions('ga','MaxGenerations',250,'PlotFcn',@gaplotbestf);
[x,fval] = ga(@MyCost,20,[],[],[],[],lb,ub,[],1:20,options);
strLog = sprintf('best value: %f, 1/fval):
disp(strLog);
for i=1:20
    strTemp = sprintf('the%d course set %d time',i,x(i));
    disp(strTemp);
end
abilitySet = getIndividualAbility(x);
for i=1:16
    strTemp = sprintf('the %d ability score:%f',i,abilitySet(i));
    disp(strTemp);
end
```

Figure 4 optimization core code of MATLAB
4 EXAMPLE ANALYSIS

The data acquisition process is based on the training of the students in the three classes of a certain unit. Due to the curriculum reform and the adjustment of the syllabus, there are some differences in the teaching and training contents of the three classes, which provides favorable conditions for the research. Taking 10 pilots from each of the three classes as samples, the instructors, commanders and teaching experts were invited to evaluate the abilities of the pilots in the flight preparation stage, the solo flight stage, the mid-training stage and the final examination stage, respectively. The five-point system was adopted to evaluate the abilities of the pilots, so as to obtain the values of the course combination and the ability evaluation. This form is shown in Table 1. The simulation data are simulated in this paper

Table1 Curriculum and capability scoring sample table

project \ Num		1	2	3	4	5	6	7	...	113
		Cur 1	50	30	30	35	35	35	40	...
curriculum
	Cur 20	45	30	30	45	45	45	45	...	30
ability score	C ₂₁	3.3	2.9	4.2	4.4	4.8	2.9	3.7	...	3.5

	C ₃₆	2.9	4.2	4.4	4.8	2.9	3.7	4.7	...	4

In this paper, we use the genetic algorithm of optimoptions optimization algorithm toolbox in Matlab2017 to solve. The ability assessment of different stages is normalized, and different combinations of 20 subjects involved in practical operation are used as input. Each combination corresponds to a set of ability scores. Taking the reciprocal of the objective function as the fitness function, the MATLAB operation is carried out, and 200 iterations are carried out to get the result as shown in Figure 6.

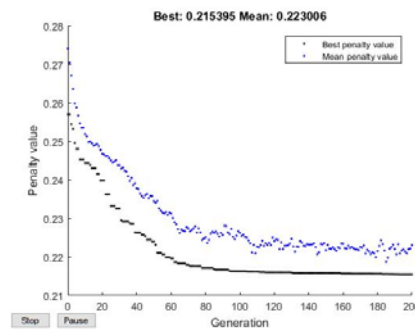


Figure 6 Optimization results

The result of the optimization of course hours is [40 44 28 60 40 20 24 40 44 29 59 41 21 25 59 40 21 24 40 43], Under this kind of curriculum combination mode, the average ability value is 4.642641, which is more than 4.5. Therefore, the result meets the requirements of constraint conditions and is a satisfactory solution to the problem.

5 CONCLUSION

Optimal design of flight Cadet curriculum is the basic work of personnel training, which is helpful to the follow-up implementation of teaching and training reform and training system optimization. Because the training data of flight cadets are relatively limited, it is difficult and times-consuming to obtain available samples, the ability foundation of trainees varies greatly, and the individual uncertainty is great, so the number of available samples is small, and the accuracy of general prediction methods is low. Support Vector Machine (SVM) method has good adaptability for nonlinear and small sample problems. Genetic algorithm has a good convergence in realizing multi-objective integer programming, which is to calculate the fitness of all solutions in the whole search space, and is beneficial to avoid the optimization result of local optimal solution.

The training of flight cadets is affected by the airport environment, training equipment, training equipment, flight instructors, training cycles and so on, and these factors are constantly changing. It is difficult to make a constant training plan to implement flight teaching, and some training resources are difficult to provide the training needed to optimize the results. Therefore, the method introduced in this paper is usually only

used as a course aided design method, the optimization results need to be adjusted according to the actual situation, to provide a reference for teaching and training managers.

REFERENCE

- [1]Su Hengshan, Wang Kangping, Xue Yong. Preliminary study on competency model of flying personnel. Air Force Military Academy. 2012(02)
- [2]Pan Bangchuan, Song Zhiyong. Research on optimization model of pilots' simulator training plan. Chinese Management Science. 2008(02)
- [3]Liu Wenbin, Zhang Shouzhi, Shi Bole. Solution of scheduling problem for pilot simulator based on GA. Computer Engineering. 2011(15)
- [4]Gao Mingang, Chang Houdong, Zhang Jianjun. Strategic planning of civil aviation pilots' human resources. Science and technology for development. 2012(03)
- [5]Gao Minggang, Chi Hong, Shao Xueyan. Analysis of pilots upgrading cycle. Operations research and management science. 2012(06)
- [6]Wang Dingcheng. Support vector machine modeling, prediction and control. Beijing: Meteorological Press. 2009.12
- [7]Yu Lei. 30 case studies of MATLAB intelligent algorithm (Second Edition). Beijing: Beijing University of Aeronautics and Astronautics Press.2015.09
- [8]Liu Haiyan, Yu Shixin. Logistics Vehicle Delivery Management Based on Genetic Algorithm. Electronic design engineering. 2017(01)

Cloud Computing Based Remote Monitoring System for Mining Equipment

Pengyu Lei, Qingli Ou, Wenhui Luo

Hunan University of Science and Technology, School of Information

Abstract: As a new Internet technology, cloud technology greatly brings convenience to People's Daily life. This system is a remote monitoring system for mining equipment developed on the basis of cloud computing. The system itself is a monitoring system constructed by a variety of sensors, data chips, total control chips, cloud server, and through the multi-level communication layer composed of ether network, CAN bus and GPRS. The monitoring system adopts the form/server architecture of cloud computing and USES the core algorithm of AES data encryption to improve data privacy and security, which greatly strengthens the application in security engineering. Based on TCP/IP protocol, two-way communication and multi-channel communication with monitoring nodes are realized, and online adjustment and optimization of data are supported while obtaining sensor data, so as to achieve the purpose of continuous monitoring. By setting up the thread pool, the data of sensor can be acquired and displayed to the user's client port in real time through asynchronous communication, and the monitoring and sensor data can be synchronized completely. Special comprehensive monitoring support is provided for matrix type data widely used in cloud computing. The three software systems, the cloud software as the main control system, the encryption system as the software copyright, and the mobile APP system constitute a comprehensive monitoring system. The real-time monitoring platform of multiple dimensions and multiple nodes makes the system more perfect. Finally, dc motor as a controlled object, adopts the speed sensor and ultrasonic ranging sensor as the monitoring data and the simulation data, by means of monitoring system software forms, dynamic simulation based on ali cloud platform and the actual experiment of local cloud platform, to prove the feasibility and practicability of the proposed cloud monitoring system, promote and perfect the supervisory system combined with cloud computing in practical application.

Keywords: Cloud computing; Mining equipment; Remote monitoring; Software encryption

1. INTRODUCTION

With the rapid development of Internet technology and computer technology, our daily life is becoming more and more convenient. In the industry, cloud technology is irreplaceable to become a newcomer in

the industry. How it will calculate, store, extract and other resources from the terminal to the cloud, forming a huge virtual processor. As an important part of cloud computing, cloud computing is a collection of services such as network analysis, system management, data storage and complex computing. In industries, services, smart agriculture and other industries have been actively applied.

In the monitoring system, the advantages of cloud computing in many aspects. The perfect cost investment greatly reduces the overall cost of the system. Excellent computing resources greatly expand the system function, and good versatility and scalability can pave the way for industrial production. As a solution, the impact of cloud computing on monitoring systems is not only high-tech content, but also targeted and perfect at the data level and even at the functional level. For example, the various restrictions of data in the ordinary storage mode, cloud computing does not require the owner to specifically purchase large-capacity storage devices, saving a lot of money. There is no need to consider the preservation and maintenance of data, and all data can be backed up. Functionally, cloud computing greatly reduces the threshold for data processing, allowing ordinary users to professionally compare, classify, and clean data. Undoubtedly a perfect solution. And these potentials for cloud technology are just the tip of the iceberg.

Of course, there are still many imperfections in the development of cloud technology. It should be noted that there are still many problems with cloud computing. The main problem for the monitoring system is the delay in the network transmission process, the data transmission performance of the data network out of order and packet loss. In response to these problems, the solution focuses on the use of data-based predictive control algorithms to solve the network-induced delay, and the time period, throughput and task completion time of the parallel processing system are used as performance indicators. The algebraic method is used to analyze and optimize the cloud. Control system parallel processing capabilities and other methods.

In practical engineering applications, the application of cloud monitoring system is relatively rare, and the key factor limiting its development is: from the perspective of data types, to solve the data delay, disorder and loss in the cloud monitoring system.

Packet problem, the above control strategy introduces the concept of state space, making vector or matrix type data become the main body of calculation and transmission. Comprehensive monitoring and control system operation data is essential for control system analysis and control strategy design. Existing cloud monitoring systems designed to monitor scalar data cannot be applied to cloud monitoring systems, thus failing to meet the engineering needs of cloud control systems; In terms of platform selection, the existing support cloud monitoring system needs to be developed for the cloud platform service provider, which has platform limitations and complicated operations. As an important part of the monitoring system, the display controls used in traditional monitoring systems and common cloud monitoring systems usually come from individuals or small businesses. Their functions are simple, maintenance and update capabilities are limited, and stability cannot be guaranteed. Moreover, it does not have the function of monitoring interface customization and online modification of control system parameters.

Compared with the existing monitoring system projects, the cloud monitoring system designed and implemented in this paper has the following

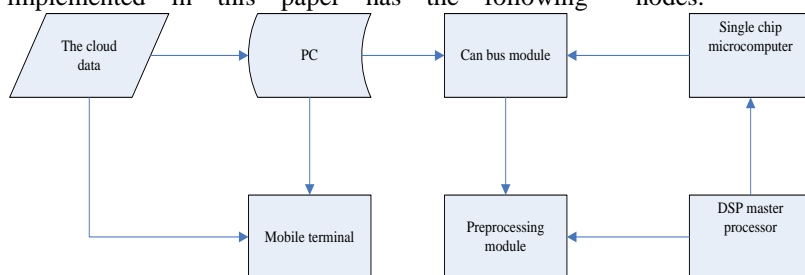


Figure 1

3. MAIN CONTROL ENCRYPTION CHIP

This design uses TMS320VC5402DSP chip, TMS320VC5402 is a fixed-point digital signal processor introduced by Texas Instruments, with the unique high performance, low power consumption and low price characteristics of TMS320VC54X series. Data can be collected, audio and other data can be encrypted, uploaded, or decrypted by downloading data from the cloud, thus avoiding the possibility of leaking in the cloud.

The structure characteristics of TMS320VC5402DSP chip are as follows;

a) Improved Harvard bus architecture with high performance, with three independent 16-bit data

characteristics:

1) It can obtain real-time information in the cloud monitoring system through the network, and realize the data display query based on the cloud network;

2) Support Alibaba Cloud and Baidu Cloud common cloud platform, the cloud environment is more liberal and free;

3) Have a self-developed encryption type encryption system, the file is more secure and more secret;

4) Adopt BBC form sensor communication scheme, the function can be Expansion, more suitable for monitoring in various environments;

5) Allow users to customize the monitoring system and support the modification of related parameters. More practical;

2. CLOUD MONITORING SYSTEM HARDWARE DESIGN

In the monitoring system of this cloud technology, in order to better enhance the reliability and stability of the system, the monitoring system uses a relatively reliable DSP as the main processor, and another SK3 MCU is used as the main chip of the encryption system and the cloud node processing system. Industrial-grade sensors are used as cloud monitoring nodes.

storage buses and one The Bit program stores the bus.

b) Has a 40bit arithmetic logic unit, including a barrel shifter and two independent algorithm.

c) Comparison, selection and storage unit with professional VITERBI butterfly algorithm.

d) The exponent decoder can find an index value of 40M accumulated number in one instruction cycle, where the index is defined as the number of bits in the accumulator that are not occupied by data minus 8.

e) Two address generators, eight auxiliary registers, and two auxiliary register arithmetic units.

Single-cycle fixed-point instruction execution time is 10ns.

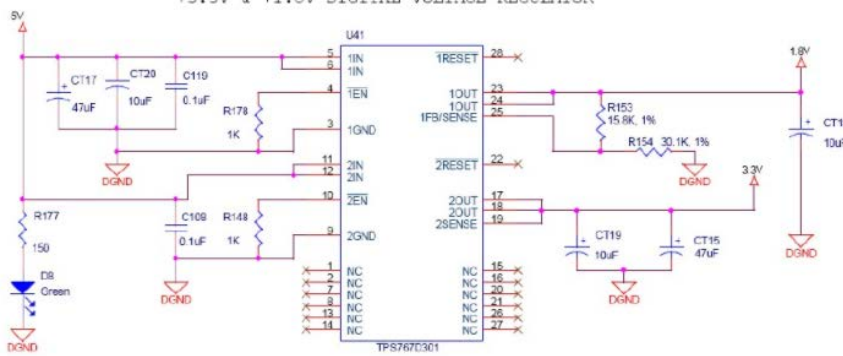


Figure 2 Power supply circuit

4. MCU SENSOR DATA RECEIVING CHIP

The monitoring system needs a chip as the main chip, and processes the system integrated data, such as encryption, packing data, decrypting data, etc., and also needs several data chips to connect the sensors, corresponding to the CAN bus module, and performs internal data processing and transmission.

From the perspective of power consumption and economy, this MCU selects a chip of AT89C51, which is a low voltage, high performance microprocessor with 4K bytes of flash memory. The following standard features are available: 4k Byte Flash Memory, 128 Byte Internal RAM, 32 I/O Line Lines,

Two 16-Bit Timer/Counters, One 5-Vector Two-Level Interrupt Structure, One Full-Duplex Serial Communication Port, on-chip oscillator and clock circuit. At the same time, the AT89C51 can be reduced to 0Hz static logic operation and supports two software-selectable power-saving modes. The idle mode stops the CPU, but allows RAM, timer/counter, serial communication port and interrupt system to continue to work. The power-down mode saves the contents of the RAM, but the oscillator stops working and all other components are disabled until the next hardware reset.

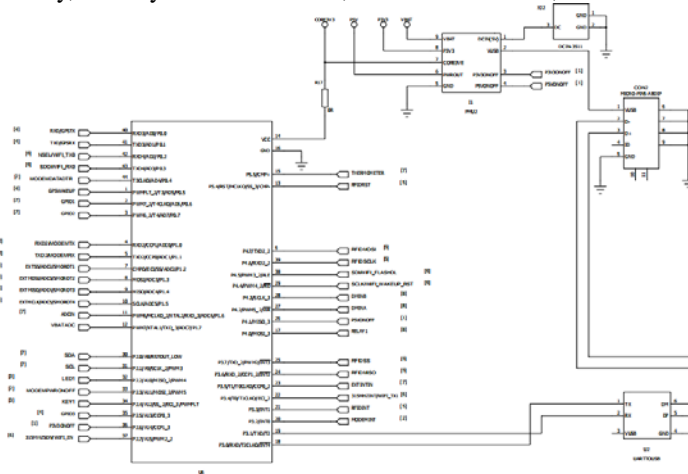


Figure 3 Main circuit diagram

5. SENSOR AND PERIPHERAL RECEIVING CIRCUIT

This monitoring defines video acquisition, vehicle speed acquisition, vehicle status acquisition, etc. It requires the acquisition of data such as camera, electromagnetic sensor (speed), hydraulic sensor, etc., so a single MCU is separately set to accept the control sensor data (for the convenience of experiment, Only ultrasonic ranging data is taken as an example).



Figure 4 Ultrasonic velocity sensor

(1)Introduction to ultrasonic distance measuring sensor

The HC-SR04 ultrasonic ranging module provides 2CM-400CM non-contact distance sensing function with a range accuracy of 3mm. The module includes an ultrasonic transmitter, receiver and control circuit. Its working principle: using IO port TRGI trigger test, give at least 10us high level signal; module automatically sends 8 40KHz square wave, automatically detect whether there is signal return; there is signal return, output high power through IO port ECHO Flat, high level duration is the time from the launch to the return of the ultrasonic wave. Test distance = (high time * sound speed (340M / S)) / 2;

(2) Ultrasonic distance measuring sensor works The ultrasonic timing diagram is as follows:

Initialize the trig and echo ports are set low, first send a high-level pulse of at least 10 us to the trig (the module automatically sends out 8 40K square waves), then wait, capture the rising edge of the echo output, capture at the same time as the rising edge, the timer is started to start counting, and again waiting to capture the falling edge of echo. When the falling edge is captured, the time of the timer is read. This is the time when the ultrasonic wave runs in the air. According to the test distance = (high level Time*

Sound speed (340M/S))/2 It is possible to calculate the distance from the ultrasonic wave to the obstacle.

6. PERIPHERAL CIRCUIT

The peripheral circuit of the monitoring system includes a control circuit, a clock circuit, a reset circuit, a power supply circuit, an output drive circuit, an AD conversion circuit and the like.

Because the work done in this thesis is mainly based on software, only a brief introduction is made.

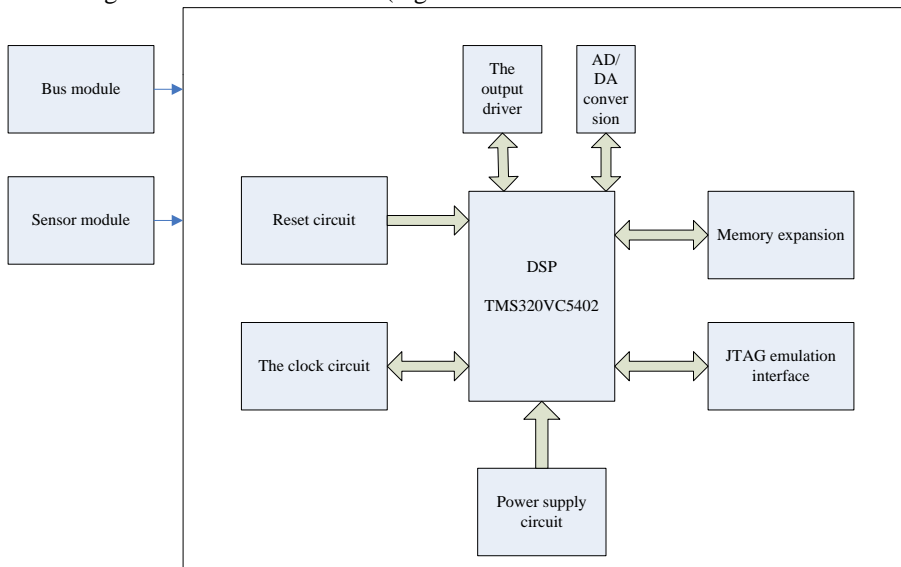


Figure 5 Peripheral circuit module

Main demand points of main control chip:

- a) it has a double-circuit output voltage which can be separately powered, with a fixed output voltage of 3.3v for one way, and a voltage of 1.3v for another way.
- b) the voltage of each circuit shall be maintained within the range of zero to 1A.
- c) there is an open leakage reset output for each line regulator, and the reset delay time is 200MS.
- d) there is a tolerance of 2% when the load and temperature are exceeded.

Power circuit

The TMS320VC5402DSP chip USES a dual power supply design to achieve better performance, with operating voltages of 3.3v and 1.8v. Among them, 1.8v mainly provides voltage for internal logic. It also includes the CPU and all external logic. The external interface pin is still powered by 3.3v, which is convenient for external interface equipment. The power supply system is designed by selecting a dual-channel output voltage TP767D318 chip.

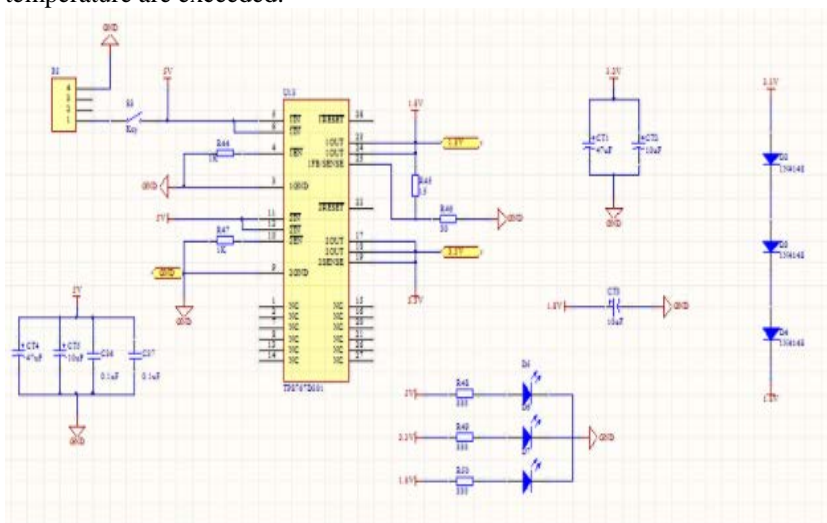


Figure 6 TMS320VC5402DSP chip power circuit diagram

Reset circuit

The reset circuit is essential to the control system, the common guard dog reset, manual reset, and on - power reset. The system adopts the first two reset modes.

Clock circuit

The clock circuit is used to provide clock signal for TMS320VC5402DSP chip, which is composed of an internal oscillator and a phase-locked loop.

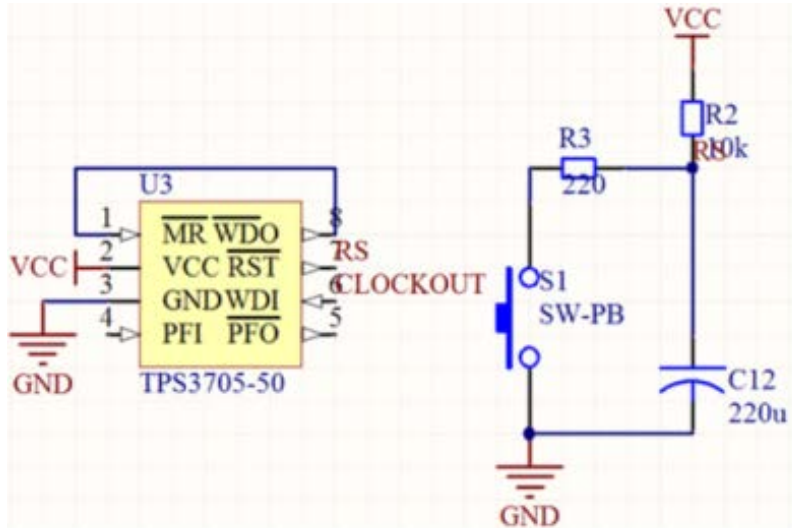


Figure 7 TMS320VC5402DSP chip reset circuit circuit diagram

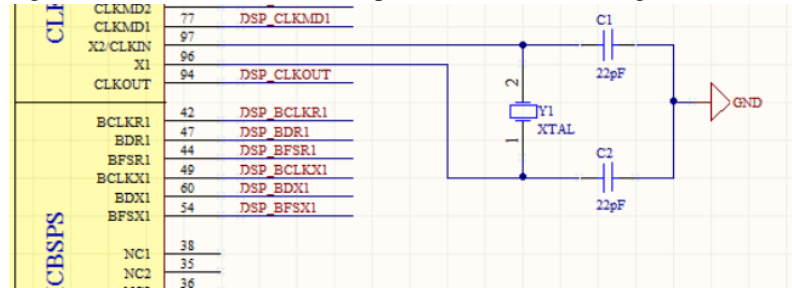


Figure 8 TMS320VC5402DSP chip clock circuit circuit diagram

7. Encryption Algorithm

It is well known that in the cloud service, the structural security of data is crucial, and the DSP data encryption software used in the monitoring system of the cloud technology equipment ensures that the data of the client is not compromised, and even if the breach is not cracked. The hardware part of the encryption system scheme is composed of USB module, DSP module and power module. The software part adopts the new data encryption standard AES. The encryption system realizes the functions of data encryption and data decryption, which greatly improves the security of data.

Process of encryption algorithm

The encryption algorithm needs to meet the following three requirements: 1) resist all known attacks. 2) fast and compact coding on multiple platforms. 3) simple design.

The AES encryption process operates on a 4-by-4 Byte matrix, also known as "state," whose initial value is a plain-text block (the size of an element in the matrix is a Byte in the plain-text block). During encryption, each round of AES encryption cycle (except the last round) contains 4 steps:

a) AddRoundKey -- each byte in the matrix is XOR

operation with the round key; Each sub-key is generated by the key generation scheme.
 b) SubBytes - replace each byte with its corresponding byte by using the non-linear substitution function in the lookup table.
 c) ShiftRows - shifts each row in the matrix in a circular fashion.
 d) MixColumns - to fully mix the operations of each straight line in the matrix. This step USES linear transformations to mix the four bytes in each column. Omit the MixColumns step in the last encryption loop and replace it with another AddRoundKey.

Software design of monitoring system

The data architecture adopted in this monitoring system is divided into client and server, in which the upper computer of the monitoring system is client, including the main control chip, peripheral chip, peripheral sensor and communication module. The cloud depends on the cloud server. The communication channel between them is established through the network, which realizes the network - based remote monitoring.

The software composition of the monitoring system is divided into three modules: the encryption software based on VS platform, the main PC terminal system

based on BBC platform, and the mobile phone client based on Android.

Design and implementation of encryption control

The encryption control is a very important part of the monitoring system, which allows users to encrypt and decrypt the device, thus protecting the privacy of the

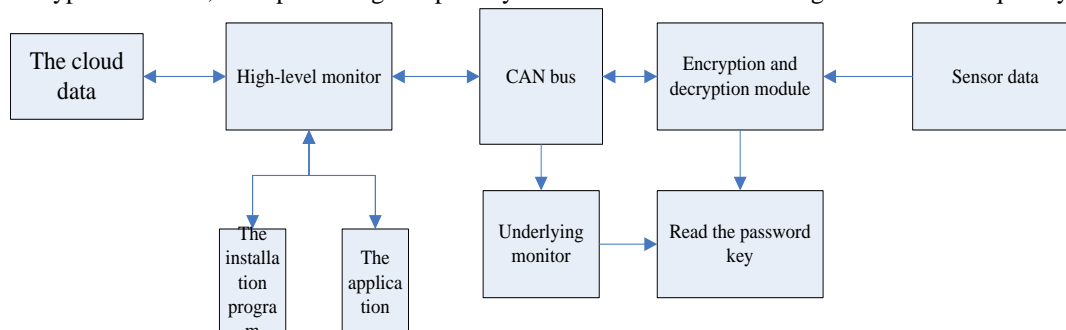


Figure 9 Block diagram of encryption software design

The creation of graphical software through VS is mainly built through various graphical controls and C++ based code, and the way of setting controls is as simple as possible.

The first thing you need to do is create a data type library, whose primary data is based on SQL native libraries, in order to implement mouse-to-mouse

For the custom operation of the meter control, you need to write a mouse-to-control response event, such as overwriting the MOUSEDOWN () event for the mouse trigger as a wrisort () event, and then establishing an enumerated type data to represent the different state of the mouse. The specific behavior represented by different states is described in a MOUSEPOINT() method. When set, the control automatically calls the SetValue() method to save the new property value.

PC terminal monitoring system software

The BBC software released through the BBC platform is an open and free instant messaging software developed by warmont information technology co., LTD., which can realize instant messaging between smart devices such as PC mobile phones and SK3 non-smart suite. It can be divided into PC and mobile versions. Based on the BBC communication mechanism, users can realize the two-way point-to-point communication between SK3 and mobile phone or PC or other SK3 without setting up a server. Users can modify the graphics interface and LOGO open to BBC software at will to complete the product development quickly, which greatly reduces the workload of the developers. The BBC is equipped with error correction and encryption algorithm to ensure the security and reliability of the product. Point-to-point communication is based on the BB number, which can be applied to obtain on mobile or PC software.

Software functional system

1. General account can be registered
2. Text data can be sent and received
3. Can send and receive sensor data, and view the

whole monitoring system. This software application scenario is mainly each monitoring room, so it is developed based on window, more adaptive and universal. The graphics software written by VS platform is simple, clear and fully functional, which enables users to get started more quickly.

received sensor data in the client

4. Configure the working status of the sensor
5. Configure sensor work status parameters (starting and ending time, sensor type, working days per week, working days, data times, etc.)
6. Query the working status of the sensor
7. Change password
8. Add and delete devices (all kinds of sensors, working equipment, etc., each of which has its own unique device number, supporting batch view and data capture)

CONCLUSION

Cloud cloud nodes distributed in the control system, the author of this paper, the types of matrix data are widely used, make the system running state observation of the problem was designed and implemented a cloud monitoring system. This paper expounds the system of client/server structure, based on the function of the remote real-time monitoring network cloud node data, support matrix type data elements to monitor all of the characteristics, the integrated NI controls the advantages of stable performance and feature rich, dynamic custom monitoring interface allows the user to convenience, support the necessity of adjusting parameters, online store extensibility of monitoring data and the relevant part of the specific implementation details. Based on the Internet cloud of electricity The feasibility and practicability of the system are verified by the computer control dynamic simulation and the LAN cloud motor control experiment. This paper not only provides a solution for the development of the monitoring system, but also promotes and improves the practical application of the combination of the control system and cloud computing.

REFERENCES

- [1] L. Qian, Z. Luo, Y. Du, et al. Cloud computing: An overview[C]. Proc of the IEEE International Conference on Cloud Computing. Berlin: Springer, 2009: 626-631.

- [2] K. Chen, W. M. Zheng. Cloud Computing: System Instances and Current Research. *Journal of Software*, 2009, 20(5): 1337-1348.
- [3] M. Armbrust, A. Fox, R. Griffith, et al. A view of cloud computing. *Communications of the ACM*, 2010, 53(4):50-58.
- [4] G. Aceto, A. Botta, W. De Donato, et al. Cloud monitoring: A survey. *Computer Networks*, 2013, 57(9): 2093-2115
- [5] A. M. Fahad, A. A. Ahmed, M. N. M. Kahar The importance of monitoring cloud computing: An intensive review[C]. Proc of the TENCON 2017-2017 IEEE Region 10 Conference. Penang: IEEE, 2017: 2858-2863.
- [6] S. Abrahão, E. Insfran. Models@ runtime for Monitoring Cloud Services in Google App Engine[C]. Proc of the 2017 IEEE World Congress on Services. Honolulu: IEEE, 2017: 30-35.
- [7] F. Rossignaux, L. Lefevre, J. P. Gelas, et al. A generic and extensible framework for monitoring energy consumption of OpenStack clouds[C]. Proc of the 2014 IEEE Fourth International Conference on Big Data and Cloud Computing. Sydney: IEEE, 2014: 696-702.
- [8] J. Wang, Y. Zhang. Monitoring System of Machine Tools Based on the In Touch[C]. Proc of the 2013 International Conference on Mechanical and Automation Engineering. Jiujiang: IEEE, 2013: 70-72.
- [9] X. Yangang, W. Han, L. Xingqi, et al. Monitor system design for machine electric spindle based on MCGS[C]. Proc of the 2010 WASE International Conference on Information Engineering. Beidaihe: IEEE, 2010, 3: 248-252.
- [10] Z. Xiao, Y. Xiao. Security and privacy in cloud computing. *IEEE Communications Surveys and Tutorials*, 2013, 15(2): 843-859.
- [11] Y. Q. Xia, Y. M. Qin, D. H. Zhai, S. C. Chai. Further results on cloud control systems. *Science China(Information Sciences)*, 2016, 59(07): 232-236.
- [12] S. Subashini, V. Kavitha. A survey on security issues in service delivery models of cloud computing. *Journal of Network & Computer Applications*, 2011, 34(1): 1-11.

Evaluation of Service Capacity of China's Membrane Separation Industry Cluster based on ANP Theory

Qiongqiong Wei^{1,*}, Gongli Luo²

^{1,*} Academy of Economics and Management, Qingdao University of Science and Technology, Qingdao, China;

Email: wqq@qust.edu.cn

² Academy of Economics and Management, Qingdao University of Science and Technology, Qingdao, China

Email: luogongli1112@126.com

Abstract: According to the characteristics of China's membrane separation industry cluster, this paper constructs an evaluation index system for China's membrane separation industry cluster service capability based on the main theory of service-oriented manufacturing, covering five key service elements: information, logistics, finance, commerce and technology. ANP was used to evaluate the service capability of China's membrane separation industry cluster.

Keywords: Membrane separation industry cluster, service-oriented manufacturing, ANP, service capability evaluation.

1. INTRODUCTION

Membrane separation industry is a newly emerged industry with the most potential development in the 21st century. As a new type of material, membrane materials occupy an important strategic position in the fields of environmental protection, energy, chemical engineering and bio-engineering. In 2010, China's "Decision of the State Council on Accelerating the Cultivation and Development of Strategic Emerging Industries" included high-performance membrane materials in strategic emerging industries. China's "Twelfth Five-Year Plan for National Economic and Social Development" clearly states that it is necessary to promote the deep integration of emerging technologies and emerging industries, and to develop strategic emerging industries into pilot and pillar industries. The development of membrane separation industry in China has a history of nearly ten years. Due to the huge market demand for membrane products in China, the membrane separation industry has developed rapidly in the past five years. By the end of 2017, China's membrane separation industry cluster contained more than 3,000 related production enterprises, and the market scale reached 194.4 billion yuan. Under this background, China's all-levels governments take the membrane separation industry as the focus of cultivation and development, and the research on membrane separation industry has become a new focus.

The membrane separation industry cluster service capability refers to the characteristics of the membrane

separation industry cluster that directly affects the service effect in serving activities. China's membrane separation industry has a new industrial morphological characteristic of service-oriented manufacturing. Therefore, it is necessary to enhance competitiveness and international status through value-added services [1]. As China's membrane separation membrane industry has just started, domestic and foreign scholars have mainly studied the membrane separation industry in terms of the strategic significance, development ideas and industrial characteristics. Research on various fields such as the service capacity of membrane separation industry clusters in China is still in its infancy.

This paper applies the theory of service-oriented manufacturing and uses the Network Analytic Hierarchy Model (ANP) decision-making method to establish the evaluation model of membrane separation industry cluster service capability and comprehensively evaluates the service capability of China's membrane separation industry cluster.

2. MEMBRANE SEPARATION INDUSTRY CLUSTER SERVICE CAPABILITY EVALUATION INDEX SYSTEM

(1) Membrane Separation Industry Cluster Service Capability Element System

The membrane separation industry cluster mainly includes the following service-oriented manufacturing forms: production process services (such as manufacturing outsourcing) between membrane manufacturing enterprises, production services provided by service enterprises for membrane manufacturing enterprises (such as engineering design, strategic planning, marketing services, etc.), and service companies. Membrane manufacturing companies jointly provide ultimate-users with utility services (such as the customization of membrane engineering) [2]. Based on the relevant literature, this paper divides the service element system of membrane separation industry cluster into five categories and takes it as the theoretical basis for the division of service capability indicators. The five service categories are information services (including technologies, software and hardware services for the processing, transmission and application of

information for enterprises.), logistics services (including transportation, logistics infrastructures, professional markets and goods agency services for enterprises), financial services (including financing for enterprises, venture capital and insurance services), business services (including procurement, sales, consulting, exhibitions and other circulation services for enterprises and professional assistant service as accounting, law, taxation, etc.), technology services (including research and development services such as product development, process design, quality control, maintenance and support, technical testing and other scientific and technological exchange services, technology intermediary, technology promotion, consulting and other professional technical services, etc.) [3].

(2) Membrane separation industry cluster service capability evaluation index system

Based on the researches of the connotation and characteristics of membrane separation industry cluster

Table 1 Membrane Separation Industry Cluster Service Capability Evaluation Index System

Aims	Primary indicator	Secondary indicators	Indicator type
<i>Membrane separation industry cluster service capability</i>	Information Service Capability A1	Business process information level a11	Qualitative positive indicator
		Management control integration level a12	Qualitative positive indicator
		Information utilization a13	Qualitative positive indicator
		Information demand satisfaction level a14	Qualitative positive indicator
	Logistics Service Capability A2	Packaging storage capacity a21	Qualitative positive indicator
		Transportation and distribution capability a22	Qualitative positive indicator
		Ration of logistics cost to total cost a23	Quantitative positive indicator
		Logistics service outsourcing satisfaction a24	Qualitative positive indicator
	Financial Service Capability A3	Financing efficiency a31	Qualitative positive indicator
		Ration of financing to total assets a32	Quantitative moderate index
		Financing yield a33	Quantitative positive indicator
		Cash flow adequacy a34	Qualitative positive indicator
	Business Service Capability A4	Service performance level a41	Quantitative positive indicator
		Market sales growth rate a42	Quantitative positive indicator
		Customer satisfaction a43	Quantitative positive indicator
	Technology Service Capability A5	Technological innovation capacity a51	Qualitative positive indicator
		Technical service capability a52	Qualitative positive indicator
			New product development rate a53

3. RESEARCH METHODS

(1) Construction of ANP

The Network Analytic Hierarchy Model (ANP) was proposed by T.L. Saaty in 1996 [4]. Analytic Hierarchy Process (AHP) can be seen as a special case of a network-level analytical model [5]. The network analytic model quantifies various types of metrics and allows multiple indicators to co-exist. The model describes the decision-making problem more accurately by fully considering the dependence and

service capability, this paper divides the membrane separation industry cluster service capability evaluation system into three levels. 1. The target layer, the membrane separation industry cluster service capability; 2. The criterion layer consists of five dimensions: information service capability, logistics service capability, financial service capability, scientific research technology service, and business service capability; 3. The indicator layer, with the 18 key highly characteristic elements of the five dimensions selected by the survey and experts. All indicators include qualitative indicators and quantitative indicators. In the process of evaluation, the qualitative indicators are quantified by expert scoring method, while the quantitative indicators are both positive and moderate indicators. A range is set with the value of the indicators. The dimensionless processing is converted to the corresponding score (see Table 1).

feedback relationships among all the elements. The ANP architecture is divided into a control layer and a network layer [6]. 1) The control layer includes the problem objectives and decision criteria and the decision criteria are independent of each other, with typical ANP hierarchical structure features. The method of determining each criterion is same as the ANP method. 2) The network layer, which describes the network relationships, is formed by the interactions and interactions between the elements governed by all

controlled layers. A comprehensive analysis of the various interaction factors leads to their integrated importance.

(2) The main steps of the ANP method

The main steps of the ANP method are: first, construct the typical structure of ANP; secondly, construct the initial super-matrix calculation weight of ANP; finally, construct the weighted super-matrix, and finally obtain the evaluation factor weight[7]. As it is shown in Figure 1, the specific operation needs to complete the super-matrix calculation and iterative convergence calculation process by applying the ANP method through the super-decision software (supar decisions) [8].

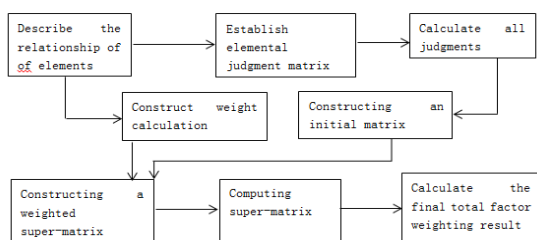


Figure 1 Basic steps of the ANP method.

4. ANP BASED MEMBRANE SEPARATION INDUSTRY CLUSTER SERVICE CAPABILITY EVALUATION MODEL CONSTRUCTION

(1) Membrane Separation Industry Cluster Service Capability Evaluation Model

According to the membrane separation industry cluster service capability index system established in the paper, the network relationship between the indicators is determined through the questionnaire survey method. The survey questionnaires are divided into two parts. One is used to determine the influence relationship of the network layer structure factor of the evaluation model and another is used to establish the weight of the evaluation index of the service capacity of the membrane separation industry cluster. The first survey

questionnaire was distributed to experts and business leaders in the field of membrane separation industry, and 18 questionnaires were distributed and all recovered. Based on the Delphi method, the results of the questionnaire were used to obtain the influence relationship of the factors in the network structure, and then the service capacity evaluation model of the membrane separation industry cluster was established (see Figure 2).

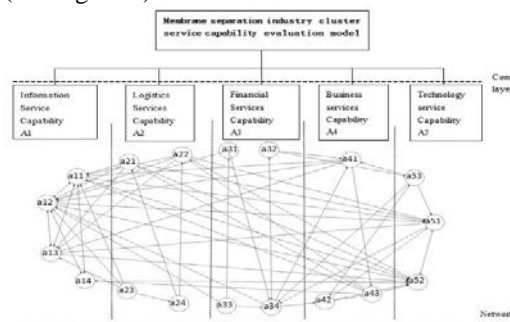


Figure 2 Membrane separation industry cluster service capability evaluation model

(2) The weight of the membrane separation industrial cluster service capability evaluation index

The second survey respondents were experts and scholars in the field of membrane industry manufacturing and leaders in membrane related companies. Based on the survey results of the first questionnaire, the hamburger model design was used, 116 questionnaires were distributed again, and 70 valid questionnaires were collected. The valid questionnaire data was used as the criteria in the questionnaire. The data of the valid questionnaire are geometric mean valued as the criteria of the questionnaire. The table was formed by the Supar Decisions software to obtain the weight of the membrane separation industry cluster service capability evaluation indicators as shown in Table 2. Due to the words limitations, the specific operation process is omitted.

Table 2. Indicator ANP weights in the evaluation system

Primary Indicator	Weights	Secondary Indicators	Weights
<i>Information Service Capability A1</i>	0.1825	Business Process Information Level a11	0.0541
		Management Control Integration level a12	0.0463
		Information Utilization Rate a13	0.0225
		Information Demand Satisfaction Level a14	0.0596
<i>Logistics Service Capability A2</i>	0.1700	Packaging Storage Capacity a21 Transportation and Distribution Capability a22	0.0400
		Logistics Cost to Total Cost Ratio a23	0.0362
		Logistics Service Outsourcing Satisfaction a24	0.0535
<i>Financial Service Capability A3</i>	0.1794	Logistics Service Outsourcing Satisfaction a24	0.0403
		Financing Efficiency a31	0.0600
		Financing as a Percentage of Total Assets a32	0.0098
		Financing Yield Rate a33	0.0250

<i>Business Service Capability A4</i>	0.2205	Cash Flow Adequacy a34	0.0846
		Service Performance a41	0.0705
		Market Sales Growth rate a42	0.0802
		Customer Satisfaction a43	0.0698
<i>Technology Service Capability A5</i>	0.2476	Technological Innovation Ability a51	0.1104
		Technical Service Capability a52	0.0829
		New Product Development Rate a53	0.0543

5. NON-DIMENSIONAL AND SERVICE CAPABILITY EVALUATION OF MEMBRANE SEPARATION INDUSTRY CLUSTER SERVICE CAPABILITY INDICATORS

(1) Non-dimensional of membrane separation industry cluster capability indicators

The Membrane Separation Industry Cluster Service Capability Index System covers 18 specific indicators in 5 categories. Due to the differences in the dimensions of the indicators, a non-dimensional transformation is required, and each indicator is converted into a number in the interval [0, 1] and then be calculated. The index used in this paper is the positive indicator-the larger the better, and its non-dimensional treatment method is

$$f(\alpha_i) = \frac{\alpha_i - \alpha_{\min}}{\alpha_{\max} - \alpha_{\min}}, \alpha_{\min} < \alpha_i < \alpha_{\max} \quad (1)$$

Another type is a modest indicator, and its non-dimensional treatment method is

$$f(\alpha_i) = \begin{cases} \frac{2(\alpha_i - \alpha_{\min})}{\alpha_{\max} - \alpha_{\min}}, & \alpha_{\min} < \alpha_i < \alpha_{opt} \\ \frac{2(\alpha_{\max} - \alpha_i)}{\alpha_{\max} - \alpha_{\min}}, & \alpha_{opt} < \alpha_i < \alpha_{\max} \end{cases} \quad (2)$$

Based on the indicator types and formulas (1) and (2) shown in Table 2, the results of the non-dimensional raw data processing of the service capacity evaluation index of China's membrane separation industry cluster are shown in Table 3. (The original data is from the statistics of China Film Industry Association.)

Table 3 Service Capability Indicators and Non-dimensional Results of China's Membrane Separation Industry Cluster

Third-level Indicator	Raw data	Infinite Tempering Value
<i>Business Process Information Level a11</i>	0.82	0.82
<i>Management Control Integration Level a12</i>	0.68	0.68
<i>Information Utilization Rate a13</i>	0.75	0.75
<i>Information Demand Satisfaction level a14</i>	0.7	0.70
<i>Packaging Storage Capacity a21</i>	0.8	0.80
<i>Transportation and Distribution Capability a22</i>	0.79	0.79
<i>Logistics Cost to Total Cost Ratio a23</i>	0.012	0.80
<i>Logistics Service Outsourcing Satisfaction a24</i>	0.80	0.80
<i>Financing Efficiency a31</i>	0.56	0.56
<i>Percentage of Financing To Total Assets a32</i>	0.30	0.70
<i>Financing Yield a33</i>	0.15	0.75
<i>Cash Flow Adequacy a34</i>	0.65	0.65
<i>Service Performance a41</i>	0.78	0.72
<i>Market Sales Growth Rate a42</i>	0.12	0.80
<i>Customer satisfaction a43</i>	0.76	0.64
<i>Technological innovation ability a51</i>	0.72	0.72
<i>Technical service capability a52</i>	0.80	0.80
<i>New product development rate a53</i>	0.20	0.70

(2) Evaluation of Service Capability of Membrane Separation Industry Cluster

Membrane separation industry cluster service capability index $Z = \sum_{i=1}^{18} \alpha_i w_i$, among them α_i

expresses i -- non-dimensionalized values of indicators, w_i expresses i --the global weight of each indicator relative to the total target, the result should be the value of the interval range [0,1], and the evaluation criteria of the service capability of the membrane

separation industrial cluster are set as: interval (0-0.2) is the worst, interval (0.2- 0.4) is the bad, interval (0.4-0.6) is the medium, interval (0.6-0.8) is the good, and interval (0.8-1) is the excellent. From Table 2 and Table 3, the service capacity of China's membrane separation industry cluster is 72.77%, among which the information service capability, logistics service capability, financial service capability, business service capability, and technology service capability are 73.66%, 79.79%, 63.65%, 72.38%, and 74.24% respectively, relative to the global weight. The financial service capacity is at a medium level, and the

remaining capabilities are at a good level, indicating that the service capacity of the membrane separation industry in China is generally good. The weight of the service capacity index of the membrane separation industry cluster can be known as the importance of the technology service capacity for the membrane separation industry service capability. The level of science and technology service in the membrane separation industry cluster should be strengthened. At the same time, aiming at the weak links of the membrane separation industry cluster, attention should be paid to improve the financial services ability of the membrane separation industry.

6. CONCLUSION

This study comprehensively considers the complex influences and feedback relationships between the elements and elements of the membrane separation industry cluster service capability, and uses the network hierarchy analysis (ANP) decision-making method to establish a membrane separation industry cluster service capability evaluation model. Systematic analysis and comprehensive evaluation of the service capacity of China's membrane separation industry cluster have been made. This research helps this industry to understand the status quo of its own services in a scientific way, so as to adopt an effective industrial service improvement strategy and enhance industrial competitiveness. It is of great significance for the correct formulation of China's membrane separation industry cluster service policy and the improvement of cluster service level.

ACKNOWLEDGEMENT

This work is supported by National Planning Office of Philosophy and Social Science Project (Grant No. 17BJY073), Humanities and Social Sciences Research

Project of the Ministry of Education (Grant No. 14YJAZH 108), Shandong Provincial Natural Science Foundation (Grant No. ZR2014GM012) and Shandong Provincial Social Science Planning Project (Grant No. 18CGLJ25)

REFERENCES

- [1]L. Sun, G. Li, and Z. Jiang, "Advanced Manufacturing Model in the 21st Century—Service-Oriented Manufacturing", *China Mechanical Engineering*, Vol.18, No.19, pp.2307-2312. 2007.
- [2]G. Li, L. Sun, and J. Gao, "Research on the Architecture and Implementation Model of Service Manufacturing Model", *Science and Technology Progress and Countermeasures*, Vol.7, 45-50. 2010.
- [3]Y. Chen, W. Wang, "Service Performance Evaluation of Strategic Emerging Industry Clusters Based on Service Manufacturing", *Commercial Economic Research*, Vol. 9, pp. 125-127. 2015.
- [4]T. L. Saaty, "Decision Making with Dependence and Feedback", *The Analytic Network Process International*, Vol.95, No.2, pp. 129-157. 1996.
- [5]L. Wang, "ANP principle and algorithm", *Systems engineering theory and practice*, Vol.3, pp.44-50. 2001.
- [6]T. L. Saaty, "The Analytic Network Process", *Pennsylvania: RWS Publications*, 2001, ch. 3.
- [7]T. L. Saaty, *Theory and Applications of the Analytic Network Process: Decision Making with Benefits, Opportunities, Costs and Risks*, *Pennsylvania: RWS Publications*, 2001, ch. 4.
- [8]T. L. Saaty, "Decision Making-The Analytic Hierarchy and Network Processes(AHP/ANP)", *Journal of Systems Science and Systems Engineering*, Vol.13, No.1, pp. 1-35. 2004.

Effect Analysis and Design Method Improvement of Expansion Tank in Heating System by Heat Transfer Fluids

Wang Lei^{1,2*}, Liu Jing¹, Liu Zhanchong¹, Li Yantong¹, Lin Chuhong²

¹Beijing Institute of Technology, Zhuhai Guangdong Zhuhai 519000

²Zhuhai Jinggong Inspection Technology Limited Company, Zhuhai 519000

Abstract: The expansion tank is a device with more accidents in the heating system by heat transfer fluids. In this paper, the analysis on the effect of the expansion tank in the heating system by heat transfer fluids and the common accidents shows that the volume of the expansion tank should be equal to the 1.3 times regulating volume required by the regulations, and the gas volume and the liquid rising volume which is caused by the gas emissions should also be added. In the meantime, the total amount of heat transfer fluids needed for cold oil displacement should be considered and compared, and the volume of expansion tank should be the maximum of both.

Keywords: Heat transfer fluids; Heating system; Expansion tank; Optimization on design

In industrial production, with the development and application of new processes and new technologies, the temperature of the heat transfer medium required by the production process is getting higher and higher, and the heat transfer temperature difference is getting smaller and smaller. With the deepening of people's understanding of heat conducting oil, heat conducting oil has been widely used in petroleum transportation, petrochemical, synthetic fiber, synthetic resin, textile printing and dyeing, food processing, drug synthesis, building materials, energy, transportation and other industries. Its prospects for development are extremely broad. But at present, the heating system by heat transfer fluids is not yet universally used in China, mainly because that people do not have a full understanding of the system, coupled with the introduction of heating system by heat transfer fluids to China for a relatively short period of time and not mature technologies, so accidents often occur in heating system by heat transfer fluids [1]. The "injection" accident often occurs in the medium expansion tank due to the unreasonable volume design. Based on the role of the expansion tank, various factors are comprehensively considered in this paper to improve the design method of the expansion tank.

1 CLASSIFICATION OF EXPANSION TANKS AND COMMON ACCIDENTS

Expansion tanks are important safety devices in liquid phase furnaces and systems, most of which are round steel vessels. According to the pressure bearing

condition of the expansion tank, it can be divided into open expansion tanks and closed expansion tanks. The atmosphere tube is installed on the expansion tank of the open structure, and the space inside the expansion tank communicates with the external environment through the atmosphere tube, and the space pressure is maintained at normal pressure, that is, atmospheric pressure. A pressure relief valve is installed on the expansion tank of the closed structure to relieve pressure. At the same time, in the closed expansion tank, the upper part of the heat transfer fluid should be sealed with nitrogen to prevent it from directly contacting with the air at high temperature to cause oxidative deterioration, reducing the service life of the heat transfer fluid, and eliminate the safety hazard [2]. The closed structure expansion tank can better ensure the closed operation of the heat transfer fluid in the heating system and ensure the service life of the heat transfer fluid, but its structure is relatively complicated, the operation management is relatively troublesome, and the investment is large. Considering the provisions of Article 21 of the *Safety Technical Supervision Regulations for Organic heat transfer material heater*: the surface temperature of the heat transfer fluid in the expansion tank should not exceed 70°C, under this temperature limitation, most heat transfer fluids are not easily oxidized when in direct contact with air, so heating system by heat transfer fluids often employ an open structure.

Expansion tank is divided into vertical and horizontal types. The height of the liquid column is increased in the vertical expansion tank, which is beneficial to the replenishment of the indenter and the smooth separation of the liquid and gas. However, since the expansion tank is generally placed at the highest position of the system, horizontal placement and installation are more convenient, so in practical applications, the horizontally placed expansion tank is more common. At present, there are frequent safety accidents in the expansion tank of the heat carrier heating system, such as (1) over-temperature of the expansion tank. When the temperature of the heat transfer fluid is $\leq 100^\circ\text{C}$, its oxidation is not obvious; when the temperature of the heat transfer fluid is $>100^\circ\text{C}$, its oxidation rate is obviously increased with the increase of the temperature of the heat carrier, and finally the heat transfer fluid is rapidly ineffective.

Therefore, it is clearly stated in the regulations that the temperature of the heat transfer fluid in the expander should not exceed 70°C , in order to prevent the heat transfer fluid from oxidizing and failing due to over-temperature, forming residual carbon deposited on the pipe wall, deteriorating heat transfer effect, burning out the heated surface tube. The over-temperature phenomenon of the expansion tank is manifested by the fact that the temperature of the heat carrier in the expansion tank exceeds the highest upper limit required by the regulations, thereby shortening the service life of the heat carrier. (2) Overflow. When the system is started, a large number of high temperature heat carriers flow into the oil storage tank through the overflow pipe on the expansion tank, causing the oil pump to work at high temperature, which affects the life of the oil pump^[5]. (3) Injection, in which the gas carries a large amount of heat carrier and is ejected from the atmospheric tube at the top of the expansion tank, which not only causes waste of energy, environmental pollution, but also threatens the safety of the workers. (4) Fire and explosion, which is the most serious and dangerous one in the expansion tank accidents. Its main performance is the sudden fire and explosion in the expansion tank, which will cause huge economic losses and even lead to casualties.

2 ANALYSIS OF THE ROLE OF THE EXPANSION TANK IN THE SYSTEM

In order to analyze the cause of the expansion tank accident, we need to specifically understand the role of the expansion tank in the heat carrier heating system. The role of the expansion tank in the heating system is as follows: (1) To store the thermal expansion of the heat transfer fluid in the storage liquid furnace and system. The heat carrier will expand by about 10% for every 100°C increase in temperature during heating, and a small amount of oil vapor will be generated, which must be released to ensure the normal circulation of the heat transfer fluids in the system. (2) To automatically supplement the system with heat transfer fluids. According to statistics, during normal operation, the heat transfer fluids in the system are consumed by 3% to 5% per year due to thermal cracking and oxidation. Due to the reduction in the amount of circulation, a pressure difference is generated between the circulation system and the expansion tank, under which the heat carrier in the expansion tank is pressed into a relatively small pressure circulation system. (3) To eliminate the gas in the system. During the start-up process of the liquid phase furnace, especially when it is put into operation for the first time, due to the hydrostatic test and the residual moisture of the heat carrier, a large amount of water vapor, air and other low-boiling volatiles are generated. With the help of the expansion tube and auxiliary exhaust pipe, the gas will be discharged from the air tube on the expander to the system to ensure the normal and reliable operation of the system.

(4) To perform a cold oil replacement during a sudden power outage. In the event of a sudden power failure, the heat carrier circulation speed in the system is zero, and the heat carrier in the heat carrier furnace suddenly heats up due to the residual heat, causing over-temperature cracking, coking, and even causing the furnace tube to be damaged by heat deformation. At this point, close the transfer pipeline of the heat carrier furnace to the user, and open the valve of the cold oil replacement tube. The "cold" heat transfer fluid in the expansion tank flows into the heat transfer fluid furnace due to the liquid level difference, and replaces the "hot" heat transfer fluid in the furnace, and then flows into the oil storage tank through the corresponding pipeline to achieve the function of cooling the furnace tube. (5) When oiling the heating system, oil may also be injected into the expansion tank and then flowed into the heating furnace and the system. (6) To isolate the high temperature heat transfer fluid in the system from contact with air. When the temperature of the heat transfer fluid is $\leq 100^{\circ}\text{C}$, its oxidation is not obvious; when the temperature of the heat transfer fluid is over 100°C , its oxidation rate is obviously increased with the increase of the temperature of the heat carrier, and finally the heat transfer fluid is rapidly ineffective. In normal operation, the heat transfer fluid in the expansion tank is low temperature (not more than 70°C), and the heated heat transfer fluid in the insulation system is in contact with the air, which weakens the oxidative decomposition of the heat transfer fluid by the oxygen in the air and prolongs the service life. (7) To stabilize the pressure. The expansion tank is installed in the upper part of the system to provide a basic head to the system to make the circulation pump work stably and reliably. (8) To relieve the pressure. The overpressure caused by mis-operation can be released through the atmospheric pipe on the expansion tank or through the overflow pipe to the atmospheric pipe on the oil storage tank to ensure that the system does not have an overpressure accident. (9) To dewater and drain. When the system is put into operation for the first time, the auxiliary exhaust pipe (also called the dewatering pipe) can be opened, so that the expander participates in the circulation, and the temperature in the tank is kept higher than the vaporization point of the water, so that the water is vaporized and discharged from the exhaust pipe to achieve the purpose of dehydration. However, after the dewatering, the valve on the auxiliary exhaust pipe must be closed to prevent the temperature in the expander from overheating for a long time and the heat transfer fluid to be invalidated. During normal operation of the system, due to various reasons, the system will inevitably be mixed with water, which will be vaporized by heat in the furnace, and separated by the separator into the expander through the expansion tube^[5]. Since the temperature of the

heat transfer fluid in the expander is lower than the vaporization point of water during normal operation, some of the water vapor will condense into water before it can be discharged from the top of the expander. Some of the vapor will return to the system and the rest will accumulate at the bottom of the expander. It can be drained by the drain pipe at the bottom of the expander to facilitate safe and reliable operation of the system^[4].

3 IMPROVEMENT OF DESIGN METHOD OF EXPANSION TANK

The design of the expansion tank mainly includes the volume design of the expansion tank and the design of the diameter of the expansion tube. The volume of the expansion tank specified by each country is not exactly the same. According to DIN4754 in West Germany, when the volume of liquid phase furnace is less than 1000litre, its volume is 1.5 times that of liquid phase furnace; when more than 1000litre, it is 1.3 times that of liquid phase furnace. The 1989 edition boiler regulation of the former Soviet Union stipulated 1.3 times. China's 1993 edition regulation by the Ministry of chemical industry stipulates that it is two times the volume of liquid phase furnace. The latest regulation of *Organic heat transfer material heater GB/T 17410-2008* stipulates that the regulating volume of expansion tank (expander) should not be less than 1.3 times of the volume expansion of heat transfer fluid. It is noteworthy that the regulating volume of the expansion tank stipulated in the regulation (i.e. *GB/T 17410-2008*) is not less than 1.3 times of the expansion volume of the heat carrier. According to the minimum requirement of 1.3 times, the expansion tank designed often has insufficient effective volume and the heat carrier flows into the oil storage tank from the overflow pipe. The reason is that only the volume of the heat carrier expanding when the system is in operation is considered in the regulation, and the "swelling volume" due to the system residue and the steam and air carried by the heat carrier itself is not considered^[6]. In addition, the regulation fails to take into account the volume of heat carrier required for "cold oil displacement" and the volume required for gas space. The reason for the frequent "injection accident" is that the gas space is insufficient, and the exhaust gas carries a large amount of oil. Therefore, it is necessary to further investigate the volume of the expansion tank.

3.1 Composition of the expansion tank volume

The volume of the expansion tank is determined by its role in the system. Therefore, it must meet the following requirements:

- 1) To be able to absorb the thermal expansion of the heat carrier in the storage liquid phase system;
- 2) To meet the amount of heat carrier required for "cold oil displacement" in the event of a power outage;
- 3) To have a certain gas space height to meet the requirements of the gas space height during the oil

and gas separation process, and to prevent excessive oil carrying (the phenomenon that the exhaust carries the heat carrier);

- 4) When the liquid phase system is put into operation for the first time, the gas in the expander oil space will cause the "expansion" of the gas-liquid interface. At this time, the expander should ensure that no overflow occurs.

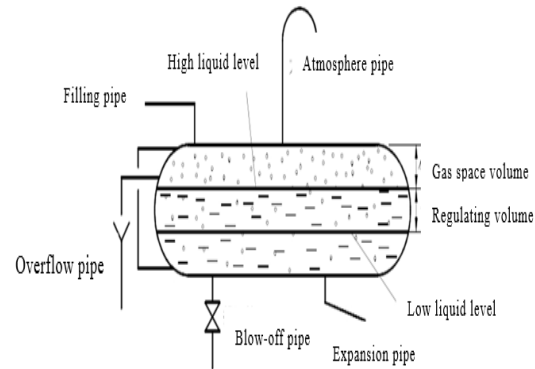


Figure 1 Schematic diagram of the horizontal expansion tank

3.2 Determination of the expansion tank volume

A schematic diagram of the common horizontal expansion tank is shown in Figure 1.

3.2.1 Determination of regulating volume

The regulating volume of the expansion tank refers to the total heat transfer fluid volume in the system when the expansion tank is at the lowest liquid level before heating, and is set to V_0 , and the total heat transfer fluid volume in the system when the expansion tank is at the highest liquid level after reaching the use temperature by heating, and is set to V_m . Then the maximum increase of the volume of the heat transfer fluid in the heating system is $\Delta V = V_m - V_0$, that is, the regulating volume of the expansion tank. According to the definition of the adjustment volume and the regulations of the *Organic heat transfer material heater GB/T 17410-2008*, when the heat transfer fluid exceeds a given temperature, the volume increase can be determined according to the formula $V_{ij} = 1.3\beta(A+B+C)(t-t_0)$.

Where,

V_{ij} —Regulating volume of expansion tank;
 A —Volume of heat carrier in the liquid phase furnace;

B —Heat carrier volume in thermal equipment;

C —The volume of the heat carrier in the system circulation pipe;

t —Working temperature of heat transfer fluid;

t_0 —Initial temperature of heat transfer fluid;

β —Volume expansion coefficient of heat transfer fluid when heated to operating temperature.

The volume expansion coefficient of the heat transfer fluid is related to the temperature of the heat carrier. In the heating system by heat transfer fluids, the heat transfer fluid does not reach the working temperature through a rapid heating in the furnace body, but passes through a slow heating process, and it usually

takes about 30 hours to reach the working temperature. Fig. 2 is the heating curve of YD series heat transfer fluids. Figure 3 is the relationship between the volume expansion coefficient and temperature of YD series heat transfer fluids.

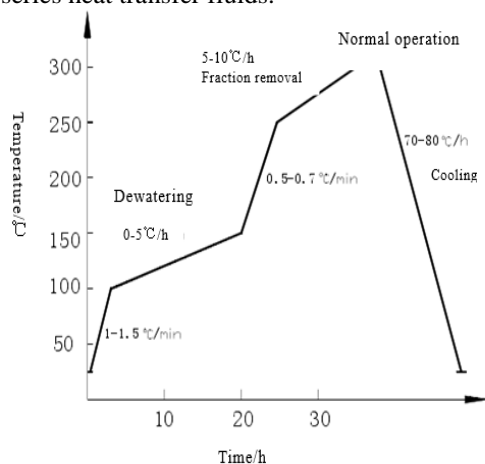


Figure 2 Temperature rise curve of YD series heat transfer fluid

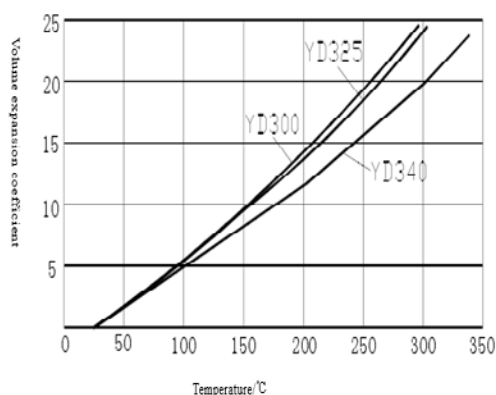


Figure 3 Diagram for relationship between volume expansion coefficient and temperature of YD

In the initial stage of the system operation, the heat transfer fluid is rapidly heated at a rate of 1 to 1.5°C/minute. At this time, the heat transfer fluid is in a cold state, the viscosity is large, and the flow speed is small. If the temperature rises too fast, it is easy to cause thermal cracking of heat transfer fluids. After reaching 100°C, the water mixed in the heat carrier is vaporized and discharged. In this case, in order to sufficiently discharge the water, the heating speed must be slowed down at a rate of 0 to 5°C/hour. The presence of moisture causes unstable system operation, corrosion of pipes, and reduction of thermal stability of heat transfer fluids^[7]. When the carrier temperature reaches 150°C, the moisture in the carrier is substantially discharged, and the heating rate of the system increases to 0.5-0.7°C/min. When the temperature reaches about 250°C, the light fraction in the heat transfer fluid starts to escape, and the temperature increase rate at this time is 5 to 10°C/hour, so that the light fraction is sufficiently discharged from the exhaust pipe, and finally heated to reach the operating temperature. Due to the

different composition and the difference in the amount of water remaining in the piping system, different types of heat transfer fluid have different heating processes when the system is put into operation. The more residual moisture or light fraction in the system, the longer the heating and heating time. In order to ensure the safe and reliable operation of the system and prolong the service life of the heat transfer fluid, the heating process should be reasonably adjusted according to the condition of the heat transfer fluid in the system, and the heating rate should not be accelerated blindly and the heating time should be shortened.

3.2.2 Determination of gas space volume

As can be seen from the temperature rise process in Fig. 3-4, a large amount of steam and light fractions are discharged during the initial operation of the system. In order to avoid the oil injection accident in the expansion tank during the dehydration and exhaust process, the gravity sedimentation method is generally adopted, that is, a certain volume space of the expansion tank is ensured, so as to fully utilize the difference in gas-liquid density to separate the heat transfer fluid carried by the exhaust gas. In practical applications, it is difficult to accurately determine the amount of gas emissions. In the absence of data, it is recommended that the expansion tank height be 400mm to 500mm. In addition, since the height of the air space required for the horizontal expansion tank is the same as that of the vertical expansion tank, in order to save material, the expansion tank should use a vertical expansion tank as much as possible.

3.2.3 Determination of the expansion volume of the expansion tank

When the system is first put into operation, the gas is discharged from the heat carrier from the temperature rise process to cause the volume of the heat transfer fluid to "swell up". Since it is difficult to determine the amount of gas discharged, the "bulging" volume caused by it is difficult to determine and can only be selected according to empirical values. According to the operating experience, the value can be selected according to the heat of the system heat carrier in the range of 0.5m³~1.0m³ [8].

3.2.4 Determination of cold oil displacement volume

When the system is unexpectedly shut down or the circulating pump suddenly breaks down, the heat transfer fluid in the furnace tube will not flow because of the stop of the circulating pump. At this time, the temperature of the heat transfer fluid in the furnace tube rises because of the continuous acceptance of the waste heat from the combustion of the fuel in the furnace. When serious, the heat transfer fluid in the furnace tube cokes. At this time, the cold oil displacement valve should be opened, the cold oil in the expansion tank is brought into the furnace by static pressure through the expansion tube, oil-gas separator, Y-type oil filter (or bypass) and circulating pump, and the hot oil in the furnace tube is discharged

into the oil storage tank through the cold oil replacement tube and pipeline. The "cold" heat transfer fluid in the expansion tank should ensure the required amount of cold oil displacement. Since the combustion in the furnace cannot be stopped immediately during a power outage or when the circulation pump is shut down, there will be a delay. Therefore, in addition to reducing the temperature of the furnace tube, the heat absorbed by the combustion needs to be considered by the amount of cold oil replacement. The heat of combustion can be considered according to the heat load of the furnace.

3.2.5 Determination of the total volume of the expansion tank

It can be estimated based on the following formula^[9].

$$V=1.3(A+B+C)t/1000$$

Where,

V—Volume of expansion tank;

A—Volume of liquid phase furnace;

B—Volume of heat transfer fluid in the thermal equipment;

C—The volume of the pipe between the boiler and the thermal equipment;

t—Boiler operating temperature.

4 IMPROVEMENT MEASURES AND CONCLUSIONS

For the installation position of the expansion tank, measures to prevent the injection of the heat transfer fluid from being fired should be considered. Generally, it is not appropriate to install the expansion tank directly above the Organic heat transfer material heater. The bottom of the expansion tank should have a distance of more than 1.5 m from the top of the Organic heat transfer material heater and the top of the heating system pipeline, and the distance between the expansion tank and the oil-gas separator should be greater than 1 m to prevent the heat from the heating system from being transferred to the expansion tank and ensure that the heat transfer fluid in the expansion tank is of low temperature. The expansion tank maintains a high liquid level during normal operation to ensure that there is sufficient heat transfer fluid to prevent overheating in the furnace tube when cold oil replacement is required. The high liquid level of the expansion tank can also prevent air from entering the heating system when the heat transfer fluid is cooled and contracted during normal shutdown. The liquid level meter on the expansion tank should have a low level alarm function to prevent gas from entering the heating system.

The heating technology of heat transfer fluid is relatively advanced in China. The main function of the expansion tank is to receive the volume expansion from the circulating heat carrier of the system. The volume of the expansion tank is required to be 1.3 times of the total volume expansion of the system. However, fuel injection accidents often occur in this design. Therefore, in the volume design of expansion tank, besides the expansion of the heat carrier itself, the volume of heat transfer fluid "swelling" caused by the residual heat carrier in the pipeline or the moisture in the heat carrier itself due to vaporization should also be considered. At the same time, it is necessary to compare the volume of heat transfer fluid needed in cold oil displacement, and choose the larger value as the basis for the design of expansion tank volume, which will effectively avoid the occurrence of accidents in heating system by heat transfer fluids.

REFERENCES

- [1] Ren Aiguo. Analysis of application technology of heat transfer fluid. China Petroleum and Chemical Industry Standards and Quality. 2013-10.
- [2] Zhao Hong. The role and maintenance of circulating pump in heat transfer fluid boiler system [J]. Science and Technology Vision. 2014-01.
- [3] Sun Minmin. Analysis of the use of heat transfer fluids. Chemical Management. 2014-08.
- [4] Shan Luliang. Discussion on structure and system design of fuel heat transfer fluid boiler. Industrial Boilers. 2002-06.
- [5] Hu Yuexin, Li Defeng, Yue Yong. Discussion on some hidden dangers in the production and use of heat transfer fluids. Industrial Boilers. 2004-01.
- [6] You Tianxiang. Feasibility and economic analysis of heat transfer fluid substituting steam in vulcanized flat plate heating. Industrial Heating. 2004-01.
- [7] Wu Shaoping. Design initiative of heating system by heat transfer fluids. Chemical Fertilizer Design. 2004-04.
- [8] Yue Yong, Han Dongtai. Commissioning and operation technology of fuel (gas) heat transfer fluid heating device. Industrial Heating. 2007-02.
- [9] Shi Zhao. Statistical analysis and countermeasures for safety accidents in the application of heat transfer fluid heating technology; Proceedings of the 20th National Heat Carrier Heating Technology Exchange Conference 2017.

A Comparison of Epidural Anesthesia with Chloroprocaine and Lidocaine for Outpatient Knee Arthroscopy

Dezhan Li¹, Shaoqun Tang^{2*}, Kun Zhang¹, Tao Xie¹

¹Department of Anesthesiology, Jingzhou Central Hospital, The Second Clinical Medical College, Yangtze University, Jingzhou, Hubei, 434020, P. R. China

²Department of Anesthesiology, Renmin Hospital of Wuhan University, Wuhan 430060, Hubei Province, China
E-Mail: 6939904@qq.com

Abstract: Objectives: To study the clinical efficacy and safety of chloroprocaine in epidural anesthesia compared to lidocaine in outpatient knee arthroscopy. Methods: Eighty patients undergoing knee arthroscopy were randomly allocated to receive either 3% 2-chloroprocaine (group C, n = 40) or 2% lidocaine (group L, n = 40) to conduct epidural block. Latency to anesthesia onset, highest block level, time to achieve peak effect, time to complete sensory and motor block regression, and vital signs including respiration and hemodynamics were measured. Complications and adverse effects related to the epidural anesthesia were assessed in follow-up visits within 24 hours and one week after the operation. Results: No significant differences were found in the latency to anesthesia onset and peak effect, duration of anesthesia efficacy, and the time for recovery of sensory function between the two groups. However, the latency to maximal block of pain sensation and the time needed to recover motor function were significantly shorter in group C than in group L ($P < 0.05$). No adverse effects or neurologic complications were found in both groups. Conclusion: Epidural chloroprocaine elicits rapid anesthetic effects, fast sensor and motor block, and more importantly, faster recovery of motor function compared to lidocaine. These characteristics make chloroprocaine more appropriate than lidocaine as the choice of epidural anesthesia in short clinical operations such as knee arthroscopy.

Keywords: Chloroprocaine; Lidocaine; Epidural anesthesia; Knee arthroscopy

1. INTRODUCTION

Outpatient surgery offers several advantages over traditional inpatient surgery, which include a shorter operation duration, relatively little trauma, faster recovery, fewer adverse reactions or complications, and earlier discharge times. Knee arthroscopy is an outpatient procedure benefitting greatly from epidural anesthesia which provides rapid and reliable anesthetic effects, predictable recovery and minimal complications. A number of local anesthetics have been de-

veloped to meet the growing need for day case surgeries including knee arthroscopy [1-4].

Lidocaine has been the choice of epidural anesthetic in many outpatient procedures. It has a rapid onset of action and long duration of efficacy. However, the neurological complications associated with the use of lidocaine, collectively named the transient neurologic symptoms (TNS), have limited its use [2, 5, 6]. Chloroprocaine, an amino-ester type of local anesthetic, when used as epidural anesthetic, has been described to display similar recovery profile as epidural lidocaine. Compared to lidocaine and other local anesthetics, chloroprocaine induces an anesthesia that is characterized by rapid onset, a very short duration of action and a favorable evolution of spinal block for short outpatient procedures [5, 7]. Therefore, chloroprocaine has been proposed by multiple studies over the past decade to be an excellent candidate anesthetic and alternative of lidocaine for short procedures. In spite of the significant advantages of chloroprocaine, use of chloroprocaine for epidural anesthesia has proven controversial and therefore, more studies are needed to determine the clinical efficacy and safety of chloroprocaine in outpatient procedures. In this study, chloroprocaine and lidocaine in epidural anesthesia were compared in patients undergoing knee arthroscopy.

2. METHODS

(1) General Information

This study has been approved by the Hospital Ethical Committee of Jingzhou Central Hospital. Patients have given consent to participate in the study. Eighty patients who underwent knee arthroscopy do not have endocrine or metabolic diseases or any nervous system disorders. They have no abnormalities in diagnostic indicators of liver and kidney function, and no epidural puncture contraindications. Using a randomized, double-blind method, eighty patients were randomly divided into two groups according to the date of surgery. The patients in the chloroprocaine group (group C, n = 40) were injected with 3% 2-chloroprocaine (30 mg/ml, Shanxi Jincheng Hayes

Pharmaceutical Co., Ltd., Shanxi, China). The patients in the lidocaine group (group L, $n = 40$) were injected with 2% lidocaine (20 mg/ml, Shanghai Xudong Haipu Pharmaceutical Co., Ltd., Shanghai, China).

(2) Anesthetic Method

The patients were monitored with a GE multi-function monitor to measure heart rate, blood pressure and respiratory rate. The L2-3 vertebral body gap was selected for epidural anesthesia in a lateral position and a 3.5 cm catheter was placed upward. 3% 2-chloroprocaine or 2% lidocaine was injected in a 5 ml test dose with the patient in supine position. It was confirmed that the conduit was in the epidural space and there were no unwanted spinal anesthesia symptoms. Five minutes later, a 10 ml dose of 3% 2-chloroprocaine or 2% lidocaine was added. The injection speed of both groups was the same, and no other local anesthetics were added during the entire operation. After the successful epidural anesthesia puncture, oxygen was taken up through a nasal catheter at 2-4 L/min. If the blood pressure dipped to lower than 30% of the base value, 10 mg ephedrine was injected intravenously. If the heart rate dropped to lower than 50 beats/min, 0.5 mg atropine was injected intravenously. The two groups of patients were not given any sedation, analgesia, or other intravenous anesthetics for assistance. Patients with unsmooth anesthesia operation or uncertain effects were excluded.

(3) Observation Items

Anesthetic effects: Latency to anesthesia onset (the time period from giving the test dose to the disappearance of cold sensation); latency to nerve block onset (the time period from giving the test dose to elimination of pain sensation, tested by pinprick); highest block level (determined by the disappearance of cold sensation), latency to peak effect (the time period from giving the test dose to appearance of highest block level); sensory recovery time (time period from giving the test dose to feeling pain in the surgical wound, scored ≥ 4 in Visual Analogue Scale (VAS), see below for detailed description); and motor recovery time (time period from giving the test dose to recovering motor function in the lower limb joints, scored 0 by Bromage scoring method, see below for detailed description). VAS scoring method: 0 indicates no pain, ≥ 4 indicates moderate pain, and the highest score of 10 represents unbearable intense pain. Bromage scoring method: 0 represents no motor nerve block (hip, knee and ankle joints are inflective); 1 represents the inability to lift legs (but knee and ankle joints are still mobile); 2 represents the inability to bend the knee (but retention of movement in ankle joints); 3 represents the inability to move the ankle joints (all three major joints - hip, knee and ankle - are immobile). The following vital signs, blood pressure, heart rate and respiratory rate, were measured and monitored before anesthesia and after drug delivery at

5, 10, 15, 20, and 30 min. Patients were also monitored for adverse reactions including: dizziness, nausea, vomiting, drowsiness, restlessness, unconsciousness, peripheral numbness of mouth, and nervous system complications such as hypotonia in the lower extremities or muscle, abnormal sensation and bladder dysfunction, etc.

(4) Statistical Analysis

Statistical analysis was performed using statistical software SPSS13. Results were presented as mean \pm standard deviation (SD). The comparison of anesthetic effects and vital signs at different time points between the two groups was determined using t-test. Changes in vital signs of both groups and the comparison of vital signs between groups before and after anesthesia were assessed using repeated measures analysis of variance. Differences in categorical variables between the groups were analyzed with χ^2 test. A p -value < 0.05 was considered statistically significant.

3. RESULTS

Eighty patients were randomized into two groups for this study. There were no dropouts or case failures in our study. Demographics including age, gender, weight and height were similar between groups and there were no significant differences in duration of operation and epidural infusion volume between groups (Table 1, $P > 0.05$). The latency to anesthesia onset and the latency to elimination of pain sensation were both shorter in group C than in group L, but the differences between the two groups were not statistically significant (Table 2, $P > 0.05$). Notably, the average time required to reach the highest level of sensory block was significantly shorter in group C than in group L (14.7 ± 3.4 min vs. 18.5 ± 4.8 min, Table 2, $P < 0.05$). Furthermore, the average motor recovery time in group C was much faster than that in group L (76.1 ± 16.3 min vs. 85.9 ± 18.8 min) and this difference was statistically significant (Table 2, $P < 0.05$). Vital signs of patients were monitored carefully throughout the procedure. The arterial pressure (AP) of group C decreased significantly 10 min after delivery of anesthesia. In contrast, the AP of group L decreased significantly 10-15 min after delivery of anesthesia, indicating a trend toward longer latency to AP reduction. Meanwhile, heart rate (HR) for both groups showed an upward trend and there was no significant difference between groups ($P > 0.05$). The percentage of patients experiencing side effects such as hypotension, bradycardia, sicchasia, dizziness or backache in each group during the operation is shown in Table 3. The percentage was small in both groups and no significant differences in the incidence of such side effects between the two groups were found ($P > 0.05$). In addition, no neurological complications such as paraesthesia of lower limbs and dysfunction of vesica urinaria was reported for patients from either group according to follow-up visits within 24 hours and one week after the operation.

Table 1. Summary of demographic data, duration of operation, and infusion volume (mean \pm SD).

Demographics	Group C (n = 40)	Group L (n = 40)
Age (years)	37.6 \pm 7.5	41.3 \pm 8.3
Gender (M/F)	21/19	23/17
Body weight (kg)	61.5 \pm 3.7	65.3 \pm 4.9
Body height (meter)	1.74 \pm 1.1	1.72 \pm 1.4
Duration of operation (min)	45.7 \pm 8.3	42.3 \pm 9.7
Infusion volume (mL)	850 \pm 65	790 \pm 70

There is no significant difference between the two groups ($P > 0.05$).

Table 2. Summary of anesthetic effects and recovery (mean \pm SD).

Material data	Group C (n = 40)	Group L (n = 40)
anesthesia onset (min)	4.7 \pm 1.4	5.2 \pm 1.9
sensory block onset (min)	9.4 \pm 2.2	9.7 \pm 3.1
highest block level (T)	9.9 \pm 1.2	10.4 \pm 1.1
latency to peak effect (min)	14.7 \pm 3.4*	18.5 \pm 4.8*
sensory recovery time (min)	74.3 \pm 15.1	73.7 \pm 21.1
motor recovery time (min)	76.1 \pm 16.3*	85.9 \pm 18.8*

* $P < 0.05$ between the two groups.

Table 3. Incidences of hypotension, bradycardia, sicchasia, dizziness and backache after operation.

Variables	Group C, n = 40 (%)	Group L, n = 40 (%)
Hypotension	1 (2.5 %)	2 (5 %)
Bradycardia	1 (2.5 %)	3 (7.5 %)
Sicchasia and dizziness	0 (0)	1 (2.5 %)
Backache	1 (2.5 %)	1 (2.5 %)

There is no significant difference between the two groups ($P > 0.05$).

4. DISCUSSION

The number of outpatient small surgeries has greatly increased over recent years due to advance in technologies. The growing popularity of outpatient surgeries calls for effective and safe local anesthetics. The ideal candidate should exhibit features such as rapid and reliable anesthetic effects with minimal to no toxicity. Chloroprocaine has been widely used in infiltration anesthesia and nerve block worldwide [8, 9] and is especially applicable to outpatient procedures [4] and daytime surgeries [1, 10]. Beginning in the late 1990s, chloroprocaine was used for epidural block and subarachnoid space block [5, 11, 12]. Neal et al. applied chloroprocaine or lidocaine epidural

anesthesia to short-duration, minor orthopedic operations of the lower limbs [13]. Casasola et al. compared the efficacy of preservative-free chloroprocaine and plain lidocaine in the same dose for spinal block in knee arthroscopy [5]. In both studies, it was discovered that the group receiving chloroprocaine required less time in the observation room following the operation. Yoos et al. compared the spinal anesthetics using 40 mg of chloroprocaine and 7.5 mg of lidocaine and found that the surgeries for patients receiving chloroprocaine were more likely to fit in the expected time frame, allowing patients to be discharged from hospitals earlier [14].

With accumulating evidences supporting the application of epidural chloroprocaine in outpatient surgeries, this study aims to test the hypothesis that chloroprocaine provides a similarly effective sensory block but with a faster recovery of motor function compared to an equivalent dose of lidocaine in Chinese patients. The results of our study indicate that 3% chloroprocaine has a slightly faster onset of anesthetic effect compared to 2% lidocaine in patients undergoing outpatient knee arthroscopy. Chloroprocaine required significantly shorter time to reach the maximal sensory blocking effect than lidocaine. The times for sensory recovery are comparable between the groups receiving chloroprocaine and lidocaine, which makes them both ideal for knee arthroscopy and other short surgical procedures of ≤ 1 h. However, the motor function of the group receiving chloroprocaine recovered significantly faster than the group receiving lidocaine following the emergence of pain sensation. This faster motor recovery may be explained by the fact that chloroprocaine can be locally hydrolyzed by cholinesterase [15,16]. The rapid metabolism of chloroprocaine also contributes to limit its potential for toxicity.

In our study, anesthesia caused a decrease in AP and an increase in HR for both groups of patients suggesting that chloroprocaine elicits the same effect on the circulatory system as lidocaine and other local anesthetics, which is to block the intraspinal sympathetic system and causes angiectasis in resistance and capacity of the blood vessel, thereby reducing blood pressure and increasing heart rate. During the operation, the incidences of hypotension, bradycardia, sicchasia, dizziness and backache were quite low and unwanted side effects were similarly infrequent in both groups. Early reports indicated that a large dose of chloroprocaine applied outside the dura mater would lead to severe, spastic backache [17, 18]. This adverse effect may be related to permeation of the local anesthetic into human tissues by needle passages after a large dose of medicine being injected. More recent reports showed that when appropriate dose of preservative-free chloroprocaine was used for spinal block, no serious backache was reported and very rare complications were observed [4, 5, 8]. In our study, the incidence of backache in both groups was very

low (1 in 40 patients), which is consistent with other reports. According to follow-up visits within 24 hours and one week after the operation, patients from either group experienced any obvious complications related to neurotoxicity which is again consistent with other reports [3, 4, 19].

In conclusion, our study has provided additional evidence supporting the hypothesis that chloroprocaine is a better alternative to lidocaine in epidural anesthesia. Chloroprocaine exhibits characteristics of rapid onset, defined efficacy, rapid motor recovery, minimal toxicity and lack of adverse reactions. Therefore, it is a good anesthetic option for patients undergoing small outpatient procedures such as knee arthroscopy. With shorter surgical procedures, faster recovery time and decreased risk of complications, the patients do not need to stay in the hospital for prolonged observation and they can return home sooner. Our findings support the use of the epidural chloroprocaine in ambulatory knee arthroscopy.

References

- [1] Forster, J.G. and P.H. Rosenberg, Revival of old local anesthetics for spinal anesthesia in ambulatory surgery. *Curr Opin Anaesthesiol.* 2001, 24:633-7. DOI: 10.1097/ACO.0b013e32834aca1b.PMID 21841475.
- [2] Goranson, B.D., et al., 1997. A comparison of three regional anaesthesia techniques for outpatient knee arthroscopy. *Can J Anaesth*, 1997. 44(4): p. 371-6.
- [3] Stewart, A.V., et al., Small-dose selective spinal anaesthesia for short-duration outpatient gynaecological laparoscopy: recovery characteristics compared with propofol anaesthesia. *Br J Anaesth*, 2001. 86(4): p. 570-2.
- [4] Vaghadia, H., G. Neilson, and P.H. Lennox, 2012. Selective spinal anesthesia for outpatient transurethral prostatectomy (TURP): randomized controlled comparison of chloroprocaine with lidocaine. *Acta Anaesthesiol Scand.*, 56:217-23. doi: 10.1111/j.1399-6576.2011.02599.x.PMID 22236346.
- [5] Casati, A., et al., 2007. Spinal anesthesia with lidocaine or preservative-free 2-chloroprocaine for outpatient knee arthroscopy: a prospective, randomized, double-blind comparison. *Anesth Analg*, 2007. 104(4): p. 959-64.
- [6] Zaric, D., et al., Transient neurologic symptoms after spinal anesthesia with lidocaine versus other local anesthetics: a systematic review of randomized, controlled trials. *Anesth Analg*, 2005. 100(6): p. 1811-6.
- [7] Kouri, M.E. and D.J. Kopacz, Spinal 2-chloroprocaine: a comparison with lidocaine in volunteers. *Anesth Analg*, 2004. 98(1): p. 75-80, table of contents.
- [8] Goldblum, E. and A. Atchabahian, The use of 2-chloroprocaine for spinal anaesthesia. *Acta Anaesthesiol Scand*, 2013. 57(5): p. 545-52.
- [9] Novikova, N. and C. Cluver, Local anaesthetic nerve block for pain management in labour. *Cochrane Database Syst Rev*, 2012. 4: p. CD009200.
- [10] Allen, R.W., J.P. Fee, and J. Moore, A preliminary assessment of epidural chloroprocaine for day procedures. *Anaesthesia*, 1993. 48(9): p. 773-5.
- [11] Smith, K.N., D.J. Kopacz, and S.B. McDonald, 2004. Spinal 2-chloroprocaine: a dose-ranging study and the effect of added epinephrine. *Anesth Analg.*, 98: 81-88, table of contents.PMID 14693591
- [12] Kopacz, D.J., 2005. Spinal 2-chloroprocaine: minimum effective dose. *Reg Anesth Pain Med.*, 30: 36-42.PMID 15690266
- [13] Neal, J.M., Deck, J.J, Kopacz, D.J and Lewis, M.A., 2001. Hospital discharge after ambulatory knee arthroscopy: A comparison of epidural 2-chloroprocaine versus lidocaine. *Reg Anesth Pain Med.*, 26: 35-40. PMID 11172509.
- [14] Yoos, J.R. and D.J. Kopacz, 2005. Spinal 2-chloroprocaine for surgery: an initial 10-month experience. *Anesth Analg.*, 100: 553-558.PMID 15673893.
- [15] Smith, A.R., D. Hur, and F. Resano, 1987. Grand mal seizures after 2-chloroprocaine epidural anesthesia in a patient with plasma cholinesterase deficiency. *Anesth Analg.*, 66: 677-678.PMID 3111302.
- [16] Kuhnert, B.R., Philipson, E.H., Pimental, R and Kuhnert, P.M., 1982. A prolonged chloroprocaine epidural block in a postpartum patient with abnormal pseudocholinesterase. *Anesthesiology.*, 56: 477-478.PMID 7081736.
- [17] Drolet, P. and Y. Veillette, 1997. Back pain following epidural anesthesia with 2-chloroprocaine (EDTA-free) or lidocaine. *Reg Anesth.*, 22: 303-307. PMID 9223193.
- [18] Stevens, R.A., Urmev, W.F., Urquhart, B.L. and Kao, T.C., 1973. Back pain after epidural anesthesia with chloroprocaine. *Anesthesiology.*, 78: 492-497. PMID 8457050.
- [19] Lennox, P.H., C. Chilvers, and H. Vaghadia, 2002. Selective spinal anesthesia versus desflurane anesthesia in short duration outpatient gynecological laparoscopy: a pharmacoeconomic comparison. *Anesth Analg.*, 94: 565-568.PMID 11867376.

Fast Convergent VHGMRES(m) Iteration Algorithm

Cuihuan Ren^{1,2*}, Lu Liu¹

¹Mathematical Modeling Innovation Lab, North China University of Science and Technology, Tangshan, Hebei, 063210, China

²North China University of Science and Technology, Tangshan, HeBei, 063210, China

*E-mail: 18713510209@163.com

Abstract: Numerical simulation of Engineering problems will form discrete equations, regardless of the Boundary Element Method or Finite Element Method. Combining with Householder transform and variable restart parameter, an iterative method named VHGMRES(m) algorithm is proposed. By properly changing a variable restart parameter for the GMRES(m) algorithm, the computation efficiency is greatly improved. Based on the orthogonalization process of VHGMRES(m) algorithm and the relevant properties of generalized inverse matrix, the projection of the error vector r_{m+1} on r_m is concluded. The result demonstrates that the VHGMRES(m) algorithm is not only fast convergent but also highly accurate. Numerical experiments further show that the VHGMRES(m) algorithm has higher computational precision and efficiency than the GMRES(m) algorithm.

Keywords: Householder transform; VHGMRES(m) algorithm; Error vector projection; Variable restart parameter; Fast convergence; highly accuracy

1. INTRODUCTION

In scientific and engineering fields, different kinds of differential equation and integral equation are usually established for many problems. By discretization, these equations can be summed up in solving a large scale linear system of equations, which can be expressed as

$$Ax = b, A \in R^{n \times n}, x, b \in R^n \quad (1)$$

where the coefficient matrix A is nonsingular. In recent years, how to solve such equations has become one of the research focuses. Many algorithms were studied. For example, Y Saad and MH. Schultz put forward a Generalized Minimal Residual algorithm (GMRES algorithm) in 2006, which gave the analysis of reliable theory and computational complexity, and K. Florikijni and K. Iiyami came up with a kind of convergence of inner-iteration gmres methods. A. Essai proposed a kind of weighted GMRES algorithm, which adopted weighted technology to speed up the residual amount of convergence. Ayachour proposed a kind of fast GMRES algorithm, and so on. At present, GMRES(m) algorithm has

gained widely popularity to solve a large sparse linear equations.

For the GMRES(m) algorithm, the selected parameter m is fixed during the whole iterative process. So the selection of m is one of the key factors for the convergence speed. Many results show that a small value of m may result in slow convergence or no convergence, while a large value of m will cause too much memory requirement. Recently, some researchers have tried to overcome these difficulties by changing the restart parameter m in the GMRES(m) algorithm. Householder GMRES(m) (HGMRES(m)) algorithm has been gaining popularity to solve a large sparse linear equations. It uses Householder transform to form the normal orthogonal bases for the GMRES(m) algorithm.

In this paper, a variable restart parameter is introduced into the HGMRES(m) algorithm, and a kind of HGMRES(m) algorithm with Variable restart parameter (VHGMRES(m) algorithm) is presented. By appropriately changing a variable restart parameter, the VHGMRES(m) algorithm has higher computational precision and efficiency than the GMRES(m) algorithm.

2. FUNDAMENTAL THEORY

(1) Galerkin principle

For a large scale linear system of equations

$$Ax = b, A \in R^{n \times n}, x, b \in R^n \quad (2)$$

Take an arbitrary initial vector $x_0 \in R^n$, and let $x = x_0 + z$. Then Eq.(2) is equivalent to

$$Az = r_0, r_0 = b - Ax_0 \quad (3)$$

For a given positive integer parameter m , K_m and L_m are two m -dimensional Krylov subspaces in R^n , which are formed by

$$K_m = \text{span}\{r_0, Ar_0, \dots, A^{m-1}r_0\}$$

$$L_m = \text{span}\{Ar_0, A^2r_0, \dots, A^m r_0\} = AK_m$$

Suppose that $V_m = \{v_1, v_2, \dots, v_m\} = \{v_i\}_{i=1}^m$ and

$W_m = \{w_1, w_2, \dots, w_m\} = \{w_i\}_{i=1}^m$ are the bases of K_m and L_m . For the solving system of Eq.(3), the Galerkin

principle is to find an approximate solution

$$z_m = V_m y_m \in K_m, y_m \in R^m \text{ so that } (r_0 - Az_m) \perp L_m .$$

(2) Householder Transform

Definition 1 Suppose that $w \in R^n, \|w\|_2 = 1$ and an elementary matrix P satisfies $P = I - 2ww^T$, then P is called a Householder transform matrix or a Householder transform. P is also called an elementary reflection matrix or an image mirror transformation, which is a kind of linear transformation.

With the norm of the vector maintains unchanged, the most important application of the Householder transform is to make some elements of a given vector be zeroes. If Householder transform is applied to each column vector of a matrix, it will be transformed into an upper Hessenberg matrix, which can simplify the relevant problems.

(3) Procedure of Householder orthogonal similarity algorithm

1) For $j = 1, \dots, n - 2$;

2) Define a vector $x = a_{*,j}$ (column j elements of matrix A);

3) Compute according to the following formula:

$$\begin{cases} \alpha = (x_{j+1}^2 + \dots + x_k^2)^{\frac{1}{2}} \\ u = (0, \dots, 0, x_{j+1} + \text{sign}(x_{j+1})\alpha, x_{j+2}, \dots, x_k, 0, \dots, 0)^T \\ t = 2\alpha(\alpha + |x_{j+1}|) \\ P_j = I - 2uu^T/t \end{cases}$$

where $\text{sign}(x)$ is a function symbol;

4) Orthogonal similarity transform $P_j A P_j = A$;

5) Until $j = n - 2$, stop.

3. VHGMRES(m) ITERATIVE ALGORITHM

(1) VHGMRES(m) Algorithm

For VHGMRES(m) algorithm, the basic thought is to accelerate the convergence speed of the GMRES(m) algorithm by using a Householder transform to quickly make the relevant matrix be orthogonal and by appropriately changing the restart parameter m in the iterative procedures. The specific process is as follow:

1) Initialization: Give a fixed integer $m \ll n$ and an error upper bound ε . Take an arbitrary initial value $x_0 \in R^n$, and compute $r_0 = b - Ax_0, s = \|r_0\|_2$.

2) Householder transform: Compute $P_1 = I - 2ww^T$, where $w_1 = r_0/s$ and $\|w_1\|_2 = 1$,

$$v_1 = P_1 e_1 (e_1 = (1, 0, \dots, 0)^T)$$

3) Iteration and Householder transform: For $j = 1, 2, \dots, m$, let $C = P^T A v_j$ ($j = 1, P = P_1$), then carry out Householder orthogonal similarity transformation for C and we can get P_j . Let

$e_1 = (1, 0, \dots, 0)^T \in R^{m+1}$ (h_j is j th column elements of matrix \overline{H}_m), compute $v_{j+1} = P_{j+1} P_j \dots P_1 e_{j+1}$, and form the matrices \overline{H}_m and V_m .

4) Solve the least squares problem:

$$\min_{y \in R^m} \|\beta e_1 - \overline{H}_m y\| \tag{4}$$

To obtain y_m , where $e_1 = (1, 0, \dots, 0)^T \in R^{m+1}$. Then compute $x_m = x_0 + z_m = x_0 + V_m y_m$.

5) Iteration control: Compute the norm of the residual vector $\|r_m\| = \|r_0 - Az_m\|_2$. If $\|r_0 - Az_m\|_2 < \varepsilon$, then $x = x_m$. Otherwise, let $x_0 = x_m, m = m + 1$ and turn to 1) until it meets the given error upper bound.

This algorithm uses Householder orthogonal transformation ($P_j (j = 1, 2, \dots, m)$) to complete QR factorization for the matrix $X = (r_0, Av_1, Av_2, \dots, Av_m)$, namely

$$Q_m (r_0, Av_1, \dots, Av_m) = (h_0, h_1, \dots, h_m) \tag{5}$$

where $Q_m = P_m P_{m-1} \dots P_1$ is a unitary matrix, and (h_0, h_1, \dots, h_m) is an $n \times (m + 1)$ dimensional upper triangular matrix, so we have

$$h_j = P_{j+1} z = P_{j+1} Q_j A v_j = Q_{j+1} A v_j \tag{6}$$

From Eq. (6), we can get

$$\begin{aligned} A v_j &= Q_{j+1}^T \sum_{i=1}^{j+1} h_{ij} e_i = \sum_{i=1}^{j+1} h_{ij} Q_{j+1}^T e_i \\ &= \sum_{i=1}^{j+1} h_{ij} v_i, j = 1, 2, \dots, m \end{aligned}$$

Obviously,

$$A V_m = V_{m+1} \overline{H}_m = V_m H_m + h_{m+1,m} v_{m+1} e_m^T \tag{7}$$

(2) Convergence analysis

Definition 2 Suppose that $A \in C^{m \times n}, X \in C^{n \times m}$, at the same time if Moore Penrose equations

$$\begin{cases} AXA = A, XAX = X \\ (AX)^H = AX, (XA)^H = XA \end{cases}$$

are established, then the matrix X is a pseudo inverse matrix of A .

Theorem 1 Suppose that $A \in C^{m \times n}$, and $A = BC$ is the maximum rank decomposition of A , then $X = C^H (CC^H)^{-1} (B^H B)^{-1} B^H$ is a pseudo inverse matrix of A .

Proof: For the matrix $X = C^H (CC^H)^{-1} (B^H B)^{-1} B^H$, since $A = BC, A \in C^{m \times n}$, we have

$$AXA = BCC^H (CC^H)^{-1} (B^H B)^{-1} B^H BC = BC = A,$$

$$XAX = C^H (CC^H)^{-1} (B^H B)^{-1} B^H BCC^H (CC^H)^{-1} (B^H B)^{-1} B^H$$

$$= C^H (CC^H)^{-1} (B^H B)^{-1} B^H = X,$$

Hereto, the first tow Moore Penrose equations are

established. The following is to verify the other two Moore Penrose equations:

$$\begin{aligned} (AX)^H &= [BCC^H(CC^H)^{-1}(B^HB)^{-1}B^H]^H \\ &= [B(B^HB)^{-1}B^H]^H \\ &= B(B^HB)^{-1}B^H = AX, \\ (XA)^H &= [C^H(CC^H)^{-1}(B^HB)^{-1}B^HBC]^H \\ &= [C^H(CC^H)^{-1}C]^H \\ &= C^H(CC^H)^{-1}C = XA \end{aligned}$$

From Definition 2, the matrix X is a pseudo inverse matrix of A . The proof is completed.

Corollary 1 Suppose that $A \in C^{m \times n}$ is a matrix with full column rank, then we have

$$A^+ = (A^H A)^{-1} A^H \tag{8}$$

Theorem 2 Suppose that r_m and r_{m+1} are the error vectors of the m and $m+1$ cycles, respectively, then we can obtain the following relationship.

$$\cos \langle r_m, r_{m+1} \rangle = \frac{\|r_{m+1}\|_2}{\|r_m\|_2}$$

Proof: For the VHGMRES(m) algorithm, when $m = m+1$, the subspace K_m becomes

$$K_{m+1} = \text{span}\{r_m, Ar_m, \dots, A^m r_m\}$$

Then the basis vectors $\{v_i\}_{i=1}^{m+1}$ and a Householder transform \bar{H}_{m+1} can be obtained, where $v_1 = \frac{r_m}{\beta}$,

$$\beta = \|r_m\|_2, \cos \langle r_m, r_{m+1} \rangle = \cos \langle v_1, r_{m+1} \rangle = \frac{v_1^T r_{m+1}}{\|r_{m+1}\|_2}$$

From Eq.(4), we can get the least squares solution $y_{m+1} = \bar{H}_{m+1}^+ (\beta e_1)$, $e_1 \in R^{m+2}$, where \bar{H}_{m+1}^+ is a real matrix with full column rank. According to Eq.(8), we have

$$\bar{H}_{m+1}^+ = (\bar{H}_{m+1}^T \bar{H}_{m+1})^{-1} \bar{H}_{m+1}^T$$

Then

$$y_{m+1} = (\bar{H}_{m+1}^T \bar{H}_{m+1})^{-1} \bar{H}_{m+1}^T (\beta e_1), e_1 \in R^{m+2} \tag{9}$$

On the other hand, we have

$$r_{m+1} = b - Ax_{m+1} = b - A(x_m + V_{m+1}y_{m+1}) = r_m - AV_{m+1}y_{m+1}$$

From Eq.(7), we have $AV_{m+1} = V_{m+2}\bar{H}_{m+1}$. Then we have

$$\begin{aligned} r_{m+1} &= r_m - V_{m+2}\bar{H}_{m+1}y_{m+1} = \beta v_1 - V_{m+2}\bar{H}_{m+1}y_{m+1}, \text{ so} \\ \|r_{m+1}\|_2^2 &= (\beta v_1 - V_{m+2}\bar{H}_{m+1}y_{m+1})^T (\beta v_1 - V_{m+2}\bar{H}_{m+1}y_{m+1}) \\ &= \beta^2 - \beta v_1^T V_{m+2}\bar{H}_{m+1}y_{m+1} - \beta y_{m+1}^T \bar{H}_{m+1}^T V_{m+2}^T v_1 \\ &\quad + y_{m+1}^T \bar{H}_{m+1}^T V_{m+2}^T V_{m+2} \bar{H}_{m+1} y_{m+1} \\ &= \beta^2 - \beta h^T y_{m+1} - (\beta y_{m+1}^T \bar{H}_{m+1}^T V_{m+2}^T v_1 \\ &\quad - \beta y_{m+1}^T \bar{H}_{m+1}^T V_{m+2}^T V_{m+2} \bar{H}_{m+1} (\bar{H}_{m+1}^T \bar{H}_{m+1})^{-1} \bar{H}_{m+1}^T e_1) \\ &= \beta^2 - \beta h^T y_{m+1} = \beta(\beta - h^T y_{m+1}) \end{aligned}$$

As the same time, because

$v_1^T r_{m+1} = v_1^T (\beta v_1 - V_{m+2}\bar{H}_{m+1}y_{m+1}) = \beta - h^T y_{m+1}$ (h^T indicates a vector formed by the first line elements in \bar{H}_{m+1}), we have

$$\cos \langle r_m, r_{m+1} \rangle = \frac{\beta - h^T y_{m+1}}{\sqrt{\beta(\beta - h^T y_{m+1})}} = \frac{\|r_{m+1}\|_2}{\|r_m\|_2} \tag{10}$$

The proof is completed.

Theorem 3 For the VHGMRES(m) algorithm, let $E = \|r_m\|_2$, $\bar{E} = \|r_{m+1}\|_2$, and then we have $\bar{E} < E$.

Proof: In Eq.(10), $\cos \langle r_m, r_{m+1} \rangle \leq 1$, namely,

$$\frac{\|r_{m+1}\|_2}{\|r_m\|_2} \leq 1. \text{ Because } h^T y_{m+1} \neq 0, \text{ we have}$$

$$\bar{E} = \|r_{m+1}\|_2 < \|r_m\|_2 = E \tag{11}$$

The proof is completed.

4. NUMERICAL EXPERIMENTS

In this section, two different numerical experiments are given to illustrate the validity and feasibility of the VHGMRES(m) algorithm.

Example 1 Consider the following linear equations:

$$Ax = b,$$

$$\text{where } A = \begin{bmatrix} 1 & 0.5 & & & 0.5 \\ & 0.5 & 2 & 0.5 & \\ & & \ddots & \ddots & \ddots \\ & & & 0.5 & n-1 & 0.5 \\ 0.5 & & & & 0.5 & n \end{bmatrix}_{n \times n}, b = \begin{bmatrix} 1 \\ \vdots \\ \vdots \\ 1 \end{bmatrix}_{n \times 1} \text{ Take an}$$

initial vector $x_0 = (0, \dots, 0)^T$ and an error limit $\varepsilon = 1e-6$. By using the GMRES (m) algorithm and the VHGMRES (m) algorithm, respectively, we can get numerical results for Eq. (12), as is shown in Figure 1.

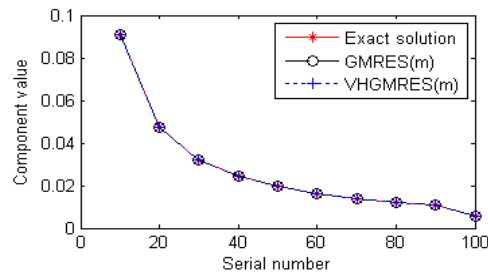
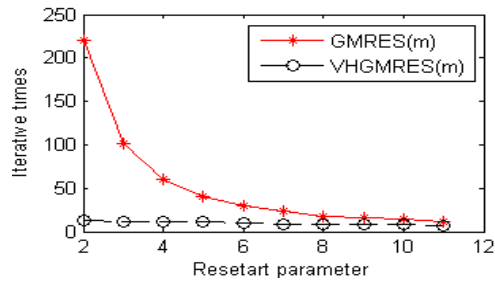


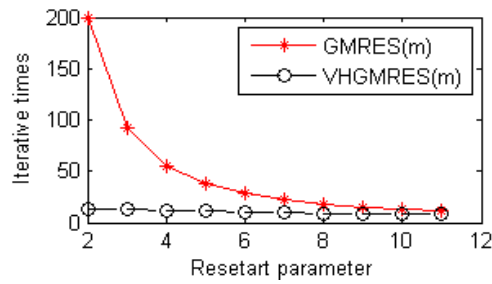
Figure 1. Computational results

From Figure 1, the numerical solution of the VHGMRES(m) algorithms is very close to the exact solution. Therefore, the VHGMRES(m) is correct and feasible.

Take the initial vectors $x_0 = (0, \dots, 0)^T$ and $x_0 = (1, \dots, 1)^T$, respectively. For the same parameter m and error limits ε , comparisons of computational efficiency and accuracy, as is shown in Figure 2, Table 1 and Table 2, respectively.



(a) $x_0 = (0, \dots, 0)^T$



(b) $x_0 = (1, \dots, 1)^T$

Figure 2 Comparison of the computational efficiency

Table1 Comparison of computational accuracy

m	4	6	8	10
GMRES(m)	8.17e-7	6.17e-7	9.63e-7	4.76e-7
VHGMRES(m)	2.12e-7	4.75e-7	1.11e-7	2.46e-7

Table2 Comparison of computational accuracy

m	3	5	7	9
GMRES(m)	9.37e-7	7.97e-7	8.62e-7	8.00e-7
VHGMRES(m)	1.58e-7	2.26e-7	1.26e-7	6.57e-7

From Figure 2, we can see that no matter how to select the restart parameter and initial vector, the iterative time of the presented algorithm is less than that of the GMRES(m) algorithm. And take the initial vectors $x_0 = (0, \dots, 0)^T$ and $x_0 = (1, \dots, 1)^T$, we can get Table.1 and Table 2. From the two tables above, we know the new algorithm is fast convergent with high precision.

5.CONCLUSIONS

In this paper, we discuss the fundamental theories of the VHGMRES(m) algorithm. Based on the Householder transform and GMRES(m) algorithm, we propose the VHGMRES(m) algorithm which can be used to solve many mathematical, mechanical and engineering problems. Through the theoretical proof, the new algorithm is proved to be fast convergent

with higher computational accuracy. Numerical experiments further show the algorithm not only has higher computational efficiency and accuracy, but it also has good stability.

ACKNOWLEDGMENT

The han nationality in our country elementary and middle schools body shape characteristics of the dynamic change rule and trend research - to 1995-2015 years students physique and health test report as the basis (14YBB027).

REFERENCES

[1] Bellalij, M., L. Reichel, and H. Sadok. Some properties of range restricted GMRES methods. Journal of Computational & Applied Mathematics, 290(2015):310-318.

[2] Yang B, Liu H, Chen Z, et al. GPU-Accelerated Preconditioned GMRES Solver[C]// IEEE, International Conference on Big Data Security on Cloud. IEEE, 2016:280-285.

[3] Matinfar M, Zareamoghaddam H, Eslami M, et al. GMRES implementations and residual smoothing techniques for solving ill-posed linear systems[J]. Computers & Mathematics with Applications, 2012, 63(1):1-13.

[4] Saad Y, Schultz M H. GMRES: a generalized minimal residual algorithm for solving nonsymmetric linear systems[J]. Siam Journal on Scientific & Statistical Computing, 2006, 7(3):856-869.

[5] Fiorikijni K, Iiyami K. Convergence of inner-iteration gmres methods for least squares problems[J]. Nii Technical Reports, 2015, 36(5):225-250.

[6] Essai A. Weighted FOM and GMRES for solving nonsymmetric linear systems[J]. Numerical Algorithms, 1998, 18(3-4):277-292.

[7] Ayachour E H. A fast implementation for GMRES method[J]. Journal of Computational & Applied Mathematics, 2003, 159(2):269-283.

[8] Najafi H S, Zareamoghaddam H. A Numerical Comparison of Two Different Implementations of GMRES Method[J].2011(8)

[9] Kyanfar F, Moghadam M M, Salemi A. Complete stagnation of GMRES for normal matrices[J]. Journal of Computational & Applied Mathematics, 2014, 263(8):417-422.

[10] Philippe B, Reichel L. On the generation of Krylov subspace bases[J]. Applied Numerical Mathematics, 2012, 62(9):1171-1186.

Color and Matter Concentration Identification based on Multiple Linear Regression

Ruiying Lou^{1,2}, Yanjing Du^{1,2}, Cuijuan Sun^{1,2}, Yang Han^{3,*}

¹ School of metallurgy and energy, north China University of technology, Tangshan city, Hebei province, China

² Engineering computing and simulation innovation laboratory, China

³ School of Science, North China University of Science and Technology, Tangshan 063210, China

*E-mail: 729420132@qq.com

Abstract: According to the experiment, the color readings of three substances at different concentrations were obtained, and the scatter plots were made to analyze the distribution trend of various material data points. The curve fitting was carried out with MATLAB software, and the variable Gray value was defined. The color readings were superimposed with MATLAB, and the color contrast images of three substances at different concentrations were obtained. The concentration function is related to H and S values by observing whether the color change is obvious. Secondly, linear regression analysis was carried out on the data of each group of substances with MATLAB, and the functional relationship between the concentration of three substances and the color reading was obtained. Finally, in order to ensure the accuracy of the results, the residual analysis of the relation function was performed to obtain the correlation coefficient comparison of three substances: urea in > histamine > milk, indicating that the fitting effect of aluminum potassium sulfate was optimal in the data of three substances used to fit the concentration function.

Keywords: Gray color model; multiple linear regression residual analysis; color dimension comparison

1. INTRODUCTION

Colorimetric method is a commonly used method to detect the concentration of substances.[1,2] Based on the experiment, the color readings of three substances at different concentrations were obtained, and a gray scale model was established for different substances.

2. STUDY ON THE RELATIONSHIP BETWEEN HISTAMINE CONCENTRATION AND COLORREADING

The correlation analysis of histamine concentration and color readings was carried out by MATLAB, and the fitting curve shown in Fig.1 was obtained. According to Figure 1, there is a negative correlation between material concentration and color reading.

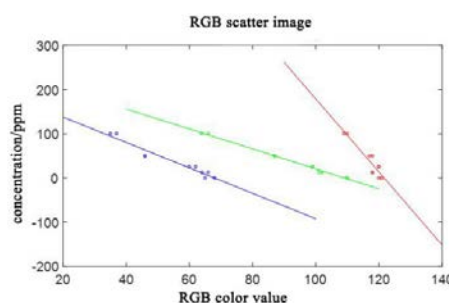


Figure 1 Scatterplot of histamine solution

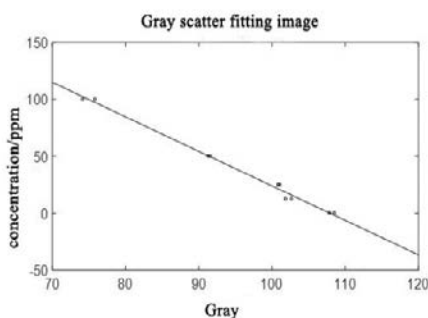


Figure 2 Gray scatter fitting images of histamine

In order to obtain the concentration of the substance directly according to the color reading, the Gray color model was established. Describe the RGB data points by defining the variable Gray. Fig.2 is a color chart synthesized by using RGB channel of MATLAB. Because histamine varies dramatically in different concentrations, the effect of tone and saturation on histamine concentration function is not considered.

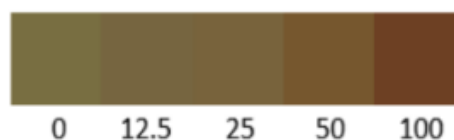


Figure 3 Color comparison of different concentrations of histamine

Set up the Gray model of RGB and obtain the following equation

$$gray = 0.299R + 0.587G + 0.114B$$

The Gray scatter fitting image of fig.3 histamine was obtained by MATLAB fitting. According to the image,

there was a linear relationship between histamine concentration and Gray value. According to the linear relation of equation (1), the regression analysis of histamine[3] fitting curve was conducted with MATLAB, and the linear function relation between histamine concentration and color reading was obtained.

$$\hat{y} = -3.0337x + 327.4322 \quad (x = \text{gray})$$

The obtained functions are tested by regression

$R^2 = 0.9926, F = 1070.8, P = 0.0000, S^2 = 11.5870$, R^2 Close to 1, so the regression line fits well with the observed value of the sample. The value is F much larger than the critical value; Significantly P smaller than the significance level of 0.05, S^2 larger, reflecting the large deviation degree between the data of this group and its average value. Generally speaking, there is a dominant linear relationship between the random variable and the explanatory variable.

Secondly, the data points of histamine were analyzed using MATLAB again based on the linear function relationship between concentration and color reading. The results are shown in Figure 4.

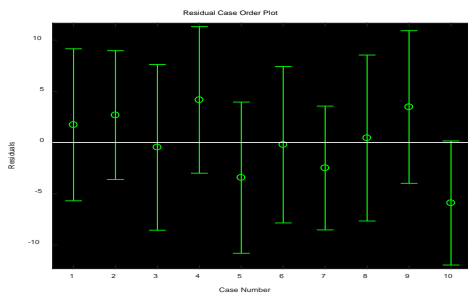


Figure 4 Residual analysis of histamine

According to the time series residual map, the residual value falls in the $y = 0$ zonal region with the central axis, so there is no singular point, which satisfies the regression model.

2THE RELATIONSHIP BETWEEN ALUMINUM POTASSIUM SULFATE CONCENTRATION AND COLORREADING

In order to facilitate the measurement of aluminum potassium sulfate concentration and color reading, the experimental data of six concentrations of aluminum potassium sulfate were averaged, as shown in Table 1. Table 1 Mean value data of aluminum and potassium sulfate

concentration /ppm	R	G	B	H	S
0.0	104	125	115	75	43
0.5	59	115	140	99	147
1.0	54	116	145	99	161
1.5	47	115	153	100	175

2.0	37	107	160	103	196
5.0	39	109	154	101	189

The color model of Gary was established. Gary values were the same as 1.1. Figure 5 was obtained by using MATLAB color channel superposition. Regression was performed on Gray value, tone H, saturation S and concentration C, as shown in figure 5.

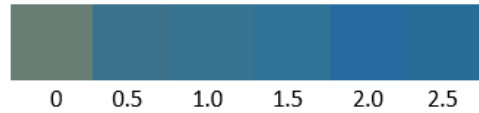


Figure 5 Color contrast of aluminum and potassium sulfate at different concentrations

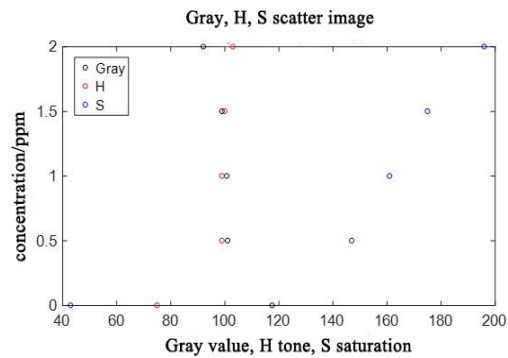


Figure 6 Scatterplot of aluminum potassium sulfate concentration

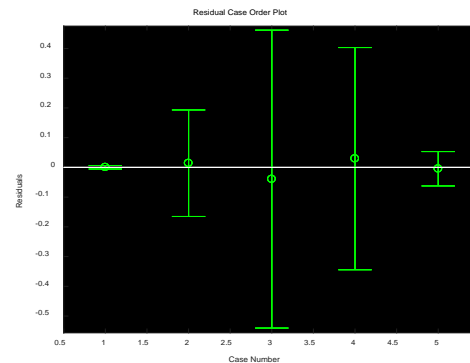


Figure 7 Residual analysis of aluminum potassium sulfate

Observation of figure 6 shows that there is no obvious linear relationship between Gray, tone H, saturation S and concentration, and the fitting function is

$$Z = 15.1199 - 0.0338\text{gray} - 0.1708H - 0.0387S$$

The regression test was performed on the function $R^2 = 0.9989, F = 315.4285, P = 0.0414 < 0.05, S^2 = 0.0026$, R^2 Close to 1, the

regression line fit well with the observed value of the sample. The value is F much larger than the critical value; P far less than the significance level of 0.05; S^2 is very small, reflecting the small deviation of the reconstructed data and its mean value, indicating that there is an explicit linear relationship between the random variable y and the explanatory variable.

The results are shown in Figure 7. The residual value falls in the zonal region with the central axis, so there is no singular point, which satisfies the regression model.

3. STUDY ON THE RELATIONSHIP BETWEEN UREA CONCENTRATION AND COLORREADING IN MILK

According to the experimental results, three groups of experimental data of urea in milk were obtained. MATLAB was used to draw the scatter diagram, as shown in Figure 8.

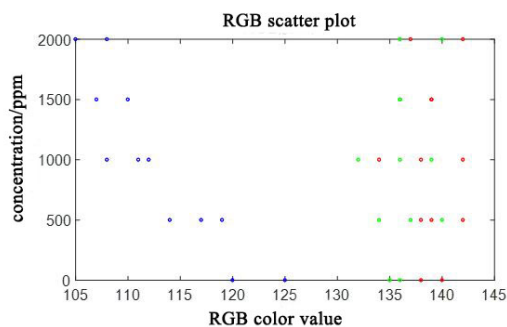


Figure 8 Scatter diagram of urea in milk

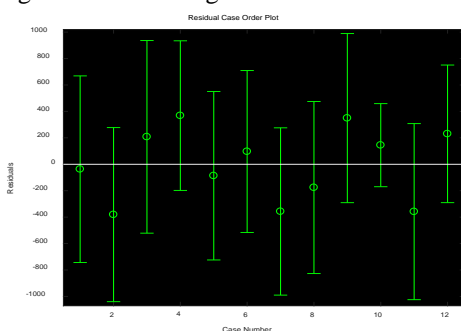


Figure 9 Residual analysis of urea in milk

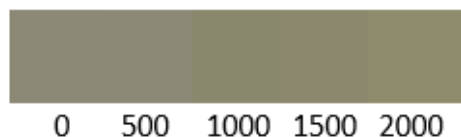


Figure 10 Color contrast of urea in different concentrations of milk

Since the color change in figure 9 obtained by MATLAB color channel superposition is not obvious,

the concentration function needs to consider the hue H and saturation S, and the fitting function is

$$Z = 3336.9 - 34.1331\text{gray} - 26.7049H - 61.9521S$$

The regression test was performed $R^2 = 0.8423, F = 14.2386, P = 0.0014 < 0.05, S^2 = 103110$, R^2 close to 1, the regression line fit well with the observed value of the sample. The value is F much larger than the critical value; P far less than the significance level of 0.05; S^2 is very large, reflecting the large deviation between the reconstructed data and its mean value, but generally there is a linear relationship between the random variable and the explanatory variable.

The residual analysis of the function is carried out, and the result is shown in Fig.10. The residual value falls in the zonal region with the central axis, so there is no singular point, which satisfies the regression model.

The correlation coefficients of the concentration functions of histamine, aluminum potassium sulfate and urea in milk were compared R^2 , Aluminium potassium sulfate > histamine > In the milk urea.

The results indicated that the data of aluminum and potassium sulfate was the best and the data of urea in milk was the worst to fit the concentration function.

REFERENCES

- [1]Shen jichen, Wang xueqing, Liu bangli, Zhang weihong. Study on determination of concentration of colored solution based on image colorimetry [J]. Optical instrument,2008(02):9-12.
- [2]Liu rui, Yang ruiqin, Chang guanqun. Determination of colored solution by image colorimetry [J]. Physical and chemical testing (chemistry),2014,50(11):1348-1350.
- [3]Mei changlin, Zhang wenxiu. Testing linear regression relation by local weighted fitting method. System science and mathematics, 2002(04):467-480.

Protective Clothing Problem based on Bidirectional Unsteady Heat Conduction

Tian zhou Zhang¹, Xin Rui Wang², Ke Xin Yu², Bin Bai^{3,*}

¹Engineering computation and simulation Innovation Laboratory, Tangshan 063210, China

²Mathematical Modeling Innovation Lab, North China University of Science and Technology, Tangshan 063210, China

³School of Science, North China University of Science and Technology, Tangshan 063210, China

*E-mail: 956201990@qq.com

Abstract: Thermal protective clothing is the most widely used special protective clothing. Based on the whole heat conduction model from thermal insulation clothing to dummy skin in high temperature environment, a multi-objective nonlinear programming model is successfully established, and the optimal thickness of each thermal insulation layer is obtained.

Keywords: Protective clothing problem; Bidirectional unsteady; Heat conduction

1. INTRODUCTION

Based on the steady-state heat transfer, the boundary temperatures of the four layers are calculated to be 25, 25.31, 26.00 and 29.40 degrees respectively when the external temperature is 25 degrees centigrade. Then, the inhibiting effect of the human body temperature on the heat transfer is neglected. Based on the principle of unsteady-state heat conduction, the intelligent calculation is used. The temperature distribution in each layer of the fabric layer is obtained preliminarily by using the method, and the temperature distribution in the final fabric layer is obtained by modifying the temperature distribution of the human body (the first layer is dominated by the external environment) when the temperature of the thermal insulation clothing is too high. In this way, the temperature distribution of the second and third layers of the fabric is obtained respectively, which is specific to problem1. The first layer is the worst, the second layer is the best, and the third and fourth layers are between I and II. Finally, BP neural network is used to verify the results of fabric layer temperature distribution, and it is found that the fabric layer temperature distribution is close to the actual situation.

2. ESTABLISHMENT AND SOLITION OF THE QUESTION

2.1 Solution of initial temperature

When a dummy wears a thermal-insulated suit and is in a normal temperature environment of 25 degrees Celsius, the temperature of the dummy remains at 37 degrees Celsius, and the environment-insulated suit-dummy model can be established. After a long

time, the temperature of the thermal-insulated suit does not change with time. Therefore, the temperature of the thermal-insulated suit is determined as a steady-state heat conduction process. The initial temperature of the contact layer between the four layers is obtained through the heat conduction at both ends.

The basic law of heat conduction is in accordance with Fourier law:

$$Q = -\lambda \text{grad}t = -\lambda \frac{\partial t}{\partial n} n \quad (1)$$

In steady state heat conduction, the heat conduction rate Q does not change with time. When the heat transfer area is A and the heat conduction resistance is R , the heat conductivity λ and the thickness X of each layer are known.

among them:

$$R = x / \lambda A$$

t_i is the junction temperature of each two layers. ($i=1, \dots, 5$), $t_1=25^\circ\text{C}$, $t_5=37^\circ\text{C}$.

Improved Fourier formula:

$$Q = \frac{t_a - t_b}{x / \lambda A} = \frac{\Delta t}{R} \quad (2)$$

Therefore, the improved Fourier formula is used to calculate the temperature of t_2 , t_3 and t_4 in 1m2.

The heat conduction rate is 42.54w, the temperature at the junction of each layer is $t_2= 25.31^\circ\text{C}$, $t_3= 26^\circ\text{C}$, $t_4= 29.40^\circ\text{C}$.

2.2 Solution of initial temperature

(1) One dimensional unsteady heat conduction of a semi-infinite thick body under the first boundary condition

For a plane wall with finite thickness, the theoretical formula of a semi-infinite body can be applied as long as the other side of the plane wall is not affected by the heating.

The temperature is not only a function of location, but also related to time, it is determined to be unsteady heat conduction.

The heat transfer is perpendicular to the skin direction, it can be regarded as one-dimensional.

From the data in Appendix 2, the temperature variation of the skin surface at any time can be

obtained, which conforms to the first boundary condition, that is, the temperature variation of each boundary of an instantaneous object on a given boundary with time:

$$t = f(x, y, z, \tau) \quad (3)$$

In the process of heat transfer, when the temperature on the boundary is constant, the temperature on the boundary is known. That is

$$t = Const \quad (4)$$

Next, we take the semi infinite object shown in figure 1 as the object of discussion.

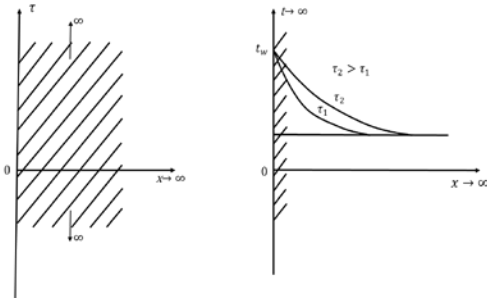


Figure 1 Temperature of a semi-infinite thick body after temperature jump

One dimensional unsteady heat conduction differential equation with constant physical properties and no internal heat source is considered:

$$\frac{\partial t}{\partial \tau} = a \frac{\partial^2 t}{\partial x^2} \quad (5)$$

The condition of solution is:

$$\tau = 0, \quad 0 \leq x < \infty \quad t = t_0 \quad (6)$$

$$\tau > 0, \quad \begin{cases} x = 0 & t = t_w \\ x \rightarrow \infty & t = t_0 \end{cases} \quad (7)$$

The Laplace transform is usually used to solve the problem, and the transformation formula is:

$$\Delta \mu = \frac{\partial^2 \mu}{\partial x^2} + \frac{\partial^2 \mu}{\partial y^2} = 0 \quad (8)$$

Solution:

$$\frac{t_w - t}{t_w - t_0} = erf\left(\frac{x}{2\sqrt{a\tau}}\right) = erf\left(\frac{1}{2\sqrt{Fo}}\right) \quad (9)$$

$$erf\left(\frac{x}{2\sqrt{a\tau}}\right) = \frac{2}{\sqrt{\pi}} \int_0^{\frac{x}{2\sqrt{a\tau}}} e^{-\xi^2} d\xi \quad (10)$$

Then

$$t = t_1 - erf\left(\frac{x}{2\sqrt{a\tau}}\right)(t_1 - t_2) \quad (11)$$

among them:

$$a = \frac{\lambda}{\rho c} \quad (12)$$

a is the mean value of heat transfer coefficient, Formula (10) is a Gaussian error function, ξ is a virtual variable, and the result of the integral is a function of its upper limit. The value of the integral can be obtained from the Gaussian error function table.

The Gauss error function table can be used to calculate the temperature at x distance from the heating surface at τ time.

(2) One dimensional unsteady heat transfer in fabric layer

According to the Gauss error function table,

when $\frac{x}{2\sqrt{a\tau}} = 3$, $\frac{t_1 - t}{t_1 - t_0} \approx 1$, it indicates that at the moment of τ , the temperature at x has not changed yet, which is still the initial temperature t_0 , and the distance that the temperature inside the wall begins to change after τ time is:

$$x = 4\sqrt{a\tau}$$

Thus, when the thickness of a finite body is $\delta = 4\sqrt{a\tau}$, the approximate solution of a semi-infinite body can be obtained, and the error caused by this solution is very small.

The bi-directional analysis of each layer of fabrics should take into account both the warming effect of high temperature environment on clothes and the inhibiting effect of human body on fabric materials at 37°C.

a) Preliminary analysis of temperature distribution in fabric layer

Because the first layer fabrics are directly in contact with the external temperature of 75°C, the influence of 75°C is the greatest, and the human body temperature can hardly affect the I layer temperature, so the inhibition of human skin on the first layer temperature is neglected.

The solution of the temperature distribution of the second layer fabric layer is transformed into one-dimensional unsteady heat conduction of a semi-infinite thick body under the first boundary condition. For the second layer fabrics, the

temperature on the left side of the layer is t_2 , and the heat on the left will heat up the right side through heat transfer, and the temperature will be t_3 .

Therefore, the left temperature t_2 is taken as the external temperature of the left side of the third layer

fabric, and t_3 is used as the external temperature of t_4 on the left side of the fourth layer fabric.

$t_1 = 75^\circ\text{C}$, $t_2 = 25.31^\circ\text{C}$ The limit value of first layers of fabric thickness, $x = 0.6\text{mm}$ The temperature distribution of layer fabric is obtained by MATLAB. As shown in figure 2, the temperature rises rapidly to 42.25°C in 0-1 seconds, to 74°C in 1426 seconds, and then to 74.49°C in 5400 seconds, which is close to the outside temperature.

The temperature distribution of layer III and IV is obtained by using the same method. As shown in

figure 2.

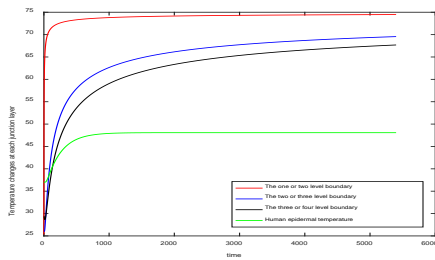


Figure 2 Boundary temperature distribution before correction

b) Further correction of temperature distribution in fabric layer

Then, considering the inhibiting effect of human body temperature on the temperature of thermal insulation clothing, the temperature distribution of fabric layer is further corrected.

When the temperature of the fabric or air is higher than that of the human body, the human body temperature will inhibit it. It is necessary to modify the right boundary temperature distribution of the second and third layers (the first layer is dominated by the external environment). Human body temperature is in direct contact with air, so the improved air temperature distribution with human body temperature suppression is calculated by using MATLAB firstly.

In the improved temperature distribution, it can be seen from figure 3 that the temperature of air layer in 1s rises from 29.40 to 32.95°C, the temperature of air layer in 1496s reaches 48.27°C, and the temperature of human body is lower than that of air layer, which makes the temperature of air layer decrease gradually until 5400s to 48.23°C, which is close to 48.08°C.

Finally, the temperature distribution of the improved air layer (the right boundary of the third layer) is taken as the outer temperature of the right boundary of the second layer. The temperature distribution of the corrected right boundary of the second layer is obtained by improving the temperature distribution of the improved air layer (the right boundary of the third layer). As shown in figure 3, the temperature gradually increased to 49.74°C from the initial 26°C, and then decreases gradually by inhibiting the temperature of the human body. The temperature is 49.22°C, slightly higher than the air layer temperature.

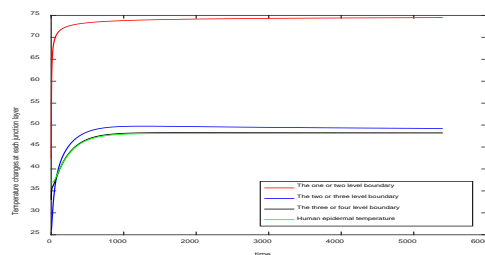


Figure 3 Boundary temperature distribution after correction

c) Temperature distribution of fabric layer

As can be seen from figure 3, Layer I has the worst heat insulation effect, almost no heat insulation effect, After 90 minutes, the temperature of Layer II is only 49.22°C, Layer II has the best heat insulation effect, after the third layer insulation, the temperature dropped by 1 degrees. The temperature of the air layer is very close to that of the surface layer of the human body, so the heat insulation effect of the second layer is the best. As shown in figure 4, the temperature distribution pattern for each fabric is corrected.

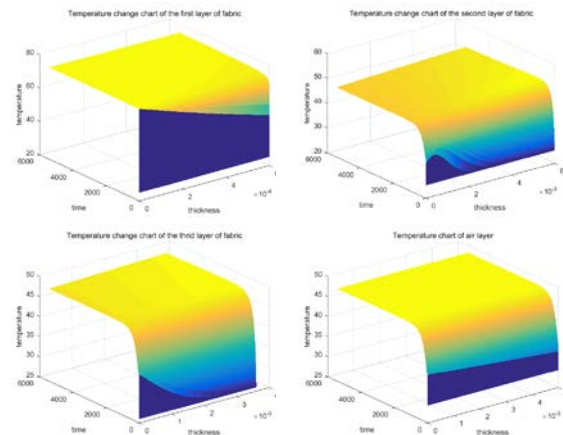


Figure 4 Temperature distribution of each fabric layer after correction

d) Result accuracy check

In order to verify the accuracy of the temperature distribution, we fit the human body temperature based on BP neural network. By comparing the fitted human body temperature change with the real temperature change, we evaluate the accuracy of the temperature distribution of each layer of the thermal insulation clothing.

Temperature distributions at the boundaries of each fabric layer (t_2 , t_3 , t_4) are taken as input layer, human body surface temperature as output layer, 75% of the total sample number as training set sample, and the rest as test data. Three-layer BP neural network with only one hidden layer can approximate any nonlinear function. Therefore, this group selects single hidden layer BP neural network and S-tangent function tansig as the excitation function of hidden layer neurons. The number of hidden layer neurons has a great influence on the network performance, so the following empirical formulas are used to select the number of hidden layers:

$$N = \sqrt{m(n+2)} + 1 \tag{13}$$

among them:

- N — Number of hidden layer nodes,
- m — Number of input nodes,
- n — Number of nodes in output layer, m=3, n=1.

Error analysis of the data shows that the root mean square error is 1.67×10^{-3} , very close to zero,

indicating that the temperature distribution is close to the actual situation, with good persuasion, can accurately and truly reflect the temperature changes of each fabric layer.

REFERENCES

- [1] Jianhua Xiong, Hong Dai, Fen Luo, Shuliang Ding, Wenyi Wang. Estimation of Unknown Parameters in Graded Response Model by Back-propagation Neural Network. *Psychosocial Science*, 2014, 37(06):1485-1490.
- [2] Dongmei Huang, Song He. Influence of air gap position on heat insulation performance of firefighters' protective clothing. *Journal of textile*, 2015, 36(10):113-119.
- [3] Linzhen Lu. Mathematical model of heat transfer within multilayer thermal protective clothing and corresponding optimal parameter determination. Zhejiang Sci-Tech University, 2018.
- [4] Bin Pan, Jingxian Yu, Na Yi. Mathematical modeling course, Beijing: Chemical Industry Press, 2016.10.
- [5] Chong Tang. Nonlinear Programming Problem Solution Based on Matlab. Computer and digital engineering, 2013, 41(07):1100-1102+1185.
- [6] Lijia Xu, Jiong Mu, MATLAB programming and Application. tsinghua university press, 2011.
- [7] Bin Pan. Mathematical modeling of heat transfer within thermal protective clothing and inverse problems of parameters determination. Zhejiang Sci-Tech University, 2017.
- [8] Dinghua Xu, Yuanbo Chen, Xiaohong Zhou. Type design for bilayer textile materials under low temperature: Modeling, numerical algorithm and simulation. *International Journal of Heat and Mass Transfer*, 2013, 60.
- [9] Dinghua Xu, Peng Cui. Simultaneous determination of thickness, thermal conductivity and porosity in textile material design. *Journal of Inverse and Ill-posed Problems*, 2016, 24(1).
- [10] Jussila Kirsi, Valkama Anita, Remes Jouko, Anttonen Hannu, Peitso Ari. The effect of cold protective clothing on comfort and perception of performance. *International Journal of Occupational Safety and Ergonomics*, 2010, 16(2).
- [11] Yishen Shen. Fundamentals of metallurgical transport principle. Beijing: Metallurgical industry press, 2003.

Accurate Treatment of Diabetes based on Big Data

Ding Zhang^{1,2,*}, Ju'an Ma^{1,3}, Bingxue Kang^{1,4}, Xu Zhou^{5,*}

¹Engineering Computing and Simulation Innovation Lab, Tangshan, 063200, China

²Innovation experiment Base of North China University of Science and Technology, Tangshan, 063200, China

³College of Metallurgy, North China University of Technology, Tangshan, 063200, China

⁴School of Architectural Engineering, North China University of Technology, Tangshan, 063200, China

⁵School of Science, North China University of Science and Technology, Tangshan 063210, China

*E-mail:625525957@qq.com

Abstract: The management and control of blood glucose level in diabetic patients play an important role in reducing morbidity and mortality, but most medical institutions are more casual in management. Therefore, it is necessary to analyze and evaluate the treatment model of diabetes patients in existing hospitals.

Keywords: Diabetes mellifluous logit; Statistical analysis; Correlation analysis

1. INTRODUCTION

Controlling the blood sugar level of inpatients plays an important role in reducing morbidity and mortality. Many medical institutions strictly control the blood sugar of ICU grade inpatients in intensive care unit, but most non-ICU inpatients do not. According to the traditional management, the management of inpatients is more casual, resulting in no treatment or changes in blood sugar. In order to improve the safety of patients, it is necessary to analyze and evaluate the treatment mode of diabetes patients in existing hospitals. A reasonable evaluation index system was established to evaluate the therapeutic effect of diabetes patients in hospitals. Data processing Preprocessing, deleting invalid and useless data, grouping all kinds of diseases, and getting the range of diagnostic value of each group and the percentage of the number of patients in each group to the total number of patients. The probability distribution of HbA1C test, sex, age, race, place of discharge, source of admission, length of stay, specialty of clinician, initial diagnosis result, glucose serum test, etc. Readmission rate and confidence interval of all patients.

2. ANALYSIS OF THE TREATMENT PATTERN OF DIABETES MELLIFLUOUS IN HOSPITALS

2.1 Analysis of variance

The two indexes of A1Cresult value and readmitted value of diabetes patients treated in hospital were selected to analyze emphatically, and the data of this part of hospitals in the United States were screened and processed. According to the analysis results of these two indexes, the therapeutic effect of diabetes mellifluous in hospital was evaluated simply. The

A1Cresult value of diabetic patients was different from that of normal subjects. A1Cresult was detected in patients with diabetes treated in hospital.

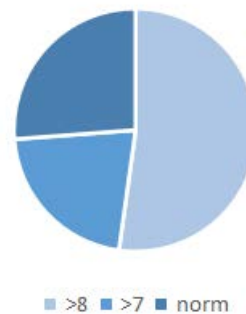


Figure 1 A1Cresult value test

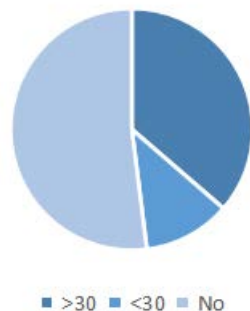


Figure 2 readmitted value percentage chart

Through analysis, we can know that after hospital treatment, norm accounts for a large part of A 1 C result, which shows that the result of hospital treatment is effective. According to the analysis of readmitted, the readmission of diabetic patients was divided into three types: no readmission, within 30 days and after 30 days. From the analysis of A1Cresult and readmitted in Fig. 1 and 2, it is obvious that hospital treatment has certain curative effect on diabetic patients. Collect hospital data, do a simple screening of the data, and group patients according to icd9 code, as in Table 1.

Table 1 grouping tables coded according to icd9

	The basic situation of ICD-9 coded list grouping
001-139	Infectious and parasitic diseases
140-239	Neoplasm
240-279	Endocrine, nutritional, metabolic and immune diseases
280-289	Diseases of blood and hematologist organs
290-319	Lunacy
320-359	Nervous system disease
360-389	Sensory organ disease
390-459	Circulation system disease
460-519	Disease of respiratory system
520-579	Digestive system disease
580-629	Disease of the genitourinary system
630-676	Pregnancy, childbirth and postpartum complications
680-709	Skin and subcutaneous tissue diseases
710-739	Musculature system and connective tissue diseases
740-759	Congenital monstrosity
760-779	Perinatal conditions
780-799	Symptoms and unknown conditions
800-999	Injury and poisoning
E and V codes	Trauma and supplementary classification

According to the classification of the disease types of the patients in Table 1, the percentage of the patients of each type is calculated, the probability distribution of the patients is drawn, and the percentage of the icd9 coding range of each group is shown in figure 3.

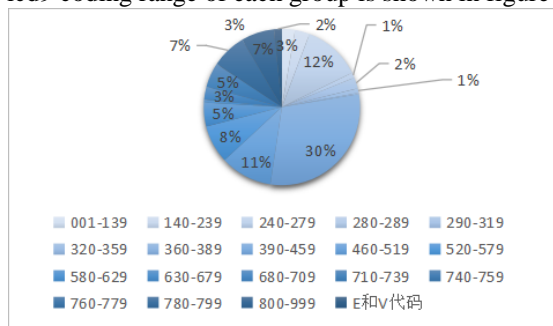


Fig. 3 percentage of icd9 coding range for each block
 2.2 Probability distribution of characteristic variables
 After the invalid data were deleted, the patients diagnosed as diabetes mellifluous were counted, and their characteristic variables were analyzed one by one, and then the probability distribution of characteristic variables was analyzed more intuitively. Figure 4 and figure 5 are HbA1C detection distribution map and race distribution map respectively. The characteristic variables of HbA1C detection results are statistically analyzed. In order to see the ratio of each item more intuitively, the percentage distribution map of characteristic variables

is drawn.

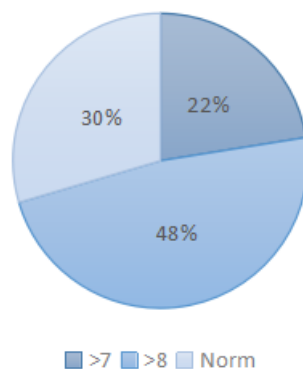


Fig. 4 HbA1C detection and analysis diagram

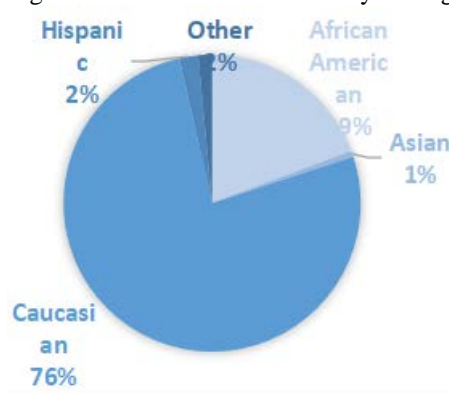


Fig. 5 ethnic distribution map

The population of diabetic patients in the data was counted, and the percentage of adult species was plotted as a percentage of the total population. The glucose serum of diabetic patients is an important basis for diabetic patients. The detection value of glucose in serum of diabetic patients is counted and the percentage of each value to the total value is analyzed.

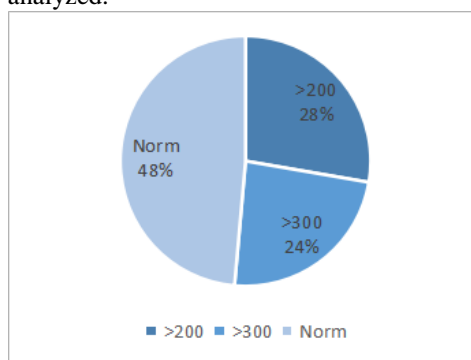


Fig. 6 Evaluation of therapeutic effect

3. EVALUATION OF THERAPEUTIC EFFECT

3.1 Readmission rate and its confidence interval
 Patients were grouped according to icd9 code, and the readmission rate and confidence interval were analyzed. After preliminary processing of the data, the patients were divided into groups according to the type of disease. SPSS was used to describe the group data. The confidence interval of all patients was 95, the revised average value was 5, the upper and lower

limits of the data trust interval were 95%, and the median and variance of each patient were obtained, respectively. Standard deviation, maximum, minimum, range, internal quartile, deflection, Kurtis, etc. Table 2, that is, the readmission rate and confidence interval of all types of patients, can be obtained.

Table 2 confidence intervals and readmission rates

	Confidence interval of the mean:95%	Confidence interval of the mean:5%
001-139	43.0%-55.0%	49.0%
140-239	38.0%-50.0%	43.0%
240-279	23.0%-33.0%	26.0%
280-289	53.0%-65.0%	60.0%
290-319	37.0%-49.0%	42.0%
320-359	31.0%-43.0%	36.0%
360-389	35.0%-46.0%	39.0%
390-459	44.0%-56.0%	50.0%
460-519	39.0%-51.0%	44.0%
520-579	33.0%-45.0%	37.0%
580-629	41.0%-69.0%	55.0%
630-676	13.1%-37.9%	22.8%
680-709	25.3%-53.1%	38.0%
710-739	41.0%-69.0%	55.0%
740-779	18.0%-45.0%	29.0%
780-799	43.0%-71.0%	58.0%
800-999	13.0%-38.0%	23.0%
E and V codes	13.0%-38.0%	23.0%

With regard to the study of various aspects of diabetes treatment, we have received a series of conclusions about the treatment of diabetes and readmission and related, from which we can see the number of outpatient visits, the number of emergencies, the number of hospitalizations, and the number of diagnosis is positively correlated; it is also clear that the hospitalization time and the age are positively related to the readmission rate, so that we consider reducing the readmission rate and improving the efficiency of the treatment, Reducing the patient's hospitalization costs should be analyzed and explored from a number of angles.

3.2 Effect of body weight on diabetes mellitus

The weight of patients with diabetes has a significant impact on the condition of the disease. By consulting relevant information and literature, it can be concluded that weight plays a significant role in the patients with diabetes, and for patients with type 2 diabetes, If obesity results in the accumulation of visceral fat, the harm is obvious: the more fat, the less sensitive insulin is, so weight control is particularly important in type 2 diabetics.

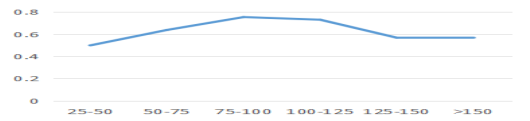


Fig. 7 weight distribution

From the statistical analysis of body weight data, we can get figure 19. Obviously, the effect of weight on the readmission rate of diabetic patients is 75-125. The effect of body weight on the readmission rate of diabetic patients was not increased when the weight was greater than a certain value. The analysis and evaluation of the treatment model of diabetes patients in existing hospitals can be applied to the analysis and evaluation of other types of diseases.

4. CONCLUSION

- (1) The detection of HbA1C should be popularized, and it is possible to better detect and treat diabetes, and reduce the admission rate;
- (2) Targeted treatment should be carried out for patients of different ages, and the emphasis on middle-aged and elderly people should be increased, and the rate of re-admission of middle-aged and elderly people should be further reduced;
- (3) Relevant drugs and dosages for the treatment of diabetes should be evaluated to minimize the loss of patients due to the drugs used;
- (4) It is necessary to pay attention to the mental health of patients. In the process of treatment, patients will have various problems during the process, which will increase the rate of re-admission, and further increase the cost of admission.

REFERENCES

- [1] Yang Yu. Analysis of big data in the diagnosis and treatment of Diabetes Mellitus. Computer knowledge and Technology 2018 (20): 14-15.
- [2] Li Jing, Li Zheng Xi Marie Nolan, Zhao Weigang, Dong Ying Yue. Research progress of psycho-social factors affecting self-management of diabetic patients. Chinese Journal of Nursing! 49 (02): 207-211.
- [3] Yuan Xiaodan, Lou Qingqing, Zhang Danyu, Yao Ping, Shen Jingxuan. Progress in the study of diabetic case management model. Chinese Journal of Nursing! 48 (01): 84-86.
- [4] Chang Zhiyun, Fan Ling, Sun Kan. Current status of Diabetes Mellitus treatment and Diabetes Education. Medicine and philosophy (Clinical decision Forum Edition) 2006 (03): 16-18.
- [5] Kirstine Brown Frandsen. Present situation of management of diabetes treatment. Foreign medicine. Endocrinology Credit Book 2005 (03): 172-173.
- [6] American Diabetes Association. Psychosocial factors affecting adherence, quality of life, and well-being: helping patients cope[M]//Kaufman FR. Medical Management of Type 1 Diabetes-5th ed. Virginia: American Diabetes Association, 2008:173-193.

Discussion on the Relationship between Substance Concentration and Color Reading

Siyu Zhai^{1,2}, Chaoqun Ma^{1,2}, Zhenling Tang^{1,2}, Lijing Feng^{3,*}

¹Mathematical Modeling Innovation Lab, North China University of Science and Technology, Tangshan 063210, China

²North China University of Science and Technology, Tangshan, 063200, China

³School of Science, North China University of Science and Technology, Tangshan 063210, China

*E-mail:785926222@qq.com

Abstract: This study deals with the relationship between the concentration of matter and the color reading. Depending on the concentration of the substance, the color readings vary. Therefore, a comprehensive variable x , which can represent the change of all color indexes, is introduced to analyze the change of substance concentration. The existing experimental data are divided into model construction group and model checking group according to 3:1 scale. Using the data in the model group to fit the matter concentration with the least square method, the function analytic formula of the matter concentration and the comprehensive influence factor “ x ” is obtained. Finally, the residual error of the model is calculated by using the data in the model checking group. The total residual value was only 4.83% of its own concentration. Therefore, the model is stable and reliable.

Keywords: Color reading; Material concentration; Lagrange interpolation; Least square method

1. INTRODUCTION

In our daily life, people measure the concentration of substances commonly used colorimetric method. Colorimetric method is to determine the content of the component to be measured by comparing or measuring the color depth of the colored material solution. This method is simple and clear, but because each person's color sensitivity and people in the observation will produce some unavoidable error, so this method has a greater impact on precision. With the improvement of photographic technology and color resolution, the accuracy of colorimetric method is increasing, and people can even get the concentration of the substance to be measured by the color reading in the photograph.

2. IMAGINE

With the improvement of photographic technology and color resolution, the accuracy of colorimetric method is also increasing. People can even get the concentration of the substance to be measured by the color reading in the photograph. Now it is planned to establish the relationship model between the color reading of the substance and its corresponding

concentration, and link the relationship between the two by using the functional relationship, and model. Make the necessary error analysis. The specific process is shown in Figure 1.

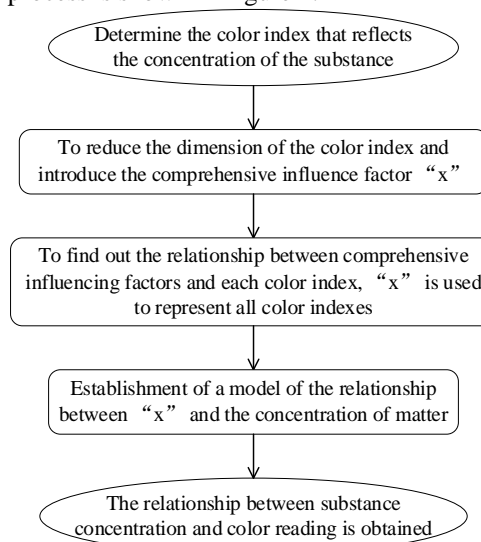


Figure 1 The specific process

3. “X” AND EACH COLOR INDEX

In order to explore the relationship between the concentration of substances and the indexes, 25 groups of data were randomly extracted with random function. The results required a group of data with different concentrations, which would be used as test data. The rest of the data builds group data as a model. The correlation coefficient between the concentration and the indexes was calculated by python programming from 18 groups of data in the constructed group, and the specific results are shown in Table 1.

Table 1 Correlation coefficient between concentration and each index

color index	R	G	B	S	H
correlat					
ion	-0.844	-0.867	0.695	-0.149	0.829
coeffici	46	29	983	53	821
ent					

The influence factor “ x ” is introduced to express the

influence of five color readings on the concentration of SO₂ solution. The specific relation is as follows:

$$x = -0.831R - 0.854G + 0.738B - 0.256S + 0.825H (x > -170) \quad (1)$$

4. "X" AND SUBSTANCE CONCENTRATION

Because the comprehensive influencing factor is related to the five color indexes, it is only necessary to seek the relationship between the comprehensive influencing factor and the concentration of the matter to express the influence of each color index on the concentration of the substance. In this subject, the least square method is used to fit the relationship between the comprehensive influence factor and the concentration of matter.

$$y = a_0 + a_1x \quad (2)$$

$$a_0 = \frac{\sum_{i=1}^n x_i^2 \sum_{i=1}^n y_i - \sum_{i=1}^n x_i \sum_{i=1}^n x_i y_i}{\sum_{i=1}^n x_i^2 - (\sum_{i=1}^n x_i)^2} \quad (3)$$

$$a_1 = \frac{\sum_{i=1}^n x_i y_i - \sum_{i=1}^n x_i \sum_{i=1}^n y_i}{\sum_{i=1}^n x_i^2 - (\sum_{i=1}^n x_i)^2} \quad (4)$$

According to the random selected number of groups, the numerical value of the comprehensive influence factors is calculated, and the scattered plot between the total influencing factors and the concentration is made, and it is found that the concentration decreases first and then rises.

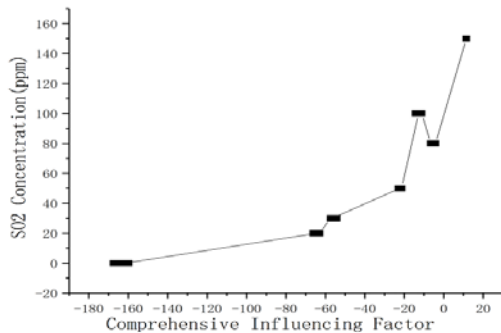


Figure 2 The trend of sulfur dioxide with Synthetical

Table 2 The data of the remaining seven groups, the result of solution and the result of residual error

Concentration(ppm)	R	G	B	S	H	Solution result	Residual result
0	153	146	158	137	20	-1.13	1.2769
20	144	115	170	135	82	22.78	7.7284
30	145	114	176	135	89	27.48	6.3504
50	141	96	174	137	109	53.5	12.252
80	141	96	182	135	119	84.76	22.6576
100	139	96	175	136	115	101.483	2.1993
150	138	86	177	137	130	150.21	0.0441

The total residual error of the test data is 7.246, which is only 4.83% of the maximum concentration in the given sulfur dioxide data, so the model error can be

influencing factor

So consider dividing the function into three paragraphs. The least square principle is used for polynomial fitting, and Lagrange interpolation is performed in this region:

$$L(x) = \sum_{j=0}^k y_j l_j(x) \quad (5)$$

$$l_j(x) = \prod_{i=0, i \neq j}^k \frac{x - x_i}{x_j - x_i} \quad (6)$$

Finally, the functional relationship between concentration and population is determined as follows:

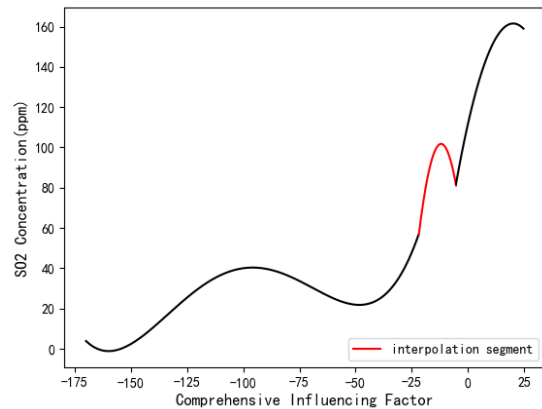


Figure 3 The trend of sulfur dioxide with Synthetical influencing factor

2. ERROR ANALYSIS

Using the relation model of sulfur dioxide and comprehensive influencing factors, the error analysis of seven groups of test data was carried out. The remaining seven groups are substituted into the above test model to obtain the corresponding concentration, and the corresponding residual error is shown in Table 2.

proved to be small. Can more accurately characterize the relationship between the five color readings and the concentration.

REFERENCES

- [1]Gao Rulin, Liu Nan, Liu Di. A stepwise regression model for sulfur dioxide concentration measurement based on colorimetric method [J]. Henan Science: 2018 (06): 837-841.
- [2]Wang Xueping. Mathematical modeling of the relationship between color reading and substance concentration [J]. Economic Mathematics 35 (02): 105-110.
- [3]Xu Yanhua. Study model of color reading and substance concentration [J]. The Chinese Journal of Multimedia and Network Teaching (Chinese Journal): 2018 (05): 111-112.
- [4]Li Jianjun. Identification of color and substance concentration based on principal component analysis [J]. Electronic Technology and Software Engineering! 2018 (07): 66.
- [5]Wen Jie, Xie Kai, Li Tong, Shi Hui Xin. Application of weighted least Square method in Color characterization of LCD [J]. Journal of Beijing Institute of Printing (06): 22-24 29.
- [6]Xu Hao, Zhang Tao, Li Xiaosong, Liu Yuanyuan. Logistic regression analysis of different Pearson residual estimation methods [J]. Journal of Sichuan University (Medical Edition) (01): 129-132.
- [7]Yang Jun, Fang Yazhi. A study on the derivation of Lagrange interpolation Formula [J]. Journal of Tonghua normal University (06): 25-28.
- [8]Ju Jiangzhou. Study on the method of selecting pathogenic SNPs based on genetic Model and Random Forest [D]. Nanjing University.
- [9]Discussion on different Pearson residual estimation methods in logistic regression [J].Journal of Sichuan University (Medical Edition), 2015,46(01): 129-132

Talking about Artificial Intelligence

Yang Wang¹, Ziqi Wei^{1,2}, Long Cheng^{1,2}, Lu Liu^{3,*}

¹North China University of Science and Technology, Tangshan, 063200, China

²Engineering Computing and Simulation Innovation Lab, Tangshan, 063000, China

³School of Science, North China University of Science and Technology, Tangshan 063210, China

*E-mail: 93665397@qq.com

Abstract: In 2016, AlphaGo defeated the world Go champion, making artificial intelligence once again the focus of people's attention. This article briefly introduces its understanding of artificial intelligence and the development of artificial intelligence.

Keywords: artificial intelligence; application field; development direction.

1. INTRODUCTION

I often hear news media introducing artificial intelligence. They all say that people's lives are inseparable from artificial intelligence, but what is artificial intelligence? Where do we use artificial intelligence in our lives? Some people often wonder why the machine also has the power of the human part. What is the means and technology it uses? Still others are always worried that artificial intelligence is too strong, will it replace humans? This article will provide a brief introduction to these issues.

2. DEFINITION OF ARTIFICIAL INTELLIGENCE

In most people's perceptions, any automation can be artificial intelligence, but this is just a paradox that confuses theory and application. Artificial intelligence is extended from computer science. It is necessary to study how to construct intelligent machines or intelligent systems to simulate, extend and expand human intelligence. Its purpose is to model and understand human behavior, even better than humans, rather than let the machine mechanically repeat one thing.

3. THE HISTORY OF ARTIFICIAL INTELLIGENCE

In 1950, the birth of the Turing machine and the Turing test laid the foundation for computers and AI. In 1956, a group of young scientists gathered in Dartmouth to propose a new topic - artificial intelligence, which caused a wave of time. Scientists competed for it. The development process was characterized by the first artificial intelligence in 1972. The birth of the robot Shakey. When people's cheers have just risen, due to lack of data, insufficient assessment of the difficulty of the project, etc., people have questioned the optimistic conjecture, and the government has begun to transfer project funds to other scientific research, causing AI to suffer. It was the first major strike, from 1974 to 1980. Until the 1980s, an AI program called "Expert System" began to be adopted by companies all over the world, and

"knowledge processing" became the focus of mainstream AI research. People once again saw the dawn of victory, and after the happy Apple and the performance of machines produced by IBM and other companies continue to develop. Compared with some old products, they have higher performance and lower maintenance costs, which quickly replaces these old products. The old products have no existing value, making artificial intelligence enter the trough again. In the later development, we can see that in 1997, IBM's computer system "Deep Blue" defeated the chess world champion Kasparov, and once again triggered a phenomenon-level AI topic discussion in the public domain. In 2006, Hinton made a breakthrough in the field of deep learning in neural networks. Once again, human beings saw the hope of machines catching up with human beings, and it was also a symbolic technological advancement. In 2011, an artificial intelligence program using artificial intelligence to answer questions in natural language was developed. Representatively, Watson, developed by IBM, used the artificial intelligence program to participate in the American quiz, defeating two human champions and achieving brilliant results. The record. In 2016, AlphaGo and the world's Go masters began a man-machine battle. The last fortress, known as human wisdom, was broken and once again pushed artificial intelligence to the spotlight of the world stage.

4. KEY TECHNOLOGIES OF ARTIFICIAL INTELLIGENCE

4.1. Machine learning: Machine learning is the core technology of artificial intelligence development now. The purpose is to enable computers to simulate human learning behaviors and to acquire new knowledge and skills. It can predict future data more accurately from the observed data.

4.2. knowledge map: Knowledge map can connect the different kinds of information it acquires to form a knowledge network, thus realizing the ability to analyze problems. At present, knowledge maps have great advantages in search engines, precision marketing, and visual display. However, if the data that the computer touches is wrong in itself, or the value is redundant, it will cause a big problem and needs to be broken.

4.3. Natural language processing: We need to let the

machine learn our language as well, which requires the machine to perform machine translation, understand the semantics and answer the questions we want to know. At present, there are still great challenges in this respect. After all, there are many uncertainties in the richness of language and the different usages of different contexts, and we do not allow the artificially intelligent data resources to make the machine accurately constitute the system.

4.4. Human-computer interaction: The main purpose of human-computer interaction is to realize the exchange of information between people and computers. The current level of development is in addition to basic interaction techniques, such as language interaction, emotional interaction, character design and so on.

4.5. Computer Vision: Computer vision is imitating the human visual system. Computers can solve very well and memorize some complicated formulas that humans can't calculate in a short time, but some humans can watch things directly. People can't, he still needs to analyze images, understand images, and so on. The current problem is that the accuracy is not very high when dealing with certain problems, and the need for a large amount of data requires a long development cycle. The emergence of artificial intelligence chips has made the visual design and development of different data acquisition devices different. Big challenge.

4.6. Biometrics: Biometrics identifies individual identities by analyzing the physiological and behavioral characteristics of an individual. Biometrics technology is also widely used in the current use, including fingerprint recognition, face recognition, iris authentication and so on.

4.7. AR/VR: Virtual reality and augmented reality are computer-based new audio-visual technologies. It can generate the same scenes in the real environment within a certain range, giving people a shock in terms of sight, hearing and touch.

Of course, these technologies will not exist alone, and there will be some cross-use. So-called intelligent robots will apply these technologies in a comprehensive way, so that machines can communicate in human language, store various information obtained by machines, and use knowledge to answer questions and extract. New conclusions, manipulating and moving objects, from "feeling" to "perception", turning "automatic execution" into "autonomous decision making", turning "scheduling knowledge" into "acquiring knowledge" through learning, making them more human.

5. APPLICATION AREAS OF ARTIFICIAL INTELLIGENCE

Artificial intelligence is entering the peak period of technological innovation and large-scale application, the pioneering period of smart enterprises and the formation period of intelligent industry. Artificial

intelligence has penetrated into all aspects of our lives, and human beings are entering the era of intelligence.

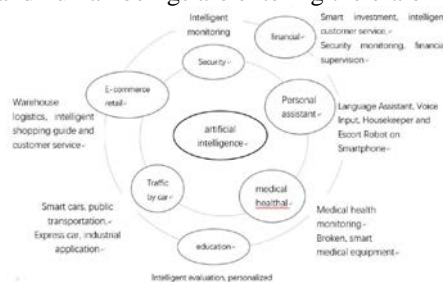


Figure1: application domain of artificial intelligence

In education, the intelligent assistant teaching system has a teaching decision module, a student model module, and a natural language interface. Therefore, the existence of artificial intelligence optimizes our traditional teaching, which can be based on each student's knowledge reserve, learning habits and learning ability. Find problems and develop appropriate ways and means, teach students in accordance with their aptitude, and provide targeted counseling to students. There is also Intelligent Computer Assisted Education (ICAI) which consists of three modules. The knowledge base contains two parts: subject knowledge and teaching knowledge. The "student model" module indicates which students know what is not known; the "teacher model" module It will provide a teaching strategy and tell the system what kind of teaching materials to present to the students.

In recent years, the developed population of traffic has gradually increased, and the incidence of traffic accidents has also increased. AI has also made significant achievements in the field of traffic self-driving. According to the road network traffic flow data, the initial timing and control of traffic signals are better. The map also intelligently provides routes to allow people to avoid traffic jams. In recent years, there have been driverless cars. It is also convenient for industrial use, such as visual analysis of application data, self-diagnosis of machines, predictive maintenance, and so on.

In terms of e-commerce retail, customer service consulting, product packaging, delivery and internal operations, etc., Alibaba's ant gold service is better. In 2015, 95% of remote customer service services were completed with big data intelligent robots.

In terms of banking and insurance, it effectively shields telephone marketing, loan approval, credit card fraud, etc., and reduces the victimization rate.

In terms of medical health, the problems we face 1. The population of China is aging, the number of elderly people with high incidence of diseases is increasing, and medical needs are increasing. 2. The number of patients with chronic diseases is increasing, and medical needs are expanding. 3. Hospitals and beds are in short supply, and urban and rural resources are not balanced. 4. The number of medical staff has grown slowly, and the overall education of health

personnel is low. 5. Excessive medical treatment, excessive consumables, unreasonable resource allocation and other serious waste phenomena. At present, it seems that we still have many diseases that cannot be solved. Relatively speaking, biotechnology is also an information technology that is a big data. When you have enough data, you can also apply artificial intelligence.

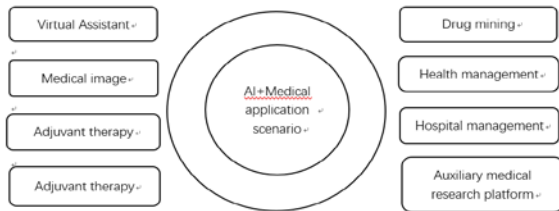


Figure 2: medical application scenarios of artificial intelligence

In terms of security, video structuring and big data technology, mainly used in image processing, pattern recognition, deep learning, etc., have brought us a higher sense of security.

When it comes to security, war and conflict are also a never-ending topic. We can use artificial intelligence to solve disputes. For example, using some virtual reality technology, people can more truly feel the fear brought by war and make everyone more Cherish the hard-won peace and happiness. This shows that artificial intelligence has penetrated into every aspect of life, and we can no longer ignore or question the value of its existence as before.

In terms of finance, investment banks and sellers attempt to automatically generate reports, intelligent and quantitative transactions, smart investment, robotics, financial search engines, etc., which can make the financial industry service model more proactive and the big data processing capability greatly improved

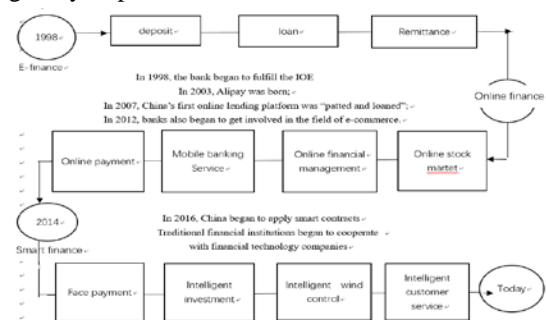


Fig 3: the development of financial services

6. FOUR CHARACTERISTICS OF THE INDUSTRY IN THE ERA OF ARTIFICIAL INTELLIGENCE

6.1. Industrial intelligence: More and more industries are supported by intelligent science and technology, and intelligent science and technology will be of great use.

6.2. Knowledge intelligence: the substitution effect of knowledge industry on material resources, the optimization effect on national economic production

factors, and the multiplication effect on national economic growth.

6.3.Industrial intelligence: The continuous breakthrough of intelligent science and technology will promote the rapid development of high-tech products.

6.4.Popularization of intelligent machines: The organic combination of natural intelligence and machine intelligence has led to an increase in man-machine collaboration and interactive work.

7.THE DEVELOPMENT DIRECTION OF ARTIFICIAL INTELLIGENCE

Now artificial intelligence researchers are studying intellectual behaviors, allowing robots to perform mathematical calculations and understanding physics, or other activities related to consciousness, but artificial intelligence is ultimately imitating human beings. Human beings cannot be a single individual, human beings. It is a group. Human beings not only have the ability to think and think independently, but also have interactions with other people, such as physical and emotional communication, but so far the field of artificial intelligence has not studied social behavior, many people I believe that robots will change our lives and turn us into lonely people in the machine world, but it will make us live in a world that cares about things. At present, the most concerned in interpersonal relationships is between people. Relationships, (such as some small games, having a small house to take care of themselves) are more likely to satisfy human needs and enrich human inner spirit), so socially conscious artificial intelligence can make us more inclined to some extent. care about others. So socially conscious artificial intelligence can be applied to children with autism or Asperger's disease, which are difficult to establish relationships with, so building such robots allows them to reach out to their cravings. Machines can make our society more social, let us hold on to what we care most about.

8. WILL ARTIFICIAL INTELLIGENCE REPLACE HUMANS

The sci-fi movies we watched include some news media that will bring us some particularly powerful information, but we look at the reality. The world's highest-selling smart speakers are alarm clocks, weather, music, news, and another intelligence. The purpose is speech recognition. Everyone will think why this is like this? The gap with our imagination is a bit big, because some of our current technologies are not very mature and have great limitations.

8.1.People will be afraid of new technologies because of work problems. Scientists are not excluded, because the development of technology will always replace the work of some people. Because some people's knowledge reserves are unacceptable, they will face unemployment and even be eliminated. This is One of the panic that new technologies bring to humans, but has to admit that new technologies

always create new jobs, and new jobs tend to be better than old ones. Just as cars have just been invented, people call them "self-propelled bombs," but with the development of technology, it can really bring human benefits. If you have more cars, you can sell cars, sell oil, get driving licenses, etc. Because of the new work brought about by the existence of the car, I believe that artificial intelligence will bring more benefits to human beings.

8.2. In the world of robots, the numbers 0 and 1 can be the logic of everything in the world, but they cannot create inspiration, have intuition, and gain emotion. The machine is always a machine, the material determines consciousness, and consciousness is the vitality of the living body to the objective world. It is reflected that the responsiveness of the machine depends on the designer's ability to think. It is impossible for human beings to multiply, write programs, and develop themselves.

8.3. Some things in the world can never be replaced by AI. For example, the works created by artists can be copied exactly the same, but the artistic conception of hand-painted characters can never be seen. There is also the crystallization of the wisdom of the Chinese people for thousands of years---the poetry, although artificial intelligence is very powerful, it can put together some beautiful words, the surface neatness and rhyming can not fill the wonderful expression of the personal experience like a poet. Or helpless. In the hands of the mother, the wandering clothes, even if the machine is sewed in the same way as the mother, can not bring the mother a needle and a line of sewing. In general, feelings, no matter how much consciousness you give to the machine, the emotion between people is that the machine will be difficult to own, so no human beings will have no intelligence, and intelligence will replace human beings with repeated worthless labor, but Will not replace humans.

9.CONCLUSION

Sixty years of sorrowful sorrows, one-piece Chunhua Qiushi. Looking back on the past, the artificial intelligence discipline has grown into a big tree, artificial intelligence technology continues to make

amazing progress, the era of artificial intelligence has come, it has had a profound impact on the world economy, human life and social progress. However, artificial intelligence is still in the initial upswing, and we still need to work hard to overcome difficulties and make artificial intelligence better serve humans. Of course, we can understand that people are afraid that artificial intelligence will bring us threats. However, in fact, the use of small technology will bring danger to human beings, so artificial intelligence is also the same. We need to use it reasonably to make artificial intelligence. Give us positive effects for the benefit of mankind.

REFERENCE

- [1]Tan Tie Niu, Sun Zhenan, Zhang Zhaoxiang. "Artificial Intelligence: Angel or Devil?" [J]. Chinese Science: Information Science, 2018 (09): 1257-1263.
- [2]Zeng Mei. "On the application of artificial intelligence in the field of medical devices"[J]. Science and Technology Plaza, 2017 (12): 57-60.
- [3]Lü Wei, Zhong Yiyi, Zhang Wei. "Overview of Artificial Intelligence Technology"[J]. Shanghai Electric Technology, 2018, 11 (01): 62-64.
- [4]Yan Rui. "Exploring the use of artificial intelligence in the medical field" [J]. China New Communications, 2018, 20 (15): 159.
- [5]Song Mingyang. "Discussion on the application of artificial intelligence in road traffic management"[J]. China Management Information, 2018, 21 (13): 143-144.
- [6]Cao Junqi. "Analysis of the application and development of artificial intelligence in the financial field" [J]. Times Finance, 2018 (21): 37+39.
- [7]Wang Xinhua, Xiao Bo. "Artificial Intelligence and Its Application in Financial Fields" [J]. Banker, 2017(12): 126-128.
- [8]Gao Jie. "The role of artificial intelligence in financial transactions and its future development direction" [J]. Electronic Technology and Software Engineering, 2017 (18): 253.

Best Design for High Temperature Professional Clothing

Wanqiu Chang^{1,2}, Yongfeng Chen^{1,2}, Shuaijie Shan^{1,2}, Aimin Yang^{3,*}

¹Mathematical Modeling Innovation Lab, North China University of Science and Technology, Tangshan 063210, China

²North China University of Science and Technology, Tangshan 063210, China

³School of Science, North China University of Science and Technology, Tangshan 063210, China

*E-mail: 43698059@qq.com

Abstract: The professional clothing used in high temperature environment needs to have good thermal insulation performance. In this study, the thermal conduction equation between different media is established by analyzing the physical properties of the thermal insulation layer of the suit, to determine the temperature change on the outside of the dummy skin. Firstly, in this study, the temperature distribution in the adiabatic medium is determined respectively in time and space, through different heat conduction modes. And the distribution of temperature in the medium will be obtained after coupling. Then, according to the temperature distribution function, the particle swarm optimization model based on single-objective optimization is established under the condition that the temperature and time of the insulation layer are limited. The minimum temperature outside the dummy skin was used as the objective function to solve the problem and the optimal thickness of layer II medium was 19mm. The solution of temperature distribution function in heat insulation medium under high temperature environment is studied, which provides theoretical basis for making high temperature work clothes.

Keywords: Partial differential equation; Thermal insulation performance evaluation; Improved particle swarm optimization; Single objective optimization

1. INTRODUCTION

With the continuous progress of science and technology and the increasing attention to the personal safety of high-risk operators, more professional clothing design for them with higher safety coefficient has become a hot spot. The high temperature environment will cause certain burns on human skin [1]. Therefore, it is necessary to make special heat insulation clothing and improve the heat insulation effect of special clothing as much as possible. Through literature review, Huang Dongmei [2] pointed out in the research on the internal heat and humidity transfer mechanism of fire fighting suit under the condition of low radiation intensity that the heat insulation result of special clothing is related to

the temperature of the external environment and the design of protective equipment, which provides guidance and Suggestions for the production of heat insulation clothing.

The high-temperature special clothing usually consists of three layers of fabric materials, in which layer I is in contact with the external environment and layer III is still in space with the skin, which is considered as layer IV. The thickness of the middle layer of the fabric and the thickness between the clothing and human skin have a great impact [3], so the effectiveness of clothing can be optimized by changing these two items. Liu hua and ai qing [4] et al. conducted a lot of experiments on common thermal insulation materials, and obtained that the thermal insulation properties of materials are related to the density, specific heat capacity, thermal conductivity and thermal diffusion rate of materials.

In order to design the fabric layer quantitatively, Pan Bin [5], in the mathematical modeling of heat transfer in thermal protective clothing and the inverse problem of parameter determination, established the heat transfer model for the thermal protective clothing -- air layer -- skin system, and obtained the temperature distribution inside and outside clothing by establishing and solving the heat transfer equation for each layer.

To every layer of high temperature special clothing quantify optimum design, this article through the establishment of evaluation of fabric heat insulation performance indicators, and combined with heat transfer equation, using particle swarm algorithm to optimization of solution set of equation, and get the optimal II, IV layer thickness of high temperature special clothing to provide better design solutions.

2. ESTABLISHED AND SOLVED THE TEMPERATURE DISTRIBUTION MODEL OF PROFESSIONAL CLOTHING THERMAL INSULATION MATERIALS FOR HIGH TEMPERATURE WORK

At first, this paper studies the parameters of a certain situation, that the external environment temperature is 75 °C, and the surface temperature of experiment dummy is constantly 37 °C, change in temperature of different space points inside the protective suit.

Because of the object of the study is professional high-temperature operation clothing, , the thermal insulation effect is good. Therefore the temperature change of each layer is slow, and the temperature of the thermal clothing at each moment can be taken as a steady state. The analysis process is shown in figure 1:

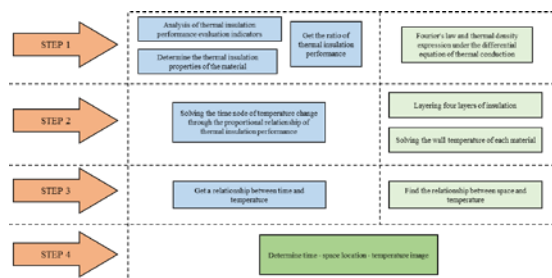


Figure 1 mathematical model analysis process of heat insulation clothing temperature distribution

2.1 STUDY ON THE TEMPERATURE DISTRIBUTION OF THERMAL INSULATION MATERIALS OVER TIME

2.1.1 ASSESSMENT MODEL OF THERMAL INSULATION PERFORMANCE OF THERMAL INSULATION MATERIALS

The function of thermal insulation materials is to prevent heat transfer from hot end to cold end. In this study, a heat insulation performance evaluation model including specific heat capacity, thermal conductivity and material thickness is proposed. The heat at the cold end of heat insulation material per unit area per unit time is used as the basis to evaluate the capability of heat insulation material. Theoretically, the smaller the heat quantity through per unit time and per unit area, the stronger the insulation capacity of the heat insulation material [6]. Then the total heat per unit area can be expressed as:

$$Q(t_m) = \int_{t=0}^{t_m} q(t)dt$$

Where t_m represents the heating time of the insulation material, $q(t)$ represents the heat flux through the unit area at time t .

The physical models of the heat insulation materials in this study are all Dirichlet conditions of the first kind, and the control equation is analyzed by the physical model:

$$\rho c_p \frac{\partial T}{\partial t} = \frac{\partial}{\partial x} (\lambda \frac{\partial T}{\partial x})$$

According to Fourier's law, the heat expression through the cold end of the unit area material in the applied time t_m is:

$$Q_{\delta}(t_m) = \int_0^{t_m} q_{\delta}(t)dt = \int_0^{t_m} (-\lambda \frac{\partial T}{\partial x} |_{x=\delta})dt$$

make this equation

$$Q^* = \frac{\delta}{\lambda(T_h - T_l)t_m} Q_{\delta}(t_m), \phi(F_{o,m}) = \int_0^{F_{o,m}} \frac{1}{F_{o,m}} dF_o$$

and get a single valued function:

$$Q^* = \phi(F_{o,m})$$

By referring to literature [7], the corresponding Fourier number range of common thermal insulation materials is obtained. Combined with the physical property and geometric parameters of four types of thermal insulation materials, the thermal insulation effect of four types of thermal insulation materials is calculated, as shown in table 1:

Table 1 physical property data of four kinds of insulation materials

Layer	Density (kg/m ³)	Specific heat (J/(kg·°C))	Pyroconductivity (W/(m·°C))	Thickness (mm)	$Q_{\delta Z}(t_m)$
I	300	1377	0.082	0.6	23.7462
II	862	2100	0.37	0.6-25	2.5858
III	74.2	1726	0.045	3.6	4.4757
IV	1.18	1005	0.028	0.6-6.4	3.5107

By calculation results available in the table in four of hot work special clothing materials under their respective thickness, application time of 5400s, the thermal insulation material II is best, the thermal insulation material IV takes second place, the thermal insulation material III again, and material I heat insulation effect is poorer.

2.1.2 DISTRIBUTION OF INTERNAL TEMPERATURE OF FOUR MATERIALS WITH TIME

By analyzing the temperature data of each moment within 90 minutes, time nodes of temperature change are obtained. The heat insulation property is used to represent the thermal insulation property of the fabric. There is a linear relationship between the thermal insulation property and the temperature duration and the temperature change.

Firstly, the data of thermal insulation performance is normalized, and the results are shown in table 2:

Table 2 normalization results of thermal insulation performance

thermal insulation material	I	II	III	IV
$Q_{\delta Z}(t_m)$	0.69	0.08	0.13	0.10

According to the inverse relation between thermal insulation performance and temperature duration and change, the function expression is:

$$\frac{Q_i}{Q_j} = \frac{\Delta t_j}{\Delta t_i} = \frac{\Delta T_j}{\Delta T_i}, i = 1,2,\dots,4; j = i + 1, i + 2, \dots, 4$$

Where, Q_i represents the insulation performance of the i th material, Δt_i represents the temperature duration of the i th material, ΔT_i represents the temperature change of the i th material.

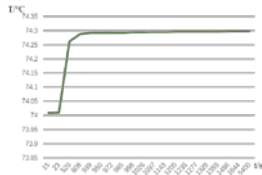


Figure2-I

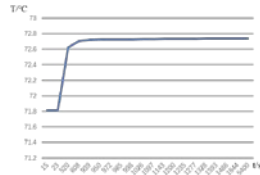


Figure2-II

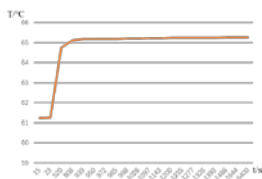


Figure2-III

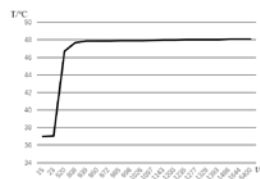


Figure2-IV

Fig.2 temperature distribution in the time axis of each layer of thermal materials

Based on the analysis of temperature distribution in the time axis of each layer of thermal materials in FIG. 2, when heat transfer of each layer of thermal insulation materials begins, the temperature value of the inner layer materials does not change within a period of time, that is, the thermal insulation materials have thermal resistance effect. When temperature difference between the two sides of the thermal insulation materials is present, heat transfer from the hot end to the cold end has time delay.

2.1.3 STUDY ON THE TEMPERATURE DISTRIBUTION IN SPACE POSITION OF THERMAL INSULATION MATERIALS

According to the multi-layer heat transfer model in this study, the temperature distribution function is solved by differential method for each layer, and the integral method is adopted for the integral steady-state case. By building an example diagram of a single-layer slab, as shown in figure 3, the mathematical expression of the Fourier heat conduction law is obtained as follows:

$$\phi = -\lambda A \frac{\partial T}{\partial x}$$

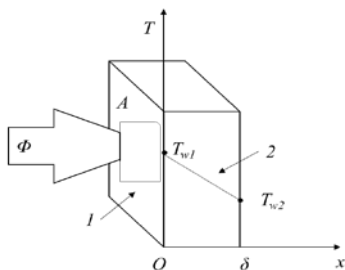


Figure3 temperature distribution of single-layer plate

Where, λ is the thermal conductivity, A is the cross-sectional area of the plate, ϕ is the heat flow, that heat passing through a certain surface in unit time.

Along the layer and the space between the skin - III layer fabric - II layer fabric - I layer fabric layer fabric direction is set to x axis, combined with Fourier law differential expression of heat flow density q is:

$$q = \frac{\phi}{A} = -\lambda \frac{dT}{dx}$$

Study overall equilibrium, set up the first I layers of wall temperature T_1 for a given temperature of 37 °C, the II layers of wall temperature is T_2 , the III layers of wall temperature is T_3 , the IV layers of wall temperature is T_4 , the steady state dummy when the outside of the skin temperature T_5 is 48.08 °C. When the temperature outside the skin of the dummy reached equilibrium, the thermal resistance function of the remaining layers reached equilibrium is:

$$\frac{T_{i+1} - T_i}{q} = \frac{\delta_i}{\lambda_i}$$

Where, λ_i represents the heat conductivity of layer i, q represents the heat flux of the entire space system, and δ_i represents the thickness of layer i.

According to the superposition principle of series thermal resistance, that is, the total thermal resistance value in series process is equal to the sum of other partial thermal resistance values. The equation of the total thermal resistance of the multilayer wall obtained by superimposing all layers is:

$$\frac{T_1 - T_4}{q} = \frac{\delta_1}{\lambda_1} + \frac{\delta_2}{\lambda_2} + \frac{\delta_3}{\lambda_3} + \frac{\delta_4}{\lambda_4}$$

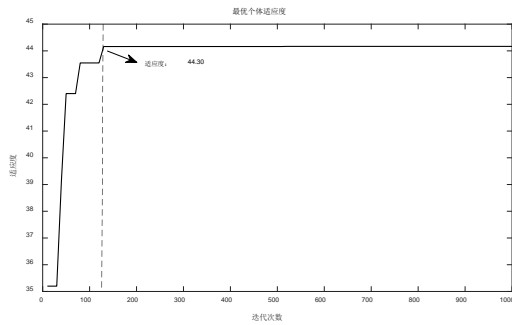
Through the transformation of the equation, the temperature T_i of each layer of wall is deduced as:

$$T_{i+1} = T_i - q \frac{\delta_i}{\lambda_i}, \quad i = 1, 2, \dots, 5$$

After several iterations, the temperature at the equilibrium state of each layer is finally obtained, as shown in the table below:

Table 3 temperature distribution of each layer in equilibrium state

Layer	I	II	III	IV	Outside
temperatu	75	74.232	72.435	64.568	48.08



The optimal solution is ($t=3300s$; $X_2=19mm$), the optimal thickness is 19mm.

3. CONCLUSION

Considering the physical insulation characteristics of hot work for clothing can be affected by specific heat, coefficient of thermal conductivity, the influence of three aspects: material thickness, get the II thermal insulation material, best IV layer of the thermal insulation material, the thermal insulation layer material III again, the worst I layer of the thermal insulation material; By analyzing the temperature distribution of the space position in the time axis, it is concluded that when the temperature difference on both sides of the fabric exceeds the balance limit that the fabric can bear, the heat is transferred from hot end to cold end and has time delay. Is obtained by using the multi-objective particle swarm optimization algorithm, when the environment temperature for 65 DHS C, working time for 60 minutes, and the I layer thickness is 0.6 mm, thickness of 3.6 mm III, IV layer thickness of 5.5 mm of external conditions, get the optimal thickness of the II material fabric for 19 mm, clothing insulation is best at this time. By repeatedly using this method, the optimal status of each influencing factor can be obtained by fixing other influencing factors, and then the optimal design of high-temperature special clothing can be obtained.

REFERENCES

- [1]Jiang peiqing, Yan yaojing, Tang shijun, Chen yuhong. "Human experiment of clothing material selection in high temperature environment" [J]. Journal of Qingdao university (engineering technology edition),2004(01):18-21.
- [2]Huang dongmei. "Study on heat and humidity transfer mechanism of fire fighting suit under low radiation intensity" [D]. University of science and technology of China,2011.
- [3]li defu, Yang weiping, liu xiaoxu. "Research status and prospect of heat transfer characteristics of multilayer thermal insulation materials" [J]. Spacecraft environmental engineering,2013,30(03): 302-309.
- [4]liu hua, ai qing, li donghui, xia xinlin. "Evaluation method for transient thermal performance of thermal insulation materials" [J]. Chinese scientific paper, 2015,10(04):463-466.
- [5]Pan bin. "Mathematical modeling and parameter determination of heat transfer in thermal protective clothing" [D]. Zhejiang university of science and technology,2017.
- [6]Wang Yuping, Liu Dalian, Cheung Yiu-Ming. "Preference bi-objective evolutionary algorithm for constrained optimization. In Proceedings of the International Conference on Computational Intelligence and Security" (CIS2005), LNAI 3801, Yuping Wang et al. (Eds.), Springer-verlag, Brln, 2005, 184-191
- [7]Wei Jingxuan, Wang Yuping. "A Novel Multi-objective PSO Algorithm for Constrained Optimization Problems. In Proceeding of SEAL06", LNCS 4247, T.-D.Wang et al. (Eds), China, Springer-Verlag, Berlin, 2006, 174-180.

Human Body Temperature Simulation of Multi-layer Thermal Protective Clothing under Constant Temperature Environment

Xueyong Jia^{1,2,*}, Jin Guan^{1,2}, Yinduo Zhao^{1,2}

¹ Engineering computing and simulation innovation, North China University of Science and Technology, Tangshan 063210, China

² North China University of Science and Technology, Tangshan 063210, China

*E-mail: 1845528549@qq.com

Abstract: Human body protection is an important research direction in the field of public safety. Firefighters in the fire environment rescue, due to exposure to high temperature heat radiation environment, physical activity intensity, and wearing thick protective clothing, may lead to heat stress response. Therefore, it is an important means to properly assess the life safety of human-clothing-environment heat exchange and human thermal response in high temperature environments to protect firefighters. Mathematical simulation of thermal protective clothing, mainly by constructing mathematical models to describe the thermodynamics of multi-layer thermal protective clothing-air layer-skin system. Provide a theoretical reference for the functional design of thermal protective clothing. In this paper, the heat transfer model is used to simulate the skin surface temperature change, and the results of the dummy experiment to achieve the simulation and experimental study of human thermal reaction fire in high temperature environment. The research results can be used to predict the temperature change of the human body surface at different temperatures, which is of great significance for the design of fire rescue and thermal insulation clothing.

Keywords: Human Body Temperature Simulation; Multi-layer Thermal Protective Clothing; Constant Temperature Environment

1. INTRODUCTION

In recent years, the multi-layer thermal protective clothing heat transfer model is a research hotspot. The existing models can be divided into single-layer thermal protective clothing models and multi-layer thermal protective clothing models according to protective clothing. Gibos et al. first proposed single-layer thermal protective clothing. Based on the model, Chitrphiromsri et al. proposed a more comprehensive multi-layer thermal protective clothing model. Ghazy further proposed a more realistic garment-air layer-skin model. This paper

constructs a protective clothing-air-skin model, which simulates the conduction process in the case of the thickness of the three-layer thermal protective clothing, the density, specific heat capacity and thermal conductivity of each layer.

2. MATHEMATICAL DESCRIPTION OF THE PROBLEM

Based on the assumptions, the problem can be abstracted into a mathematical problem as shown in Figure 1.

The special clothing is usually composed of three layers of fabric materials, which are referred to as layers I, II and III, wherein the layer I is in contact with the external environment, and there is a gap between the layer III and the skin, and the gap is recorded as an IV layer. The ambient temperature is 75 °C and the dummy temperature is controlled at 75 °C. Taking the I layer boundary as the origin of the coordinate axis, L_1, L_2, L_3, L_4 represent the thickness of layers I, II, III, and IV. The specific volume, code, and thermal conductivity of the material are given in Annex 1.

The thermal conductivity of the multilayer fabric used in this work. This is determined by considering a similar circuit model in series as shown in Figure 2.

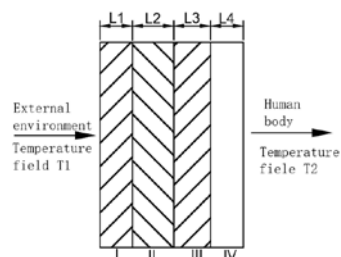


Figure 1 Schematic diagram of the heat transfer model through a multi-layer garment component

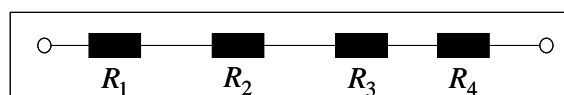


Figure 2 Resistance series circuit model

The special clothing is usually composed of three layers of fabric materials, which are recorded as layers I, II and III. The layer I is in contact with the external environment, and the ambient temperature is 75°C. There is also a gap between the layer III and the

skin, and the gap is recorded as the IV layer. The density, specific heat, thermal conductivity, and thickness of the I, II, and III layers of fabrics are given in Table 1.

Layering	density (kg/m ³)	Specific heat (J/(kg·°C))	Thermal conductivity (W/(m·°C))	thickness (mm)
I layer	300	1377	0.082	0.6
II layer	862	2100	0.37	0.6-25
III layer	74.2	1726	0.045	3.6
IV layer	1.18	1005	0.028	0.6-6.4

The dummy whose body temperature is controlled at 37°C is placed in a high temperature environment of 75°C in the laboratory. If there is a certain temperature difference along the x direction, the direct life experience tells us that there must be heat transfer in the x direction. Experiments have shown that k is related to the material of the medium. Strictly speaking, it is also related to temperature. However, if the temperature does not vary widely, k can be regarded as independent of u.

3. ESTABLISHMENT OF HEAT TRANSFER MODEL

According to Fourier's law, the object flows in an infinitesimal time interval $[t, t + \Delta t]$, the heat ΔQ flowing through an infinitesimal rectangular block area ΔS and the length of time Δt , the rectangular block area ΔS and the object temperature u along the normal direction ΔS of the rectangular block n

The direction derivative $\frac{\partial u}{\partial n}$ is directly proportional to the three

$$\Delta Q = -k \frac{\partial u}{\partial n} \Delta S \Delta t \quad (1)$$

Among them, in question 1, $\frac{\partial u}{\partial n} = 75^\circ\text{C}$, To be more general, we write it in this form. $k > 0$ becomes the heat transfer coefficient, and the negative sign indicates that the heat flows from a place where the temperature is high to a place where the temperature is low, that is, from the outside environment of the temperature of 75°C to the inside of the work clothes. Therefore, in any time interval $[t, t + \Delta t]$, the total heat flowing into the region Ω through the plane Γ is:

$$Q_1 = \int_{t_1}^{t_2} \left(\iint_{\Gamma} k \frac{\partial u}{\partial n} dS \right) dt \quad (2)$$

Second, the specific heat of the object $c(x)$, density is $\rho(x)$, Then the heat required to change the temperature of the micro-e dV containing the point x from $u(x, t_1)$ to $u(x, t_2)$ is

$$dQ = c\rho [u(x, t_1) - u(x, t_2)] dV \quad (3)$$

From time t_1 to time t_2 , the total amount of heat increase of the object is

$$\begin{aligned} Q_2 &= \iiint_{\Omega} dQ = \iiint_{\Omega} c\rho [u(x, t_1) - u(x, t_2)] dV \\ &= \int_{t_1}^{t_2} \left[\iiint_{\Omega} c\rho \frac{\partial u}{\partial t} dV \right] dt \end{aligned} \quad (4)$$

According to the law of conservation of heat, there are arbitrariness of $Q_1 = Q_2$, and t_1, t_2, Ω .

$$k \frac{\partial u}{\partial n} = c\rho \frac{\partial u}{\partial t} \quad (5)$$

Let $a^2 = \frac{k}{c\rho}$, $f = \frac{F}{c\rho}$, get the one-dimensional heat conduction equation

$$\frac{\partial u}{\partial t} = a^2 \frac{\partial^2 u}{\partial x^2} + f(x, t) \quad (6)$$

The heat transfer equation describes the temperature dependence of temperature in a high-temperature garment as a function of time and position, and heat flows from a higher ground direction. The equation relates to physical quantities such as specific heat capacity, density, and thermal conductivity of high-temperature work clothing fabrics.

4. LEAST SQUARES FITTING TO DETERMINE BOUNDARY CONDITIONS

The least squares method can find the best function match of these data based on the principle of minimizing the sum of squared errors by a given set of experimental data. According to the data in Annex II, the data of the temperature outside the skin of the dummy can be obtained with time. The data is fitted by the least squares method, and the fitting result is shown in Figure 3.

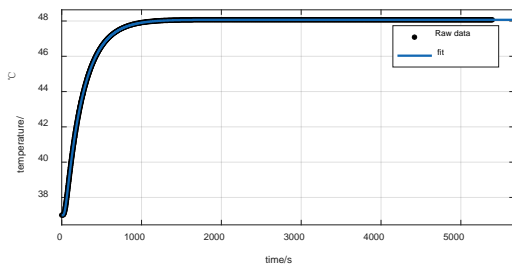


Figure 3 Innermost temperature fitting curve
From Fig.3, it can be concluded that the temperature outside the skin of the dummy is 1000s before the temperature rises continuously with time. After 1000s, the temperature outside the skin of the dummy is basically unchanged. In addition, the curve fitted by the least squares method is completely consistent with the actual data, achieving a very good fitting effect, and the fitting results are shown in Table 2:

Table 2 Analysis of fitting results of least squares method

Result analysis	(SSE) Sum of squared errors (SSE)	(R ²) Correlation coefficient (R ²)
Fitting result	0	1

5. SOLUTION OF HEAT CONDUCTION EQUATION BASED ON DIFFERENCE METHOD

The basic idea is to replace the continuous solution area with a grid of finite discrete points called the nodes of the grid, and the function of the continuous variables on the continuous solution area is used on the grid. The discrete variable function is approximated; the original equation is approximated by the micro-commercial difference quotient in the condition of the solution, and the integral is approximated by the integral sum, so that the original differential equation and the fixed solution condition are approximated by the algebraic equations, the finite difference equations. Then, using the interpolation method, the approximate solution of the solution problem over the entire region can be obtained from the discrete solution[5].

Discrete analysis of heat conduction equation

As shown in Figure 4, the temperature of any node (j,n) in the figure is expressed as $t_j^{(n)}$: the lower foot code represents the spatial interval sequence, and the upper foot code represents the time interval sequence.

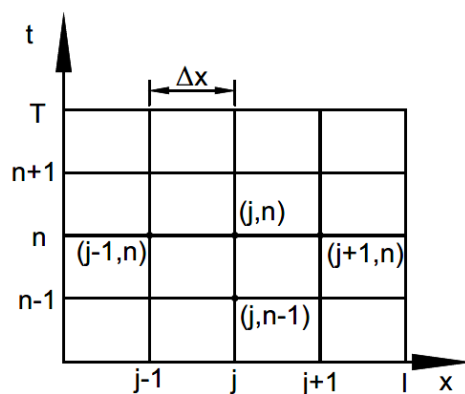


Figure 4 Heat conduction equation implicit format meshing

Use $u(x,t)$ the forward difference quotient [10]:

$$\frac{\partial u}{\partial t} \approx \frac{u_j^n - u_j^{n-1}}{\Delta t} \tag{7}$$

Because of the heat transfer process in the garment from the thermal field to the high temperature, the

temperature difference in the molecule is determined by the difference between the value of the previous time interval and the latter value in time, so the second difference center difference quotient is determined by the center difference quotient:

$$\frac{\partial^2 u}{\partial x^2} \approx \frac{u_{j+1}^n - 2u_j^n + u_{j-1}^n}{(\Delta x)^2} \tag{8}$$

The discrete equations are:

$$\frac{u_j^n - u_j^{n-1}}{\Delta t} = a^2 \frac{u_{j+1}^n - 2u_j^n + u_{j-1}^n}{(\Delta x)^2} \tag{9}$$

which is $(1 + 2r)u_j^n - ru_{j+1}^n - ru_{j-1}^n = u_j^{n-1}$

The above formula can be transformed into a matrix form and converted into a solution problem of a linear system of equations.

In this question, the fabric is equally divided into four units, each thickness has been given by an additional,

and the node can be expressed as $x_i, i = 1, 2, 3, 4$, the initial condition is $u_n^{(0)} = 75^\circ C, n = 1$ and $n = 5$ the two formulas are boundary condition expressions.

6. CONCLUSION

According to the model established in this paper, combined with the parameters provided in the attachment of the topic, the temperature distribution is obtained under the conditions of ambient temperature of 75°C, thickness of layer II of 6 mm, thickness of layer IV of 5 mm, and working time of 90 minutes. Firstly, a curve of temperature change with time is randomly selected from each layer, as shown in Fig. 5. It can be clearly seen from the figure that the closer to the environment, the higher the temperature, the faster the temperature rises. As shown in Fig. 6; the temperature distribution at 50s, 100s, 500s, and 1000s is exhibited. It can be observed from Fig.6. As time increases, the thickness and temperature gradually become completely negatively correlated. As shown in Figure 7, the change in temperature is shown when time and thickness change [6].

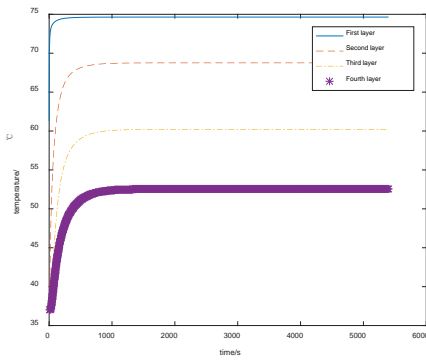


Figure 5 Temperature distribution of different layers

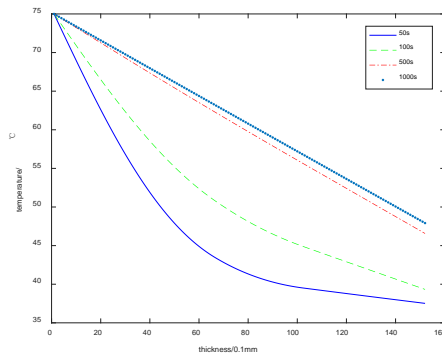


Figure 6 Temperature distribution at different times

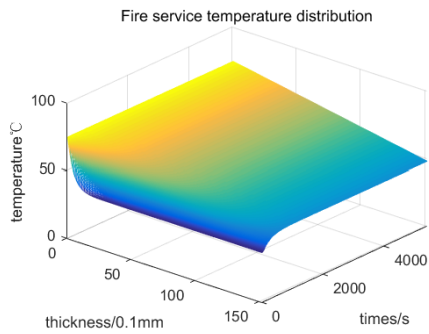


Figure7 Overall temperature distribution of

REFERENCES

[1]Gibson P W, Charmchi M. “Coupled heat and mass transfer through hygroscopic porous materials: Application to clothing layers”. *Fiber*, 1997, 53(5):183-194.

[2]Chitrphiomsri P, Kuznetsov A V. “Modeling heat and moisture transport in firefighter protective clothing during flash fire exposure”. *Heat & Mass Transfer*, 2005, 41(3):206-215.

[3]AhmedGhazy, Bergstrom D. “Numerical Simulation of Transient Heat Transfer in a Protective Clothing System during a Flash Fire Exposure”. *Numerical Heat Transfer*, 2010, 58(9):702-724.

[4]Das A, Alagirusamy R, Kumar P. “Study of heat transfer through multilayer clothing assemblies: a theoretical prediction”. Retrieved from,(Jun. 2011), 2011.

[5]Su Y, He J, Li J. “Modeling the transmitted and stored energy in multilayer protective clothing under low-level radiant exposure”. *Applied Thermal Engineering*, 2016, 93: 1295-1303.

[6]Kadri R L, Boctor F F. “An efficient genetic algorithm to solve the resource-constrained project scheduling problem with transfer times: The single mode case”. *European Journal of Operational Research*, 2018, 265(2): 454-462.

Design of High Resolution Nuclear Magnetic Resonance Magnet

Chen Lele^{1,2}, Zou Changchun¹, Wang Rong², Sun Dianqing², Sun Wei²

¹ China University of Geosciences (Beijing), Beijing, 100083, China

² Research Institute of Petroleum Exploration & Development, Beijing, 100083, China

*E-mail: chenll69@petrochina.com.cn

Abstract: The high-resolution NMR logging instrument is consistent with other NMR logging instruments in working principle. By adopting gradient magnetic field and multi-frequency measurement mode, it is faster in measurement speed, and can measure fluid diffusion coefficient, making recorded data more complete and accurate. With much higher resolution than conventional NMR instruments, it can measure the NMR data of thin reservoirs. This paper introduces parameter calculation, magnetic material selection, finite element calculation and analysis of magnets, probe assembly and debugging, and other aspects of the high-resolution NMR logging instrument.

Keywords: nuclear magnetic resonance; high resolution; well logging.

1. INTRODUCTION

In recent years, a set of expert system for nuclear magnetic logging has been developed and promoted abroad. The expert system uses measurement mode of gradient field, multiple frequencies, and multiple shells, and adopts two-dimensional inversion algorithm. This not only improves the measurement speed of the instrument, but also increases the depth of investigation (DOI), thus allowing the instrument to obtain more information on petrophysical properties, especially the diffusion coefficient of the molecule.

The high-resolution NMR logging tool also uses an acquisition mode of gradient field and multi-frequencies to obtain the transverse relaxation time (T₂) and the diffusion coefficient (D). In addition, the instrument can do measurement on thin reservoirs, making up for the deficiencies of traditional NMR instruments.

2. DESIGN OF MAGNET

At present, high-resolution magnets commonly used in the world are characterized by large volume, complex design, and shallow DOI. In comparison, the magnet designed in this paper is simple in structure, small in size and high in efficiency. The theoretical basis of the magnet design is the numerical calculation method of electromagnetic field. Finite difference method, finite element method, and integral equation method etc are used to design the high resolution magnet. The dimensions of each part of the magnet are worked out first, and then each part is optimized and corrected by 2D and 3D finite element analysis to achieve the

best result.

(1) Design parameters of magnet

The magnetic parameters of the constant gradient field are as follows:

① Magnetic field strength of the detection area B₀=1000Gs -1500Gs

② Magnetic field gradient 17Gs/cm

③ Linear degree of magnetic field gradient $\leq \pm 5\%$

(2) Selection of magnetic materials

Three factors, the maximum magnetic energy product, intrinsic coercivity and Br temperature coefficient, were considered in selecting magnetic materials. The nature of the magnetic material itself is the main factor affecting the three properties, so choosing a suitable magnetic material is one of the major tasks in the development of this magnet. The following table shows the magnetic properties of two kinds of magnetic materials. See Table 1 for details.

Table 1 Performance parameters of permanent magnet materials

Material	Maximum magnetic energy product (unit) kJ/m ³	Intrinsic coercivity (unit) kA/m	Br temperature coefficient (%)	Maximum operating temperature
NeFeB(250/240)	266	2560	-0.12	80-200°C
2:17SmCo II (150/210)	200-220	1660-2100	-0.03	150-250°C

Table 1 shows that 2:17SmCo has better temperature stability. In order to ensure the magnet stability of the constant gradient field and the linearity degree of the gradient, 2:17 SmCo was selected.

(3) Shape design of the magnet and fine-tuning of the magnetic field

The shape of the magnet determines the overall distribution of the magnetic field. Because of influencing factors such as magnetic flux leakage and calculation accuracy, whether it is a finite element 2D model or a 3D model, the results are different somewhat from the actual ones. Therefore, after completing the design of the overall shape of the

magnet, it is necessary to fine-tune the magnet so as to compensate for the design flaw and reach the requirement of application. The magnet shape designed is shown in Figure 1:

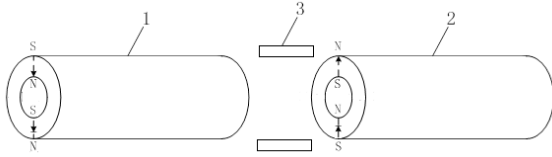


Figure 1 Structure of a high resolution detector Part 1 and 2 in Fig. 1 are SmCo II permanent magnets. The two magnets are identical in size and shape, and symmetrically arranged, and part 3 is a transmitting antenna. The two magnets produce a gradient magnetic field of about 1000 Gs at about 10 cm directly above and below the antenna.

3. FINITE ELEMENT CALCULATION OF MAGNET

The static magnetic field can be described by the following equation:

$$\nabla \cdot B = 0 \tag{1}$$

$$\nabla \times H = J \tag{2}$$

$$B = \mu H \tag{3}$$

The magnetic flux density B can be expressed as:

$$B = \nabla \times A \tag{4}$$

The following second-order differential equation can be obtained by formulae (1-1) to (1-4)

$$\nabla \times \left(\frac{1}{\mu} \nabla \times A \right) = J \tag{5}$$

In formula (5), B is magnetic flux density, H is magnetic induction intensity, J is current density, μ is magnetic permeability of medium, and A is vector potential. Let $\nabla \cdot A = 0$, then unique numerical solution of A can be obtained by equation (1) and its corresponding boundary conditions. After the post-processing, magnetic flux density and other field quantities can be derived.

4. THREE-DIMENSIONAL FINITE ELEMENT ANALYSIS OF MAGNETS

(1) Control equation and boundary conditions of three dimensional static magnetic field

The three-dimensional static magnetic field satisfies the following vector equation:

$$\nabla \times \left(\frac{1}{\mu_r} \nabla \times A \right) = \mu_0 J \tag{6}$$

Its boundary conditions are Dirichlet principle

$$\hat{n} \times A = P \tag{7}$$

and homogeneous Norman criterion for symmetry planes

$$\hat{n} \times (\nabla \times A) = 0 \tag{8}$$

Application of μ_r continuity conditions at the abrupt interface

$$\hat{n} \times A^+ = \hat{n} \times A^- \tag{9}$$

And

$$\frac{1}{\mu_r^+} \hat{n} \times \nabla \times A^+ = \frac{1}{\mu_r^-} \hat{n} \times \nabla \times A^- \tag{10}$$

(2) Variational formula

According to the variational principle, by solving the extremes of the following functionals under the conditions of (7) and (8), the solutions to Equations (7) to (11) can be obtained.

$$F(A) = \frac{1}{2} \iiint_V \frac{1}{\mu_r} (\nabla \times A) \cdot (\nabla \times A) dV - \mu_0 \iiint_V J \cdot A dV \tag{11}$$

(3) The cell division of magnet

In order to identify each cell of the magnet, a $4 \times M$ array was introduced to encode them, each of the cell was denoted by $n(i, e)$, where $i=1, 2, 3, \dots$, and $e=1, 2, 3, \dots, M$. M represents the total number of cells. In addition to the above data, other data are also needed in the finite element formula, such as:

- ① The coordinates of each node x_i, y_i, z_i ($i=1, 2, 3, \dots, N$), where N represents the total number of nodes;
 - ② The value of each cell μ_r, μ_0, j_z ;
 - ③ The p value corresponding to the node of Γ_1 must be added parallel condition $p=0$;
 - ④ γ and q values for each segment of Γ_2
- (4) Interpolation

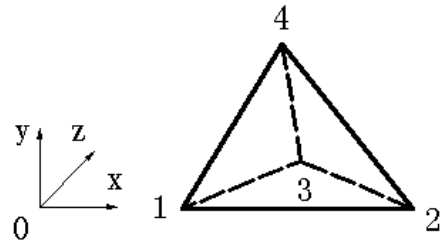


Figure 2 Tetrahedral cell of three-dimensional finite element

The unknown function A in the tetrahedral cell can be approximated as:

$$A^e(x, y, z) = a^e + b^e x + c^e y + d^e z \tag{12}$$

Introducing equation (12) into the four nodes, the four coefficients a^e, b^e, c^e and d^e in the above equation can be determined. When the value of A on the Jth node is denoted as A_j^e , the following formula can be obtained:

$$\begin{aligned} A_1^e(x, y, z) &= a^e + b^e x_1 + c^e y_1 + d^e z_1 \\ A_2^e(x, y, z) &= a^e + b^e x_2 + c^e y_2 + d^e z_2 \\ A_3^e(x, y, z) &= a^e + b^e x_3 + c^e y_3 + d^e z_3 \\ A_4^e(x, y, z) &= a^e + b^e x_4 + c^e y_4 + d^e z_4 \end{aligned}$$

According to the above formulas, we have:

$$a^e = \frac{1}{6V^e} \begin{vmatrix} A_1^e & A_2^e & A_3^e & A_4^e \\ x_1^e & x_2^e & x_3^e & x_4^e \\ y_1^e & y_2^e & y_3^e & y_4^e \\ z_1^e & z_2^e & z_3^e & z_4^e \end{vmatrix} = \frac{1}{6V^e} (a_1^e A_1^e + a_2^e A_2^e + a_3^e A_3^e + a_4^e A_4^e)$$

$$b^e = \frac{1}{6V^e} \begin{bmatrix} 1 & 1 & 1 & 1 \\ A_1^e & A_2^e & A_3^e & A_4^e \\ y_1^e & y_2^e & y_3^e & y_4^e \\ z_1^e & z_2^e & z_3^e & z_4^e \end{bmatrix} = \frac{1}{6V^e} (b_1^e A_1^e + b_2^e A_2^e + b_3^e A_3^e + b_4^e A_4^e)$$

$$c^e = \frac{1}{6V^e} \begin{bmatrix} 1 & 1 & 1 & 1 \\ x_1^e & x_2^e & x_3^e & x_4^e \\ A_1^e & A_2^e & A_3^e & A_4^e \\ z_1^e & z_2^e & z_3^e & z_4^e \end{bmatrix} = \frac{1}{6V^e} (c_1^e A_1^e + c_2^e A_2^e + c_3^e A_3^e + c_4^e A_4^e)$$

$$d^e = \frac{1}{6V^e} \begin{bmatrix} 1 & 1 & 1 & 1 \\ x_1^e & x_2^e & x_3^e & x_4^e \\ y_1^e & y_2^e & y_3^e & y_4^e \\ A_1^e & A_2^e & A_3^e & A_4^e \end{bmatrix} = \frac{1}{6V^e} (d_1^e A_1^e + d_2^e A_2^e + d_3^e A_3^e + d_4^e A_4^e)$$

Where

$$V^e = \frac{1}{6} \begin{vmatrix} 1 & 1 & 1 & 1 \\ x_1^e & x_2^e & x_3^e & x_4^e \\ y_1^e & y_2^e & y_3^e & y_4^e \\ z_1^e & z_2^e & z_3^e & z_4^e \end{vmatrix} = \text{cell volume}$$

After the determinant is expanded, the coefficients a_j^e , b_j^e , c_j^e and d_j^e can be worked out.

Substituting the values of a_j^e , b_j^e , c_j^e and d_j^e into formula 12, the following equation can be obtained

$$A^e(x, y, z) = \sum_{j=1}^4 N_j^e(x, y, z) A_j^e \quad (13)$$

The interpolation function $N_j^e(x, y, z)$ in the upper equation is:

$$N_j^e(x, y, z) = \frac{1}{6V^e} (a_j^e + b_j^e x + c_j^e y + d_j^e z) \quad (14)$$

The interpolation function has the following properties:

$$N_j^e(x, y, z) = \delta_{ij} = \begin{cases} 1 & i = j \\ 0 & i \neq j \end{cases} \quad (15)$$

(5) Finite element calculation

Firstly, it is necessary to express Equation (12) as the component form of scalar

$$F(A) = \frac{1}{2} \iiint_V \mu_r \left[\left(\frac{\partial A_z}{\partial Y} - \frac{\partial A_y}{\partial Z} \right)^2 + \left(\frac{\partial A_x}{\partial Z} - \frac{\partial A_z}{\partial X} \right)^2 + \left(\frac{\partial A_y}{\partial X} - \frac{\partial A_x}{\partial Y} \right)^2 - \mu_0 (A_x J_x + A_y J_y + A_z J_z) \right] dV \quad (16)$$

Discrete Equation (16), then in Figure 2, the three components AX, AY and AZ can be expressed as:

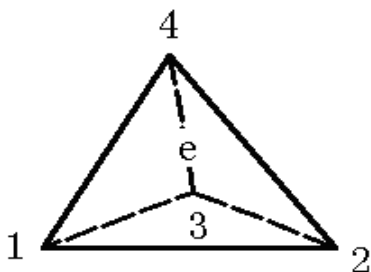


Figure 3 Tetrahedral cells in discrete areas

$$A_x^e = \sum_{j=1}^4 N_j^e A_{xj}^e = \{N^e\}^T \{A_x^e\} = \{A_x^e\}^T \{N^e\}$$

$$A_y^e = \sum_{j=1}^4 N_j^e A_{yj}^e = \{N^e\}^T \{A_y^e\} = \{A_y^e\}^T \{N^e\} \quad (17)$$

$$A_z^e = \sum_{j=1}^4 N_j^e A_{zj}^e = \{N^e\}^T \{A_z^e\} = \{A_z^e\}^T \{N^e\}$$

Substituting Equation (17) into Equation (16), we can get the F part of e-th cell, and then find the partial derivatives of A_{xj}^e , A_{yj}^e , A_{zj}^e , the following equation can be obtained

$$\left\{ \frac{\partial F^e}{\partial A_x^e} \right\} = [K_{xx}^e] \{A_x^e\} + [K_{xy}^e] \{A_y^e\} + [K_{xz}^e] \{A_z^e\} - \{b_x^e\}$$

$$\left\{ \frac{\partial F^e}{\partial A_y^e} \right\} = [K_{yx}^e] \{A_x^e\} + [K_{yy}^e] \{A_y^e\} + [K_{yz}^e] \{A_z^e\} - \{b_y^e\} \quad (18)$$

$$\left\{ \frac{\partial F^e}{\partial A_z^e} \right\} = [K_{zx}^e] \{A_x^e\} + [K_{zy}^e] \{A_y^e\} + [K_{zz}^e] \{A_z^e\} - \{b_z^e\}$$

Combine all the cells and impose a stagnation condition, the following equation sets can be obtained:

$$\left\{ \frac{\partial F}{\partial A_x} \right\} = \sum_{e=1}^M ([K_{xx}^e] \{A_x^e\} + [K_{xy}^e] \{A_y^e\} + [K_{xz}^e] \{A_z^e\} - \{b_x^e\}) = \{0\}$$

$$\left\{ \frac{\partial F}{\partial A_y} \right\} = \sum_{e=1}^M ([K_{yx}^e] \{A_x^e\} + [K_{yy}^e] \{A_y^e\} + [K_{yz}^e] \{A_z^e\} - \{b_y^e\}) = \{0\} \quad (19)$$

$$\left\{ \frac{\partial F}{\partial A_z} \right\} = \sum_{e=1}^M ([K_{zx}^e] \{A_x^e\} + [K_{zy}^e] \{A_y^e\} + [K_{zz}^e] \{A_z^e\} - \{b_z^e\}) = \{0\}$$

Changing the Equation (19) into the following form

$$\begin{bmatrix} K_{xx} & K_{xy} & K_{xz} \\ K_{yx} & K_{yy} & K_{yz} \\ K_{zx} & K_{zy} & K_{zz} \end{bmatrix} \begin{Bmatrix} A_x \\ A_y \\ A_z \end{Bmatrix} = \begin{Bmatrix} b_x \\ b_y \\ b_z \end{Bmatrix} \quad (20)$$

and imposing Dirichlet's boundary conditions, magnetic potential of each node can be got.

According to the above principle, the magnetic field potential can be calculated by using the electromagnetic field module of the ANSYS (a software for finite element calculation). Then the

formula $B = \nabla \times \left(A_z \hat{Z} \right)$ can be used to obtain the

magnetic flux density B_0 .

5. MACHINING AND ASSEMBLY OF MAGNETS

(1) Machining

① The machining of pad is shown in Figure 4

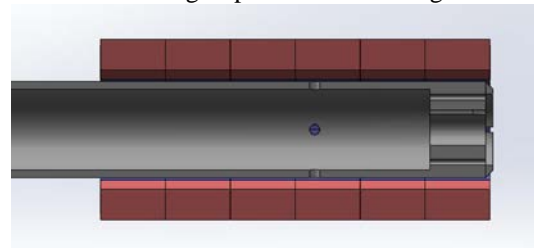


Figure 4 Schematic of the pad

The pad has two main functions: The first is to fix the magnet. Because SmCo II magnets are too strong in magnetism but not strong in material strength, metal skeletons are needed to fix them; the second is to control

the magnetic field distribution in the air gap of the annular space to achieve better magnetic field distribution.

② The machining of magnets shown in Figure 5, which includes the bonding of magnets and the assembly of centering pins. In the figure, 1 is the center positioning pin, and 2 is the magnet block for bonding.

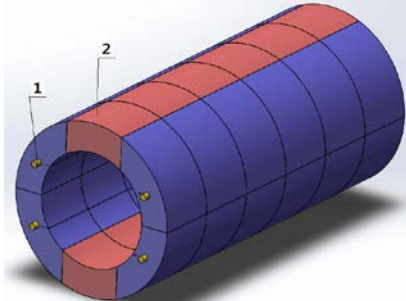


Figure 5 Machining and assembly of magnets
(2) Assembly of magnet

Since the magnetic material has large repulsion and not high enough strength, it is necessary to first bond the magnetic blocks into the form shown in Figure 5, and then the entire magnet block is inserted into the metal pad and bonded with a high-temperature adhesive. In Figure 6, 1 is a metal pad, 2 is a magnet after bonded, 3 is the center positioning pin of the magnet.

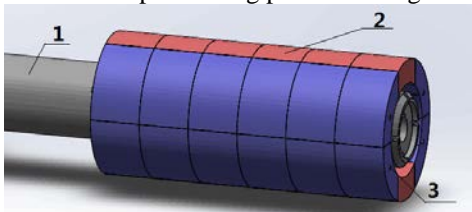


Figure 6 Bonding of magnets

The constant gradient field magnet is the most critical part of the constant gradient field NMR core analysis system. It needs a magnetic field with a certain gradient intensity and gradient linearity degree, and this magnetic field can remain relatively stable when the external temperature does not change much. This requires the precise calculation, processing, assembly and commissioning of the magnets.

6. NUMERICAL SIMULATION RESULTS

The magnetic field distribution curves and the magnetic field equipotential surface obtained by numerical simulation are shown in Figure 7:

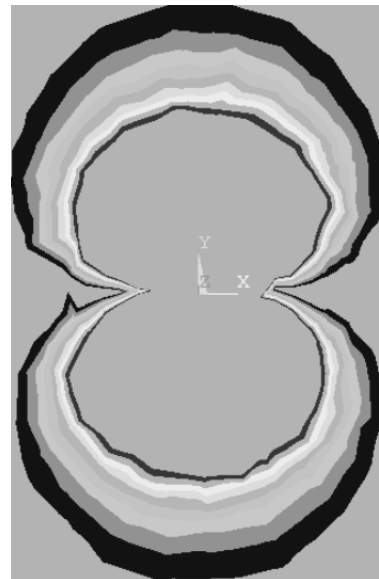
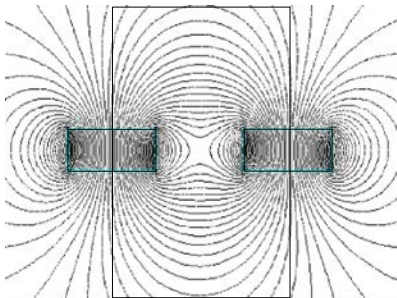


Figure 7 Magnetic field distribution curves and magnetic field isopotential surface

After the magnets were made, the actual measurement results and numerical simulation results are basically the same. However, there are still some differences. The reasons for the difference are the differences of magnetic properties of the magnetic material and the machining techniques.

7. CONCLUSIONS

(1) The core technology of NMR instrument is the design of magnets, which affects the strength and accuracy of NMR signals, and the signal-to-noise ratio required for two-dimensional spectrum inversion. It is the key to the design of the entire instrument.

(2) From the experimental data, the results of numerical simulation and actual measurement are basically consistent, which indicates that numerical simulation is an effective means for designing magnets.

(3) In order to improve the signal-to-noise ratio of NMR analyzer, magnetic field intensity, magnetic field distribution, lateral uniformity, and longitudinal linearity degree of the magnet gradient must be properly adjusted. In the numerical simulation, magnetic flux leakage and temperature change need to be considered to obtain more accurate design data and improve the overall performance of the magnet.

REFERENCES

- [1] Feng Qiao, Numerical analysis and control circuit design of AC controllable reactor magnetic field, Zhejiang University, 2002.
- [2] Tian Mingxing, Li Qingfu. Calculation of magnetic field and parameters of transformer controllable reactor, Journal of Xi'an Jiaotong University, 2005, 39(6): 656-658.
- [3] Zhang liuchen, Xu Song, The application of finite element method in electromagnetic calculation. Beijing: China Railway Publishing House, 1996.
- [4] R. Mehasni, M. Feliachi and M. E. Latreche. Effect of the magnetic dipole interaction on the capture

efficiency in open gradient magnetic separation, *IEEE Transactions on Magnetics*, 2007, 43(8): 3488–3493.

[5] Jin Jianming, Wang Jianguo, Translate, Finite element method for electromagnetic field. Xi'an: Xi'an Electronic and Science University Press, 2001.

[6] Yin Zhongdong, Liu Hong, Chen Baichao, Chen Weixian, Study of magnetic valve controlled reactor, 1998, 35(7): 1-4.

[7] Liu Dichen, Chen Baichao, Tian Cuihua, Application and lectotype analysis of new controllable reactor in power grid, *Power grid technology*, 1999, 24(2): 56-59.

[8] Heinz W. Engl, Martin Hanker, Andreas Neubauer. Regularization of inverse problems, Dordrecht, Kluwer academic publishers. 1996.

[9] M.B. Crowe et al. Measuring Residual Oil Saturation in West Texas Using NMR, SPWLA 38th Annual Logging Symposium, June 15-18, 1997.

[10] S. Chen et al. Methods for Computing Swi and BVI from NMR Logs, SPWLA 39th Annual Logging Symposium, May 26–29, 1998.

[11] Stefan Menger and Manfred Prammer, Can NMR Porosity Replace Conventional Porosity in Formation Evaluation. SPWLA 39th Annual Logging Symposium, May 26–29, 1998.

[12] W.J. Looyestijn, Determination of Oil Saturation from Diffusion NMR Logs. SPWLA 37th Annual Logging Symposium, June 16–19, 1996, S.

[13] G.R. Coates, H.J. Vinegar. Restrictive Diffusion From Uniform Gradient NMR Well Logging. SPE 26472, 1993, 575–590.

Quad-rotor Aircraft Control based On Fractional Order PID

Chen Yimei, Zhang Tengyun

School of Electrical Engineering and Automation, Tianjin Polytechnic University, Tianjin 300387, China

Abstract: In view of the characteristics of non-linearity, parameter perturbation, environment disturbance and the requirement of fast attitude control for four-rotor aircraft, a control scheme based on fractional order PID (FOPID) is proposed in this paper. By adding two adjustable parameters, The FOPID controller can make the system have better dynamic performance and robustness. The simulation results show that the fractional order PID has better speediness and smaller overshoot than the traditional PID controller, and has a better suppression effect on the parameter perturbation. Finally, the controller designed in this paper is applied to the Qball2 quad-rotor platform. The experimental results show that the pitch angle, roll angle and yaw angle can track 15 degrees angle in 2.5 seconds. hovering experiment can achieve stable hovering, the error is 0.02 meters.

Keywords: Quad-rotor aircraft; Fractional order control (FOC); FOPID; $PI^\lambda D^\mu$; Qball2 platform

1. INTRODUCTION

In the last few decades, the quad-rotor aircraft has been paid more and more attention because of its simple mechanical structure, small size, flexible flight and easy maintenance. It can complete vertical take-off and landing, hovering, erection of cloud platform and so on [1]. Quad-rotor widely used in agriculture, military investigation, fire monitoring, express transportation, video entertainment and many other fields.

The quad-rotor aircraft is a nonlinear, strong coupling, under actuated and time-varying system [2]. During the flight, the quad-rotor will be disturbed by the gust and the airflow of its own rotor, which will bring great challenge to the control of the quad-rotor. In the control method of quad-rotor aircraft, the PID control algorithm and the combination of PID and some nonlinear algorithms are commonly used. For example, the PID was applied to quad-rotor control earlier in reference [3]. The PID attitude controller is designed in reference [4], and the IAE index is used to optimize the controller parameters. In reference [5], the control effect of PID, LQR, LQRPID controller on the height of quad-rotor is compared. Although the above methods can achieve stable control effect, there are many shortcomings such as overshoot, long adjustment time and so on. In nonlinear PID control scheme, the fuzzy PID controller is designed by

reference [6]. Under the condition of no position controller, the quad-rotor track circular trajectory is realized only by the control the pitch angle and roll angle. In reference [7], a multivariable neural network adaptive PID control method based on RBF is proposed. In reference [8], a multi-mode PID controller is proposed to suppress actuator saturation in yaw channels. As an extension of the traditional PID controller, I.Podlubny proposed fractional order PID controller [9] in 1999. Compared with the traditional PID controller, the FOPID has two more regulating parameters, which can control the nonlinear link better, and has better dynamic performance and strong robustness [10-11]. The introduction of FOPID controller promotes the application of fractional order control theory in engineering. For example, the robust fractional order PID controller is designed for missile pitch angle control [12]. The reference [13] applies fractional PID controller to trajectory tracking of vehicle mobile robot. However, the research on the FOPID applied to the quad-rotor control is less.

Based on the above considerations, the fractional order PID is used to control the quad-rotor aircraft system. The fractional order PID controller is designed for the quad-rotor attitude and height control. The simulation results show that fractional order PID has good dynamic performance and strong robustness under the case of general and parameter perturbation. The attitude and height control experiments also were carried out on the Qball2 experimental platform to further verify the effectiveness of the controller.

2. DYNAMIC MODEL

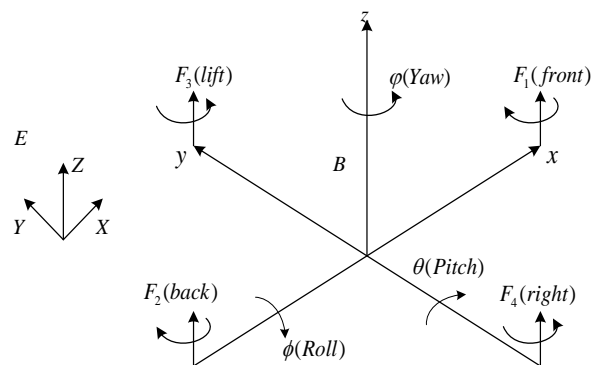


Figure 1 Quad-rotor structure diagram

This paper constructs the body coordinate frame

$B-xyz$ and the ground coordinates frame $E-xyz$, as shown in figure 1. The established coordinate frame obeys the right-hand rule. The origin of the body coordinate frame is in the center of the quad-rotor. The rotation angles of the aircraft around the X,Y and Z axes are defined as the roll angle, the pitch angle and the yaw angle, respectively. The four motors of Qball2 are numbered respectively (hereinafter 1.2.3.4 motor), in which 1 and 2 motor drive rotor clockwise rotation, 3, 4 motor drive rotor turn counterclockwise. The lift generated by each

motor is expressed in terms of $F_i (i = 1, 2, 3, 4)$. According to Newton Euler's laws[6], the dynamic model of quad rotor UAV is [12,14]:

$$\begin{cases} \ddot{x} = (F_1 + F_2 + F_3 + F_4)(C_\phi S_\theta C_\phi + S_\phi S_\theta) / m + \Delta(x) \\ \ddot{y} = (F_1 + F_2 + F_3 + F_4)(S_\phi S_\theta C_\phi - S_\phi C_\theta) / m + \Delta(y) \\ \ddot{z} = (F_1 + F_2 + F_3 + F_4)(C_\theta C_\phi) / m - g + \Delta(z) \\ \ddot{\phi} = [l(F_3 - F_1) + \dot{\phi}\theta(I_y - I_x)] / I_x + \Delta(\phi) \\ \ddot{\theta} = [l(F_1 - F_2) + \dot{\phi}\phi(I_z - I_x)] / I_y + \Delta(\theta) \\ \ddot{\varphi} = [(\tau_1 + \tau_2 - \tau_3 - \tau_4) + \dot{\phi}\dot{\theta}(I_x - I_y)] / I_z + \Delta(\varphi) \end{cases} \quad (1)$$

Where (ϕ, θ, φ) is the roll angle, pitch angle and yaw angle of the quad-rotor; $F_i (i = 1, 2, 3, 4)$ is the thrusts produced by the four propellers; $C_{(\square)}$ denotes $\cos(\square)$, $S_{(\square)}$ denotes $\sin(\square)$; l represents the distance from the center of the propeller to the midpoint of the quad-rotor. m is the mass of the four-rotor and g is the acceleration of gravity. (I_x, I_y, I_z) is the moment of inertia with respect to the axes. $\Delta(\square)$ is the unmodeled part of the system.

The thrusts generated by each rotor and the PWM input of the motor in Qball2 can be expressed by first order transfer function.

$$F_i = k_f \frac{w}{s + w} u_i \quad (i = 1, 2, 3, 4) \quad (2)$$

The k_f is positive gain coefficient and the w is the bandwidth of the motor.

The torque τ_i generated by each rotor is approximately proportional to the PWM input u_i of the motor.

$$\tau_i = k_q u_i \quad (i = 1, 2, 3, 4) \quad (3)$$

In order to facilitate the design of the controller, the virtual control volume U_1, U_2, U_3, U_4 is introduced.

$$\begin{cases} U_1 = u_1 + u_2 + u_3 + u_4 \\ U_2 = u_3 - u_4 \\ U_3 = u_1 - u_2 \\ U_4 = u_1 + u_2 - u_3 - u_4 \end{cases} \quad (4)$$

By taking formula (2) (3) (4) into form (1) and ignoring unknown disturbances, the simplified mathematical model of four-rotor is obtained as follows.

$$\begin{cases} \ddot{x} = K\omega U_1(C_\phi S_\theta C_\phi + S_\phi S_\theta) / (m(s + \omega) + \Delta(x)) \\ \ddot{y} = K\omega U_1(S_\phi S_\theta C_\phi - S_\phi C_\theta) / (m(s + \omega) + \Delta(y)) \\ \ddot{z} = K\omega U_1(C_\theta C_\phi) / (m(s + \omega)) - g + \Delta(z) \\ \ddot{\phi} = [Kl\omega U_2 / (s + \omega) + \dot{\phi}\theta(I_y - I_x)] / I_x + \Delta(\phi) \\ \ddot{\theta} = [Kl\omega U_3 / (s + \omega) + \dot{\phi}\phi(I_z - I_x)] / I_y + \Delta(\theta) \\ \ddot{\varphi} = [K_y U_4 / (s + \omega) + \dot{\phi}\dot{\theta}(I_x - I_y)] / I_z + \Delta(\varphi) \end{cases} \quad (5)$$

3. FRACTIONAL ORDER PID CONTROLLER

The fractional order PID controller is proposed by Professor Podlubny and is generally written as $PI^\lambda D^\mu$. λ, μ are the order of the integral operator and the order of differential operators respectively. When λ, μ take 1, it is the traditional PID controller. The FOPID controller is basically the same as the traditional PID structure. The introduction of λ, μ can improve the performance of the controller and obtain better dynamic performance and robustness.

The transfer function of the traditional integer order PID is:

$$G_1(s) = K_p + K_i s^{-1} + K_d s \quad (6)$$

The transfer function of the fractional order PID controller is:

$$G_2(s) = K_p + K_i s^{-\lambda} + K_d s^\mu \quad (7)$$

Where K_p is proportional gain, K_i is integral coefficient, and K_d is differential coefficient.

$$0 < \lambda, \mu < 1$$

The mathematical realization and improvement of fractional calculus operator s^λ have always been the focus of research. In this paper, the improved approximation method [15-16] is used to approximate s^λ as a continuous rational transfer function model. The approximation process is as follows:

1)The range (w_b, w_h) of the approximate frequency section and the approximate order $2N + 1$ are selected.

2)According to the order and frequency range of fractional calculus, we get w'_k, w_k, K from the formula 8,9,10.

$$w'_k = \left(\frac{b}{d}\right)^{\frac{2k-\lambda}{2N+1}} w_h^{\frac{N+k+1/2(1-\lambda)}{2N+1}} w_b^{\frac{N-k+1/2(1+\lambda)}{2N+1}} \quad (8)$$

$$w_k = \left(\frac{b}{d}\right)^{\frac{2k+\lambda}{2N+1}} w_h^{\frac{N+k+1/2(1+\lambda)}{2N+1}} w_b^{\frac{N-k+1/2(1-\lambda)}{2N+1}} \quad (9)$$

$$K = (w_b w_h)^\lambda \quad (10)$$

In the formula, b , d coefficient introduced to optimize the approximate effect at both ends of the approximate frequency band. $-N \leq k \leq N$.

3)The rational transfer function approximated by fractional calculus operator s^λ is obtained by substituting formula (8), (9), (10) in (11).

$$G_3(s) = K \left(\frac{ds^2 + bsw_h}{d(1-\lambda)s^2 + bsw_h + d\lambda} \right) \prod_{k=-N}^N \frac{1 + \frac{s}{w'_k}}{1 + \frac{s}{w_k}} \quad (11)$$

In the same way, the approximate rational transfer function of s^μ is obtained.

$$G_4(s) = K \left(\frac{ds^2 + bsw_h}{d(1-\mu)s^2 + bsw_h + d\mu} \right) \prod_{k=-N}^N \frac{1 + \frac{s}{w'_k}}{1 + \frac{s}{w_k}} \quad (12)$$

From the expression (7), (11), (12), the transfer function of FOPID controller can be written as follows:

$$G_5(s) = K_p + K_i / G_3(s) + K_d G_4(s) \quad (13)$$

4. CONTROL SYSTEM DESIGN

This paper adopts the design of double closed loop control system (shown in Figure 2). The position loop adopts the traditional PID control method. In order to obtain a better tracking effect, the fractional-order PID control method is adopted in the attitude loop. In the graph, we give the expected value of position and yaw is $(x_0, y_0, z_0, \varphi_0)$, and the expected value of pitch angle and roll angle is obtained by solving the nonlinear constraint condition. The output of the controller U_1, U_2, U_3, U_4 is the virtual control value. The virtual control value is converted to the input of four motors u_1, u_2, u_3, u_4 by the inverse operation of the formula (4). The position and attitude of the aircraft can be controlled by the input of the motor.

(1)Design of position controller

The outer loop controller is divided into two modules. Because z is an independent control channel, the virtual control volume U_1 can be directly obtained by fractional PID controller. x, y two channel and attitude angle θ, ϕ constitute a double closed loop mode, the outer loop is a fixed value control system, and the inner loop

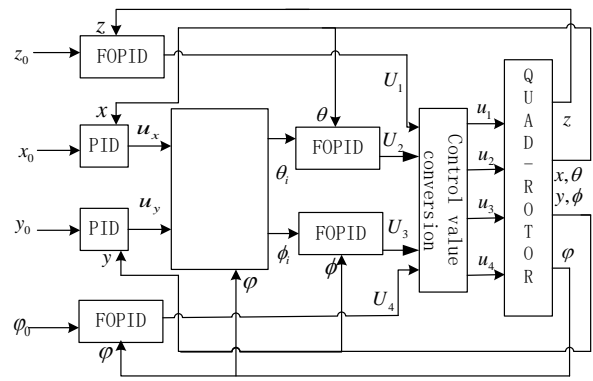


Figure 2 Block diagram of quad-rotor control system is a servo system. In order to achieve the speed of inner loop control and the stability control of the outer ring, the x, y outer loop channel adopts the traditional PID control. The output of the position controller is obtained by the combination formula (6) and formula (13).

$$\begin{cases} U_1 = [K_p + K_i / G_3(s) + K_d G_4(s)](z_0 - z) \\ U_x = K_p(x_0 - x) + K_i \int (x_0 - x) + K_d(x_0 - x)' \\ U_y = K_p(y_0 - y) + K_i \int (y_0 - y) + K_d(y_0 - y)' \end{cases} \quad (14)$$

(2) Nonlinear constraint condition

In the position control of the aircraft, the pitch angle and the roll angle are the control state in the middle, and the actual expected value can not be given directly. The expected value must be calculated by the output of the position controller u_x, u_y [17]. The nonlinear constraint relationship between position control u_x, u_y and attitude expectation (θ_i, ϕ_i) is as follows:

$$\begin{cases} u_x = \cos \varphi \sin \theta_i \cos \phi_i + \sin \varphi \sin \phi_i \\ u_y = \sin \varphi \sin \theta_i \cos \phi_i - \cos \varphi \sin \phi_i \end{cases} \quad (15)$$

In the indoor low altitude flight, it is generally considered that the pitch angle and roll angle of the aircraft are very small. Here, we use the small angle hypothesis to simplify equation (15) (small angle approximation $\sin \theta_i \approx \theta_i, \cos \theta_i \approx 1, \sin \phi_i \approx \phi_i, \cos \phi_i \approx 1$). The expected value of attitude (θ_i, ϕ_i) is calculated as follows:

$$\begin{cases} \phi_i = u_x \sin \varphi - u_y \cos \varphi \\ \theta_i = u_x \cos \varphi + u_y \sin \varphi \end{cases} \quad (16)$$

(3) Design of attitude controller

As the basis of position control, attitude control is directly related to the control effect of the whole aircraft. Due to the interference of indoor low-altitude air flow, unmodeled factors and adverse effects caused by parameter perturbation, the attitude controller adopts fractional order PID controller with better robustness. According to equation (14), the

output of attitude controller is:

$$\begin{cases} U_2 = [K_p + K_i / G_3(s) + K_d G_4(s)](\theta_i - \theta) \\ U_3 = [K_p + K_i / G_3(s) + K_d G_4(s)](\phi_i - \phi) \\ U_4 = [K_p + K_i / G_3(s) + K_d G_4(s)](\varphi_0 - \varphi) \end{cases} \quad (17)$$

5. EXPERIMENTAL VERIFICATION

(1) Simulation verification

In order to verify the speediness and robustness of the proposed control scheme , a simulation experiment was carried out on the MATLAB/Simulink. The simulation parameters are consistent with the parameters of the Qball2 experimental platform (as shown in Table 1). In the simulation experiment, the attitude inner loop was adjusted first, and then the parameters of the position outer loop are adjusted after the requirement of fast and stable internal loop control was met. In the simulation and physical experiment, the fractional calculus operator parameters are selected as $w_b = 0.01$, $w_h = 100$, $N = 3$, $b = 10$. $d = 9$.

Table 1 Qball2 parameter table

parameter	value	parameter	value
m	1.79kg	g	9.8m / s ²
l	0.2m	I_x	0.03kg□m ²
k_f	12N	I_y	0.03kg□m ²
k_q	0.4N□m	I_z	0.04kg□m ²

Set pitch angle, roll angle, yaw angle expectation value is 5 degrees, initial value is 0 degrees. After debugging, the pitch angle, yaw angle, roll angle controller parameters are shown below. The fractional PID attitude tracking curve shown in Fig. 3 .

$$\begin{cases} K_p = 0.01 \\ K_i = 0.005 \\ K_d = 0.007 \\ \lambda = 0.5 \\ \mu = 0.78 \end{cases} \begin{cases} K_p = 0.04 \\ K_i = 0.006 \\ K_d = 0.006 \\ \lambda = 0.3 \\ \mu = 0.8 \end{cases} \begin{cases} K_p = 0.05 \\ K_i = 0.018 \\ K_d = 0.01 \\ \lambda = 0.3 \\ \mu = 0.75 \end{cases}$$

As shown in figure 3, the overshoot of pitch angle and roll angle is 0.4 degrees, and the time of stabilization is 0.5 seconds. The yawing angle overshoot is 0.3 degrees, and the stabilization time is 1.5 seconds.

In order to verify that the proposed FOPID has better dynamic performance and stronger robustness than the

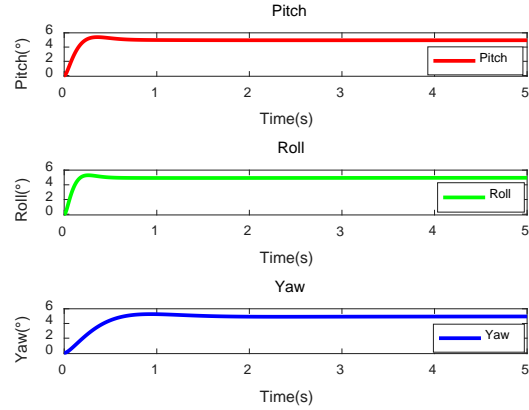


Figure 3 Simulation curves of pitch, roll and yaw traditional PID, this paper makes a comparative experiment on the pitching channel. Figure 4 shows the control effect of FOPID and PID in turning inertia I_x from 0.03 to 0.04 and l from 0.2 to 0.18. The comparison results show that FOPID has smaller overshoot and shorter stable time when the system parameters are the same. Under the condition of system parameter perturbation(PP), the stability time and overshoot of FOPID have less change and stronger robustness.

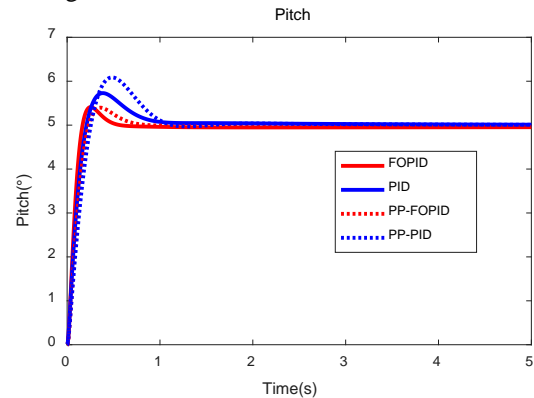


Figure 4 Simulation comparison between PID and FOPID under parameter perturbation(PP)

After the inner loop meets the rapidity requirement, the position simulation is carried out. Set the expected value of position (x, y, z) to be 1 meter, and the initial position to be 0 meters. The parameters of the position controller are shown below, and the response curve shown in Figure 5.

$$\begin{cases} K_p = 1.8 \\ K_i = 0.005 \\ K_d = 3.4 \end{cases} \begin{cases} K_p = 2 \\ K_i = 0.005 \\ K_d = 3.5 \end{cases} \begin{cases} K_p = 0.08 \\ K_i = 10 \\ K_d = 0.03 \\ \lambda = 0.9 \\ \mu = 0.7 \end{cases}$$

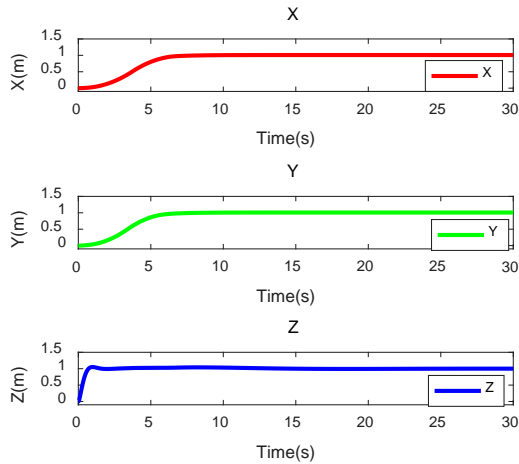


Figure 5 Position simulation curve
From Figure 5, we can see that the position simulation curve is not overshoot, relatively smooth, stable time is 5.5 seconds. The height overshoot is 0.05 meters, and the stable time is 1.5 seconds.

(2) Physical experiment

The proposed algorithm is applied to the Qball2 experimental platform, which includes a console host, a WiFi router, 6 OptiTrack cameras and a Qball2 quad-rotor. The OptiTrack camera is responsible for the real-time positioning of the Qball2 in the flight range of the quad_rotor. The positioning information is transmitted to the operating platform via WiFi, and the control information is processed and sent to the aircraft. The experimental scene is shown in Figure 6.



Figure 6 Qball2 quad-rotor and OptiTrack camera
Expectations set pitch angle, roll angle, yaw angle is 15 degree angles. The three Angle controller parameters are shown as follows. The attitude tracking curve shown in figure 7,8.

$$\begin{cases} K_p = 0.012 \\ K_i = 0.01 \\ K_d = 0.0006 \\ \lambda = 0.8 \\ \mu = 0.85 \end{cases} \begin{cases} K_p = 0.02 \\ K_i = 0.03 \\ K_d = 0.0003 \\ \lambda = 0.85 \\ \mu = 0.75 \end{cases} \begin{cases} K_p = 0.08 \\ K_i = 3 \\ K_d = 0.007 \\ \lambda = 0.8 \\ \mu = 0.85 \end{cases}$$

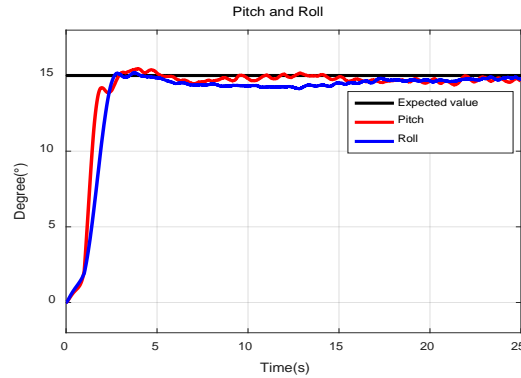


Figure 7 Pitch angle and Roll angle tracking curve

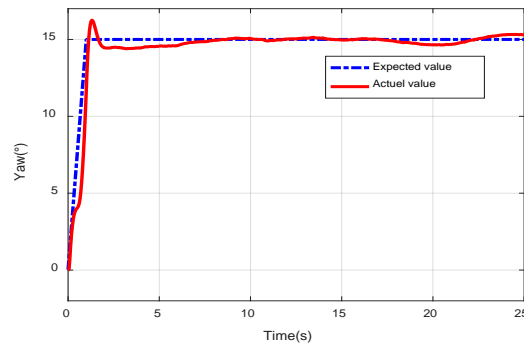


Figure 8 Yaw angle tracking curve

The above figure shows that the pitch angle reaches the expected value in 2.5 seconds, the error range is 0.5 degrees. The roll angle response time is 2.5 seconds and the error range is 0.8 degrees. In the actual system, the relative independent yaw angle has the control slope limit, the yaw angle overshoot is 1.25 degrees, stable time is 2 seconds, error range is 0.6 degrees. The experimental results show that the fractional PID control algorithm can achieve fast and stable inner loop control.

In order to further verify the superiority of the proposed fractional order controller compared with the traditional PID control, a contrast experiment of the pitching channel is carried out in this paper, and the experimental results are shown in Figure 9.

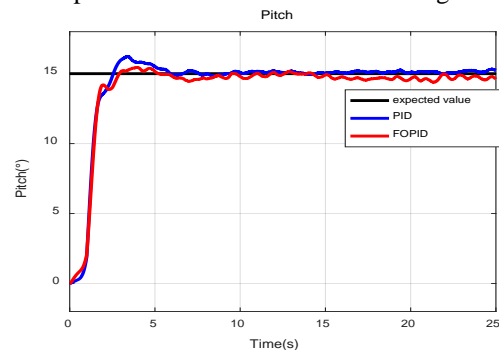


Figure 9 Contrast experiment between FOPID and PID in the pitch channel

As can be seen from Figure 9, both FOPID and traditional PID satisfy the requirements of attitude control stability, but FOPID has faster response speed and smaller overshoot.

In hovering test, the height expectation is set to 0.3 meters. And the experimental system is run in fifth seconds, then is closed in forty-seventh seconds. The parameters of the position controller are shown as follows. Figure 10, 11 and 12 respectively show the height response curve, attitude control curve at suspension and motor PWM input value curve.

$$\begin{cases} K_p = 0.3 \\ K_i = 0.4 \\ K_d = 0.8 \end{cases} \begin{cases} K_p = 0.3 \\ K_i = 0.4 \\ K_d = 0.8 \end{cases} \begin{cases} K_p = 1 \\ K_i = 0.7 \\ K_d = 0.5 \\ \lambda = 0.85 \\ \mu = 1 \end{cases}$$

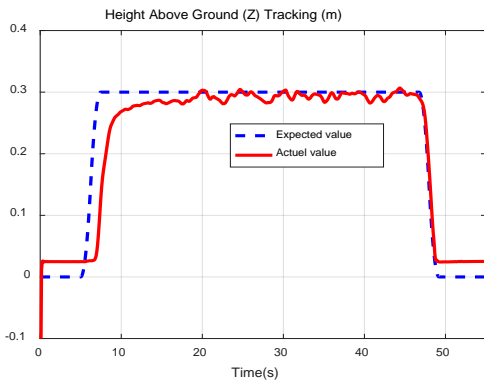


Figure 10 High response curve

The figure 10 shows that aircraft starting position is 0.025 meters (protective sponge pad height). The system runs in 5 seconds, and the quad-rotor starts to take off in 1.5 seconds. At the 10th second, the height error reached 0.27 meters. After stabilization, the height error was 0.02 meters. 47 seconds, stop the system, and the vehicle lands steadily.

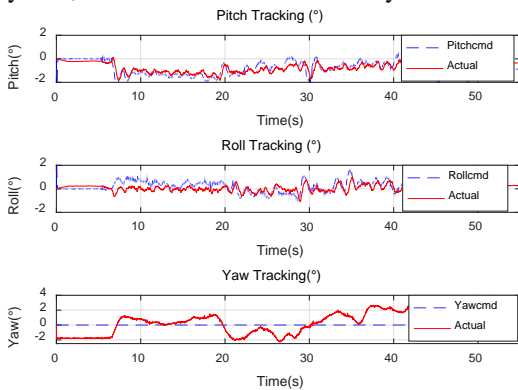


Figure 11 Attitude curve during hovering experiment

Figure 11 shows the control curve of the inner ring attitude in hovering test. The fluctuation range of pitch and roll is ± 2 degrees, and the fluctuation range of yaw angle is ± 4 degrees. The fluctuation range of three angles is small, which can realize the stable hovering of quad-rotor.

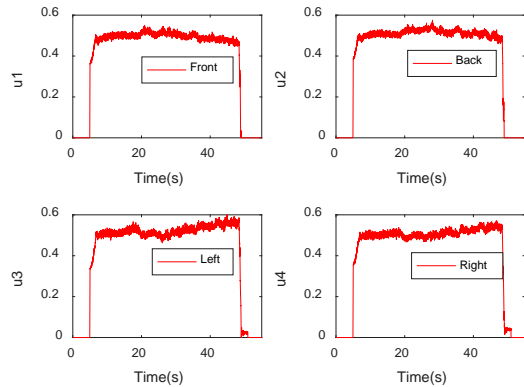


Figure 12 PWM input value of motor

Figure 12 shows that the PWM input value of the motor starts from 0.36, which is set to offset the gravity acceleration. The PWM input reaches about 0.5 in 6.5 seconds, corresponding to the 6.5 second take-off point of the height response curve. During the whole experiment, the input value of the motor PWM is around 0.5, which satisfies the takeoff condition[20]. The fluctuation range of the input value of PWM is ± 0.02 , within the controllable range.

6. CONCLUSION

In this paper, the mathematical model of quad-rotor aircraft is established, and the control scheme of attitude inner loop and position outer loop is adopted. According to the fractional PID control algorithm, the inner loop attitude controller and height controller of quad-rotor aircraft are designed. The proposed control algorithm is verified on the MATLAB and the Qball2 quad-rotor experimental platform. The simulation and experimental results show that the proposed algorithm can achieve the tracking control of the attitude and height, and has strong robustness and dynamic performance. In the future work, on-line optimization of control parameters will be carried out.

REFERENCES

[1]Nie Bowen, Ma Hongxu, Wang Jian. WANG Jian-wen Study on actualities and critical technologies of micro mini quadrotor. ELECTRONICS OPTICS & CONTROL, 2007(6):113-117.(in Chinese).
 [2]Zhen Hongtao, Qi Xiaohui, Xia Mingqi, Zhao Hongrui. A survey on flight control technology of four rotor unmanned helicopter. FLIGHT DYNAMICS, 2012, 30(4): 295-299.(in Chinese).
 [3]Salih A.L,et al. Flight PID controller design for a UAV quadrotor. Scientific Research and Essays,2010, 23(5) : 3660 – 3667.
 [4]Bolandi H, Rezaei M, Mohsenipour R, et al. Attitude Control of a Quadrotor with Optimized PID Controller. Intelligent Control & Automation, 2013, 04(3):342-349.
 [5] Argentim L M, Rezende W C, Santos P E, et al. PID, LQR and LQR-PID on a quadcopter platform International Conference on Informatics, Electronics & Vision. IEEE, 2013:1-6.

- [6]Kuantama E, Vesselenyi T, Dzitac S, et al. PID and Fuzzy-PID control model for quadcopter attitude with disturbance parameter. *International Journal of Computers Communications & Control*, 2017, 12(4): 519 -532.
- [7]Li Yan-nong, Li Ting-lan, Jiang Yi, Fan Jia-lu. Adaptive PID Control of Quadrotor Based on RBF Neural Network. *Control Engineering of China*, 2016, 23(3):378-382. (in Chinese).
- [8]Peng Cheng, Bai Yue, Qiao Guanyu, Gong Xun, Tian Yantao. Anti-windup and Multi-Mode PID Control of Yaw Movement for a Quad-Rotor UAV. *ROBOT*,2015,37(4):415-423.(in Chinese).
- [9]Podlubny I. Fractional-order systems and $PI^{\lambda}D^{\mu}$ controllers. *IEEE Transaction on Automatic Control*. 1999,44(1) : 208-214 .
- [10] Pritesh Shah, Sudhir Agashe. Review of fractional PID controller. *Mechatronics*, 2016,38.
- [11] Zhu Chengxiang, Zhou Yun. Summary of research on fractional-order control. *Control and Decision*, 2009,24(2):161-169.(in Chinese).
- [12]Qi Naiming, Qin Changmao, Song Zhiguo. Robust Fractional PID Missile Autopilot Design. *Control Engineering of China*, 2011,18(5):715-718.(in Chinese).
- [13]Al-Mayyahi A, Wang W, Birch P. Design of Fractional-Order Controller for Trajectory Tracking Control of a Non-holonomic Autonomous Ground Vehicle. *Journal of Control Automation & Electrical Systems*, 2016, 27(1):29-42.
- [14] Zhang Y.M, YU X, Wang B, LIU Ding. Design and Implementation of Fault-Tolerant Control Algorithms for an Unmanned Quadrotor System. *Control Engineering of China*, 2016,23(12):1874-1882.
- [15]Xue D, Zhao C, Chen Y Q. A Modified Approximation Method of Fractional Order System, *IEEE International Conference on Mechatronics and Automation*. IEEE, 2006:1043-1048.
- [16]Li Ying-shun, Zhao Chun-na, Lu Tao. Research and Application of Fractional Advanced Control system. Beijing: Beijing Normal University Publishing Group,2012.(in Chinese).
- [17]Wang C, Song B, Tang C, et al. Trajectory Tracking Control for Quadrotor Robot Subject to Payload Variation and Wind Gust Disturbance. *Journal of Intelligent & Robotic Systems*, 2016, 83(2):315-333.
- [18]Walter Lucia, Mario Sznaier, Giuseppe Franzè. An obstacle avoidance and motion planning Command Governor based scheme: the Qball-X4 Quadrotor case of study. 2014 IEEE 53rd Annual Conference on Decision and Control, 2014:6135-614.

Thermal Analysis and Research of Electronic Pump for Passenger Vehicles

Penghong Yang¹, Binwei Duan^{1,*}

¹School of Electrical Engineering and Automation, Tianjin Polytechnic University, Tianjin, 300387, China

*E-mail: binweitpu@163.com

Abstract: There is no prototyping plan in the thermal simulation analysis of the new energy automobile cooling pump. The thermal simulation scheme of the automobile pump is designed to solve this problem, by using the structural characteristics of the existing pump as the reference. Based on the ANSYS Icepak, the heat transfer analysis of conducting, convection and radiation conjugate on printed circuit boards and electronic components provides the solutions for automobile cooling systems, which is more productive effectiveness and cost saving.

Keywords: Water pump; Natural convection; Icepak

1. INTRODUCTION

With the upgrade of computer hardware and the development of software integration technology, the thermal analysis of electronic equipment by numerical calculation has become the main means of the thermal design of electronic equipment. Thus, the thermal design of electronic equipment is based on the results of the thermal analysis. Compared to the traditional thermal analysis method, the numerical simulation technology can effectively reduce the design cost, shorten the design time, master the vulnerable link in the design in advance, and avoid the design risk, resulting in the improvement of the success rate of the product. According to statistics, 55% of the failure of electronic equipment is caused by excessive temperature. With the increase in temperature, the component failure efficiency increases exponentially. Research shows that the temperature of semiconductor elements rises every 10 °C, its reliability reduces by 50%; For every one degree Celsius drop in temperature, the failure rate will decline 4% [1]. The pump, as an important part of the cooling system of the automobile engine, is used to pump the cooling liquid to make it flow quickly in the cooling liquid circulation channel of the battery pack, which is to ensure that the battery pack works at a normal temperature. In this paper, the feasibility of the design scheme is verified by theoretical analysis and simulation, and the optimization scheme is proposed. The actual pump is shown in figure 1.



Figure 1 The actual water pump.

2. SOURCE AND ORIGIN OF HEAT

The analysis of the MOSFET characteristics shows that the opening and switching speed of the MOSFET is related to the current. The opening time of MOSFET is affected on the current value provided by the drive circuit directly. Because of the influence of Miller charge and interelectrode capacitance, it takes a longer time to charge the MOSFET, resulting in the increased switching loss of MOSFET and a large amount of heat, which can easily cause the burning of MOSFET [2]. In addition, since the high switching frequency of MOSFET in this product design, the crossover loss cannot be ignored when the moment of MOSFET turned on or off leading the crossing of voltage and current at the very short time. On the other hand, the long load of the working time will lead to the accumulation of heat, while the motor has no forced cooling function, thus the high temperature of the motor will weaken the load capacity and shorten the service life of the motor [3].

3. SIMULATION SCHEME

Electronic thermal simulation mainly uses a numerical calculation to get the results of the flow field, temperature field and other physical fields in the environment of electronic products, belonging to the category of CFD. By analyzing the CFD calculation results, we can guide the engineers to optimize the structure and circuit and achieve the optimal design. For an electronic equipment, natural cooling is a relatively reliable method of heat dissipation, so as to guarantee the normal operation of the equipment within a reasonable temperature range. The criterion equation of natural convection is $Nu = CRa^n$ (Nu is Nusselt number, the relation between Nu and h_c is $Nu = \frac{h_c D}{\lambda}$; Ra is Rayleigh number)

3.1 SIMULATION ENVIRONMENT

- (1)Environmental properties:ambient temperature is 75°C, pressure is 101325Pa;
- (2) Coolant properties: the coolant is air, density is 1.225kg/m³
- (3)The motor is mainly composed of enamelled wire, contact pin and injection material pps&GF40;
- (4)The material of the heat sink is 6061 aluminium alloy

3.2THE HEAT SOURCE PARAMETERS

Power device	Magnitude&Quantity
Driving MOSFET	1W*3
Anti-reverse contact MOSFET	0.5W*1
Winding	3W*6
Capacitance	0.1W*2
Sampling resistor	1W*2
Inductance	0.9W*1

3.3PARAMETER OF EACH COMPONENT IN THE MODEL

Material Composition	Thermal Conductivity W/(m • K)
silicon	82
copper	390
silicon lamination	20
Thermal pad	3
pps+GF40	1.5
Al6061-T4	154

3.4CFD MODELING

The geometrical model of CAD must be "clean", and the geometrical features of the model, such as screw, nut and small feature chamfers should be simplified and omitted without affecting the heat dissipation[4]. The simplified model is shown in figure 2.

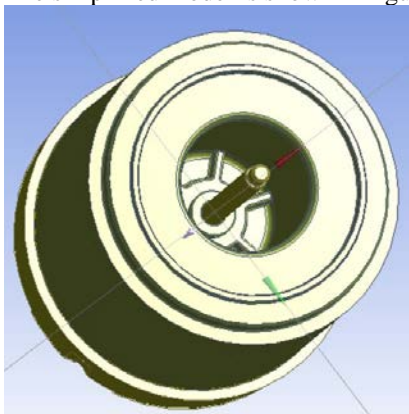


Figure 2 Simplified model

3.5MESH GENERATION

The hexahedral dominant grid type is used to divide the grid. Set the maximum grid size to be 0.005m and the minimum grid size to be 0.0005m, with only the refining for the PCB required. Mesh control is shown in figure 3. The final grid number is 570105.

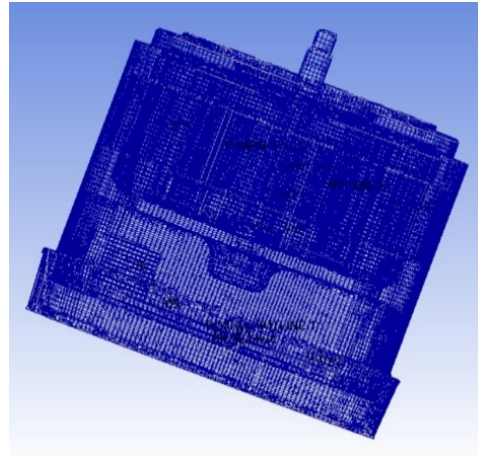


Figure 3 Final grid

4.SIMULATION RESULT

The Simulation is based on icepak software. The overall size of the pump is 0.072m×0.072m×0.069m. Figure 4 is a cloud diagram of the overall temperature distribution of the pump. Figure 5 is a temperature distribution cloud map of PCB surface devices[5]. MOSFET junction temperature is 133°C lower than the maximum allowable working temperature 175 °C.The design meets the actual demand can work stably in the car.

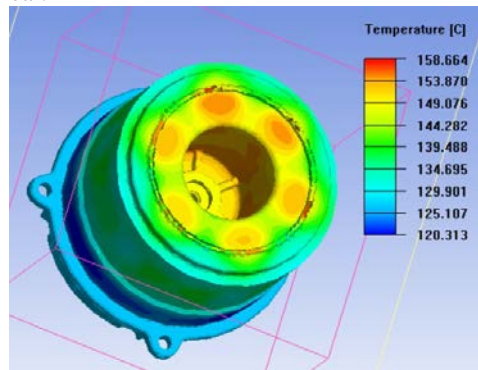


Figure 4 Overall temperature distribution

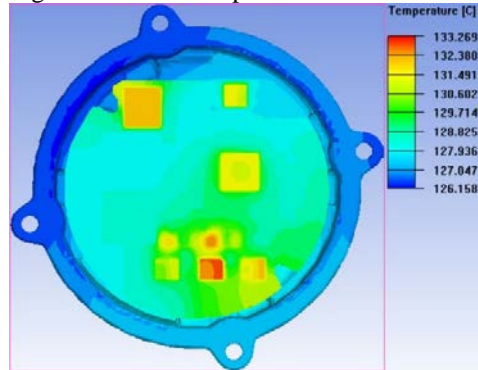


Figure 5 Temperature distribution cloud map of PCB

5.CONCLUSION

The paper uses icepak simulation, the feasibility of the design of the electronic pump was analyzed, and the cloud chart of the thermal distribution of components under typical working conditions was obtained, which saved time and cost. It provides a reference for future program improvement.

REFERENCES

[1]T. Yu, C. Zhou, and Y. Ma, Thermal Analysis and Optimization of a Servo Control Module, *Electro-Mechanical Engineering*, 2017, 33(02): 41-43+47.
[2]X. Qian, C. Liu, A method of sort based on FPGA is used in radar system, *Electronic Design Engineering*, 2015, 23(23): 136-137+140.
[3]Y. Wang, X. Yao and Y. Qin, Analysis of the Motor Heat Transfer and Structural Optimization on the

Automatic Cooking Machine with Rotary Drum, *Mechanical Engineer*, 2015(12): 162-164.
[4]Y. Wang, "ANSYS Icepak electronic thermal foundation course," National Defense Industry Press, 2015.
[5]Z. Li, Finite Element Analysis and Research of the Thermal Fatigue of Electronic Packaging QFP Components, *Reliability and Environmental Testing of Electronic Products*, 2015, 33(03): 51-54.

Software Engineering Course Practice Teaching

Gui-ping Lei

Guangdong University of Science & Technology, Dongguan, 523083, China

*E-mail: 122432141@qq.com

Abstract: The "Software Engineering" course is an important professional compulsory course in software engineering, network engineering and computer science and technology and related professional teaching programs. The course is very practical and involves many disciplines and comprehensive. Through the course of Software Engineering, students can understand the software development process and familiar with process management related technologies, and lay a foundation for students to work on graduation design and future software development and application. However, in the practical teaching of practical software engineering courses, the specific methods and approaches have become the topic of discussion among many experts and scholars. This paper is also based on such a background, from the practical problems of practical teaching of software engineering courses, the purpose of practical teaching, teaching This issue is discussed in many aspects, such as the realization of reform.

Keywords: software engineering; curriculum; practical teaching; teaching reform

1. INTRODUCTION

The current training of software engineering talents is facing the challenges of rapid development of technology, continuous growth of software system scale and complexity, and increasing industrial engineering requirements for engineering capabilities. How to cultivate high-quality, system-oriented software engineering talents to meet industrial needs has become a major challenge for the current education and higher education institutions. The actual situation is that there is still a big gap between the software engineering talents cultivated by higher education institutions and the requirements of the industry. Therefore, we need to objectively understand the gap between the two and seek effective means to bridge the gap. Software engineering practice teaching plays a key role in the cultivation of computer software talents. How to strengthen the teaching of software engineering practice, solve its universal contradictions and problems, adapt to current educational concepts and software engineering technology development, meet the needs of industry, etc. has become a very urgent educational research topic.

2. THE PRACTICAL PROBLEM OF PRACTICAL 2.

2. TEACHING IN SOFTWARE ENGINEERING COURSES

The current software engineering practice teaching usually adopts a team approach to organize students to participate in practice, conducts practice in the form of projects, and uses teachers or TAs as the main help objects for the students to complete the curriculum practice, with the tasks and requirements given by the teachers (such as time, progress, evaluation). Standards and assessment criteria, etc.) drive students to practice. [1]In the course of the course practice, students mainly use physical space (such as classroom or campus), or local area network (such as some teaching platforms), through the interaction with teachers and TA, to obtain the required resources to solve the existing problems.

To sum up, this practical teaching method has the following shortcomings: 1 The closedness of the participants, the participants of the curriculum practice are limited to students, teachers and TAs who participate in practical teaching, and other objects are difficult to join and contribute to practical teaching. Therefore, the role of the teacher is very important; 2 the limited resources channels, students can only get the resources needed to support the curriculum practice from the teacher or TA, it is difficult to get help from other channels, so the teacher's counseling is very important; 3 The locality of the implementation space, curriculum practice is usually limited by the local physical space and information space, students are difficult to interact and collaborate with individuals or groups outside the implementation space, so interaction with the teacher is critical.

3. THE PURPOSE OF PRACTICAL TEACHING OF SOFTWARE ENGINEERING COURSES

(1) Cultivate students' ability to innovate

Constructing a platform for college students' innovation and entrepreneurship is a good way to comprehensively test and enhance the ability of innovation and entrepreneurship. The platform includes three parts: the University Student Innovation Center, the College Student Entrepreneurship Center, and the Enterprise High-Tech Demonstration Experience Center. The high-tech experience display center includes the enterprise high-tech demonstration experience area, the teacher-student independent research and development product display experience area, and is

open to students all the time. It introduces the industry's cutting-edge technology, the latest ideas, and high-tech products to the campus, allowing students to feel the impact of high-tech, and stimulate students' interest in technological innovation to guide students to learn independently, practice independently, and start their own businesses. The University Student Innovation Center and the Entrepreneurship Center allow students to strengthen their hands-on ability, innovation ability and entrepreneurial ability in addition to theoretical study and their own hobbies and specialties. By participating in various science and technology competitions and entrepreneurship guidance, students can be trained in team management, creative motivating, engineering design, entrepreneurial practice, market management, etc., in the practice of training innovative ability, in the pursuit of training innovative thinking. Through the platform of innovation and entrepreneurship practice base, build a bridge between "teaching" and "engineering", "theory" and "practice", "scientific research" and "transformation of results", "starting business appeal" and "professional incubator". Promote the transformation of the concept of talent cultivation and the reform of education and teaching.

(2) Strengthening students' professional cognition

In the process of cultivating software engineering students, educators should pay attention to scientific literacy training, integrate the results of scientific research into the experimental teaching system, and enhance students' professional expansion ability and research ability. For example, the wireless sensor network experiment course and the Internet of Things sensing technology experiment course are set up, paying attention to the design and implementation of the basic sensor node of the IoT professional, the comprehensive design of the Internet of Things system, and the wireless information security experiment in the direction of information security. Computer virus detection experiments, etc. Focus on guiding students' scientific interest, emphasizing "student-centered", forming project teams, students' independent learning and innovation, teachers providing guidance and constructive opinions, and comprehensively improving students' overall quality. The professional direction experimental platform consists of a software development and testing laboratory, an embedded system laboratory, an information security laboratory, a service science laboratory, and a digital media laboratory. It focuses on cultivating students' comprehensive skills and innovative abilities in this field. And continue to improve the software development and testing direction, embedded system direction, information security direction, service science direction and other experimental courses, build a professional experimental teaching platform for the direction of the Internet of Things and digital media technology,

improve students' recognition of professional direction Knowledge and engineering practice.

(3) Cultivate students' practical ability

The training teaching should be carried out in the senior grade of software engineering, the time is 3 to 6 months, and the training adopts the "double true" mode, which is the real enterprise environment and real project case. Students are required to play the role of team leader, developer, tester, system analyst and other roles in the training base according to the standards of the company's employees. [2]The company assigns experienced employees to be project managers, and guides students according to the software development process such as corporate culture understanding, business negotiation, demand analysis, summary design, detailed design, coding implementation, online simulation, etc., so that students can truly experience the standards in the enterprise. How the project was made. At the same time, during the training process, the company will send personnel managers to train and train soft skills, including professionalism, expressiveness, teamwork, and dual foreign language skills. Enhance students' practical ability in team building, corporate culture and values, business etiquette, work skills, time management, and results presentation to better cultivate outstanding engineering and technical talents with comprehensive quality.

(4) Strengthen the training of students' basic skills knowledge system

The software engineering basic experimental platform, the following can set up 7 software labs and 10 hardware labs, undertake the basic class computer and experimental courses of nearly 3,000 undergraduates, including computer and IT entry, programming foundation and C language, object-oriented methods and C++, data structure and algorithm design and other computer courses, computer basic experiments, digital-analog electrical experiments, computer network integrated experiments, computer components experiments, operating system experiments and information security comprehensive experiments and other experimental courses.[3] These courses focus on general education in the development of elite software engineering talents, focusing on the development of students' basic skills and basic practical skills. And continue to improve the construction of a basic experimental teaching platform for software engineering, implement standardized, unified management, broaden the knowledge level of students, and enrich the experimental basis of students.

4. REALIZATION OF SOFTWARE ENGINEERING TEACHING REFORM

(1) Fully integrate the high-quality resources of existing laboratories, strengthen the construction of basic experimental platform for software engineering, strengthen basic programming and program verification training, and consolidate the basic

knowledge of students. Develop innovative, scalable and high quality software systems. Require students to conceive and creative software requirements, put forward explicit requirements for the scale, integration, comprehensiveness and quality of the development software system, adopt iterative methods for requirements analysis, software design, writing code, test verification, etc., and encourage students to reuse open source. Code and Internet services, through software-based distributed collaboration, continuous integration and inspection, open source community-based communication and discussion to develop software to solve problems encountered in development.[4] The results of the practice include software requirements creative documentation, software design models, program code, test reports, operational and demonstrable software systems, product introductions to software systems, demonstration videos, and reporting materials.

(2) Build a software engineering professional experimental platform, strengthen comprehensive training in the professional field of students, cultivate students' professional practice ability, and broaden students' knowledge. This practice requires students to read high-quality, open-source software of a certain scale, label the code according to the understanding of open source software, analyze the quality of the code, maintain the open source software on this basis, improve its function, and correct it. defect. Figure 1 below is the related products of open source software.

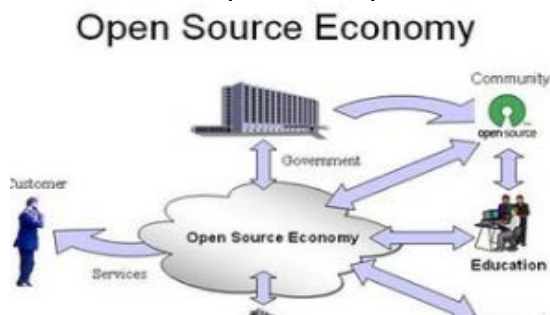


Figure 1 Open source software peripheral information. The purpose of this practice is to enable students to master the basic style and requirements of high-quality program code, learn how to write high-quality program code, feel the importance of program code quality, and understand the impact of software demand changes and scale growth on code quality. The results of the practice include open source code annotations and annotations, open source code quality analysis reports, maintained open source code, runnable and demonstrable software systems, software system product introductions, presentations, and reporting materials.

(3) Strengthen school-enterprise cooperation, establish an on-campus training base with internationally renowned enterprises, introduce

enterprises into the campus, cultivate students' professional qualities, simulate the corporate environment, let students feel the needs of enterprises in close quarters, and develop the teaching of joint training of talents in school enterprises. New mode.

(4) Build a software innovation and entrepreneurship practice platform, build a high-tech display experience center, a university student innovation practice center, and a university student entrepreneurship incubation base to cultivate students' innovative practice ability and entrepreneurial ability.

After a period of construction and practical exploration of previous students, practical teaching based on grouped software engineering courses will achieve positive results in strengthening engineering practice and innovation capabilities. Students can basically master the technologies and skills based on the Internet for group collaborative development. [5]The software systems they envision and implement in the future are new and will receive certain awards in many competitions and competitions.

5. CONCLUSION

Software engineering is a core course in computer science and technology, involving technology, methods and management, and plays an important role in the development of students' development ability and quality. The reform of software engineering teaching is related to the cultivation and improvement of students' practical ability and comprehensive quality. It is a very valuable and meaningful subject. This paper is based on the current practice of software engineering curriculum to explore and analyze, I hope to make a certain contribution to the curriculum practice teaching of software engineering.

REFERENCES

- [1]Xu Fengsheng, Li Tianzhi, Li Haijun. Analysis of the Construction of Computer Science and Technology Course Group; Fujian Computer, 2007-03.
- [2]He Zhaoqing, Yang Xishu, Peng Li, Hu Xiangyong. Research and Practice of Computer Professional Software Design Course Group Construction, Journal of Chifeng College (Science Education Edition), 2011-12.
- [3]Lin Song. Discussion on Teaching and Practice of "Software Engineering" Course in Colleges and Universities, Fujian Computer; 2008-01.
- [4]Liu Xiaoyuan. Discussion on Teaching Reform of Software Engineering Course in Higher Vocational Colleges, Journal of Mudanjiang College of Education, 2011-04.
- [4]Zhou Qiuping, Fan Qingchun. Research on Teaching Reform of Software Engineering Course, Journal of Hefei Teachers College, 2008-06.

Hyperspectral Images Classification based on Multifractal Spectrum

Luo Jing^{1,2}, Li Yun-lei^{1,2}, Hu Fei^{1,2}

¹ Key Laboratory of Advanced Electrical Engineering and Energy Technology, 300387, China;

² College of Electrical Engineering and Automation, Tianjin Polytechnic University, Tianjin, 300387, China

*E-mail: m18039178933@163.com

Abstract: To reduce the effects of information redundancy caused by noise and band correlation on the hyperspectral image analysis, a method for hyperspectral images classification using Spectral Correlation(HCSC) is proposed. Firstly, the hyperspectral images are preprocessed. Secondly, band selection algorithm based on correlation coefficient(BCCS) is proposed to reduce the information redundancy caused by adjacent bands. Thirdly, The spatial pixel purity index(SPPi) is used to extract the pure pixel and end-member extraction is accomplished. The experiments have been done on AVIRIS database. The experimental results have shown the proposed algorithm(HCSC) can improve the efficiency in the pure pixel extraction and classification, and the classification accuracy is 86.4%.

Keywords: multifractal spectrum; feature extraction; hyperspectral images; support vector machine

1. INTRODUCTION

In the modern remote sensing system, compared with other remote sensing technology, there are a number of advantages in hyperspectral remote sensing technology, such as its strong waveband continuity, approximate spectral information of object, stronger recognition ability to ground objects. The hyperspectral remote sensing technology has been more and more widely used in the field of land resources investigation and development and natural disaster monitoring. However, the hyperspectral data is exceedingly huge, and there is a strong correlation between spectrum and a lot of redundant information[1-5], which will increase while the number of bands in hyperspectral images becomes larger. Therefore, in order to improve the accuracy of object classification and reduce computation without losing significant information, it's necessary to select an appropriate sample set and compress the data properly for the end-member extraction rapidly and efficiently.

For hyperspectral image data compression [6-10], the main methods used in domestic and foreign research can be divided into two categories: one is to carry out some mathematical transformation on all bands to find the most important feature, that is, feature

extraction, the commonly used method is principal component analysis (PCA) [11] and Independent Component Analysis (ICA). Secondly, according to certain judgment criteria, the band selection algorithm, such as Spectral Angle Mapping (SAM) and Euclidean Distance (Euclidean Distance), is selected from all the bands of interest. ED) and so on. Feature extraction saves the information in the original data as much as possible through matrix transformation of spectral data to avoid the loss of information. However, the information itself is provided by the original data, which inevitably retains the external noise information, the phenomenon of "isomerism" between hyperspectral image pixels [12-14] can not be effectively improved. The band selection algorithm retains the original data of the interested band and improves the information redundancy problem between bands. However, the information loss caused by the part of the bands removed by the algorithm has a certain impact on the classification results. Multifractal spectrum can realize the detailed description of the texture features of the data at multiple scales. By expanding the similarity between the same object pixels, the phenomenon of "same object and different spectrum" between the pixels of hyperspectral image can be improved, and the efficiency of object recognition can be improved. In this paper, multifractal is introduced into hyperspectral image feature extraction. On the one hand, feature extraction effectively compresses the data and solves the problem of high dimensionality of pixel spectrum; On the other hand, the multi-fractal spectrum features can describe the texture information of terrain more precisely, solve the problem of pixel spectral difference of the same terrain under different illumination conditions, and improve the efficiency of terrain classification. In this paper, a hyperspectral image classification method based on multifractal spectrum (MFS) is proposed. First, the hyperspectral data are preprocessed, then the multifractal curve of pixel spectrum is calculated and the corresponding multifractal features are extracted. Finally, the pixels are classified by combining support vector machine (SVM) [15] and k-nearest neighbor (KNN) classifier. In order to verify the effectiveness of the proposed feature (MFS), experiments were carried out on

Hyperspectral database AVIRIS and compared with SPPI features. Experimental results show that the accuracy and stability of feature classification are better than those of contrast features, and the combination of different classification algorithms to achieve the classification of terrain has a good classification effect.

2. FEATURE EXTRACTION

Multifractal originates from fractal theory. By introducing the concept of generalized dimension and calculating a spectral function containing multiple measures, the accurate description of the classification features of different levels of things is realized, which greatly improves the calculation efficiency of single fractal. There are two main definitions of multifractal: the definition based on generalized fractal dimension and the definition based on measure theory. The two definitions are based on the same theory. Because the generalized fractal dimension method is more convenient to verify the multifractal property of the object and to calculate, this paper uses the multifractal definition method based on the generalized fractal dimension to calculate the multifractal spectrum.

(1) Multifractal spectrum calculation

Generally, the multifractal spectrum is calculated by the generalized dimension. In this paper, the box dimension is used to calculate the multifractal spectrum. The calculation steps of box dimension of pixel spectra in hyperspectral images are as follows: Suppose the one-dimensional vector of pixel spectrum $x=[x_1, x_2, \dots, x_d]$ is covered by a non-overlapping grid of scale δ . $x=[x_1, x_2, \dots, x_d]$ is divided into N elements, which are denoted as $\{\Delta_i\}$ ($i=1, 2, \dots, N$), The unit probability measure of unit I is $p_i(\delta)$ under scale δ , like the following formula:

$$p_i(\delta) = \frac{\sum_{j=1}^m e_{ij}}{\sum_{k=1}^n \sum_{j=1}^m e_{kj}} \tag{1}$$

In the formula, e_{ij} represents the value of the j sample data in the i box. For $p_i(\delta)$ weighted summation, the partition function $M(q, \delta)$ is obtained.

$$M(q, \delta) = \sum_i^N p_i^q(\delta) \tag{2}$$

Among them, q represents the weight of unit probabilities. Due to the self similarity of fractals, the relationship between $M(q, \delta)$ and scale δ satisfies the formula (3).

$$M(q, \delta) \sim \delta^{\tau(q)} \tag{3}$$

In the formula, $\tau(q)$ is the quality index, which is a monotonically increasing convex function of q . α is defined as the singularity index. Each element $\{\Delta_i\}$ has a corresponding value, which is used to reflect the fractal dimension of the corresponding element. $\alpha(q)$ is a monotonic decreasing function of q . In order to calculate the frequency of occurrence of α , $f(\alpha)$ is introduced, which represents the fractal dimension of the same α . It is a continuous spectral function used to describe the fractal dimension of a unit, i. e. multifractal spectrum. According to the relationship among multifractal spectrum $f(\alpha)$, generalized dimension $D(q)$ and $\alpha(q)$ of pixel spectrum, Legendre transform is satisfied, such as equation (4).

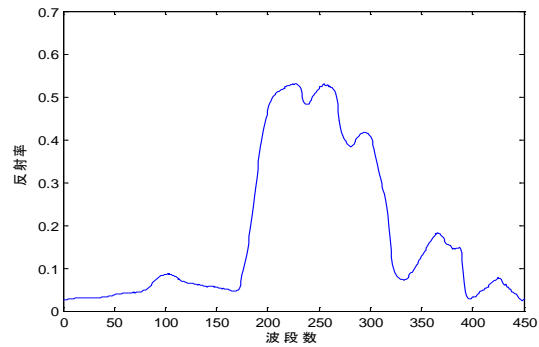
$$\begin{cases} \alpha(q) = \frac{d\tau(q)}{dq} \\ f(\alpha) = q \cdot \alpha(q) - \tau(q) \\ D(q) = \frac{\tau(q)}{q-1} \end{cases} \tag{4}$$

Simultaneous (1) ~ (4) and sum (5), (6):

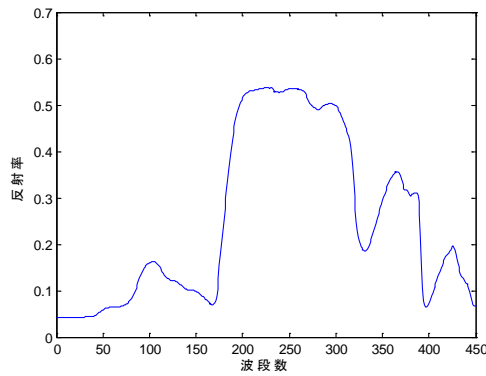
$$f(\alpha(q)) = q \cdot \frac{\sum [p_i^q(\delta) \cdot \ln p_i(\delta)]}{\ln \delta \cdot \sum p_i^q(\delta)} - \frac{\ln[\sum p_i^q(\delta)]}{\ln \delta} \tag{5}$$

$$\alpha(q) = \frac{\sum p_i^q(\delta) \cdot \ln p_i(\delta)}{\ln \delta \cdot \sum p_i^q(\delta)} \tag{6}$$

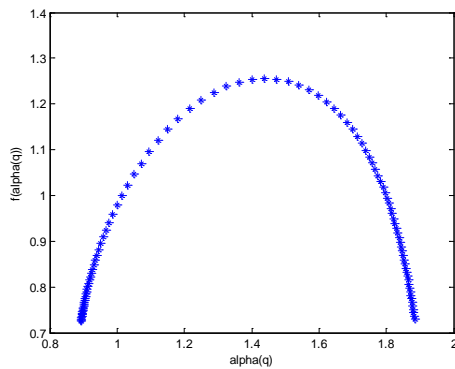
Take the United States Geological Survey (USGS) spectrum database as an example, The curve of spectrum and the corresponding multifractal spectrum of 2 surface features are selected as shown in Figures 1 and 2.



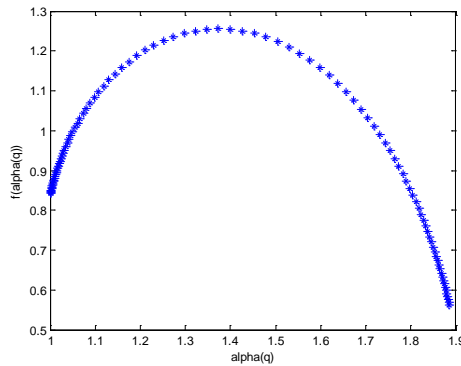
(a) Tar shrubs



(b)Walnut
Figure 1 Pixel spectra of 2 kinds of surface features



(a)Tar shrubs



(b)Walnut

Figure 2 Multifractal spectrum of 2 kinds of objects
The multifractal curves select the partition curves of the same size δ and take $q \in [-5, 5]$ to calculate the corresponding curves $f(\alpha)-\alpha$ of the two objects in turn as shown in Figure 2. The hyperspectral curves of the 2 surfaces have similar structures, but their multifractal curves are different. Therefore, the multifractal spectrum extracted from hyperspectral data has a certain degree of recognition.
(2) Multifractal feature extraction

Generally, the multifractal spectrum $f(\alpha)$ is the unimodal function of α . $\alpha(q)$ is a monotonically decreasing function of weight factor q . In order to further extract the spectral features of pixels, the

feature points of part of curve $f(\alpha)-\alpha$ are selected to replace the multifractal spectrum as the final multifractal features. The value range of recording curve is $[\alpha_{\min}, \alpha_{\max}]$, and the corresponding $f(\alpha)$ values for the boundary are $f(\alpha_{\min})$ and $f(\alpha_{\max})$ respectively. It reflects the property of the probability measure part in the pixel spectrum and the property of the small probability measure part. When $q = 0$, $f(\alpha)$ takes the maximum value, the curve satisfies $q < 0$ monotonically decreasing, and $q > 0$ increases monotonically, at this time we have $\alpha = \alpha_0$; The width of the curve is $W = \alpha_{\max} - \alpha_{\min}$. The multifractal feature (7) is obtained by extracting the above feature points.

$$P = [\alpha_{\min}, \alpha_{\max}, f(\alpha_{\min}), f(\alpha_{\max}), \alpha_0, W] \quad (7)$$

3. CLASSIFICATION

A hyperspectral image classification method based on multifractal spectrum is proposed in this paper. By calculating the multifractal spectrum of the pixel spectrum and extracting its multifractal features, SVM classifier is used to classify the pixels. The specific steps are as follows:

- (a)The multifractal spectrum of pixel spectrum is calculated.
- (b)The multifractal feature of pixel spectrum is extracted.
- (c)Select training pixel special collection and complete SVM classifier training.
- (d)We use training model to classify pixels.

4. ANALYSIS

The data recorded in the experimental area include 16 kinds of objects. Typical objects include: corn, grassland, trees, alfalfa, soybeans and oats. In this paper, raw hyperspectral data are preprocessed first. Then we calculate the MFS characteristics of each pixel and classify the pixels using this feature. The hyperspectral ideal terrain distribution is shown in Figure 3.

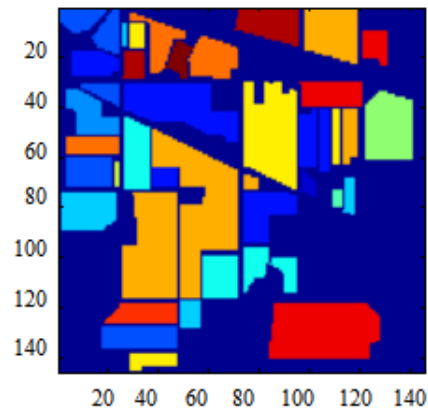


Figure3 Hyperspectral ideal distribution map
In order to verify the characteristics of this paper, it is better than other features to improve the classification efficiency of hyperspectral images. In this paper, two

groups of experiments are designed, one is based on the spatial pixel purity index characteristics as a comparison, to verify that the proposed method has better performance. The other group chooses the nearest neighbor classification algorithm and the support vector machine algorithm separately to carry on the contrast experiment to this article proposed the characteristic, in order to verify this article characteristic union different classification algorithm, has the same superiority.

Table 1 experimental results of different feature classification

type	SPPI Correct rate	This paper
alfalfa	0.65	0.8
Corn	0.935988	0.923497
Forage grass	0.217391	0.608696
Haystack	0.804598	0.862069
oats	0.125	0.625
soybean	0.868762	0.881701
Wheat	0.815217	0.842391
wood	0.871795	0.864721
Accuracy (OA)	0.868875	0.880747
Kappa coefficient	0.8689	0.8807

It can be seen that the overall classification accuracy of spatial pixel purity index features is 86.88%, while the overall classification accuracy of this method for different types of terrain based on multifractal theory is 88.07%.

Furthermore, in order to verify that the proposed features have the same advantages for different classification algorithms, the k-NearestNeighbor (KNN) classification algorithm and the support vector machine(SVM) algorithm are selected to classify hyperspectral images, and their classification effects are compared.

It can be seen that the overall classification accuracy of this feature combined with KNN algorithm is 88.07%, and the overall classification accuracy is 88.42% when combined with SVM algorithm, and the recognition rate is higher than 88%. And the Kappa coefficients are greater than 0.81, the results of two categories are almost identical. Therefore, it is concluded that the proposed features combined with different classification algorithms have good classification efficiency.

type	KNN Correct rate	SVM Correct rate
alfalfa	0.8	0.875
Corn	0.923497	0.921155
Forage grass	0.608696	0.652174
Haystack	0.862069	0.862069
oats	0.625	0.625
soybean	0.881701	0.887246

Wheat	0.842391	0.869565
wood	0.864721	0.864721
Accuracy (OA)	0.880747	0.8842
Kappa coefficient	0.8807	0.8842

Table 2 results of different classification methods

5. CONCLUSION

A hyperspectral classification method based on multifractal spectrum is proposed in this paper. In order to solve the problem of "homology and heteroscedasticity" between hyperspectral image pixels, the multifractal spectrum has the advantage of accurate description in detail information, and good classification results are obtained. The results showed that:

The accuracy and stability of feature classification are better than that of SPPI method. The combination of the proposed features and different classification algorithms achieves good classification efficiency.

REFERENCES

- [1]N. H. Ly, Q. Du, J. E. Fowler. Reconstruction From Random Projections of Hyperspectral Imagery With Spectral and Spatial Partitioning. IEEE Journal of Selected Topics in Applied Earth Observations & Remote Sensing, 2013, 6(2): 466-472.
- [2]Chen C, Li W, E. W. Tramel et al. Reconstruction of Hyperspectral Imagery From Random Projections Using Multihypothesis Prediction. IEEE Transactions on Geoscience & Remote Sensing, 2013, 52(1): 365-374.
- [3]Lu X, Li X. Multiresolution Imaging. IEEE Trans Cybern, 2013, 44(1): 149-160.
- [4]U. Srinivas, Chen Y, V. Monga et al. Exploiting Sparsity in Hyperspectral Image Classification via Graphical Models. IEEE Geoscience & Remote Sensing Letters, 2012, 10(3): 505-509.
- [5]Sun K, Geng X, Wang P et al. A Fast Endmember Extraction Algorithm Based on Gram Determinant. IEEE Geoscience & Remote Sensing Letters, 2014, 11(6): 1124-1128.
- [6]Wen J, Tian Z, Liu X et al. Neighborhood Preserving Orthogonal PNM Feature Extraction for Hyperspectral Image Classification. IEEE Journal of Selected Topics in Applied Earth Observations & Remote Sensing, 2013, 6(2): 759-768.
- [7]Ratto C R, Morton K D, Collins L M. et al. Bayesian Context-Dependent Learning for Anomaly Classification in Hyperspectral Imagery. IEEE Transactions on Geoscience & Remote Sensing, 2014, 52(4): 1969-1981.
- [8]Pu H, Chen Z, Wang B et al. A Novel Spatial-Spectral Similarity Measure for Dimensionality Reduction and Classification of Hyperspectral Imagery. IEEE Transactions on Geoscience & RemoteSensing, 2014, 52(11): 7008-702.
- [9]Mei S, He M, Wang Z et al. Unsupervised Spectral Mixture Analysis of Highly Mixed Data With Hopfield Neural Network. IEEE Journal of Selected

Topics in Applied Earth Observations & Remote Sensing, 2014, 7(6): 1922-1935.

[10]Wu X Y, Huang B M, Antonio Plaza et al. Real-Time Implementation of the Pixel Purity Index Algorithm for Endmember Identification on GPUs. IEEE Geoscience and Remote Sensing Letters, 2014, 11(5): 955-959.

[11]Yang P Y, Tsai J T, Chou J H. PCA-Based Fast Search Method Using PCA-LBG-Based VQ Codebook for Codebook Search. IEEE ACCESS, 2016, 4: 1332-1344.

[12]Xia J, Chanussot J, Du P et al. Semi-Supervised Probabilistic Principal Component Analysis for Hyperspectral Remote Sensing Image Classification. IEEE Journal of Selected Topics in Applied Earth Observations & Remote Sensing, 2014, 7(6): 2224-2236.

[13]Samat A, Li J, Liu S C et al. Improved hyperspectral image classification by active learning using pre-designed mixed pixels. PATTERN RECOGNITION, 2016, 51: 43-58.

[14]Wang Z, Nasrabadi N M, Huang T S. Spatial-Spectral Classification of Hyperspectral Images Using Discriminative Dictionary Designed by Learning Vector Quantization. IEEE Transactions on Geoscience & Remote Sensing, 2014, 52(8): 4808-4822.

[15]Kuo B C, Ho H H, Li C H et al. A Kernel-Based Feature Selection Method for SVM With RBF Kernel for Hyperspectral Image Classification. IEEE Journal of Selected Topics in Applied Earth Observations & Remote Sensing, 2013, 7(1): 317-326.

Research on the Maintenance Spare Parts Support Risk Model of Insufficient Reserve Starting Point

MA Quan-yue¹, CHENG Zhong-hua¹, WANG Ya-bin¹, LIU Shen-yang²

¹. Shijiazhuang Campus, The Army Engineering University of PLA, Shijiazhuang 050001, Hebei, China;

². Air Force Logistics College, Xuzhou 221000, Jiangsu, China

Abstract: Maintenance spare parts factory reserve needs to meet the starting requirements of variety, quantity, amount, etc., the factory can obtain benefits. If the reserve (mainly the amount of money) is too small, the plant storage sites, facilities and equipment investment may be greater than the income, it will lead to loss of the factory. The risk of profit and loss should be considered comprehensively.

Keywords: Reserve starting point; risk; model

When the maintenance spare parts reserved in a factory are in need of maintenance, it is necessary for the factory to send a person to escort the goods to the construction unit. The number of the escort personnel is generally related to the variety and quantity of the maintenance spare parts reserved, and is related to the number and distance of the insured units.

1. SYMBOL EXPLANATION

$f_i(x_i)$ —the density function of the demand for maintenance spare parts;

d_i —the unit price of the maintenance spare parts;

J_1 —the starting point of the factory reserve is insufficient and the total amount of loss;

J_{10} —the amount of factory reserve critical point in established units;

J'_1 —the total starting point of local factory reserves;

J'_{10} —the amount of the critical point of the local factory reserve;

λ_k —determine the parameters of the first station to be guaranteed by which supplier.

2. RISK DEFINITION

When the total amount of spare parts reserve is insufficient, the income of the factory is less than the expenditure, resulting in loss and risk. When the total amount of reserve is 0, the factory has no reserve task, that is, no reserve income for maintenance spare parts, but also has to bear the wages of employees, facilities and equipment maintenance costs. The maximum risk is 100%. When the total reserve is reached, the risk is 0. When the total reserve is greater, the revenue of the factory is greater than the expenditure, and the risk is

0.

$$g_1(J) = \begin{cases} 100\% & J = 0 \\ \frac{J_{10} - J}{J_{10}} & 0 < J < J_{10} \\ 0 & J \geq J_{10} \end{cases} \quad (1)$$

Similarly, the local factory has the following risk expressions:

$$g'_1(J') = \begin{cases} 100\% & J' = 0 \\ \frac{J'_{10} - J'}{J'_{10}} & 0 < J' < J'_{10} \\ 0 & J' \geq J'_{10} \end{cases} \quad (2)$$

3. RISK CALCULATION

$$J = \sum_i d_i \bar{X}_i \quad (3)$$

The total amount of factory reserve maintenance spare parts is

$$\bar{J} = \sum_i d_i \bar{X}_i = \sum_i d_i E(X_i) = \sum_i d_i \int_0^\infty x_i f(x_i) dx_i \quad (4)$$

At that time, the amount of factory loss is only

$$J_1 = J_{10} - J \quad (5)$$

The average risk of factory reserve maintenance spare parts is

$$g_1(\bar{J}) = \frac{J_1}{J_{10}} = \frac{J_{10} - J}{J_{10}} = \quad (6)$$

$$1 - \frac{1}{J_{10}} \sum_i d_i \int_0^\infty x_i f(x_i) dx_i$$

Similarly, the average risk of maintaining spare parts in local factories is

$$g'_1(\bar{J}') = \frac{J'_1}{J'_{10}} = \frac{J'_{10} - J'}{J'_{10}} = \quad (7)$$

$$1 - \frac{1}{J'_{10}} \sum_i d_i \int_0^\infty x_i f(x_i) dx_i$$

Thus, the average risk of reserve maintenance spare parts of several stations can be obtained under the joint civil and military joint guarantee.

$$g_1 = \lambda_k \left[1 - \frac{1}{J_{10}} \sum_i d_i \int_0^\infty x_i f(x_i) dx_i \right] + (1 - \lambda_k) \left[1 - \frac{1}{J'_{10}} \sum_i d_i \int_0^\infty x_i f(x_i) dx_i \right] \quad (8)$$

4. EXAMPLE ANALYSIS

Three kinds of maintenance spare parts are reserved in the two factories. The reserve quantity of the three known maintenance spare parts obeys the normal distribution N (10, 22), N (12, 32), N (15, 42). The unit price is 10, 000, 25, 000 and 30, 000 respectively. The critical reserve value of the two factories is 300, 000. The average distance between the two factories is 300 km, 1650 km and 2800 km; 3500 km, 1250 km and 2600 km. The average daily escort of the escorts is 400 km, and the average one-time delivery of four maintenance spare parts. The average man-hour cost rate of the factories is 20/h, and the critical total man-hour of the factories is 500 days. The three kinds of maintenance spare parts (corresponding to three kinds of equipment) are stored in the factories. The 10-year reserve quantity of equipments is 8 pieces, 7 pieces and 12 pieces respectively. The unit demand of three known maintenance spare parts obeys normal distribution N (10, 22), N (12, 32), N (15, 42), and the unit price is 10, 000, 25, 000 and 30, 000, respectively. The critical point of the storage cost of the maintenance spare parts is 80, 000. The average maintenance cost of the three maintenance spare parts is 1, 000/piece, 2, 500/piece, 3, 000/piece. The unit price of the three kinds of maintenance spare parts is 10, 000, 25, 000, 30, 000 and the storage life of the three kinds of maintenance spare parts is 1-1-distributed. There are 10 pieces in stock (5 of them are 2 years old, 5 of them are 1 year old), 15 pieces (3 of them are 3 years old, 7 of them are 2 years old, 5 of them are 1 year old), 20 pieces (10 of them are 2 years old, 10 of them are 1 year old). Calculate the risk of insufficient reserve starting point. Table 1 probability of transfer of maintenance spare parts

Number	Ordinal equipment has been allocated time			
	5	10	15	20
1	0.1	0.4	0.7	0.9
2	0.3	0.5	0.8	0.9
3	0.2	0.3	0.4	0.5

Table 2 maintenance cost of spare parts 123

Maintenance spare parts	1	2	3
Average demand for units	10	12	15
Existing inventory	10	10	10

Single piece	1	1.5	2
Send and receive charges	800	600	900
Quality inspection fee	980	970	960
Maintenance cost	850	820	700

$J_{10} = J'_{10} = 30, d_1 = 1, d_2 = 2.5, d_3 = 3,$ substituted, the risk expression of factory reserve maintenance spare parts is

$$g_1(J) = \begin{cases} 100\% & J = 0 \\ \frac{30 - J}{30} & 0 < J < J_{10} \\ 0 & J \geq J_{10} \end{cases}$$

Similarly, the local factory has the following risk expressions:

$$g'_1(J') = \begin{cases} 100\% & J' = 0 \\ \frac{30 - J'}{30} & 0 < J' < J'_{10} \\ 0 & J' \geq J'_{10} \end{cases}$$

Since the demand for 3 maintenance spare parts is subject to normal distribution, the average annual order quantity is

$$E(X_1) = 10, E(X_2) = 12, E(X_3) = 15$$

The risk of insufficient reserve starting point is

$$g_1 = \lambda_k \left[1 - \frac{1}{J_{10}} \sum_i d_i \int_0^\infty x_i f(x_i) dx_i \right] + (1 - \lambda_k) \left[1 - \frac{1}{J'_{10}} \sum_i d_i \int_0^\infty x_i f(x_i) dx_i \right] = 19\%$$

5. CONCLUDING REMARK

Maintenance spare parts military and civilian joint support, need to carry out maintenance spare parts reserve in the factory, the risk may appear in the factory. Reserve starting point insufficient risk, occupy too many people risk, repair spare parts production risk, storage cost risk and quality assurance costs too high risk. For the purpose of win for both the army and the people.

REFERENCES

[1]LU Guansheng. Consideration on equipment support of the army in joint operations. Research on air defense equipment technology of artillery. 2015, (6):21-27.
 [2]LU Hongtao. A preliminary study on the supporting capacity of synthetic army equipment system under informatization condition. Journal of artillery college, 2011, (3):35-39.
 [3]LI Zhishun. Military equipment assurance. Military science press, 2009.

Practical Teaching Reform of Graduation Design in Civil Engineering

Jianbo Zheng

Binzhou University, Binzhou, 256600, China

Abstract: Graduation design is an important practical teaching link in the comprehensive practicality of civil engineering. The present situation and problems of the practical teaching of graduation design for civil engineering are expounded. Aiming at the problems in graduation design, the targeted and innovative direction of reform are put forward, and the teaching design methods are made clear, so as to ensure the overall quality level of graduation design.

Keywords: Graduation design; Civil engineering; Teaching design method

1. INTRODUCTION

The graduation design is the last stage of comprehensive practice teaching for undergraduate education of civil engineering students in this process, comprehensive use of basic knowledge and professional skills in four years of practical training, can improve the analysis and solving practical engineering problems, but also lay the foundation for the design, construction and management in the field work. The quality of graduation design directly affects the students' ability to play in the job post after graduation [1]. It is also a direct reflection of the quality of education and teaching in a university. How to improve the teaching quality of graduation design is an important content that needs deep thinking and continuous exploration in the stage of undergraduate education.

2. ANALYSIS OF MAIN PROBLEMS IN GRADUATION DESIGN

The existing topic types of graduation design mainly include structure, construction, geotechnical and cost orientation, and the topic selection is relatively narrow, and most of them have "proposition style" design questions. Graduate design instructors provide detailed graduation design tasks, which clearly define the design content and schedule. Students' graduation design is only a large assignment under the predetermined plan. The design is difficult, but the task is arduous. The number of graduates has increased year by year because of the enrollment expansion in colleges and universities. The number of students under the guidance of each instructor is too large, and other teaching and scientific research tasks are heavy. Limited by time and energy, instructors have been guiding the same types of topics for many years. Students generally feel that graduation design and actual engineering derailment, there is no

enthusiasm and desire for innovation, and cannot give full play to the subjective initiative [2].



Figure1 Design sketch of residential building

The graduation design is generally arranged in the eighth semester of the undergraduate stage, and most of the graduates have been successfully signed at this time. A considerable number of students believe that graduation design can get their diploma and degree certificate if they are qualified, so there is no need to spend much time and energy in graduation design. And some of the students who have not found the job are busy with all kinds of job fairs, and they can't do the graduation design at all. However, a small number of graduate students prepare for postgraduate interviews and reexamination work, which also involve a lot of time and energy, which affect the progress and quality of graduation design. In addition, some students don't pay enough attention to the graduation design itself. They neglect that graduation design is the last "warm-up" before going to work, so as to waste a great opportunity. In view of the above conditions, the overall quality of the graduation design is not high [3].

Including the student's daily attendance management system and process management, but the graduation design process often have students who participate in the recruitment, interview, and other reasons not regular and absenteeism, graduation design in the late part of no need computer, notebook computer, students cannot type fixed classroom machine to do graduate design, the attendance system flow form. In addition, the design cycle is relatively long, during the guidance of teachers and other teaching and

research tasks, sometimes on the graduation design management and monitoring is not in place, the student level is uneven, some students do not get effective supervision and the problems are not let things drift, take the initiative to contact the instructor, resulting in design progress is seriously lagging behind. The design of pre graduate slack, and the late night combat is almost every year of graduation design have a phenomenon, so the high quality of the graduation design results cannot be guaranteed [4].

The number of books, national standards, technical specifications, standard atlas and related industry standards required for graduation design is small and slow to update. Students who do structural and construction graduation design often share a set of

specifications and atlas in groups or groups. The relevant reference materials for the graduation design of the deep foundation pit and highway bridge are scarcer. It mainly relies on guidance and online search data to solve the problem by instructing teachers two times a week. And the computer room of the computer room is limited, the related computing software is not complete, the student's calculation is basically hand calculation, not equipped with the necessary electrical calculation content. Even though some of the computerized part of graduation project is mostly calculated by pirated software or incomplete software, such factors will also affect the progress and quality of graduation design objectively [5].



Figure 2 building elevation

The fairness and rationality of the graduation design assessment method is the "lifeblood" of the students with serious and rigorous attitude to the graduation design. Considering the graduation design grade of teachers, teachers, Defense Review Group three aspects of weight, but the specific operation also has some disadvantages [6]. Teachers are relatively reliable results, but it usually teachers on students usually understand a handful, only by correcting the students' graduation design results in a short time the results are given. The final result of the defense team is also questionable, because the time limit of reply and the question of defense are not enough to evaluate students' ability to master and apply knowledge, and lack of examination of the whole graduation design process. In addition, the judges, the respondent group between the direction of teachers' professional study and differences, leading to graduation design results were compared to the students. This also greatly reduces the enthusiasm of the students to graduate design.

3. RESEARCH ON THE REFORM OF GRADUATION DESIGN

According to the status quo before the graduation design of civil engineering, from the timing, select topic, process guidance, marking the defense and other aspects, based on improving the teaching quality

of graduation design, the main line of students' engineering practice ability training, to carry out the project as the background, the implementation of teaching reform and practice of tutorial system and combining graduation design, fully play a leading role of teachers, strengthen the quality management of the whole process, fully and effectively improve the teaching quality of graduation design [7].

Most of the graduate work in civil engineering is distributed in the production and management frontlines, which requires the graduates to have a strong practical ability. As a comprehensive practical teaching link, the first step of graduation design is particularly important. Topic selection should combine engineering practice, advocate the combination of professional theory and practical projects, and start from actual combat, which is conducive to mobilize the enthusiasm, initiative and innovation consciousness of students. In order to ensure every question, the instructor requires multi aspect and multi-channel acquisition task: can the actual project topics with the construction unit or Design Institute; can combine research and professional guidance teachers to design or research topics; can be combined with the employment of students and the characteristics of interest to study etc.. After the selection of topics, the college set up a

leading group of graduation design to collectively demonstrate all the topics, requiring comprehensive knowledge structure, full work tasks and practical application. At the same time, the teachers and students with double, graduation design students and guiding teachers [8].

In order to solve the contradiction between graduation design and employment, the task arrangement of graduation design is arranged in advance at the end of the seventh semester, which actually increases the effective time of graduation design, and is conducive to the development of follow-up work. Before the winter vacation, the graduation design mobilization meeting was organized to arrange the students to meet with the instructors. The instructor can issue the graduation design task book to the students ahead of time, so that the students can seriously reflect on the tasks and requirements of the graduation design in their vacation time, and do well in the basic skills training such as data collection and CAD. The eighth semester graduation design is first to 2 weeks after the beginning of the graduation practice stage, the main task is to combine the topic and content of graduation design for special research. 3 to 4 weeks for the design stage, through access to a large number of students and their related research data, specification and reference, further digestion and absorption, put forward feasible design plan and conduct a comprehensive and detailed demonstration, based on carefully written report [9]. A good report helps students to deepen understanding of the task, to reduce the blindness of time and initial stage to the graduation design and graduation design is also carried out the following work to create favorable conditions.

4. DESIGN OF PRACTICAL TEACHING METHOD

The correct way of grouping is very important to the success or failure of teaching. In order to stimulate the students' learning motivation, the competition mechanism is introduced among the groups, so the design results are best comparable [10]. In order to ensure the balance of each group, we should take full consideration of the students' basic knowledge level and adopt the interspersed collocation method. This will facilitate the design of the competition according to the results of the calculation.

After a good project team, each team shall appoint the chief engineer and designer, review, copywriting, namely role playing method. In order to ensure the quality of teaching, this division of labor should be changed in four teaching projects. When the course is finished, the students can be qualified for each post.

Before carrying out the specific design tasks, each group can be divided again, and each person is responsible for different design calculations, such as load calculation, structural internal force calculation, flexural strength checking, shear strength checking and stiffness checking [7]. All teams responsible for

similar problems are reconstituted into groups, read the information provided by teachers with common problems, and discuss the final conclusion, so as to master the calculation method in this area. Then return to the original group, report with the original team members and cooperate to complete the final design and checking. This method requires that every student should be fully invested, otherwise it will cause a lack of a group in one aspect. Therefore, teachers should pay special attention to the observation of students' learning state [11].

The following guidance is issued, and specific design tasks, reference materials, similar engineering cases, design steps, evaluation criteria, checklists, and notices are given. With similar engineering cases, students can imitate and carry out their own preliminary design calculations.

The same type of graduation design guidance teachers form a team to guide the students. The person in charge of the teaching team conducts business guidance and coordination of the team teachers. Responsible for the strict control of the graduation design topic, through the research of the design institute and construction units, engineering design and construction of the current understanding of the main types, construction methods, grasp the latest information, combined with the actual engineering, the knowledge and technology of new method to teach the students [7]. According to each student's knowledge of professional knowledge and ability, teach students in accordance with their aptitude, in order to achieve the best results of graduation design.

5. PRACTICE TEACHING EVALUATION

The reform of graduation design must break through the traditional teaching mode of graduation design. The teaching evaluation is carried out in a combination of the process evaluation and the result evaluation. The process evaluation accounted for 50%. The teachers observed the results of students' performance and students' mutual evaluation. The results of the results were 50%, based on the results of the competition of four design projects. In order to carry out the design competition smoothly, the rules of competition and the standard of scoring should be clearly defined in the guide [12]. The evaluation standard has two aspects, one is the overall structure calculation, structure by checking the safety for the pass, to select the appropriate stress ratio, the amount of steel of the province team out; two is the construction drawing and construction drawing to complete without missing pass, to correct, standard, reasonable layout drawing full marks.

6. CONCLUSIONS

The teaching process of graduation design is an important stage to achieve the goal of undergraduate training, and it is the last important part of the undergraduate program. In the increasingly severe employment market for college graduates, it is very important for college students to succeed in

employment to reexamine and coordinate university education and teaching, especially for graduation design teaching in important practical links. Improving the quality of graduation design of civil engineering is conducive to the overall improvement of students' professional quality, effective implementation of professional training objectives and improvement of graduates' professional level.

REFERENCES

- [1]Chen Zhansheng, Liu Xiaoyu. Research on the quality guarantee mechanism of undergraduate graduation design management in Colleges and Universities. *Computer Education*, 2016(02): 163-166.
- [2]Zhang Donghai, Zhang Yindi. Research on quality control strategy of civil engineering graduation design and course design. *Jiangxi Building Materials*, 2016(19): 260-262.
- [3]Rao Lingping, Ding Jianyong, Hu Bo. An exploratory practice that combines undergraduate graduation design with scientific research and engineering practice. *University Education*, 2015(11): 36-38.
- [4]Wang Qianyun. The reform and innovation of the graduation design model of the Engineering Cost Specialty. *Journal of Higher Education*, 2016(03): 131-132.
- [5]Xu Zhi. Discussion on the reform of graduation design teaching for engineering. *University Education*, 2015(05): 144-145.
- [6]Zhang JinYuan, Lu Yan, Han Qinghua. Innovation and practice of graduation design for civil engineering. *Journal of Architectural Education in Institutions of Higher Learning*, 2016(01): 162-166.
- [7]Qin Xun. The innovation research on the graduation design of the applied undergraduate college. Anhui University, Hefei, 2017.
- [8]Zhang Jian, Liu Xiaoying, Wang Denggui. Research on the topic selection of graduation design oriented by innovation ability training. *Experiment Science and Technology*, 2015(02): 157-159.
- [9]Li Jun, Zhang Yandi. The thought shift on the undergraduate thesis project in engineering major. *Higher Education of Sciences*, 2014(05): 108-112.
- [10]Gao Hongyan, Liu Fei. Reflection on the reform of the practical teaching of engineering graduation design. *China Modern Educational Equipment*, 2017(01): 69-71.
- [11]Mou Zaigen, Wang Ke. Research on the training mode and method of the innovation practice base of undergraduate graduation design. *University Education*, 2017(12): 156-159.
- [12]Wang Guolin, Ding Wensheng, Zhao Haidong. Research and Practice on teaching reform of graduation design for civil engineering major in Applied Undergraduate Colleges. *Journal of Architectural Education in Institutions of Higher Learning*, 2014, 23(02): 119-122.

Is Self-Enhancement Restricted to Individualistic Cultures?—the Evidence from Risk Decision Making

Wei-fang Song

Railway Police College, Zhengzhou, Henan, 450053, China

Abstract: Whether self-enhancement motive is culturally relative or universal is a hot debated topic. The universalist proposed that the motive is pervasive all cultures, whereas the relativistic perspective posited that the motive is restricted to western cultures but absent in eastern cultures. The purpose of this study is to provide the evidence that self-enhancement is palculture by looking at individual's risk decision-making behaviors. A large number of studies have been documented to show that individuals in Asian culture (e.g., Chinese) are more risky than individuals in Western culture (e.g., American). Two studies were conducted in mainland China to explore the relation of self-enhancement and risk decision-making. Study 1 ($N = 158$) shows that self-enhancement is a significant predictor of risk decision making (adjusted $R^2 = 0.039$). Study 2 ($N = 148$) replicated the results by another scenario of risk decision-making relating one's self-esteem. These results of self-enhancement positively correlated with risk-taking behavior among Chinese participants provide an indirect evidence for self-enhancement is palcultural, because it is consistent with the universalist perspective.

Keywords: Self enhancement; risk taking; Pal culture

1. INTRODUCTION

Self-enhancement is known as the tendency to maintain a positive view of the self [1]. People think of themselves as better than others, for example, they believe they drive better than most other drivers [2], are fairer than most other people [3], and are smarter, warmer, more thoughtful, and more talented [4]. More than the expected 50% people evaluate themselves as above average on these desirable traits [5]. Therefore, self-enhancement is also called as "above-average-effect" that denotes the drive to affirm the self [6]. Hundreds of studies have found that people behave in way that minimize shame and humiliation feeling and maximize feeling of pride [7]. As a basic motivating factor, researcher confirms that self-other bias beyond their own personality, they also believe their friends and loved ones are better than most other people [8], their romantic relationship are better than most other people's [9], and they also believed that the groups they belong to are better than the groups to which they do not [10]. That is to say, anything that carries the designation "my" or "mine"

tends to be evaluated in an overly positive manner. However, whether self-enhancement is culturally relative or universal is a hot debated topic. There mainly have two completely opposite viewpoints on this.

The purpose of the present study is to investigate whether self-enhancement is pan-cultural from the risk-taking perspective. Most literature above indicated that the self-enhancement tendency is not shared by all cultures, but is a unique phenomenon of western culture. However, some studies on risk-seeking state that individuals in Asian culture were more risky than individuals in western culture. From this perspective, risk-seeking, self-enhancement and culture has such a progressive logic relationship that: (1) individuals in Eastern Asian are more risky than westerners; (2) people who have positive self-regard are generally more risky. We can make a conclusion that individual in Eastern Asian have high average positive self-regard (self-enhancement). If we can improve the casual relationship between self-enhancement and risk-seeking, we believed that this can provide an indirect evidence that people in east culture also is self-enhancement. We conducted two study to verify the hypothesis of the relationship between self-enhancement and risk-taking intention.

2. STUDY 1 PARTICIPANTS

Participants were recruited from several universities in Beijing. Announcements were made in various classes at these universities inviting them to participate this experiment. There are 158 undergraduate students involved the experiment at the end (52 male, 106 female; Mean age = 21.6 years, $SD = 4.8$). Most of them from rural areas (107) and they don't from one-child family. They were all recruited on a voluntary basis and thanked by 10 Yuan after they finished it.

(1) Procedure

There are two steps of the experiment. First, we asked the participants to complete a measurement of self-enhancement. After this they should accomplish an invest game. They filled in all their demographic information like age, sex etc. at the end of the experiments.

(3) Materials

A. Self-enhancement scale

The study first ask participants to indicate to what extent their traits higher than the average age college

students with the same sex of other college students. The scale included 28 personal traits (positive: independent, creative, distinctive, attractive, talent, easygoing, cooperative, honest, courtesy, sincere, moral; negative: independent, uncreative, untalented, incompetent, uncooperative, discourtesy, inconsiderate). The question is: "Suppose you are a student in a common college, according the below personality traits, to what extent do you think you are better than the other students who has the same sex, same age to you?" The participants should sign the number on a 1-6 likert scale to indicate what extent do they agree with the description of the traits be in line with themselves. Among that, 1 stand for "absolutely higher" and 6 means "absolutely lower". The individuals who gain more scores means that they are much more self-enhancement and the Cronbach alpha is 0.863 in this study.

B. Risk-seeking measurement

After the participant finished the self-enhancement scale, they should make a choice on two invest games expression. The stimuli were presented in booklets which measure individual's degree of risk-seeking read as follows [11]:

Suppose that you are faced with 2 investment options, A and B.

If you choose OPTION A, you may either make 920 Yuan or lose 200 Yuan.

If you choose OPTION B, you may either make 110 Yuan or lose 10 Yuan.

Please indicate your choice by circling a number on the 7-point scale given below:

7	6	5	4	3	2	1
Definitely					Definitely	
Choosing					Choosing	
OPTION A					OPTION B	

Subjects were instructed that there were no right or wrong answers, and the experimenters were only interested in the subject's own thoughtful answer. After all of these finished, they were thanked by 10 RMB.

3. RESULTS

(1) Primary analyses

Primary analyses revealed that no statistically significant main effects or interactions effects of participant's gender and the type of family (whether he/she in the one-child family) on self-enhancement ($t = 0.269$, $p = 0.789$; $t = 1.01$, $p > 0.05$). So we combined men and women participants in the further analysis. However, results shows that there is significant difference of birth place on self-enhancement ($M_{\text{city}} = 4.67 > M_{\text{rural}} = 4.10$, $t = 2.01$, $p < 0.01$). For risk-seeking, there is only has significant difference of gender ($M_{\text{male}} = 5.68 > M_{\text{female}} = 4.69$, $t = 2.554$, $p < 0.01$), other geographic variables not. We also checked the descriptive of the responses to the 28 traits to explore an overall index of explicit positive self-presentation ($a = 0.887$). The mean score of self-enhancement is 4.55 in the 1-7 point linket

scale that above the midpoint 4. The results states that participant in this study have a moderate higher level self-enhancement.

C. Regression analysis

We conducted the correlation analysis to explore the relationship between self-enhancement and risk-taking. The results show that there is a positive relationship between self-enhancement and risk seeking in this study by the self-esteem related scenario ($r = 0.214$, $p < 0.001$). We can make the conclusion from the results that people in Eastern culture may be have high level of positive evaluation because people are more risk-seeking in previous study. We conducted the stepwise regression analysis to further explore the causal relationship between the two. The results show that there is a significance predictive effect of self-enhancement on risk-seeking. After controlling the birth place and gender variables, the adjusted R^2 is 0.039 ($p < 0.001$) which indicated that people's self-enhancement is an important predictor variable on risk seeking. Individuals having higher level self-enhancement are more risk seeking from this results.

(4). Discussion

Though gender and the type of family has no significant difference on self-enhancement, the birth place has. Specifically to say, individuals in city has higher level positive evaluation than rural one's. According to the gender, male participants are much more risk seeking than female ones. There is a significant r coefficient between self-enhancement and risk seeking. Results of the regression analysis indicated that self-enhancement is an important predictor of risk seeking which can explain 0.039 variation. This verified the causal relationship between the two that people who have higher level positive evaluation are more risk seeking. According to the existed study, people in Eastern culture context are more risky than western people that we can believed that Eastern people are more self-enhancement or at least equivalent with western people. This results confirmed the hypothesis that self-enhancement are pal-culture, not only belong to some special culture. However, the invest game used in this study is from economic exchange only. As an important concept of self, we try to use a self-esteem related paradigm of decision making to further verify our hypothesis.

3. STUDY 2 PARTICIPANTS

The sample of the study is consisted of 148 college students who were recruited by announcements. There are 49 male (33%) and 99 female (67%) students whose mean age is 22.4 years. There are 79 participants (53.4%) from rural areas and their family has more than one child. They take part in the experiments on the voluntary basis and will receive 10 RMB as payment after they finished the experiment.

(1) Procedure

Participants in this study accomplished two tasks in sequence. Firstly, they were asked to complete the measurement of self-enhancement. Then the participants read a self-esteem related scenario about a joke which he/she will talk on the college graduation. After this, they should make the choice between the two to decide which joke they would like choose. They received the payoff after they finished all of the tasks and thanked by experimenters.

(2) Materials

A. Self-enhancement scale

We used the same self-enhancement measurement as in the study 1 whose Cronbach alpha is 0.863.

B. Risk seeking scenarios

We ask the participants to read a scenario related to self-esteem that on the topic of jokes. They should imagine giving the commencement speech at their college graduation and having to choose a joke between two choices. Joke A (**high payoff/ high risk**), which is hilarious and touching if successful but could fail completely, or Joke B (**low payoff/low risk**), which is less impressive but has a 100% likelihood of success. Participants were asked to decide between the jokes at 10 trials, where the likelihood of Joke A being successful decreases at each trial. For example, at Trial 1, Jokes A and B both have 100% likelihood of success: it thus makes sense to choose Joke A at this trial (which all participants did). At trial 2, the likelihood of Joke A success if 90%, at Trial 3 is dwindles to 80%, and so forth. At trial 10, there is a 0% chance that joke A will be successful (as might be expected, all participants opted for Joke B at this trial). The scenario was read as below:

Imagine that you have been asked to give a speech at your graduation ceremony. You are speaking to hundreds of your classmates. Now imagine that you can begin your speech with one of two jokes: joke A OR Joke B. If you tell Joke A, it can turn out to be **extremely funny and touching**. However, Joke A is a little complicated and there's a chance that no one will laugh. Joke B is mildly funny, but not as funny as joke A. however, Joke B is guaranteed to work—everyone will get it. The circles in the tables below represent your chances of successfully delivering each joke. If each box contains a circle, you chances of successfully delivering the joke are guaranteed, whereas if there are no circles, you have no chance of successfully delivering the joke. Imagine that for each numbered pair below, you must choose to deliver only Joke A OR Joke B. Note that you are offered varying chances of Joke A being successful, while your chances of Joke B being successful are always guaranteed. For each row, indicate which joke you would choose to tell by placing a checkmark in one of the two boxes.

Following completion of the decision making scenarios, participants were fully debriefed.

(3) Results

A. Primary analysis

We first analyzed the difference of geographic variables on self-enhancement and risk-seeking. The primarily results revealed no statistically significant main effects or interactions effects involving participant gender ($t = 1.186, p > 0.05$), so we combined men and women in all remaining analyses. Also, the number of child in a family also has no significant difference both in self-enhancement ($t = 0.961, p > 0.05$) and risk-taking ($t = 1.137, p > 0.05$) respectively. However, there is significant difference of birth place on self-enhancement ($M_{\text{city}} = 4.70 > M_{\text{rural}} = 3.85, t = 2.49, p < 0.01$). And also there is a significant difference of gender on risky decision make. Specifically, male students are more risky than female students ($M_{\text{male}} = 6.05 > M_{\text{female}} = 5.17, t = 4.24, p < 0.001$). We also checked the descriptive statistics of the self-enhancement and risk seeking. The mean score of self-enhancement scale is 4.831 which above the midpoint 4 in 1-7 linket. This results revealed that people have a moderate positive self-evaluation. The mean choice of risk taking is 5.94 on the adventure choice of A which state that people are likely to choose the 60% risky answer.

B. Regression analysis

We first did the correlated analysis of self-enhancement and risky seeking to explore the relationship between the two. The correlation coefficient is positive significant ($r = 0.247, p < 0.001$). The results is the same as in the study 1 which reveals that individual who have a higher positive self-evaluation are more risk seeking.

To further explore the causal relationship between risk seeking and self-enhancement we did the stepwise regression analysis. The result show that risk seeking has a significant predictive effect on self-enhancement. After controlled the birth place and gender, the adjusted R^2 of risk-taking on self-enhancement is 0.045, $p < 0.001$. This results verify the causality that self-enhancement is an important predictor of risk-seeking. Generally speaking, individual who have a high level self-enhancement always have high risk seeking intention.

(4) Discussion

The results of this study verify the assumption t that individual in eastern culture also have positive evaluation of self from the risk seeking perspective. According to the two joke choice, most people are likely to choose the “choice A” which is at the point of risk level 60%. Adopt the self-related paradigm, the results indicated that people are moderate risk seeking above the midpoint. The correlation coefficient is significant in the correlation analysis of self-enhancement and risk seeking as in study 1. We also conducted the regression analysis to explore the causal relationship between the two and verify again that self-enhancement is a significant prediction of risk seeking. This study verified our hypothesis that individuals have positive regard motivation with the

self-esteem related scenario in Eastern culture.

4. GENERAL DISCUSSION

Whether the need for positive self-regard (i.e., self-enhancement motive) is culturally relative or universal is a topic of intense debate. We address this issue with a study that test the causal effect of risk-seeking on self-enhancement in eastern cultures. The results showed that there is a significant relationship between self-enhancement and risk-seeking intention, and individual's risk-seeking intention is an important prediction of self-enhancement. That is to say, individual's who risk-seeking are self-enhancement.

In the present world economy, China and United States, Chinese from China are more-risk-seeking than Americans from the United States, and Chinese were found to exhibit markedly higher degrees of overconfidence than Americans in their general knowledge and probability judgments. There are several cultural explanations for differences in risk preference between Chinese and American respondents. Some argue that in socially-collectivist cultures like China, family or other in-group members will step in to help out any group member who encounters a large and possibly catastrophic loss after selecting a risky option. In individualist cultures like the United States, on the other hand, a person making a risky decision will be expected to personally bear the (possibly adverse) consequences of their decisions. Collectivism thus acts as a cushion against possible losses, that is, as social diversification of the risks of risky options. In the same sense that the purchase of an insurance policy reduces risk, social diversification in paying for the downside of risky options quite objectively reduces the risks of risky options for the members. Cultural values and collective culture have a hand in influencing risk preference and self-enhancement.

Is Self-enhancement Restricted to Individualistic Cultures?

According to the existed study, the existence or absence of a motive is difficult to study and is usually analyzed indirectly. The present study revealed such indirect findings that support the existence of self-enhancement motive in the East Asian culture of China from the risky decision making perspective. The results of some study believed that modesty plays in self-enhancement of agentic traits [12, 13]. When requirements for modesty are less internalized, that is to say, when modesty is lower, the self-enhancement motive can function more freely and higher self-enhancement is registered.

People in all culture have the motive striving to maintain and achieve positive self-regard. People have the same goal but may use different tactics to do so. In a similar vein, both individualistic and collectivistic cultures permit self-enhancement, but they do so through different norms. In the west, it is accepted or tolerated to flaunt one's successes. In the

east, it is accepted or tolerated to expect reciprocity relying on the seniority rule. Both in the West and in the East, self-enhancement is sanctioned through upward mobility, status seeking, forms of artistic expression, the promotion of the self on dimensions that matter. Both in the west and in the East, people self-enhance tactically, strategically, and opportunistically by making the culture work form them—a feat that deserves to be seen as a tribute to human resourcefulness, flexibility, and adaptability.

5. LIMITATIONS AND DIRECTIONS FOR FUTURE RESEARCH

The present study support that self-enhancement is palculture that both Eastern and Western people have self-positive of themselves from the perspective of risk-seeking. However, there are several question in this study and the future research should pay attention to and explore it.

The first question is why self-enhancement low in certain collectivist cultures? Except for our study, there still other study from other perspective to confirm and confirmed that self-enhancement is palcultre. However, there are also many study indicated that in certain collectivist cultures self-enhancement is low. The common explanation is that the self-enhancement motive is not prevalent in East Asian cultures due to basic differences in their typical self-construal patterns. The independent self, dominant in individualist cultures, is autonomous and self-contained, whereas the interdependent self typical of collectivist cultures is part of a comprehensive social relationship and is partially defined by others in that relationship [14]. Other scholars have suggested that cultural restrictions on the self in collectivist cultures are strong. One of the implications of such restrictions is a low need for uniqueness. In line with this model, it was suggested that the need for positive self-regard exists in East Asian cultures as well, but its manifestation is restricted by the culture and specifically by cultural demands for modesty [15]. Several previous indirect findings have shown the relevance of cultural restrictions on the self to the manifestation of self-enhancement. Comparisons of elf-enhancement levels for different types of traits have shown that when the self-enhancement of a trait does not vilate cultural norms, the bias toward self-enhancing this trait increases. Self-enhancement in Singapore was found to be stronger than in Israel for communal trait, as opposed to agentic traits. Another study conducted in Singapore showed that the degree of sensitivity of the self-enhancement measure to modesty norms affected the magnitude of measured self-enhancement. Thus, the grater the sensitivity of the self-enhancement measure to self-presentation norms, the lower the measured self-enhancement level. It was also found that Japanese students described themselves less favorably in public on traits defined as self-profitable traits as compared to descriptions they gave in private context.

The second question lack comparison between difference culture. The present study give the evidence from the perspective of risk-seeking only with the China culture context. There is no direct evidence that more or less or equivalence level with the western culture individual. The existed results considered that individual's self-enhancement is much lower than westerns. And the other parts study related to risk-seeking indicated that Eastern are more risky than westerns. What is the specific relationship between self-enhancement and risk-taking in the two different culture? There are may be have four types about the relationship easterns higher self-enhancement, more risk-seeking than westerns, or lower self-enhancement, low risk-seeking than westerns. The future study should compare the relationship among different cultures to gain the culture difference.

REFERENCE

- [1]C. Sedikides, L. Gaertner, and Y. Toguchi. Pancultural self-enhancement. *Journal of Personality and Social Psychology*, 2003, 84(1): 60-79.
- [2]O. Svenson. Are we all less risky and more skillful than our fellow drivers? *Acta Psychologica*, 1981, 47: 143-148.
- [3]D. M. Messick, S. Bloom, J. P. Boldizar, and C. D. Samuelson. Why we are fairer than other? *Journal of Experimental Social Psychology*, 1985, 21(5): 480-500.
- [4]J. D. Brown, and S. A. Smart. The self and social conduct: linking self-representations to prosocial behavior. *Journal of Personality and Social Psychology*, 1991, 60: 369-375.
- [5]J. D. Brown, R. L. Collins, and G. W. Schmidt. Self-esteem and direct versus indirect forms of self-enhancement. *Journal of Personality and Social Psychology*, 1988, 55: 445-453.
- [6]S. J. Heine, D. R. Lehman, H. R. Markus, and S. Kitayama. Is there a universal need for positive self-regard. *Psychological Review*, 1999, 106(4): 766-794.
- [7]S. E. Taylor, and J. D. Brown. Illusion and well-being: a social psychological perspective on mental health. *Psychological Bulletin*, 1988, 103(2): 193-210.
- [8]S. L. Murray, and J. G. Holmes. A leap of faith? Positive illusions in romantic relationships. *Personality and Social Psychology Bulletin*, 1997, 23(6): 586-604.
- [9]P. A. Van Lange, and C. E. Rusbult. My relationship is better than and not as bad as yours is: the perception of superiority in close relationships. *Personality and Social Psychology Bulletin*, 1995, 21(1): 32-44.
- [10]C. Sedikides, and M. J. Strube. The multiply motivated self. *Personality and Social Psychology*, 1995, 21(12): 1330-1335.
- [11]Li S. Y., Fang Y., and Zhang M. What makes frames work? *Acta Psychologica Sinica*, 2000, 32: 229-234.
- [12]J. Kurman. Self-enhancement: is it restricted to individualistic cultures? *Personality and Social Psychology Bulletin*, 2001, 3: 1705-1712.
- [13]C. Sedikides, L. Gaertner, and J. Vevea. Evaluating the evidence for pancultural self-enhancement. *Asian Journal of Social Psychology*, 2007, 10: 201-203.
- [14]H. R. Markus, and S. Kitayama. Culture and the self: implications for cognition, emotion, and motivation. *Psychological Review*, 1991, 98(2): 224-241.
- [15]J. Kurman, and N. Sriram. Interrelationships among vertical and horizontal collectivism, modesty, and self-enhancement. *Journal of Cross-cultural Psychology*, 2002, 33 (1): 71-86.
- [16]Acker, D., & Duck, N.W. Cross-cultural overconfidence and biased self-attribution. *The journal of Socio-Economics*, 2008, 377, 1815-1824.
- [17]Bond, M.H., Cheung, T.S. College students' spontaneous self-concept: the effect of culture among respondents in Hong Kong, Japan, and the United States. *Journal of Cross-cultural Psychology*, 1983, 14(2):153-171.
- [18]Borkenau, P., Zaltauskas, K, & Leising, D. (2009). More may be better but there may be too much: optimal trait level and self-enhancement bias. *Journal of Personality*, 77(3), 825-858.
- [19]Brown, J.D., & Kobayashi, C. (2003). Self-enhancement in Japan and America. *Asian Journal of Social Psychology*, 5(3), 145-168.
- [20]Diener, E., Diener, M., Diener, C. (1995). Factors predicting the subjective well-being of nations. *Journal of Personality and Social Psychology*, 69(5), 851-864.
- [21]Heine, S.J., Kitayama, S., & Lehman. (2001). Cultural differences in self-evaluation—Japanese readily accept negative self-relevant information. *Journal of Cross-cultural Psychology*, 32(4), 434-443.
- [22]Heine, S.J., Lehman, D.R., Markus, H.R., & Kitayama, S. (1999). Is there a universal need for positive self-regard. *Psychological Review*, 106(4), 766-794.
- [23]Heine, S.J., Takata, T., Lehman, D.R. (2000). Beyond self-presentation: evidence for self-criticism among Japanese. *Personality and Social Psychology Bulletin*, 28(1), 71-78.
- [24]Hsee, C.K., Weber, EU. (1999). Cross-national differences in risk preference and lay predictions. *Journal of Behavioral Decision Making*, 12, 165-179.
- [25]Kitayama, S. (2002). Culture and basic psychological processes—toward a system view of culture: comment on Oyserman et al. (2002). *Psychological Bulletin*, 128(1), 89-96.
- [26]Kitayama, S., Takagi, H., & Matsumoto, H. (1995). Causal attribution of success and failure: cultural psychology of the Japanese self. *Japanese Psychological Review*, 38, 247-280.

- [27]Kwan, V.S., John, O.P., Robins,R.W., & Kuang, L.L. (2008). Conceptualizing and assessing self-enhancement bias: a componential approach. *Journal of Personality and Social Psychology*, 94(6), 1062-1077.
- [28]Li, S., Chen, W.W., & Yu, Y. (2006). The reason for Asian overconfidence. *Journal of Psychology*, 140, 615-618.
- [29]Rosenberg, M. (1965). *Society and adolescent self-image*. Princeton, NJ: Princeton University.
- [30]Sedikides, C., Herbst, K., Hardin, D.P., Dardis G.J. (2002). Accountability as a deterrent to self-enhancement: the search for mechanisms. *Journal of Personality and Social Psychology*, 83(3), 592-695.
- [31]Triandis, H.C. (1989) The self and social behavior in differing cultural contexts. *Psychological Review*, 96(3), 506-520.
- [32]Yates, J.F., Lee, J.W., & Shinotsuka, H. (1996). Beliefs about overconfidence, including its cross-national variation. *Organizational Behavior and Human Decision Processes*, 65, 138-147.
- [33]Yates, J.F., Lee, J.W., Shinotsuka, H., Patalano, A.L., & Sieck, W.R. (1998). Cross cultural variations in probability judgment accuracy: beyond general knowledge-overconfidence. *Organizational Behavior and Human Decision Processes*, 74, 89-107.

Study and Evaluation of Concrete Durability of Plastic Impervious Wall

Jianbo Zheng

School of Architectural Engineering, Binzhou University, Binzhou, 256600, China

E-mail: zjb2006@163.com

Abstract: For its low elastic modulus and better flexibility, the plastic concrete cut-off wall can adapt to the deformation of the sandy pebble foundation, which greatly improves the crack resistance and the overall seepage control effect of the cut-off wall structure. The durability of the plastic concrete wall material is tested and studied, the safety operation life is evaluated and discussed.

Keywords: Plastic impervious wall; Concrete durability; Safety operation life

1. INTRODUCTION

During the operation of hydraulic concrete structures, aging and various diseases are caused by repeated actions of water, atmosphere, corrosive medium and positive and negative temperature. According to the survey of the durability and disease of the national hydraulic concrete, the leakage corrosion is one of the main diseases of the hydraulic concrete building because of the poor durability. The leakage and dissolution of concrete under the action of pressure water is actually an intrinsic and essential disease caused by leakage of cement hydration products $\text{Ca}(\text{OH})_2$ and lost by leakage. Under the action of pressure water, the dissolution rate of $\text{Ca}(\text{OH})_2$ in concrete gradually increased in the early stage, which was basically stable in the middle period and gradually declined in the later period. With the continuous loss of $\text{Ca}(\text{OH})_2$ in concrete, concrete compressive strength and tensile strength will continue to decline, when $\text{Ca}(\text{OH})_2$ was dissolved in 25%, the compressive strength of the concrete will be decreased by 35.8%, the tensile strength will be decreased by 66.4%, and corrosion effect on the tensile strength of concrete is more obvious.[1]

2. MACROSCOPIC CORROSION CHARACTERISTICS OF CONCRETE

The dissolution process of concrete under the action of pressure water is expressed under certain pressure and continuous determination of CaO content dissolved in leakage water, and the test pressure is 2 MPa. Concrete leakage in pressure water, the dissolution of early small CaO, showed a gradual increasing trend, to a certain time (about 50 days) dissolution rate unchanged, dissolution curve is a straight line segment, and later (about 100 days) dissolution rate decreased gradually, the dissolution curve showed a steady trend[2].

The test of macroscopic characteristics of concrete is carried out at different dissolution stages of CaO. The first stage is about 6% dissolution of CaO in concrete, and the dissolution of CaO in the second stage is about 16%, and in the third stage, the dissolution of CaO is about 25%.

The test of the macroscopic characteristics of concrete includes three indexes, the compressive strength, the tensile strength and the dry water absorption of the saturated surface. The test of compressive strength and tensile strength is based on two kinds of non-destructive methods, namely resonance frequency method and ultrasonic speed method [3]. Meanwhile, the standard method of compressive strength and tensile strength is also tested.

Test data result shows:

(1) The compressive strength of concrete decreases with the continuous dissolution of CaO in concrete. When CaO dissolves 6%, the compressive strength decreases by 11.5%, and when CaO dissolves 16%, the compressive strength decreases by 25%, and the compressive strength decreases by 35.8% when CaO dissolves in 25%.

(2) The decrease of tensile strength of concrete is higher than that of compressive strength. When the CaO dissolves 6%, the tensile strength decreases by 44.7%, and the tensile strength decreases by 59.6% when CaO dissolves 16%, and the tensile strength decreases by 66.4% when CaO dissolves 25%. Therefore, it is shown that the dissolution of CaO in concrete has a more obvious effect on the tensile strength.

(3) With the dissolution of CaO in concrete, the dry water absorption of the concrete is gradually increased. When CaO dissolves 6%, the water absorption increases by 21%, and when CaO dissolves 16%, the water absorption increases by 53%, and the water absorption rate increases by 90% when CaO is dissolved in 25%. It is shown that with the dissolution of CaO, the pores in the concrete are increasing and the density decreases continuously.

3. DURABILITY TEST OF CONCRETE IMPERVIOUS WALL

As an effective basic seepage control facility, concrete impervious wall has been widely used in water conservancy and hydropower projects. Since the first anti seepage wall was built in 1958, the area of the water cut of the impervious wall has reached about

500 thousand square meters, which is the first in the world [4].

The plastic concrete cut-off wall because of its low elastic modulus, good flexibility, can adapt to the deformation of gravel foundation, thus greatly improve the crack resistance and anti-seepage effect of anti-seepage wall structure, so as a kind of new wall materials and attention all over the world. In the United States, France, Canada and other countries, its plastic concrete impervious wall has been preliminarily applied in the project since 1970s. In the middle and late 80s of China, the experimental research and preliminary trial of plastic concrete impervious wall have been carried out, and good results have been achieved. However, whether abroad or in China, the study of long-term performance of plastic concrete cut-off wall, that is, durability, is still in the exploratory stage. Therefore, the application scope of the plastic concrete cut-off wall is also under study.

According to the actual operating conditions of the impervious wall, the durability of the concrete of the impervious wall is mainly reflected in the anti-leakage and corrosion resistance of the wall materials. Starting in late 70s, to demonstrate double mixing (i.e., adding fly ash and adding new admixture) impervious wall concrete durability problems, the author carried out the first assessment of durability and corrosion test of concrete diaphragm wall material in China; mid 80s will test macro and micro corrosion test and analysis (differential thermal analysis of electron microscope scanning, etc.) combined to do further exploration in the leakage corrosion regularity and mechanism on concrete dam. In order to cooperate with the test of plastic concrete cut-off wall material in the national foundation treatment project, the durability test and safety operation life assessment of plastic concrete wall materials are specially discussed.

(1) Experimental design

For the durability of impervious wall materials, the dissolution test is mainly used, that is, under the condition of a certain amount of leakage, the safe operation life of wall materials is evaluated by the results of the dissolution of CaO in the wall concrete material (mortar block). Therefore, this test still adopts the method of infiltration type corrosion test to test the durability of the plastic concrete wall material. At the same time, in order to explore the dissolution mechanism of plastic concrete, the micro test and analysis of plastic concrete before and after the dissolution of plastic concrete were also carried out. The test items include differential thermal analysis, scanning electron microscopy and energy spectrum analysis. The durability of the plastic concrete impervious wall is evaluated synthetically through the combination of macro corrosion test and micro test.

(2) Dissolution test result

The dissolution rule of plastic concrete and ordinary

concrete is basically similar. The dissolution rate and corrosion rate are very large at early age. However, with the extension of age, the dissolution rate gradually slows down. After 30 days, the dissolution rate is stable and the corrosion curve tends to be gentle.

Compared with ordinary concrete, the dissolution rate of CaO is quite different from that of ordinary concrete. Under the same leakage rate (1000 mL/d), the dissolution rate of plastic concrete CaO is much lower than that of ordinary concrete. The average daily dissolution rate of plastic concrete CaO is 154.188 mg/d, the ordinary concrete is 350 mg/d, the daily CaO dissolution of plastic concrete is only about 40% ~ 50% of the ordinary concrete. The total amount of 100D dissolution is 35032 mg for ordinary concrete, and 15494 to 18820 mg for plastic concrete, and 1.86 to 2.26 times for common concrete CaO.

In the same amount of leakage in the process of dissolution, although three kinds of plastic concrete CaO the actual dissolution rate is much smaller than ordinary concrete, but because the amount of plastic cement in concrete is very few, CaO reserves are low, therefore, CaO in cement dissolution percentage was relatively higher than that of ordinary concrete. The dissolution percentage of CaO in plastic concrete cement is 36% to 38%, while the percentage of CaO dissolution of ordinary concrete is 27.4%. The increase of relative dissolution rate of CaO in plastic concrete may be related to the fact that a lot of clay and expansive soils are used in plastic concrete to make the material dense.

(3) Microscopic test

The micro test of the corrosion of plastic concrete mainly carried out the differential thermal analysis, scanning electron microscope and energy spectrum analysis before and after the dissolution of various specimens [5]. Differential thermal analysis was used to determine the change of chemical composition before and after dissolution, especially the relative change of Ca(OH)_2 content. Scanning electron microscopy mainly observed the type, morphology and relative number of hydration products before and after dissolution, and the energy spectrum analysis was based on scanning electron microscopy to further determine the chemical composition of a certain measuring point.

A. Differential thermal analysis

Ordinary concrete and plastic concrete in dissolution were determined before had Ca(OH)_2 , and the higher the amount of cement, hydration of Ca(OH)_2 peak is higher, the more content of Ca(OH)_2 ; and after dissolution, the peak value of Ca(OH)_2 in the hydration products were significantly reduced, indicating the hydration product of Ca(OH)_2 has been a large number of stripping.

Ordinary concrete in the solution before peak has obvious calcium silicate hydrate gel (C-S-H) and ettringite, and after the dissolution, C-S-H and

ettringite has decreased but peak. It shows that after the corrosion of ordinary concrete, with the gradual decrease of $\text{Ca}(\text{OH})_2$ content, the hydration products such as hydrated calcium silicate will also be decomposed, and the content will gradually decrease, which will destroy the structure of cement paste step by step.

For plastic concrete, the peak before the dissolution of calcium silicate hydrate gel and ettringite is low, and with decreasing cement content of concrete, calcium silicate hydrate peak is reduced [6]. With the cement content of 140 kg/m^3 , the peak value of calcium silicate gel is not obvious, which indicates that the gel content in the plastic concrete is lower. After dissolution, with the dissolution of $\text{Ca}(\text{OH})_2$, the hydrated calcium silicate gel was decomposed and the content was further reduced. Therefore, the peak value of calcium silicate gel is not reflected on the differential heat curve of the plastic concrete after corrosion.

B. Results of scanning electron microscopy and energy spectrum

Regardless of ordinary concrete or plastic concrete in the solution before scanning electron microscopy observed the lumpy cement hydration product structure is compact, and the solution structure of hydration products is relatively loose, the apparent porosity between hydration products, at the same magnification can clearly see the rest of the individual the crystallization of $\text{Ca}(\text{OH})_2$ and ettringite crystal. It is indicated that the dissolution of $\text{Ca}(\text{OH})_2$ and the decomposition of other hydration products make cement paste become porous and porous structure from a dense structure, thus reducing the macroscopic characteristics of concrete [7].

4. DURABILITY EVALUATION OF PLASTIC CONCRETE IMPERVIOUS WALL

(1) Evaluation criteria

For the concrete cut-off wall, the evaluation index of its durability should be the long-term seepage control effect, and the main factor affecting the long-term seepage control effect is the integrity of the wall itself and the density of the wall material [8]. Crack is the main factor to destroy the integrity of cut-off wall, and the generation of cracks depends on the stress state of the wall and the quality of the construction, such as the quality of drilling and pouring, the treatment of joints, etc. This problem is more complicated. It involves not only the structural problems and material problems of cutoff walls, but also the basic character problems and construction quality problems [9]. Therefore, in the case of simply evaluating the durability of the wall material, the crack problem cannot be considered for the time being.

As a result, the durability of the wall material is mainly dependent on the long-term compactness of the wall concrete. If the wall concrete can maintain good density in a longer running life, it can ensure the

long-term seepage resistance of the impervious wall and thus has better durability. The existing research results at home and abroad believe that the compactness of concrete in the impervious wall mainly depends on whether or not the leakage and corrosion are produced [10].

(2) Evaluation of the safe service life of plastic concrete impervious wall

According to the above evaluation criteria, the safe operating life of the impervious wall can be calculated in a specific project [11]. This study does not combine with specific projects, only discusses the durability of plastic wall concrete, and compares it with ordinary concrete wall materials.

If the plastic concrete cutoff wall is applied, if the crack resistance is increased, if the 50% leakage is reduced, the safe operation life of the wall will increase by 40% to 60% than that of the ordinary concrete cut-off wall. The plastic concrete cut-off wall, if leakage and ordinary concrete cutoff wall, the safe operation of life just ordinary concrete cutoff wall is 70% ~ 90%, this is because the plastic concrete while the dissolution amount was lower than ordinary concrete, but because of the amount of cement is very low, CaO reserves too little in the same leakage situation, it is possible to shorten the running life safety situation.

5. CONCLUSIONS

In the case of leakage and dissolution of plastic concrete, the dissolution of CaO in concrete will be significantly lower than that of ordinary concrete. After the dissolution of plastic concrete, its microstructure and structure change are similar to those of ordinary concrete, resulting in the loss of $\text{Ca}(\text{OH})_2$ and the decomposition of hydration products, resulting in the loose structure and decreasing density of hydration products. The plastic concrete cut-off wall is suitable for foundation deformation and has well anti cracking effect. Therefore, the safe service life of cut-off wall can be prolonged under the condition of reducing leakage. However, due to the low strength of plastic concrete, structural cracks may also occur in the case of deep wall and high stress, which will increase the amount of leakage. If the leakage of the plastic wall increases to the same as that of the ordinary wall, its safe operating life may be reduced. The durability research of plastic concrete impervious wall, especially the evaluation of safe operation life, is the first time in China, and it is also in the exploration stage in foreign countries. The results of this study are still to be further perfected in the future.

REFERENCES

- [1]Liu Jiaping, Shi Liang, Yu Cheng, Wang Yujiang. Requirements for the development of high performance concrete for cement performance and production. Jiangsu Building Materials, 2016(3): 11-16.

- [2]Luo Dongxiang. Numerical analysis of the effect of concrete elastic modulus on the stress of concrete impervious wall. *Hunan Hydro & Power*, 2017(1): 43-45.
- [3]Zhang Shengli, Ju Hongchang, Li Hongyuan, Wang Tangrui, Zhang Peng. Experimental study on the mix ratio of marine durable concrete. *Concrete*, 2016(3): 26-28.
- [4]Li Song. Study on the properties of plastic concrete with impervious wall. Northwest Agriculture and Forestry University, Xianyang, 2015.
- [5]Li Bingwei, Wu Jichun. Study on seepage parameters of borehole pressure water test for seepage proof wall. *Chinese Journal of Rock Mechanics and Engineering*, 2016(2): 396-402.
- [6]Yang Lin. Experimental study on the basic properties of high performance plastic concrete. Zhengzhou University, Zhengzhou, 2012.
- [7]Guo Shihong, Chang Qianqian, Wei Yingying. Discussion on the effect of design index on the performance of concrete impervious wall. *Shandong Water Resources*, 2017(1): 5-6.
- [8]Wang Shaokai. The influence of the components of plastic concrete on its properties [J]. *Henan Water Resources & South-to-North Water Diversion*, 2014(18): 67-68
- [9]Yu Kaijia, Lang Xiaoyan, Ji Zhongyuan. Analysis of the property of concrete impervious wall based on prototype observation data. *Zhejiang Hydrotechnics*, 2017(3): 62-67.
- [10]Zhang Yanli. Study on the quality control of the reinforcement construction of the dam body of the plastic concrete impervious wall. *Technical Supervision in Water Resources*, 2017(1): 4-6.
- [11]Wang Li, Li Qing. Experimental study on resistance to corrosion resistance of wall material of impervious wall. *Water Resources and Hydropower Engineering*, 2012, 43(9): 30-32.

Study on Ultra-high Strength and Impact Abrasion Concrete of Iron Ore Aggregate

Jianbo ZHENG

School of Architectural Engineering, Binzhou University, Binzhou, 256600, China

E-mail: zjb2006@163.com

Abstract: Concrete is a poly-phase formed by mixing water, sand and gravel and admixtures and admixtures. From the iron ore aggregate and improve the two aspects of the overall strength of the concrete, to develop new varieties of concrete in hydraulic high speed flow abrasion resistance, mechanical properties of iron ore aggregate mortar and concrete was studied, which provided a theoretical basis for the application of new materials.

Keywords: iron ore aggregate; ultra-high strength; abrasion; concrete

1. INTRODUCTION

The emergence of a new structure is often closely related to the birth of a new material. The optimization design of any building is always on the basis of ensuring the function and durability, and how to reduce the size of the section and reduce the direction of the project. The basic design is mainly based on concrete dam stability, strength and durability, therefore, if we can develop special concrete material with high density, high strength, high durability, it may bring new changes to the design of concrete dam, will also provide the basis for other concrete design and optimization structure innovation [1]. This is the basic starting point for our development of high density and super high strength special concrete.

In many hydraulic concrete buildings built in China, with the increase of operation years, various diseases due to durability problems are more common, some of them are more serious, and even affect operation safety. According to the national survey in 2012, in the hydraulic concrete buildings, the engineering of the damaged structures was accounted for 70% because of the erosion and cavitation erosion of the high-speed water flow [2]. According to the practice of repair engineering for many years, the development of patching materials has developed from purely organic resin materials to high-strength or even super high strength cement concrete materials and inorganic and organic composite concrete materials [3]. Therefore, the development of large bulk and super high strength special concrete will also provide a new variety of material for the development of the anti-impact and wear resistance technology of the hydraulic concrete building.

2. EXPERIMENTAL DESIGN

Concrete is a poly-phase formed by a mixture of cementing material, water, sand and aggregate, admixture and admixture. There are mainly two aspects to decide the impact and wear resistance of the poly-phase, one is the abrasion resistance of the material body, and the other is the combination of various materials. The latter performance can be represented by the strength of the concrete, and the improvement of the abrasion resistance of the bulk material is the first to take the advantage of hard aggregate, because the aggregate accounts for about 70% of the total concrete consumption. Therefore, from the two aspects of iron aggregate and improving the overall strength of concrete, this project develops a new type of concrete suitable for high-speed erosion and abrasion of hydraulic engineering.

(1) Selection of test raw materials

According to the above basic ideas, through market research, we chose iron ore and sand with hard texture and large apparent density as the basic sand and gravel for this experiment. At the same time, the natural river sand and eggs and gravel made from the Yongding River in Beijing are also used [4]. The cement is No. 525 ordinary portland cement. Silicon powder is used for the new type of active mixture. The content of active silica is not less than 90%. The high efficiency water reducing agent uses low bubble DH3 high efficiency water reducing agent and retarded DH4 to reduce water efficiency. The expansion agent is also used in the test.

(2) Test project

A. Characteristic test of iron ore aggregate.
B. Characteristic test of iron ore aggregate mortar: the compressive strength; the flexural strength and the modulus of elasticity; bond strength; anti abrasion strength and the shrinkage deformation; in the freeze-thaw test.

C. The characteristics test of iron ore aggregate concrete: compressive strength; modulus of elasticity; bond strength; resistance to grinding strength; resistance to freezing and thawing test.

(3) Test method

A. Testing method for bond strength of mortar

The pre formed concrete specimen (10cm×20cm) with a drawing ring at both ends and 28d is split from the middle cross section as an old concrete specimen. When the bonding strength is formed, new mortar material is poured on the old concrete specimen, and

the ring is placed in the center [5]. The standard maintenance room is delivered to the 3d after being sent to the old concrete pull ring. After 28d, the axial tensile test procedure is applied to measure the bond strength value.

B. Testing method for bond strength of concrete

Concrete bond test is based on the splitting of the combination surface of the cube, 28d will be the maintenance of 300 concrete specimens (15cm×15cm×15cm) by splitting test method is divided into two halves, half of the specimens into mold, fracture upward, people will pour fresh concrete mold smooth surface [6]. After 28d, the bond strength of concrete was measured by the method of splitting tensile test in the concrete joint.

3) Test of abrasion resistance

The test is basically carried out according to the regulations, only to enhance the wear effect. Instead of using standard sand to use iron ore sand, the added quantity is still 150g. The test results are only compared.

3. TEST RESULTS AND ANALYSIS

(1) Experimental study on the properties of iron ore aggregate

The main components of iron ore and iron ore are Fe₂O₃ (69.53%) and SiO₂ (24.59%).

It can be seen from the test results: (1) the dry density of iron ore aggregate is about 50% higher than that of ordinary aggregate, which creates a good condition for improving the density of concrete. (2) The water absorption rate of the saturated surface of iron ore aggregate is about 25% smaller than that of the ordinary sand stone, indicating that the ore aggregate has a good compactness. (3) The crushing index and the sturdiness coefficient of the ore Department of orthopedics are all less than the ordinary sand stones, which further indicates that the ore aggregate has higher density and strength. From the above three points, it can be seen that the use of ore Department of orthopedics can not only improve the density of concrete, but also improve the overall strength of concrete.

(2) Experimental study on the properties of iron ore aggregate mortar

In the experiment, the control mortar fluidity of the jump table in about 120mm, water cement ratio from 0.28 to 0.34, the cement sand ratio by 1:2.5 and 1:3.0 in two cases, with low foam and high efficiency water reducing admixture of DH3 and DH4 two, also tested the effect of expansion agent for composite doped, for high strength, were mixed with silica fume mixed material (10%).

A. Compressive and flexural strength of mortar

When iron ore aggregate mortar is mixed with silica fume and super plasticizer, water cement ratio 0.30 ~ 0.34 and sand to cement ratio 1:2.5, the compressive strength of 28d can reach more than 90MPa, and its flexural strength is more than 9MPa. The ratio of water to cement decreased to 0.28, and the amount of

water reducing agent was increased at the same time. Under the same flow degree, the compressive strength of 28d could reach 100MPa.

With high efficiency water reducing agent in the ore aggregate mortar, it can be added with expansive agent at the same time, which has some advantages to the compressive strength [7].

B. Elastic modulus of mortar

For the high strength, the elastic modulus of the iron ore mortar is high, and the modulus of elasticity can reach (4~4.8) x 10⁴MPa within the range of the test.

C. Bonding strength of mortar

The study of bond strength is mainly to discuss the characteristic index of iron ore aggregate as repair material. Improving the bonding property of the repair material to the old concrete material is the main index to improve the overall durability of the repair material.

D. Abrasion resistance of mortar

In order to verify the performance of the abrasion resistance test of the iron ore aggregate mortar, the ordinary mortar specimen was formed and the grinding test was carried out under the same conditions. From the test results, we can see that when the water cement ratio is basically the same, the mortar abrasion resistance of the iron ore department of orthopedics is 77% higher than that of the ordinary mortar, indicating that iron ore Department of orthopedics can produce high impact abrasion resistant materials [8].

E. Dry shrinkage test of mortar

Dry shrinkage is one of the main indexes affecting the crack resistance of cement mortar and concrete, especially for the construction of thin layer large area repair works [9]. In comparison, the dry shrinkage test of ordinary mortar is also carried out.

The dry shrinkage property of iron ore aggregate mortar is basically similar to that of ordinary mortar at early stage (before 7d), but after 7d age to 180d, the dry shrinkage value of iron aggregate mortar is much smaller than that of ordinary mortar, only 50% to 68% of ordinary mortar. Especially for the mineral aggregate mortar mixed with expansive agent, the dry shrinkage value is only 30% to 40% of the ordinary sand at the early stage or later stage, which indicates that the ore aggregate can be made into cement mortar with smaller dry shrinkage, which is good for the crack resistance performance in large area construction.

(3) Test on the properties of iron ore aggregate concrete

A. Compressive strength

In the experiment the same ratio, iron ore aggregate concrete strength of 28d can reach 86 ~ 90MPa, additive changes little influence on strength; in other conditions the same conditions, only to replace the pebble ore aggregate, the strength is about 15% lower, indicating the department of orthopedics products have a certain impact on the compressive strength. It

is beneficial to improve the compressive strength of concrete by using hard material of iron ore.

B. Elastic modulus

The modulus of elastic modulus of ultra-high strength concrete of ore aggregate is also larger. When the strength is above 80MPa, the modulus of elasticity is more than 5×10^4 MPa. At the same time, the modulus of elasticity of concrete decreased (about 15%) when the gravel was used to replace the ore elbow, which was basically similar to the magnitude of the strength reduction.

C. Bond strength

The aggregate strength of the ore aggregate concrete is higher than that of the old concrete [10]. The test results are all above 2.5MPa, which is 1 times higher than that of the ordinary concrete (0.6~1.2MPa). Using aggregate concrete repair damage site, can effectively improve the durability.

D. Abrasion resistance

The impact strength of ore aggregate is higher than that of ordinary sand aggregate concrete with the same water cement ratio, which is more than 2 times higher than that of the ordinary sand aggregate concrete. The abrasion resistance of concrete consisting of ore sand and ordinary pebble is 87% higher than that of ordinary aggregate concrete, but it is slightly lower than that of all aggregate concrete. The combination of expansive agent has no effect on improving the resistance and abrasion resistance of the whole concrete [11].

E. freeze-thaw test

The frost resistance level of the concrete in the ore Department of orthopedics can reach more than F400. The frost resistance grade of mixed aggregate concrete composed of ore sand and pebble can reach more than F400. It is beneficial to improve the frost resistance of concrete with the addition of expansive agent [12]. This may be related to the increase of the compactness and impermeability in the concrete after the addition of expansive agent.

4. ANALYSIS AND INDUCTION

Iron ore can be used as aggregate of high density and high quality concrete because of its large density, small water absorption and high sturdiness. The density of mortar made of iron ore aggregate can reach 3120kg/m³, which is nearly 50% higher than that of ordinary mortar. The density of concrete made from iron ore aggregate can reach 3300kg/m³, which is nearly 60% higher than that of ordinary concrete.

The iron ore aggregate can be made into super high strength mortar and super high strength concrete without changing the existing main raw materials and processes. The compressive strength of 28d age is more than 100MPa, and the concrete can reach more than 80MPa. The ultra-high strength ore aggregate mortar and concrete have high impact resistance and wear resistance, and the abrasion resistance is nearly 1~2 times higher than that of ordinary concrete with water cement ratio.

The super high strength ore aggregate mortar and concrete also have high frost resistance, and their frost resistance levels can be above F300 and more than F400, respectively. Made of mortar and concrete using ore aggregate, the dry shrinkage of mortar and concrete than ordinary had significantly decreased, decreased about 30% ~ 40%; such as the use of mineral aggregate, and then mixed with expansive agent, mortar and concrete shrinkage value will be further reduced, only ordinary mortar and concrete 1/3. The obvious decrease of dry shrinkage deformation will be beneficial to the increase of crack resistance of mortar and concrete. The mortar, concrete and old concrete made with ore aggregate have higher bonding strength, which is 50% ~ 100% higher than that of ordinary mortar and concrete.

In view of the characteristics of ore aggregate mortar and concrete has high density, high strength, high abrasion resistance, high resistance, low shrinkage, high adhesion, so this kind of special mortar and concrete can be used as structural materials for hydraulic concrete structures, but also can be used as hydraulic building repair materials, especially for high resistance red, high frost resistance, low dry shrinkage of the part of the project, such as dam spillway, water hole spillway, the floor of the gate engineering parts of the main material or repair materials.

5. CONCLUSIONS

From the iron ore aggregate and improve the two aspects of the overall strength of the concrete, mechanical properties of iron ore aggregate mortar and concrete was studied, which provided a theoretical basis for the application of new materials. The development of large bulk and super high strength concrete will provide a new material for the development of the anti-impact and wear resistance technology of the hydraulic concrete building.

REFERENCES

- [1]Tu Erhong. Experimental research on high performance anti impact and abrasion resistant concrete of hydraulic engineering [J]. Coal Ash, 2015(1):38-41.
- [2]Huang Junwei. Research on the protection technology of the anti-erosion grinding of the discharge structure of water conservancy and hydropower project [J]. Building Technology Development, 2017(22):140-141.
- [3]Ma Yu, Sun Zhiheng, Zhang Xin. Experimental study on high elastic mending mortar [J]. Dam & Safety, 2013(2):44-47.
- [4]Zhang Bin, Fan Weili, Zhang Lei, Zheng Jun. Experimental research on concrete punching resistance based on underwater steel ball method [J]. Water Power, 2014(8): 126-128.
- [5]Lei Weili. Experimental study on the impact of ecological fiber on the performance of hydraulic concrete [J]. Development Guide to Building

Materials, 2016(20):53-55.

[6]Xin Yuliang. Experimental study on strength and abrasion resistance of steel slag concrete mixed with steel slag [D]. Xinjiang Agricultural University, Urumchi, 2014.

[7]Luo Liwen, Wang Xunzhen. Influence of different admixture on the resistance to abrasion of concrete [J]. Shanxi Architecture, 2016(35):119-120.

[8]Liu Zhihao. Experimental study on durability of reinforced concrete surface reinforced with existing structural concrete [D]. Nanjing University of Aeronautics and Astronautics, Nanjing, 2016.

[9]Ding Zhaoxiang. Experimental research on high performance concrete in high arch dam construction

[J]. Water Resources Development & Management, 2012(10):5-8.

[10]Zhu Xiaoliang, Ding Jiantong, Cai Yuebo, Fu Qionghua. Early creep theory and experimental study of micro expansion anti punching concrete [J]. Journal of China Institute of Water Resources and Hydropower Research, 2017(3):193-199.

[11]Wang Wenlong. Countermeasures to improve the erosion and abrasion performance of hydraulic structures [J]. China Rural Water and Hydropower, 2012(10):98-101.

[12]Ma Jinquan. Study on the resistance to abrasion of freeze-thaw concrete [D]. Beijing Jiaotong University, Beijing, 2017.

Research on the Selection of Diode based on ESD Simulation

Sun Yinjie^{1,*}, Wu Qi²

¹ Intertek Testing Service Ltd, Buliding T52-8, No. 1201 Gui Qiao Road Jingqiao Development Area Pudong District Shanghai, 201206, China

² Shanghai Jiao Tong University, Shanghai, 200240, China

*E-mail: sunljmy@126.com

Abstract: In EMC (Electromagnetic compatibility) test, the electrostatic discharge (ESD) is a critical test for the electronic device. Previously, we select the relevant device, always only consider the functional requirements, and select the device according to the experience to satisfy with the EMC requirement. Sometimes, it will take a lot time and money to debug the samples which failed in the ESD test. There is another risk that the product can't be delivered on time which will decrease customer's satisfaction, even bring customer's complaints. This paper based on actual engineering project, preliminary selection of diode by saber simulation, then the actual test verified simulation, and finally selected a specific diode. It can increase the efficiency and save the cost of R&D to use the simulation to guide the practice.

Keywords: EMC, ESD, Diode

1. INTRODUCTION

Electrostatic discharge (ESD) testing which has great destructive power for electronic devices is a critical test that must be performed before delivery of an electronic product. In product development, it is usually designed from the perspective of theoretical calculations and engineering experience, and then samples are taken for actual electrostatic discharge testing. On the one hand, electrostatic discharge process is complex, involves many disciplines, often will use some approximate calculation method, which may lead to deviations final products produced with the theoretical calculation of static level; on the other hand, although the project experience can help us make some anti-static discharge design, after all, are not exactly the same but different products in terms of circuit design, functional requirements, testing requirements, etc., which may also lead to deviations from the ideal products produced antistatic grade. So, often after a sample project before production is completed, the test was found to electrostatic discharge failure, then the need for product rectification, after rectification good, reproduce, re-testing. If good luck may be resolved in a short time, but more practical situation is that it needs to be repeated for many times to pass the test. Such a traditional design method will not only consume a lot

of financial resources and material resources, but may also result in failure to deliver on time due to experiments, resulting in a decrease in customer satisfaction and even in attracting customer complaints. Therefore, it is very necessary to carry out specific electrostatic discharge analysis and design for different projects. Based on practical engineering projects, preliminary diode selection can be performed by Saber simulation. Finally, only a small number of confirmatory tests are needed to confirm the credibility of the simulation results to finally determine the specific diodes that need to be selected. It can be seen that in the actual project, the method which is to guide the diode selection can effectively improve the efficiency of the project to select the right device, and can effectively reduce the number of repeated design, test time and test waste caused by repeated verification. Through forward design, simulation to guide the diode selection saves R&D costs.

2. PROBLEM DESCRIPTION

A circuit with a diode is used in a real project. During the development of the C sample, the diodes should be referred to the chip's pin1 and pin2 as required by the customer to prevent external signals to enter the chip.

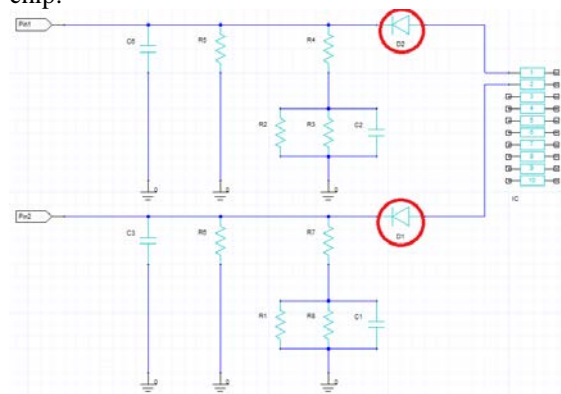


Figure 1 circuit schematic

In the figure 1, D1 and D1 are connected directly to pin 1 and pin 2. There is a potential problem with such a directly connected circuit design. According to the EMC standards and test plan, each pin of the TCU needs to discharge static electricity directly to the pin

foot without being powered on. The purpose is to simulate the situation where the pin of the device is directly contacted by the human body during transportation, assembly and disassembly. If the voltage applied to the pin port exceeds the reverse breakdown voltage of the diode, the device may be damaged. Therefore, it is required to increase the reverse breakdown voltage of the diode as much as possible. However, for a diode, increasing the reverse breakdown voltage will increase the forward conduction voltage, which is unacceptable for the module design. Therefore, a suitable diode must be selected through simulation and experimental verification.

3. PROBLEM ANALYSIS

During ESD testing, ESD capacitors and ESD guns share voltage. As we all know, the larger the ESD capacitance is, the smaller the capacitive reactance is, and the less the divided voltage is. However, due to the complexity of ESD guns, it is difficult to directly calculate the voltage across the ESD capacitor. In this example, we can get the voltage value of the ESD capacitor if we can simulate it. Comparing with the reverse withstand voltage of the diode, it is easy to select the appropriate device.

4. SIMULATION MODELING

According to the circuit schematic of Fig. 1, an ESD simulation model, showed in Fig. 2 is built. [1-2] According to the standard, the severity of the test is III (contact 6KV; air 8KV). For the purpose of protecting intellectual property, this article does not show the ESD gun body model in detail. It is only replaced by a schematic diagram. [3-4] At the same time, in order to simplify the simulation model, this paper only takes the contact discharge of 6KV as an example for simulation research. The risk of breakdown of the diode is determined by reading the voltage at the front of the diode (shown at the red point) in Figure 2.

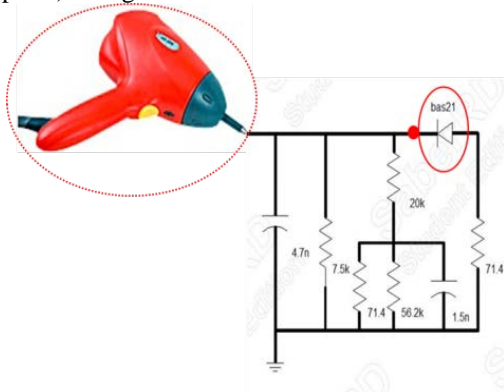


Figure 2 Simulation circuit model diagram

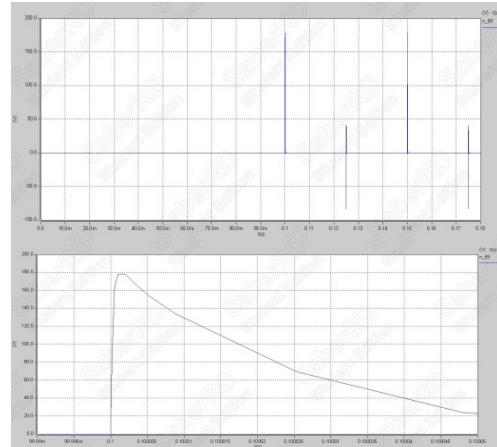
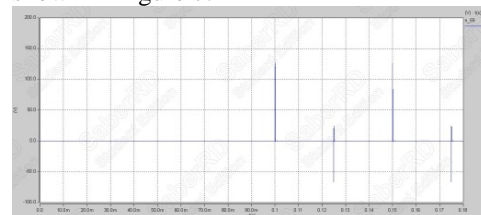


Figure 3 Simulation result with 4.7nF ESD capacitor Since the port voltage is already around 180V, it is recommended that the project team use a diode with a reverse voltage of about 200V. The project team decided to use a BAS21 diode with a reverse voltage of 200V.

After the diode was selected, the module was tested for WC (worst case) and found new problems. The diode voltage drop is about 0.8V at low temperatures. At this point, the minimum current of 3.029 mA is very close to the open-circuit threshold of the chip (1.25mA~3.0mA). There is a greater risk of false alarms for open circuit faults. The probability of false alarms for open circuit faults is also found to be as high as 10% in the actually selected test samples.

In order to avoid this risk and maximize the margin, the most direct way is to reduce the diode tube voltage drop. So the project looked for a BAS40-05 with a lower positive pressure drop but a reverse withstand voltage of only 40V. Taking into account the previous simulation results, the solution was directly denied at the point of view of the ESD. Then another material BAS70-05 was found, the reverse voltage of which is 70V. From the previous simulation results, the diode still can't meet the ESD requirements. According to the theory of ESD, we can reduce the port voltage by increasing the ESD capacitance. Therefore, the capacitance of the ESD capacitor is increased to 6.8nF, 10nF, and 22nF, respectively. The simulation results are shown in Fig. 4-6. In order to more clearly show the influence of ESD capacitance on ESD, this paper compares the simulation results of different capacitance values, as shown in Figure 7.



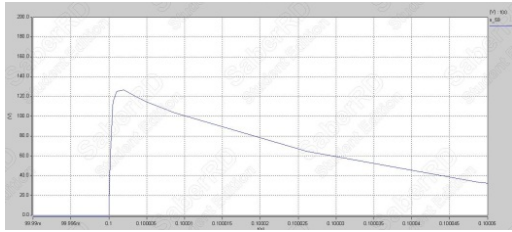


Figure 4 Simulation result with 6.8nF ESD capacitor

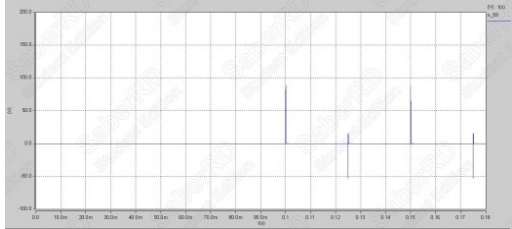


Figure 5 Simulation result with 10nF ESD capacitor

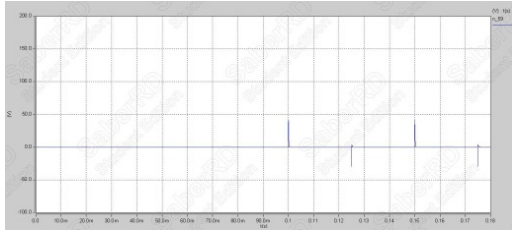


Figure 6 Simulation results with ESD capacitor capacitance 22nF

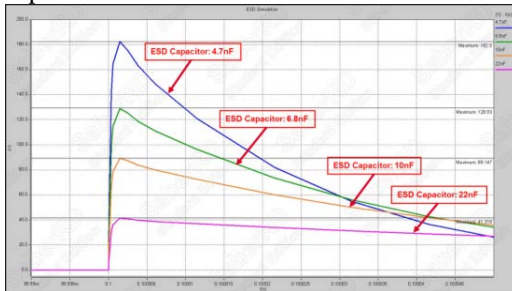


Figure 7 Comparison of simulation results with different capacitance values

Discharge Sequence	Type of Discharge	Test Voltage Level	Pass/Failure Criteria	Minimum Number of Discharges at each polarity
1	Contact discharge C=150pF,R=2kohm	+/-4kV	Status IV	3
2	Contact discharge C=150pF,R=2kohm	+/-6kV	Status IV	3
3	Air discharge C=150pF,R=2kohm	+/-8kV	Status IV	3

Through the comparison of Figure 7, it can be clearly seen that increasing the capacitance of the ESD capacitor can effectively reduce the voltage at the front end of the diode. This result is a very good proof of the ESD theory, and provides a reference solution for circuit rectification.

5. MEASUREMENT VALIDATION

Although the simulation is very intuitive, its effectiveness needs to be confirmed by measurement. In particular, tests such as ESD that can cause fatal damage to devices can be difficult to persuade without the support of experiments. In order to ensure the validity of the experiment, this experiment was arranged by a third-party certification laboratory. The laboratory shall set the experimental conditions strictly in accordance with the requirements of Table 1, and perform ESD gun calibration and actual testing according to Table 2. The reference standards used in the experiments are shown in Table 2.

Table 1 ESD Test Condition Requirements

Temperature	23+/-5.0 degrees C
Humidity	20 to 80% relative humidity(RH)

Table 2 ESD discharge network parameters and discharge levels

According to the plan, the experiment is divided into the following steps.

- (1) Sample preparation. Use a normal sample and apply a BAS21 diode.
- (2) A multimeter is used to measure the forward and reverse voltage drops of the diode before testing and record it.
- (3) After the 4KV contact discharge, use a multimeter to measure the forward voltage drop and reverse voltage drop of the diode and record.
- (4) After the 6KV contact discharge, use a multimeter to measure the forward voltage drop and reverse voltage drop of the diode and record.
- (5) After the 8V contact discharge, use a multimeter to measure the forward voltage drop and reverse voltage drop of the diode and record.
- (6) Replace the BAS21 diode with a BAS70-05 diode

on the same sample and repeat the above procedure.
 Note: If diode damage occurs in the process of (3)-(5), proceed directly (6); if diode damage occurs after (6), the experiment is completed.
 According to the standard, take the setup as shown in Fig. 8 to test, and measure the forward voltage drop and reverse voltage drop according to the plan before and after each discharge level test, record and judge whether the diode is damaged, and finally get the test results of Table 3.

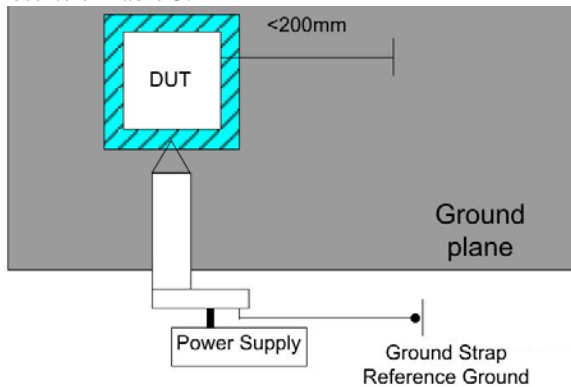


Figure 8 ESD test setup

Table 3 Test results

	BAS21		BAS70-05	
	Forward pressure drop (V)	Reverse pressure drop (V)	Forward pressure drop (V)	Reverse pressure drop (V)
Before ESD test	0.618	-	0.388	-
After 4KV contact discharge	0.617	-	0.389	-
After 6KV contact discharge	0.617	-	0.243	0.276
After 8KV air discharge	0.596	-		

Through testing, we can see that the BAS21 remains intact after 8KV of air discharge. However, the BAS70-05 was reversed in breakdown after a contact discharge of 6 kV, and obviously cannot be directly used in this project. In the actual project, later also gave up the scheme that replaces the diode, choose BAS21 that simulation and test all meet the

requirement.

6. SUMMARY

Through the previous simulation analysis and actual verification test, we can draw a conclusion: In this project, only the BAS21 diode with a reverse withstand voltage of 200V can be selected, and other types of diodes with a withstand voltage of 70V or 40V can't be used. Through this simulation case, it can be seen that the simulation can guide the selection of diodes in this project very effectively and avoid the waste of raw materials, manpower and time caused by blind selection. It truly solves the actual problems encountered in the project, has a certain practical value and saves the economic value of R&D costs. At the same time, the simulation ideas and models can be well transplanted to other projects and the selection of other devices, with a certain promotional value.

REFERENCE

[1]Omid Hoseini Izadi, Ahmad Hosseinbeig, David Pommerenke, Hideki Shumiya, Junji Maeshima, Kenji Araki. Systematic analysis of ESD-induced soft-failures as a function of operating conditions[C].
 2018 IEEE International Symposium on Electromagnetic Compatibility and 2018 IEEE Asia-Pacific Symposium on Electromagnetic Compatibility (EMC/APEMC),2018,5: 1193 - 1197
 [2]Tohlu Matsushima; Mayumi Aoki; Takashi Hisakado; Osami Wada. Equivalent circuit model with nonlinear characteristics of zener diode extracted from SPICE model for ESD simulation[C]. 2017 11th International Workshop on the Electromagnetic Compatibility of Integrated Circuits (EMCCompo).2017: 152 – 155
 [3]Kuo-Hsuan Meng; Robert Mertens; Elyse Rosenbaum. Piecewise-Linear Model With Transient Relaxation for Circuit-Level ESD Simulation[J]. IEEE Transactions on Device and Materials Reliability. 2015, Volume 15:464-466
 [4]Stanislav Scheier, Friedrich zur Nieden, Bastian Arndt, Stephan Frei. Simulation of ESD Thermal Failures and Protection Strategies on System Level[J].IEEE Transactions on Electromagnetic Compatibility.2015, Volume 57:1309-1319

Design Of Intelligent Steelmaking System

Jingna Bi^{1,2}, Jinzhen Hu², Shengdi Luo², Aimin Yang^{3,*}

¹Mathematical Modeling Innovation Lab, North China University of Science and Technology, Tangshan 063210, China

²North China University of Technology Institute of Metallurgy and Energy, Tangshan 063210, China

³School of Science, North China University of Science and Technology, Tangshan 063210, China

*E-mail: 43698059@qq.com

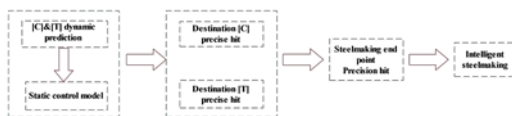
Abstract: In this paper, the BP neural network algorithm was first used to take four characteristic variables of oxygen consumption proportion, total oxygen consumption, CO content in flue gas and CO₂ content in flue gas, the influence of C content and temperature on molten steel was simulated, The prediction model of [C]&[T] on flue gas composition based on BP neural network is established; The second, It is found that all the data applied to the same model will generate large errors. Therefore, SPSS is used to standardize the data and obtain the data after standardization. Finally, the processed data are simulated and analyzed, and the prediction model [C]&[T] of flue gas composition based on BP neural network after standardization of SPSS is obtained.

Keywords: BP neural network; Data normalization; the numerical simulation

1. INTRODUCTION

At present, there are more than 500 small and medium-sized converter with less than 100 tons in China, accounting for about 50% of the national steelmaking capacity, these converters play an important role in local iron and steel enterprises. As the auxiliary gun system cannot be installed in small and medium converter, the terminal control percentage is low, and faces the "de-capacity, green manufacturing and market competition" the coupling pressure, Therefore, it is imperative to break through the technical bottleneck of middle and small converter steelmaking and create the precedent of intelligent steelmaking.

The key way to realize intelligent steelmaking is shown in the following figure:



The dynamic control of flue gas analysis in converter is to continuously detect the flue gas components (CO, CO₂, N₂, O₂, Ar, H₂) and flue gas flow generated during converter blowing. The instantaneous decarburization speed and decarburization amount of molten pool are calculated, and the distribution ratio

of oxygen in C, Si, Mn, P, S and other elements is calculated according to the instantaneous oxygen supply and slag addition amount. The content of each element and slag in the molten pool are calculated. The flue gas analysis system is used in some converter in China to control the steelmaking terminal. However, the accuracy of the dynamic prediction of carbon content and temperature value of the molten steel depends on the circumstance of the flue installation and the synchronization of data information.

In this paper, not only established the [C]&[T] prediction model of flue gas composition for the same group of data, but also used SPSS data for standardized processing, and obtained the [C]&[T] prediction model of flue gas composition for different groups of data, and tested that the method of data processing is feasible.

2. MODEL ESTABLISHMENT AND SOLUTION

2.1 BP neural network model is established

BP neural network is the back-propagation algorithm (back-propagation) in the neural network model. The algorithm is also one of the reasons for the rapid development of artificial neural network research.

The main formula is

$$E(W) = \frac{1}{2} \sum_{i,s} (T_i^s - O_i^s)^2 \quad (1)$$

Where T_i^s is the ideal output of sample s .

2.2 Establishment of [C]&[T] model based on BP neural network

We will be 5 attached PQ, Q, [CO], [CO₂], [C] and [T] data import in MATLAB software, the data of each attachment individually, in annex 1, for example: the 60% of the data in the attachment 1 as the training sample, 15% of the data as the test sample, 25% of the data as the test sample, use these data training a four input corresponding to the two output network model. The other four attachments are treated the same as annex 1.

The input training data matrix input in annex 1 has 4 features, a total of 266 samples (input=4×266), and the output is 2 results. The input training data matrix input of annex 2 has 418 samples with 4 characteristic values (input=4×418), and the output is 2 results. The

same is true for annex 3~ annex 5: In annex 3: input=4×293, output=2; In annex 4: input=4×287, output=2; In annex 5: input=4×321 and output=2.

This article uses a three-tier network structure, the number of neurons in the first input layer is determined by the sample characteristics of the input matrix, the number of neurons in the hidden layer is set to 20, the number of neurons in the output layer is determined by 2 results of the expected sample, as shown in figure 1.

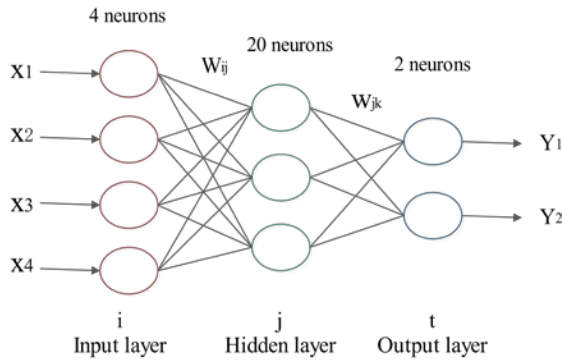
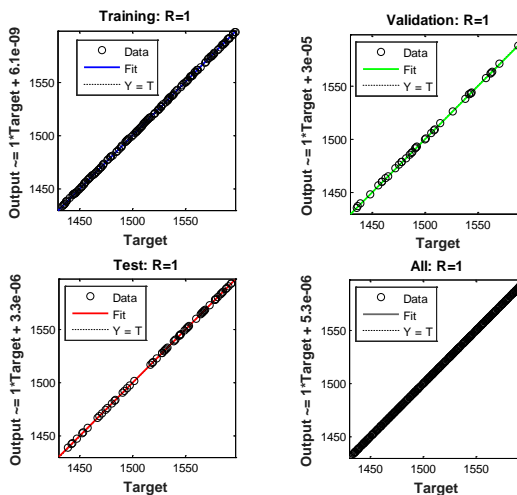


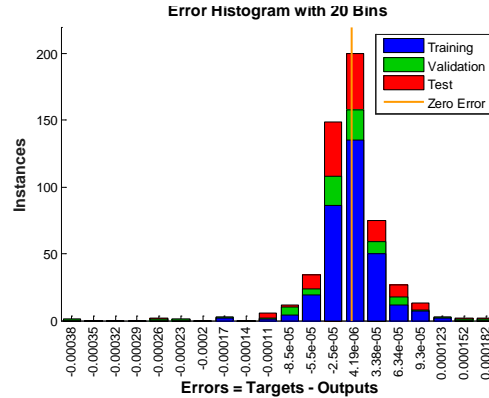
Fig. 1 BP neural network

By counting the number of samples in each attachment, four index data input networks and the simulation of three-layer neural network is obtained; By comparing the network training with the actual situation, the simulation results and the error analysis are obtained, that is, figure 2.

(Figure 2 shows the processing results for annex 1, The processing result of annex 2~ annex 5 is the same as that of annex 1, Similar results are obtained, and the images are not given in this paper.)



Simulation chart of [C]&[T] prediction model



Error analysis chart of [C]&[T] prediction model

Fig. 2 data processing results of [C]&[T]

According to the [C]&[T] prediction model and error analysis diagram of the flue gas composition in Fig. 2, it can be seen that the BP neural network model adopted in this paper is feasible.

2.3 Use SPSS to standardize the data

Since the data in the 5 attachments are variables representing the same meaning, there is a certain connection between the attachments. By referring to the data, we use SPSS software to standardize all the data.

After the processed data is obtained, table 1 is the part of data after standardization in annex 1 (Because the total amount of data in the 5 attachments is large and the same algorithm is used, only some data in attachment 1 is selected to represent, but all data is still imported in the problem).

Table 1 standardized data

PQ	Q	[CO]	[CO ₂]	[C]	[T]
-1.746	-1.746	1.82033	-2.37141	1.83631	-1.746
-1.729	-1.729	1.72183	-2.31286	1.81984	-1.729
-1.712	-1.712	1.66578	-2.17066	1.80316	-1.712
-1.712	-1.712	1.66578	-2.17066	1.80316	-1.712
-1.69496	-1.69496	1.66578	-2.15393	1.78624	-1.69496
-1.67796	-1.67796	1.59955	-2.07029	1.76915	-1.67796
-1.66102	-1.66102	1.60124	-2.07029	1.75194	-1.66102
-1.66102	-1.66102	1.60124	-2.07029	1.75194	-1.66102
⋮	⋮	⋮	⋮	⋮	⋮

2.4 The standardized prediction model is solved

Respectively the appendix 1 ~ 5 after standardization of data in the import table I ~ in table V, import the standardized data in 5 tables into MATLAB software, Process five tables, In the attachment I, for example: To I accessories in 60% of the data as the training sample, 15% of the data as the test sample, 25% of the data as the test sample, use the data training a four input corresponding to the two output network model. The other four I processing the same attachments and

accessories.

Attachment I input training data matrix input has four features a total of 266 samples (input = 4×266), the output for the two results; Attachment II input training data matrix input has four eigenvalues, a total of 418 samples (input = 4×418), the output for the two results; Annex III ~ V similarly available: attachment III input = 4×293, output = 2; Attachment IV input = 4×287, output = 2; Attachment V input = 4 ×321, output = 2.

This paper uses a three-layer network structure. The number of neurons in the input layer of the first layer is determined by the sample features of the input matrix, the number of neurons in the hidden layer is set to 20, and the number of neurons in the output layer is determined by 2 results of the expected sample.

The non-own data are respectively substituted into the established model for data simulation processing and error testing. The following results can be obtained by taking appendix 1 as an example:

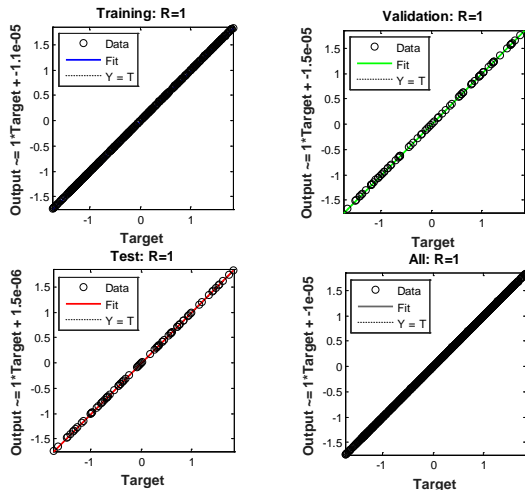


Fig. 3 simulation chart after data standardization

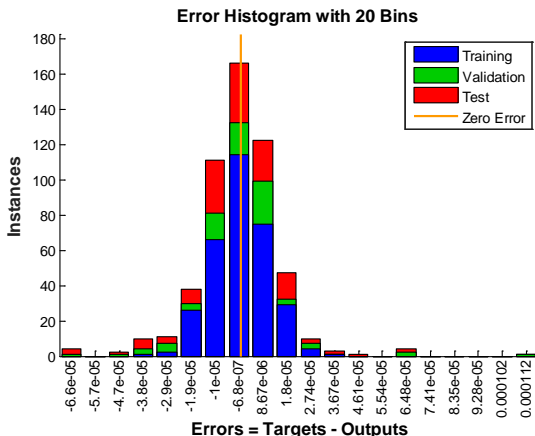


Fig. 4 error after standardization of data

It can be seen from FIG. 3 and Fig. 4 that the establishment of [C]&[T] prediction model of flue gas composition is feasible.

Since the standardization of data may cause some deviation to the original data when solving the second

question, this paper adds a comparison between the data after standardization of SPSS and the original data.

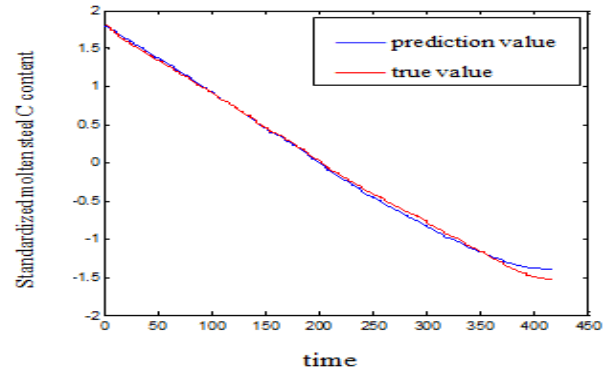


Fig. 5 prediction and true value of carbon content after data standardization

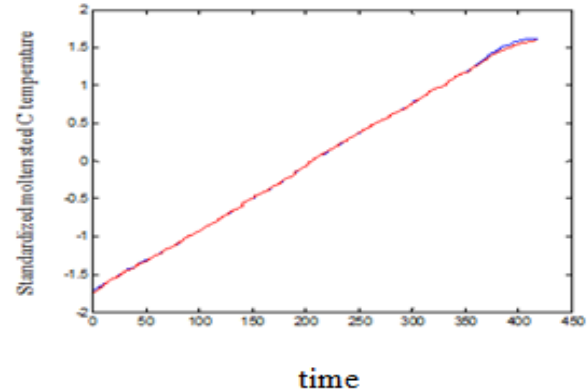


Fig. 6 prediction and true value of temperature after standardization of data

According to fig.5 and fig.6, the deviation from the original data after the standard processing of the data by SPSS software does not lead to large error in the results. Therefore, it is also proved that it is feasible to conduct standard processing of SPSS before the establishment of the prediction model of flue gas composition [C]&[T].

3. CONCLUSION

1. By studying the relationship between PQ, Q, [CO], [CO₂] and [C]&[T], the BP neural network model was established, and the forecast model based on the flue gas composition [C]&[T] was obtained.
2. The models established by different data are different from each other after analysis. If different data are applied to the same model, certain errors will be generated.
3. Carry out simulation and error analysis on the results obtained by substituting the standardized data of SPSS into the same model, and the strategy is feasible.

REFERENCES

[1]Liang Huawei, Yuan Yandong, Xue Hongwei. Sports event risk early warning model based on BP neural network.Statistics and decision-making, 2018 (16): 85-88.
 [2]Zeng Ying, Yang Chen, Wang Xiying and Fang

Zhenxing. Prediction of bicarbonate mineral water quality in Wudalianchi basin based on BP neural network. *Heilongjiang Science*, 2018, 9(16): 20-21.

[3]Zhang Lei, Li Dongyan, Sun Ziyang, Huaishuo, Xu Leirui, Zhou Peng, Li Jiankuang, Li Yuan, Li Yan, Qu Dongwei. Based on SPSS software, the analysis of the questionnaire on the transformation of scientific and

technological achievements. *Journal of Inspection and Quarantine*, 2018, 28 (04): 46-50.

[4]Tian Zhiliang. Research on the Reform of Virtual Simulation Teaching in the Age of Big Data --- Taking Accounting as an Example. *Journal of Shaoguan University*, 2018, 39 (05): 95-99.

Study on Control of Postharvest Diseases of Fruits and Vegetables and Storage Performance of Yeast

Ying Lai*, Qingzhi Li, Nanchi Zhan

College of Agriculture and Life Science, Zhoukou Normal University, Zhoukou, Henan, 466001 China

*E-mail: 23798542@qq.com

Abstract: In order to study the performance and corruption properties of different concentrations of yeasts during postharvest storage of fruits and vegetables. Using Angel active dry yeast as the experimental strain, nine kinds of yeast strains with different concentration were used to treat nine kinds of fruits and vegetables, and the untreated fruits and vegetables were taken as control. Taking the vitamin C content and relative conductivity of fruits and vegetables as the main index, The results show that: The effect of Angel brand high active dry yeast with concentration 0.06% in the storage process was the best, under this concentration, fruits and vegetables to reduce the water loss, soluble solids and vitamin C, respiration rate and membrane permeability of fruits and vegetables decreased. Finally, the yeast can prolong the storage time of fruits and vegetables, the best concentration of yeast is 0.06%.

Key words: Fruits and Vegetables; Yeast; Postharvest; Storage

1. INTRODUCTION

Fruits and vegetables often suffer diseases and spoilage during the storage, transportation and preservation process, thus causing huge economic losses [1]. In the developing countries, the spoilage rate is as high as 20%-50%. At present, the common methods for disease prevention of fruits and vegetables includes chemical preservation, low temperature storage, controlled atmosphere storage and so on [2]. Among them, the chemical preservation has the obvious effect. However, the side effect of drug resistance due to the drug residues force people to explore more safe, scientific and effective methods. At present, many kinds of yeast and germ are found effective for disease prevention. Chalutz et al. [3] found the *Debaryomyces hansenii* has distinct prevention effect for penicillium, green mold and acid rot of citrus. Fan et al. [4] found that *Trichosporon cutaneum* has an inhibition effect for gray mold penicillium of "Fuji" apple. The research of Liu et al. [5] also showed that the beer yeast has a fresh-keeping effect on strawberry. Yeast was considered as important research subjects of postharvest biological control due to its characteristics

of low nutritional requirements, no toxins, harmless to human and antagonism [6]. Yeast with unique action mode and biological characteristics can reproduce in a short time by utilizing nutrient, and survive in a dry environment, which draws a lot of attention [7]. In our experiment, the effect of yeast solution concentrations on the storage effect of the picked fruits and vegetables were studied in order to obtain better methods for postharvest diseases prevention and storage.

2. MATERIALS AND METHODS

2.1 Experimental materials

2.1.1 test strain

High activity dry yeast of anqi brand (commercially available)

2.1.2 sample

All the vegetables used in the experiment, including *Pleurotus ostreatus*, nectarines, grapes, cucumbers, bananas, tomatoes, cauliflower, leeks and spinach were supplied by vegetable market.

2.1.3 experimental reagents

All of the chemicals, including Sodium hydroxide, oxalic acid, barium chloride, phenolphthalein indicator, 2,6-dichloroindophenol, ascorbic acid, potassium iodide, potassium iodate, starch, hydrochloric acid, sodium bicarbonate and wort medium were used as received.

2.1.4 experimental instrument

TD-35 Digital refractometer, purchased from Zhejiang Tuopu Instrument Co., Ltd; DHG-2150B electric heating and drying oven, purchased from Zhengzhou Shengyuan Instrument Co., Ltd; JW-1042R low speed refrigerated centrifuge, purchased from Anhui Jiawen Instrument and Equipment Co., Ltd; Constant temperature water bath cauldron, purchased from Gongyi Yuhua Instrument Co., Ltd; TS-1 decolorizing shaker, purchased from Haimen Qi Lin Bei Instrument Manufacturing Co., Ltd; ZHWY-2102 constant temperature training rocking bed, purchased from Jintan Jingda Instrument Manufacturing Co., Ltd; FD-1B-50 freeze dryer, purchased from Beijing Boyikang Experimental Instrument Co., Ltd; DDS-307W conductivity meter, purchased from Seiko instrument (Dongguan) Co., Ltd.; JD200-3 electronic balance, purchased from

Shenyang Longteng Electronics Co., Ltd; JJ-CJ-2FD clean workbench, purchased from Suzhou Jinjing purifying equipment Technology Co., Ltd; LDZX-75KB vertical electric pressure steam sterilizer, purchased from Shanghai Shenan medical device factory.

2.2 Experimental

2.2.1 the preparation of bacterial liquid

The active dry yeast of 2 g, 4 g, 6 g and 8 g were inoculated in 200 mL wort under 30 °C with 200 r/min for 30 h. Then, it was mixed with 800 mL aseptic water to obtain the yeast solution with weight percentage of 0.20%、0.40%、0.60%、0.80%.

2.2.2 the treatment of fruits and vegetables

First, the selected fruits and vegetables were sterilize under ultraviolet light for 1 h on a clean work table. Then, the nine kinds of fruits and vegetables were soaked in four different concentrations of bacteria solution for 1 min, and dried quickly. Finally, the obtained fruits and vegetables were put in a beaker, sealed with plastic wrap, and stored at room temperature for 14 days for the experiment [8]. For comparison, the fruits and vegetables that have not been soaked in bacteria solution were also prepared.

2.2.3 the sensory evaluation and water loss rate determination

The sensory evaluation includes five sensory indicators, including overall morphology, water loss, length of bacteria, hardness and color. Each of which is divided into three grades: 0, 0.5 and 1. Finally, the

total score of each group is compared. The determination of water loss rate: the water loss rate of each group was calculated by measuring the weight before and after the experiment.

2.2.4 the determination of physiological and biochemical indexes of fruits and vegetables

The content of soluble solids in fruits and vegetables was determined by using a hand-held refractive instrument. The respiration intensity of fruits and vegetables was measured by static method. The content of Vc in fruits and vegetables was determined by 2,6 - dichloroindigol method. The relative electrical conductivity of fruits and vegetables was measured by electrical conductivity meter.

3. RESULT AND ANALYSIS

3.1 The analysis of Sensory evaluation of fruits and vegetables

Figure 1 shows the sensory evaluation scores of fruits and vegetables in 14 d storage after 5 different concentrations of yeast treatment. It can be seen that the banana, leek and spinach treated with a concentration of 0.40% yeast, and the pleurotus, nectarine, grape, cucumber, tomato and cauliflower treated with 0.60% yeast solution show the better condition. Herein, the fruits and vegetables treated with 0.40% and 0.60% yeast solution have the best preservation state, followed by the controlled group. While those treated with 0.20% and 0.80% yeast solution show the worst state.

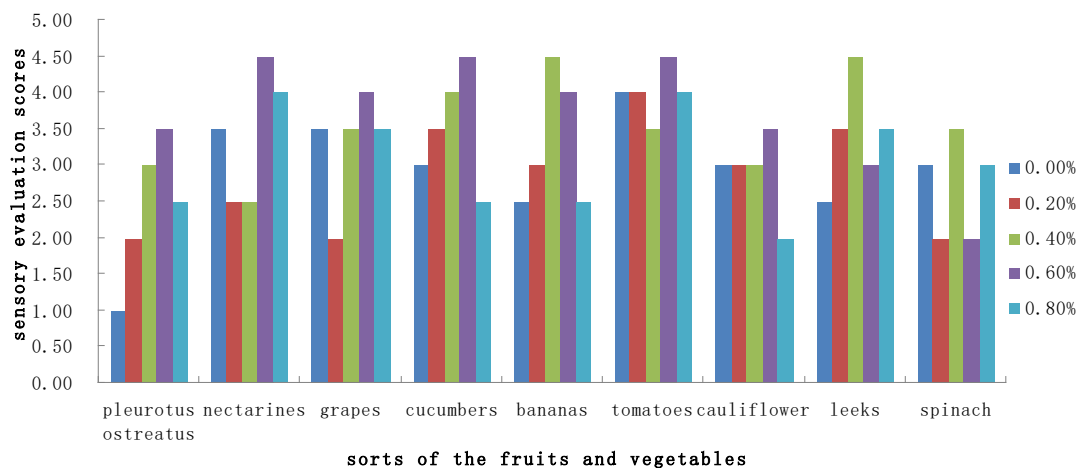


Figure 1 Sensory evaluation scores of fruits and vegetables in 14 d storage after 5 different concentrations of yeast treatment

3.2 The analysis of Water loss rate of fruits and vegetables

As can be seen from figure 2, the pleurotus, nectarine, grape, cucumber, banana, tomato, cauliflower and spinach treated with 0.60% yeast solution present the lowest water loss rate, while the leek shows the lowest water loss rate after treated in 0.40% yeast solution, which are consistent with to the results analyzed by the sensory evaluation of fruits and vegetables. In addition, the controlled group of

nectarine, grape, cucumber, tomato, cauliflower, leek, spinach, pleurotus ostreatus and banana have the highest water loss rate, indicating that the yeast solution treatment plays a water preservation effect on fruits and vegetables. Therefore, according to the above analysis, the fruits and vegetables treated with 0.60% yeast solution have the excellent water preservation performance, while the water loss in the controlled group was obvious.

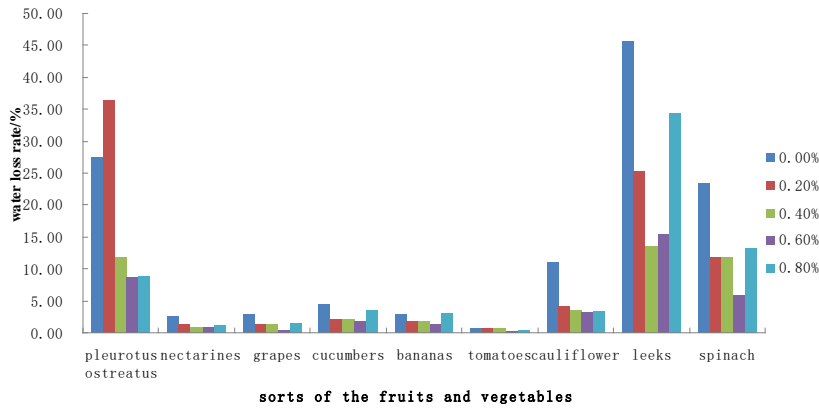


Figure 2 Water loss rate of after 5 different concentrations of yeast treatment of fruits and vegetables after in 14 d storage

3.3 The analysis of soluble solids content fruits and vegetables

Generally, more than 80% soluble solids in the fruits and vegetables of are sugar, followed by acids, pectin, vitamins and soluble pigments. To a certain extent, the level of soluble solids can well reflect the amount of nutrient reserved in the fruits and vegetables [9]. From figure 3, it can be seen that the nectarine, grape, cucumber, tomato, cauliflower and leek group with 0.60% yeast solution treatment have the lowest soluble solids content, while pleurotus eryngii, banana and spinach group show the lowest soluble solids content after treated in 0.80% yeast solution. For pleurotus, grape, nectarine, cauliflower and banana,

the highest soluble solids content are shown in the controlled group. While for the cucumber, leek and spinach, the highest soluble solids content are presented in that group with 0.20% of the yeast solution treatment. The contents of soluble solids in tomato are similar in each groups. Therefore, based on the above analysis, the fruits and vegetables treated with 0.60% yeast solution can well be preserved, and for those treated with 0.20% yeast solution, the preservation effect are poor. However, the yeast treatment has little influence on tomatoes, which shows similar soluble solids content in each group, probably due to its difficult to corruption and low nutrient loss.

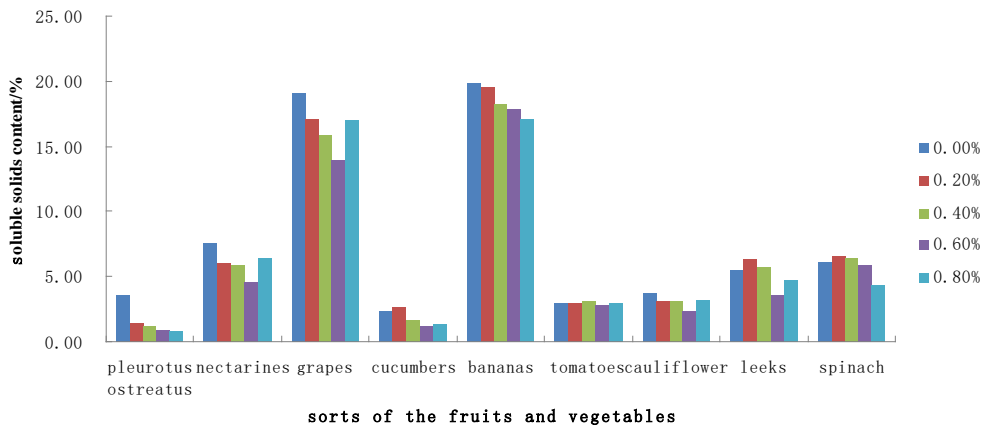


Figure 3 Soluble solids content of after 5 different concentrations of yeast treatment of fruits and vegetables after in 14 d storage

3.4 The analysis of the vitamin C content in fruits and vegetables

Vitamin C, as one of the most important nutrients in fruits and vegetables, is one of the important indicators to evaluate fruits and vegetables quality due to its easy to be oxidized [10]. Figure 4 shows the the Vc contents of nine kinds fruits and vegetables after different bacteria concentrations treatment and storage for 14 days. The lowest Vc contents for grapes and cucumbers are found in the group with 0.20% yeast solution treatment, and for nectarine, cauliflower and leek are observed in that with 0.20% yeast solution treatment. While for pleurotus and

spinach, the lowest Vc contents are present in the controlled group. In the determination of Vc content, the phenomenon in the analysis of soluble solids content also appears, showing no obvious difference for tomato with different yeast solution treatment. Combined with the results of the Vc contents of nine kinds fruits and vegetables after bacteria treatment, the 0.60% yeast solution treatment are advantageous to the Vc preservation for most fruits and vegetables. Based on the above discussion, we can see that the yeast can effectively protect the Vc in the fruits and vegetables during storage, thus slowing down the corruption rate of fruits and vegetables to some extent.

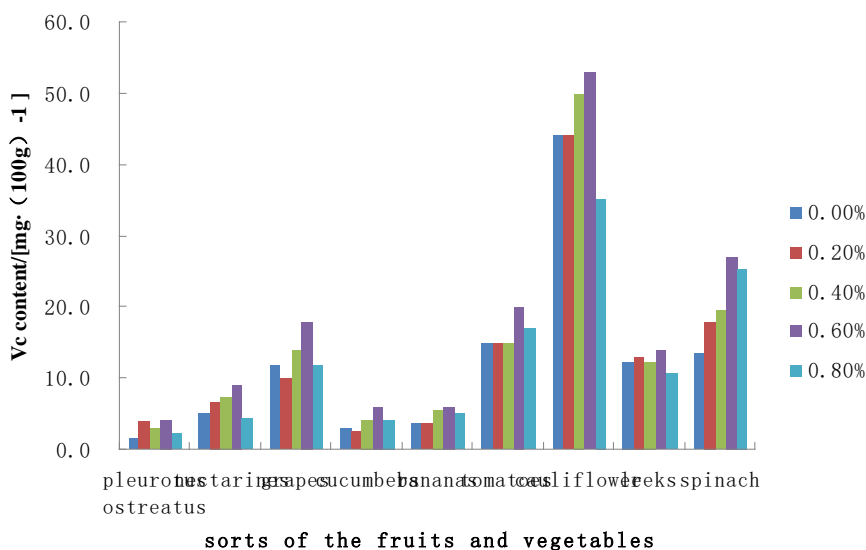


Figure 4 Vc content of after 5 different concentrations of yeast treatment of fruits and vegetables after in 14 d storage

3.5 The analysis of respiratory intensity of fruits and vegetables

The respiratory intensity also determine the corruption rate of fruits and vegetables due to combined reasons that the fruits and vegetables no longer produce organic after picking and the respiration of cells will consume organic. Generally, the stronger the respiration intensity of fruits and vegetables after picking, the shorter its life is. Therefore, reducing the respiration intensity after picking is one of the effective methods to extend the preservation time of fruits and vegetables after picking. According to Figure 5, the respiratory intensity for the treatment group with 0.80% yeast solution of pleurotus, nectarine, grape, cucumber, banana, tomato, cauliflower and leek is the strongest. The reason is probably due to the high yeast solution, which can emit much amount of CO₂, thus effecting the result. For the controlled group, the spinach is the

strongest. Among the treatment groups of fruits and vegetables, those with 0.20%, 0.40% and 0.60% yeast solution treatment have the weakest respiration intensity, while all of them lower than that of controlled group, suggesting that the yeast treatment can weaken the respiration intensity of fruits and vegetables to a certain extent. According to the analysis, the yeast treatment can lower the respiratory intensity and prolong the storage time of fruits and vegetables. And the optimal is found in the group with 0.60% yeast solution treatment. In addition, the respiration intensity in most groups have no relation to the yeast concentration, except for that pleurotus with the respiration intensity increases with the increase of the yeast concentration. Therefore, the yeast concentration especially for the lower one has little influence on the respiratory intensity of fruits and vegetables, and did not affect the overall analysis results.

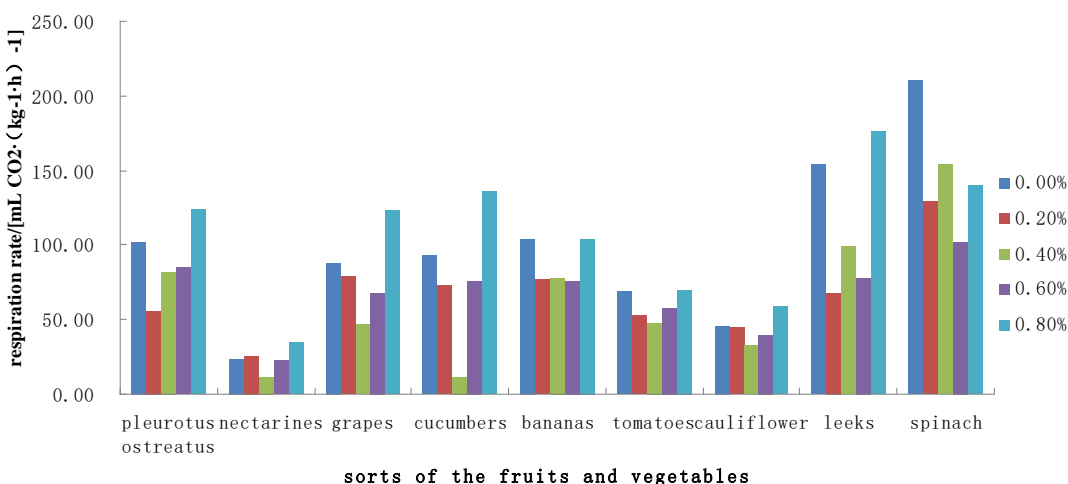


Figure 5 Respiration rate of after 5 different concentrations of yeast treatment of fruits and vegetables after in 14

d storage

3.6 The analysis of relative electrical conductivity of fruits and vegetables

The relative electrical conductivity is an important index to measure the cell membrane permeability of pulp tissues. The higher the value, the more electrolyte leakage, the heavier the damage degree of cell membrane. The value of cell membrane permeability can be indirectly measured by the relative conductivity. The higher the relative conductivity, the greater the damage degree of cell membrane integrity, and the more serious the corruption of fruits and vegetables. During the storage, the gradual decay of fruits and vegetables usually result in the increase of cell membrane permeability and also the relative electrical conductivity. As shown in Figure 9, the group treated with 0.60% yeast solution has the lowest relative conductivity. In

addition, the controlled group of pleurotus, nectarine, grape, tomato and cauliflower have the highest relative conductivity. The relative conductivity for controlled group of cucumber, banana, spinach and leek are not the highest, but the conductivity of fruits and vegetables in most treated groups was lower than that of the controlled group, and the highest conductivity is close to that of the controlled group. Therefore, it can be concluded that the treatment with yeast solution for fruits and vegetables after picking can effectively protect the cell membrane integrity of fruits and vegetables, reduce the damage degree of cell membrane, and slow down the corruption rate of fruits and vegetables during the storage. Among them, the fruits and vegetables after picking treated with 0.60% yeast solution has better results, showing more significant effect on the relative conductivity.

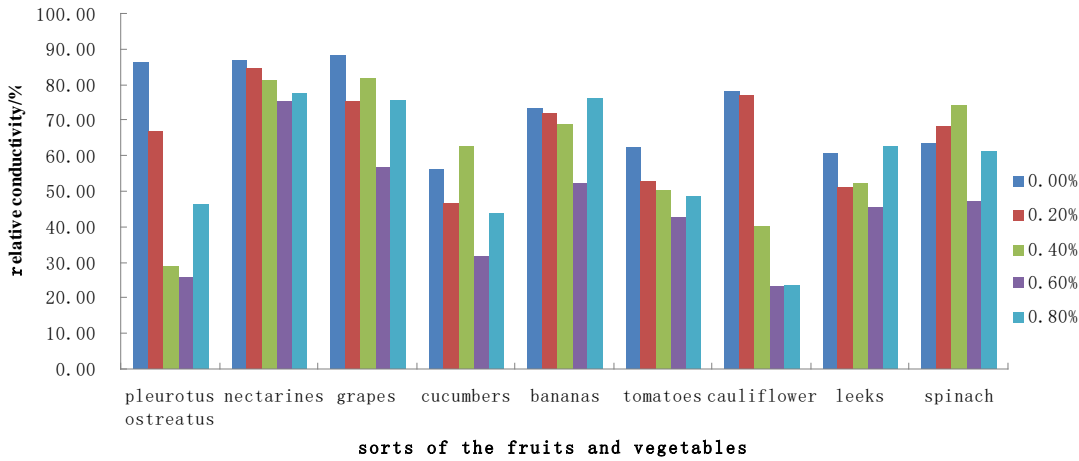


Figure 6 Relative conductivity of after 5 different concentrations of yeast treatment of fruits and vegetables after in 14 d storage

4. CONCLUSIONS

In this work, nine kinds of fruits and vegetables (i.e. pleurotus, nectarine, grape, cucumber, banana, tomato, cauliflower, leek and spinach) were pretreated with four different concentrations of yeast solution, and the untreated fruits and vegetables were taken as control. Combined with the analysis results of the sensory and water loss rates, soluble solids, vitamin C content, respiratory rate and relative electrical conductivity, we concluded that the yeast can to some extent lower the water loss rate, reduce the changes of soluble solid, vitamin C changes, the respiration rate and the cell membrane permeability, preserve freshness, prevent the diseases and prolong corruption, thus slowing down the speed of nutrients loss and aging, and improving the storability of fruits and vegetables. By comparison all physiological and biochemical indexes of groups with various yeast concentrations treatment and taking vitamin C content and relative electrical conductivity as the main indexes, it was found that the fruits and vegetables treated with 0.60% yeast solution was optimal, which showed relatively better state after storage for 14 days.

The action mechanism of most biocontrol bacteria and biocontrol mold were producing antibacterial substances, but yeast does not produce antibacterial substances. The main action mechanism of yeast on disease prevention of fruits and vegetables after picking is: i) nutrition or space competition. Yeast expanded the number of colonies through proliferation, which can form dominant colonies, consume the surrounding nutrients, occupy most of the living space, and inhibit the growth and reproduction of pathogenic bacteria. ii) The direct parasitic effect of yeast on pathogen. Many yeasts can decompose the mycelium or cell wall of the pathogen by secreting extracellular hydrolytic enzymes. Also some yeast can be attached to the pathogen, forming a direct parasitic effect for pathogen. iii) The yeast induced disease resistance in the host. Some yeasts can induce hosts to produce substances that inhibited the growth of bacteria after massive reproduction on the fruits and vegetables, and some yeast can induce the production of enzymes such as glucanase and chitinase in fruit and vegetable, which can decompose

the walls of pathogen and inhibit the growth of pathogen. In addition, some yeast can change the tissue structure of the fruits and vegetables, thereby enhancing the disease resistance and prevention of the host. IV) The influence of other substances on antagonistic effect. In general, the effect of single strain on disease prevention was less than chemical fungicides [11]. Qin et al. found that the combination of yeast and some special substances can increase the antagonistic effect of yeast.

Although yeast to some extent played a role in disease prevention of picked fruits and vegetables, some questions still existed. For example, if the yeast can ferment and produce ethanol by using the sugar in fruits and vegetables, thus accelerating the aging of fruits and vegetables? When the fruits and vegetables after being treated by yeast are stored in a lower or higher temperature environment, can yeast still play a role in preserving freshness? How about the effect of combining the yeast with other strains, physical or chemical methods? These questions are needed for further study.

ACKNOWLEDGMENT

This paper is supported by Zhoukou Normal University school-based project (2018 year) (project number :No. ZKNUB2201805)

REFERENCES

- [1] ZHANG Xi, LI Yang *, WANG Lei – ming, FENG Gang. Research progress of application of biological preservative in the preservation of fruits and vegetables [J]. *Science and Technology of Food Industry*, 2015, 39(6): 742-746.
- [2] Chiumarelli M, Pereira LM, Ferrari CC, et al. Cassava starch coating and citric acid to preserve quality parameters of fresh-cut "Tommy Atkins" mango[J]. *Journal Food Science*, 2010, 75(5): 297-304.
- [3] Bosquez-Molina E, Ronquillo-de Jesús E, Bautista-Banos S, et al. Inhibitory effect of essential oils against *Colletotrichum gloeosporioides* and *Rhizopus stolonifer* in stored papaya fruit and their possible application in coatings[J]. *Postharvest Biology and Technology*, 2010, 57: 132-137.
- [4] Velazquez-Nunez M J, Avila-Sosa R, Palou E, et al. Antifungal activity of orange (*Citrus sinensis* var. Valencia) peel essential oil applied by direct addition or vapor contact[J]. *Food Control*, 2013, 31: 1-4.
- [5] Tao N G, Jia L, Zhou H. Anti-fungal activity of *Citrus reticulata* Blanco essential oil against *Penicillium italicum* and *Penicillium digitatum*[J]. *Food Chemistry*, 2014, 153: 265-271.
- [6] Shao X F, Wang H F, Xu F, et al. Effects and possible mechanisms of tea tree oil vapor treatment on the main disease in postharvest strawberry fruit [J]. *Postharvest Biology and Technology*, 2013, 77: 94-101.
- [7] Kumar V, Mathela C S, Tewari G, et al. Chemical composition and antifungal activity of essential oils from three Himalayan erigeron species[J]. *LWT-Food Science and Technology*, 2014, 56: 278-283.
- [8] Cao S F, Zheng Y H, Wang K T, et al. Effect of methyl jasmonate on cell wall modification of loquat in relation to chilling injury after harvest[J]. *Food Chemical*, 2010, 118(3): 641-647.
- [9] Ibrahim S M, Nahar S, Islam J M M, et al. Effect of low molecular weight chitosan coating on physicochemical properties and shelf life extension of pineapple[J]. *Journal of Forest Products and Industries*, 2014, 3(3): 161-166.
- [10] Sara E, Martam H, Abdorreza M, et al. Effect of nano chitosan based coating with and without copper loaded on physicochemical and bioactive components of fresh strawberry fruit during storage[J]. *Food and Bioprocess Technology*, 2014, 7(8): 2397-2409.
- [11] Gol N B, Patel P R, Rao T V R. Improvement of quality and shelf-life of straw berries with edible coatings enriched with chitosan[J]. *Postharvest Biology & Technology*, 2013, 85 (3): 185-195.

Research on Logistics Demand Forecasting Model Combining Time Series and Neural Network

Lu Liu^{1*}, Yaning Zhao¹, Xinyan Dong¹, Yuanshuo Liu¹, Peng Qiao¹, Zhiyuan Xie¹, Cuihuan Ren¹, Fengchun Liu², Chunying Zhang¹

¹North China University of Science and Technology, Tangshan, Hebei, 063210, China

²Qian'an College North China University of Technology, Tangshan, Hebei, 063210, China

*E-mail:hblg_llu@126.com

Abstract: Logistics demand forecasting requires fast response and dynamic adjustment. Combining the characteristics of time-series and BP neural network, this paper proposes an algorithm innovatively in which time-series autoregressive-moving average model(ARMA) and back propagation (BP) neural network are fused together to predict logistics demand. First, the freight data of different time periods are regarded as a time series, the linear part is fitted with the time series autoregressive-moving model method to obtain the residual sequence, and the BP neural network is used to deal with the nonlinear residual part. Then, through index synthesis and quantitative screening, the input and output indexes of the model are determined. Finally, the data of Tangshan freight from 1978 to 2015 are selected as the original data for experimental comparison, which shows that this method is more accurate than using time series or neural network alone.

Key words: time-series;neural network;residual sequence;logistics demand forecast

1. INTRODUCTION

With the further development of e-commerce, forecasting freight volume and delivering goods to customers efficiently have become the research focus of all major e-commerce enterprises [1]. The prediction of logistics demand mostly adopts a single model such as time-series, rough neural network or improved neural network. Document [2] applies the ARMA model of time-series to the prediction of logistics demand. The generalized autoregressive conditional heteroscedasticity model proposed in document [3] is fitted, and the prediction effect is slightly better than that of autoregressive model. Document [4] constructs a logistics demand scale prediction model based on three-layer BP artificial neural network. However, the single model has the disadvantage of unstable prediction results. Therefore, a combined prediction method combining time-series method, gray prediction method and correlation analysis method is proposed in document[5], which is

applied to the prediction of wharf throughput and solves the problem of complicated factors and less available data in the previous prediction process. Shi Zejun et al. combined the grey model and exponential smoothing method and put forward a new combination forecasting method[6]; Ling Zhou et al. selected exponential smoothing method, ARIMA method and neural network method to form a combination method according to the applicability and differentiation principle of the selection method, studied the short-term demand forecast of a LTL carrier[7], and proved the superiority of the combination forecasting method of time series and neural network.

In this paper, the ARMA - BP combination method is adopted. For a single linear sequence of freight data, the ARMA model method is applied, while for a nonlinear sequence of multiple variables, BP artificial neural network method is introduced so as to establish a general prediction model. The final prediction error is further reduced by combining the two methods.

2. BASIC KNOWLEDGE

2.1 Time Series Autoregressive-Moving Average Model ARMA

According to the characteristics of time series, it can be divided into stationary and non-stationary sequences. Stationary time series models include autoregressive model (AR), moving average model (MA) and autoregressive-moving average model (ARMA)[8].

The principle of AR model is shown in Equation (1):

$$y_t = \mu + \frac{1}{1 - AR(1) * B \cdots AR(p) * B^p} \varepsilon_t \quad (1)$$

The principle of MA model is shown in Equation(2):

$$y_t = \mu + (1 - MA(1) * B \cdots MA(q) * B^q) \varepsilon_t \quad (2)$$

The principle of ARMA model is shown in Equation

(3):

$$y_t = \mu + \frac{1 - (MA(1) * B \dots MA(q) * B^q)}{1 - AR(1) * B \dots AR(p) * B^p} \varepsilon_t \quad (3)$$

Where B is the lag operator, $By_t = y_{t-1}$, p, q are the order of the model, y_t is the current value of the time series, ε_t is the random interference, μ is a constant term[9].

However, for non-stationary time series, differential processing is generally performed first to make it a stationary time series [10], and then the stationary time series model method is used for processing. For this reason, an ordered difference operator $\nabla = 1 - B$ is introduced, $\nabla^d = (1 - B)^d$, and the non-stationary time series is transformed[9] by using the first-order difference to obtain equation (4):

$$\nabla y_t = (1 - B)y_t = y_t - y_{t-1} \quad (4)$$

This difference transformation needs to be repeated until it becomes a stationary sequence. The sequence after D-order difference satisfies Equation (5):

$$\nabla^d y_t = (1 - B)^d y_t \quad (5)$$

How to select the model and determine the order needs to be determined according to the self-correlation coefficient and partial correlation coefficient, which can generally be determined according to Table 1.

Table 1 Model Type and Order Determination

self-correlation coefficient	partial correlation coefficient	Model ranking
trailing	p-order truncation	AR(p) Model
q-order truncation	trailing	MA(q) Model
trailing	trailing	ARMA(p,q)Model

2.2 Basic Principles of BP Neural Network

BP neural network uses multi-layer forward neural network to learn the nonlinear function in the system difference equation, and uses gradient search technology to minimize the network output error and the mean square value of the network expected output. As shown in fig. 1, BP neural network is composed of input layer, hidden layer and output layer [11].

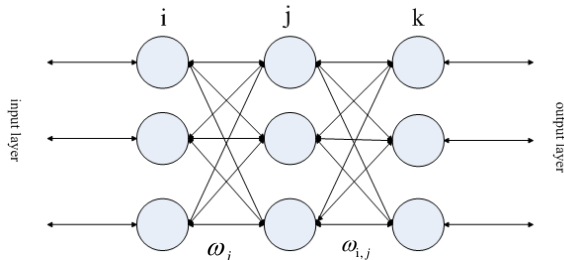


Figure 1 BP neural network structure

The relationship between input and output is shown in Equation (6):

$$x_t = \omega_0 + \sum_{j=1}^q (\omega_{0,j} + \omega_{i,j}x_{t-i}) e_t \quad (6)$$

Where $\omega_{i,j} (i = 0,1,2, \dots, p; j = 0,1,2, \dots, q)$, and $\omega_j (j = 0,1,2, \dots, q)$ represent connection weights; p is the number of input layer nodes and q is the number of hidden layer nodes.

3. ARMA - BP MODEL

3.1 Combination Method

In the process of data fitting, freight volume data of different years are regarded as a time series, divided into linear part and non-linear part. The ARMA method is used to fit the linear part and obtain the residual sequence, and then BP neural network is used to deal with the non-linear residual part [12]. The specific method is as follows:

In the first step, the ARMA method is used to fit the time series and calculate the residual error

$$e_t = \hat{L}_t - y_t \quad (7)$$

In equation (7), \hat{L}_t is the predicted value of ARMA method, y_t is the actual value.

In the second step, for e_t calculated in the first step, the BP neural network method is used for a series of training studies to predict the non-linear residual part .

3.2 Selection of Input Indicators and Output Indicators

Logistics demand is related to a variety of factors. We selected the following factors, then conducted index synthesis and quantitative screening, and finally determined six factors, as shown in Figure 2.

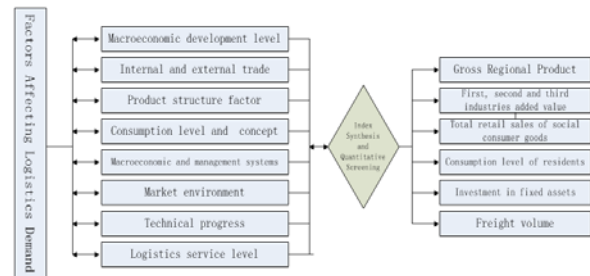


Figure 2 Determination of Input Indicators

The highway freight volume is selected as the output index of the logistics demand model. On the input index of freight volume, the residual value of freight volume obtained by time series processing is taken as the input of the model.

3.3 Algorithm Design and Analysis

The process shown in fig.3 carries out time series processing, mainly including the main processes such as stationarity test and processing and white noise test.

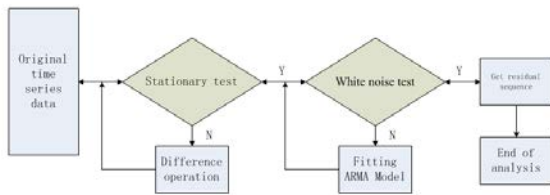


Figure 3 Time series processing flow

1)Smoothness test

Testing methods have time series diagram test, self-correlation diagram test and ADF test, combined with the characteristics of logistics data, the method use of time series diagram test is the most convenient and fast. The time series of a stationary sequence has significant boundary, no obvious change of movement and periodicity.

2)data stabilization

The N-order difference is performed using the difference principle, and the sequence obtained by the difference is tested for stability in step 1.

3)Determination of Model Order

The self-correlation and partial self-correlation coefficient maps of the sequence processed in step 2 are obtained, and the model type and order are preliminarily determined by the image and table 1 method.

4)white noise test

According to the mathematical characteristics of the self-correlation coefficient and partial self-correlation coefficient of the residual sequence, whether the residual sequence is a white noise sequence or not is judged, if the residual sequence passes the white noise test, the model is determined, the predicted value and the residual sequence value are obtained, and the analysis is finished [13].

After that, BP - ARMA model processing is used to simulate and predict the data, as shown in fig.4, the main steps are as follows.

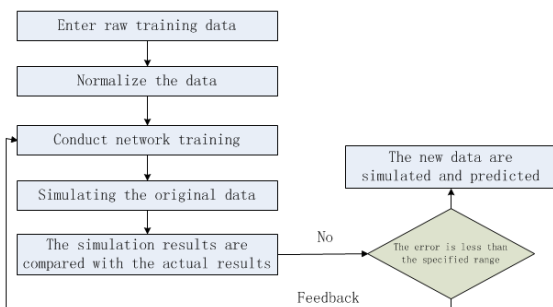


Figure 4 BP - ARMA Processing Flow

1) Selecting the residual sequence obtained by processing the time series and the confirmed indexes as the original data of the training neural network.

2) Selecting the MIN - MAX normalization function to normalize the data, and the processed original data are of the same order of magnitude.

3) Carry out the first network training to obtain a training result. Comparing with the actual value, if the error value is greater than the specified value, feedback the adjustment weight value and threshold

value and continue training until the error value are small to a certain range.

4) After the network training is over, input the prediction data for simulation and prediction so as to obtain the prediction result.

4. EXPERIMENTAL ANALYSIS

4.1 Experimental environment

The data of Tangshan Statistical Yearbook are obtained, and the data of Tangshan highway freight volume from 1978 to 2015 are used as the original data. The original data are shown in Table 2, and the data are modeled by using the time series method preliminarily.

Table 2 Freight Traffic Volume of Tangshan City from 1978 to 2015

Year	Freight volume	Year	Freight volume
1978	2444	2011	33005
1979	2692	2012	37625
1980	2228	2013	43043
1981	1885	2014	33479
.....	2015	36358

When establishing and predicting the model, the processing of time series and the acquisition of residual series are completed by EViews 9.0 data processing software. BP neural network uses Python language to build models to make analysis and prediction.

4.2 ARMA experiment

The freight volume data is imported into the software and named as the X sequence, and the trend graph and correlation graph of the sequence X are shown in Figure 5 and Figure 6 below. After observation, the obvious upward trend of the sequence can be found, and the P value is observed in the correlation graph, the sample data is found to be non-stationary, so first-order difference is performed on the original sequence.

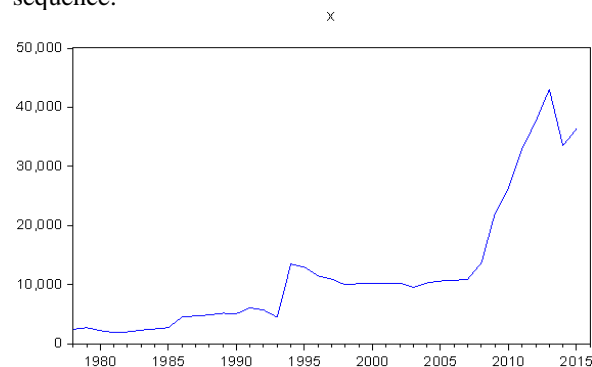


Figure 5 Trend chart of sample data

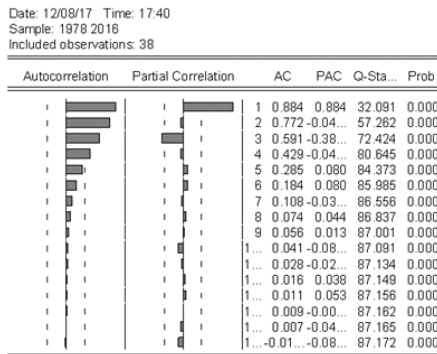


Figure 6 Sample data correlation diagram
Using the difference function, input the command $genrx_t = d(x)$ to get the new sequence x_t , draw the trend chart of the new sequence x_t , and judge x_t as a stationary sequence by combining the method of timing chart checking and fig. 7.

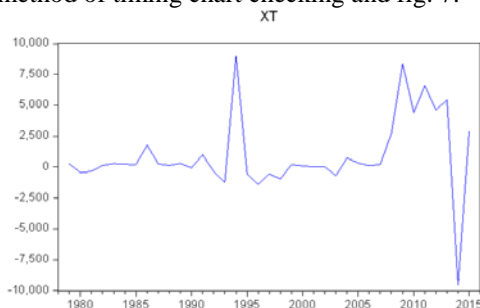


Figure 7 Trend diagram of first-order difference sequence

The correlation graph of sequence x_t is obtained as shown in fig.8. We can see that the self-correlation coefficient and partial self-correlation coefficient are always within the range of twice the standard deviation, so $\{x_t\}$ is identified as $ARMA(p, q)$ model.

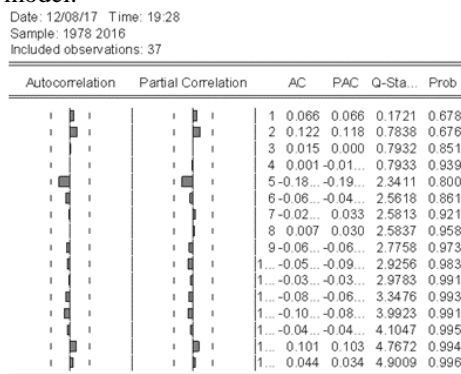


Figure 8 Correlation graph of sequence x_t
After many experiments and combining with AIC (Red Pool Criterion) minimization principle, the N and M values of each time are compared, and the final result is ARMA (20, 2) model. Draw a trend chart of predicted values and actual values, and the fitting results are shown in fig. 9.

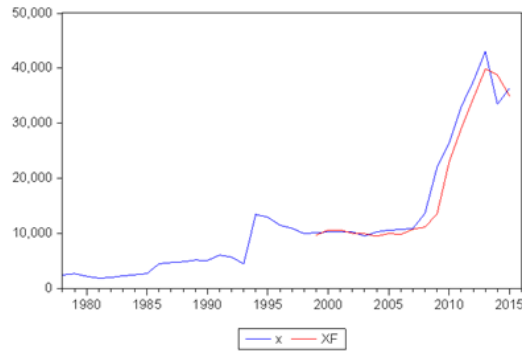


Figure 9 Trend chart of predicted value and actual value

XF in the figure is a sequence of predicted values and X is a sequence of actual values. As can be seen from fig.9, the trend charts of the two are basically consistent, but the data results are quite different.

4.3 ARMA - BP Experiment

Enter the input indicators from 2001 to 2014; The output index of one year after the input data is selected as the output of the learning model. In order to make the prediction result more accurate, the input data are trained individually several times, and the error changes during the training are shown in fig.10.

At the same time, BP neural network is used alone to provide a reference for comparative analysis of errors. See Figure 11 shows the comparison between predicted values and actual values of the three methods.

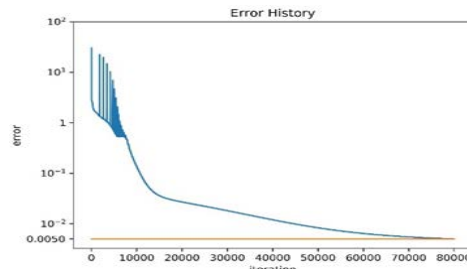


Figure 10 BP - ARMA model training error diagram

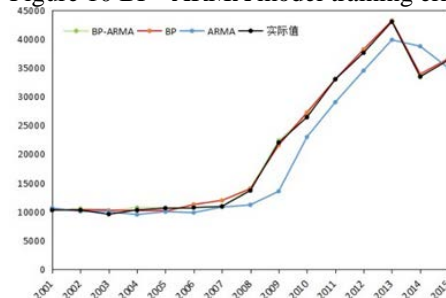


Figure 11 Comparison chart between predicted value and actual value

4.4 Comparative Analysis of Results

As can be seen from fig.11, the predicted value of the method combining the time series with the neural network agrees with the real value, and the prediction accuracy is significantly better than that of the single time series model, with the error value reaching 0.005. when comparing with the single BP model, it is difficult to see the superiority only through the trend

chart, so the error chart [14]of the single BP model is drawn, as shown in fig. 12.

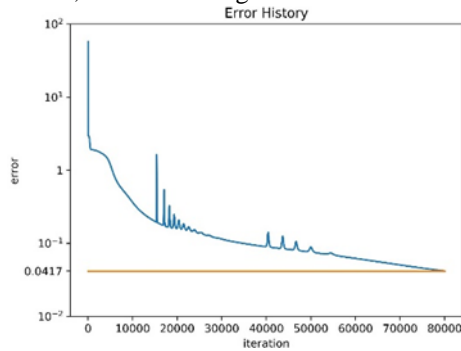


Figure 12 BP model training error diagram

Combined with fig. 12 and fig.10, it can be seen that the error of BP-ARMA model is smaller than that of single BP model, and the prediction accuracy is further improved.

In summary, the ARMA-BP combined model is more accurate and reliable than the single model method. Finally, based on this model, the freight volume in 2016 is predicted, and the predicted results are summarized in the table below.

Table 3 Comparison of Actual and Predicted Freight Volume

Year	Actual Value	Predicted Value	Year	Actual Value	Predicted Value
2011	33005	33312.10	2014	33479	33439.75
2012	37625	37688.73	2015	36358	36437.77
2013	43043	43221.51	2016	-	31279.28

5. CONCLUSIONS AND PROSPECTS

This paper combines the time series with BP neural network, integrates the characteristics of the time series and BP neural network, establishes a time series - neural network combination method, and obtains a more reliable ARMA - BP model, giving e-commerce enterprises enough time to adjust goods and enhance their advantages.

Compared with the previous model, the accuracy of this model is further improved, but when forecasting logistics demand at some future time, multiple use of the one-step forecasting method will accumulate errors, and the effect of direct multi-step forecasting is not ideal. Therefore, the future research direction should start with the improvement of neural network multi-step forecasting method, so that it can meet the demand of logistics demand forecasting in current and future markets.

At the same time, in the process of practical application, it cannot be dogmatically believed that the long-term trend is stable. For example, the upstream seller's operation strategy has changed, adding such activities as "Double Eleven" has greatly affected the trend. Therefore, the operator should grasp the latest data in combination with the actual situation, revise the forecast equation in time, and determine the optimal order quantity so as to maximize the revenue.

ACKNOWLEDGMENT

This paper is supported by Hebei Natural Science Foundation (No.F2016209344, F2018209374)

REFERENCES

[1] LI Zhuangkuo, LV Heng. Research on Guilin Logistics Forecast Based on Improved PSO-BP Neural Network[J]. Popular Science & Technology, 2017,19(06):5-8.

[2] ZHAO Yanjun, CHEN Yu. Application of Time Series Analysis Method in Logistics Demand Forecasting[J]. Logistics Technology, 2017,40(06):12-14.

[3] Bahram Adrangi, Arjun Chatrath, Kambiz Raei. The demand for US air transport service: a chaos and nonlinearity investigation[J]. Transportation Research Part E, 2001(37),337-353

[4] LUO Jianfeng, MA Tianshan. An Integrated Predicting Model of New-Built Regional Logistics Center's Demand Based on the Artificial Neural Network[J]. Applied Mechanics and Materials, 2013, 2155 (253).

[5] MO Yanfang, ZHAO Yifei. Throughput Prediction of Roving Wharf Based on Combined Prediction Model[J]. Journal of Chongqing Jiaotong University: Social Science Edition, 2014,14(2).

[6] SHI Zejun, LI Kai. Prediction of Container Throughput Based on Grey Model and Exponential Smoothing Method[J]. Journal of Traffic Humanities in Chongqing: Natural Science Edition, 2008,27(2).

[7] Ling Zhou. Prediction of a service demand using combined forecasting approach[J]. Journal of Physics: Conference Series, 2017,887(1).

[8] TIAN Genping, ZENG Yingkun. Application of Time Series Model in Logistics Demand Forecasting [J]. Logistics Technology, 2007,30 (9):96-99.

[9] CAI Kai, TAN Lunnong, LI Chunlin, TAO Xuefeng. Short-term Wind Speed Prediction Based on Time Series and Neural Network[J]. Power Grid Technology, 2008,(08):82-85+90.

[10] YANG Lei, ZHANG Miaomiao. Application of Time Series Model in Logistics Demand Forecasting [J]. Commercial Times, 2013(13): 26-27.

[11] FU Haibing, ZENG Huanglin. BP neural network algorithm and improvement[J]. Science and Technology of West China, 2012, 11(08): 23 - 24.

[12] SONG Yuqiang. Application of Artificial Neural Network in Time Series Prediction[D]. Xi'an University of Architecture and Technology, 2005.

[13] FANG Yingguo, WANG Fen. Overview of Time Series Prediction Methods[J]. Journal of zhejiang shuren university (Natural Science Edition), 2006, 6 (02): 61 - 65.

[14] JIANG Chunlei, ZHANG Shuqing, ZHANG Ce, LI Huapeng, DING Xiaohui. MODIS Leaf Area Index Time Series Modeling and Prediction Based on S ARIMA-BP Neural Network Combination Method [J]. Spectroscopy and Spectral Analysis, 2017, 37 (1): 189 - 19.

Meta-Analysis of Relationship between Ionizing Radiation and Chromosome Aberration Rate of the Radiation Workers

Xin ZHANG

North China University of Science and Technology, Department of Discipline Construction, Tangshan 063210, China

*E-mail: zhangxin_ncst@163.com

Abstract: To further analyze the relationship between ionizing radiation and chromosome aberration rate of the radiation workers by meta-analysis. The relevant literatures were searched, the number of testing cells, chromosome aberration number and chromosome aberration rate were basic data, the heterogeneity of data was tested, the risk difference was as effect size, and the fixed effects model or random effects model was used to meta-analysis. Six papers were selected in this study. Through this study, it can be concluded that medical diagnostic X-ray can increase the chromosome aberration rate of peripheral blood lymphocytes, so we must do a good job in radiation health protection.

Keywords: Medical diagnostic X-ray, Chromosomal aberration, Meta-analysis

1. INTRODUCTION

With the progress of society, the use of ionizing radiation equipment is very common. Medical diagnostic X-ray workers have long been exposed to low doses of ionizing radiation, and their health deserves attention. Chromosome aberration, as a specific sensitive indicator of biological effects of low dose radiation, is closely related to the occurrence of human tumors, abortion, congenital malformations and genetic diseases. In recent years, there have been many investigations on chromosomal aberrations in peripheral blood lymphocytes of radiologists by medical diagnostic X-ray, but the results of chromosomal aberrations reported are different [1-3]. In order to determine whether there is any difference in chromosome aberration rate between medical workers engaged in X-ray exposure and non-professional clerks in China, the meta-analysis method was used to analyze the related literatures reported in many regions of China.

2. MATERIALS AND METHODS

2.1 Literature Search

The electronic medical database was searched with the keywords of "medical diagnostic X-ray" and "chromosome aberration", mainly including "Chinese biomedical journal literature database" and "China Journal Network full text database" [4-6]. The

literature published in China from 2009 to 2018 were collected.

2.2 Inclusion

Criteria The published studies on chromosomal aberrations in peripheral blood lymphocytes of medical diagnostic X-ray workers in China need to provide the number of observations, the number of cells examined, the number of chromosomal aberration cells and the aberration rate of the radiation group and the control group. The methods of literature research are similar [7].

2.3 Exclusion

Criteria Exclud small sample size, no control group literature, repeated reports, case reports, little information or incomplete data and inability to use the original data and review literature.

2.4 Statistical

Analysis According to the inclusion and exclusion criteria of this study, a total of 6 articles were obtained by strict screening. Review Manager 5.3 software was used to collate relevant information. Heterogeneity test was performed on all selected literature data. The test statistic were Chi² and P, and the test level α was 0.05. Fixed effect model or random effect model were selected according to the test results. If the independent results were homogeneous, fixed effect model (F) was used, whereas random effect model (R) was used. The difference of chromosome aberration rate between the two groups was merged and the corresponding effect combination value and 95% CI were calculated. Publication bias was expressed by funnel plot [8].

3. RESULTS

3.1 Basic information on research

A total of 6 articles were selected according to the standard, with 2237 cases in the cumulative radiation group and 1287 cases in the control group.

3.2 Heterogeneity test

Six papers showed heterogeneity (Chi² = 88.60, P < 0.005) by consistency test, which was suitable for random effect model analysis.

3.3 Meta analysis

According to the results of heterogeneity test, the weighted mean D and 95% CI of the difference

should be calculated by the random effect model. Results 95% CI of $D = 0.22$ and $d = 0.13-0.31$, which did not include 0, showed that there was a significant difference in the overall rate between the two groups, indicating that the chromosome aberration rate of medical diagnostic X-ray workers in China was higher than that of the control group, as shown in Figure 1. Publication bias is shown in Figure 2.

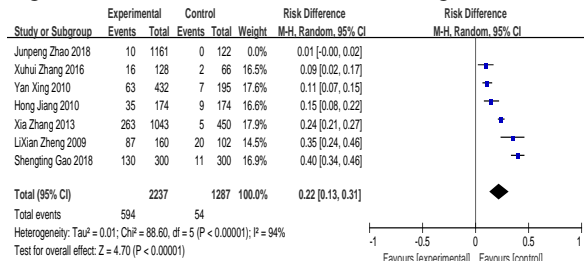


Figure 1 The Rate difference of chromosome aberration rate between radiation group and control group and its 95% confidence interval

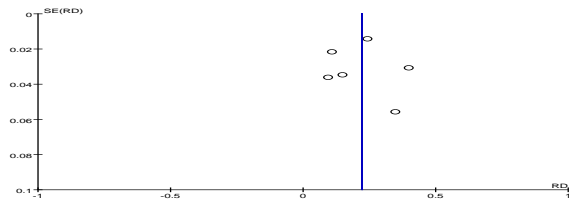


Figure 2 The Funnel plot analysis of chromosome aberration rate in two sets of data

4.CONCLUSION

It has been reported that the chromosome aberration rate of peripheral blood lymphocytes of medical X-ray workers is higher than that of other normal people, but there are also many reports that the difference between them is not significant. [7,8]. Based on the latest data on chromosome aberration rates of medical X-ray workers and other normal persons reported in most parts of China, the chromosome aberration status of medical diagnostic X-ray workers in China in the past 10 years was analyzed by using Meta-method. The results showed that the lymph nodes in peripheral blood were significantly elevated than those in the control group. The rate of chromosome aberration increased significantly. The analysis shows that medical diagnostic X-ray can increase the chromosome aberration rate of peripheral blood lymphocytes. Therefore, the high chromosome aberration rate of

X-ray workers should be highly valued by the relevant departments.

ACKNOWLEDGMENT

This work was supported by National Natural Science Foundation of China (no. 51504080), by Science and technology project of Hebei Education Department (no. BJ2017021), by NCST Natural Science Funds for Distinguished Young Scholars (no. JQ201711), by Hebei Province Natural Science Fund for Excellent Young Scholars (no. E2018209248).

REFERENCES

[1] Zhao Junpeng, Wang Yu et al. Detection analysis on peripheral blood lymphocytes chromosome aberration rate and micronucleus rate of the radiation workers in Tangshan City Hebei Province[J], 2018, 34(08):786-789.

[2] Zhang Xuhui, Sun Yuanhai, Zhang Xiaoguo. Health Survey Analysis of 128 Interventional Radiology Workers in Chifeng[J]. Chinese Journal of Radiological Health, 2016, 25(04):430-433.

[3] Xing Yan, Analysis of chromosome aberration and micronucleus rate in peripheral blood lymphocytes of radiation workers in Nanjing[J]. Chinese Journal of Radiological Health, 2010, 19(02):176-178.

[4] Jiang Hong et al, Analysis of chromosome aberration rate and micronucleus rate in peripheral blood of radiation workers in Guizhou[J]. Chinese Journal of Radiological Health, 2012, 21(01):50-52.

[5] Zhang Xia, Zhang Yan, Shi Wen. Analysis on chromosome aberration and micronucleus rate of peripheral blood lymphocytes among radiation workers in Cangzhou City[J]. Occup and Health, 2014, 30(10):1292-1441.

[6] Gao Shengting, Wu Shuibin, Lin Bo. Chromosome aberration and micronucleus rate in peripheral blood lymphocytes of radiation workers in Zhuhai [J]. Modern Chinese Medicine Application, 2018, 12(14): 213-214.

[7] Jia Li, Gao Shulan, Yang Ping. The analysis of chromosomal aberrations in 149 medical X-ray workers[J]. Ningxia Medical Journal, 2000, 22(8): 499.

[8] Liu Guanjian, Wu Taixiang, Kang Deying. Statistical process in meta analysis[J]. Clinical rehabilitation in China, 2000, 7(4): 538-539.

Optical Character Recognition

Zhuo Li^{1,2}, Yue Ma^{1,2}, Yitao Liu^{1,2}

¹North China university of technology by rising innovation education base, Tangshan, hebei 063210, China

²Mathematical Modeling Innovation Lab, North China University of Science and Technology, Tangshan, Hebei 063210, China

Abstract: Optical character recognition is the core of OCR. However, image data is often noise data, and there are many influencing factors. Therefore, how to process image to achieve effective character recognition has become a common concern of enterprises. Aiming at problem 1, the statistical description and analysis model of optical character data set was established. By importing the optical character data set into SPSS, p-p diagram of normal frequency graph was used to test the rationality of normal distribution curve, and the conclusion that it satisfied normal distribution was obtained. The data is preprocessed by removing the boundary value so that the remaining data can be recognized better. Aiming at problem 5, a BP neural network model is established. The array is fitted and trained to fit two curves. The two curves are compared to obtain the error change between the prediction results of the neural network and the actual results. **Keywords:** statistical description and analysis; Pearson correlation coefficient; Linear least square method; BP neural network

1. MODEL ASSUMPTIONS

Assuming that optical electronic devices can operate normally, they can carry out character recognition. Assume that the characters recognized by optical electronic devices are complete and there are no incomplete characters. assuming that the data is practical and the error caused by the data is very low.

2. THE ESTABLISHMENT AND SLUTION OF THE MODEL.

(1). Statistical and analytical models for optical character datasets

The optical character data set is imported into SPSS for data statistics, and then the frequency distribution histogram is established with the black pixel number as abscissa and the frequency as ordinate. Then through the induction and observation of the histogram, we can get the data which will affect the final result to some extent, and then delete it. The result is more realistic. Frequency distribution histogram is shown in Figure 1:

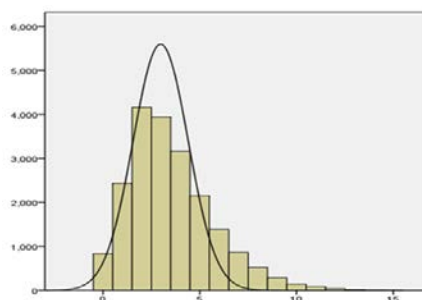


Fig. 1 frequency histogram of character data

As can be seen from the histogram, the distribution of black pixels in the rectangular region is approximately bell-shaped with high middle and low ends. In order to give a more precise numerical description, we need to give further study the so-called "statistics" that reflect the characteristics of the data. The distribution shape of the number of black pixels in the rectangular area shown in the histogram can be regarded as a normal distribution. Verify as shown in Figure 2:

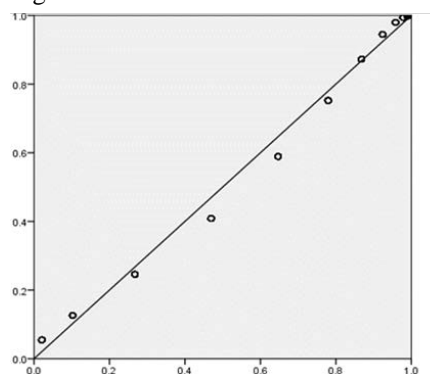


Fig. 2 normal P-P diagram of black pixels in rectangular area

Fig. 2 shows that 95% of the values fall within the range of two standard deviations from the mean value.

$$P\{\mu - 2\sigma \leq X \leq \mu + 2\sigma\} \approx 0.95 \quad (1)$$

That is to say, the optical character data set in the title is about 95%. And the remaining 5% of the data deviated from this "peak", that is, do not conform to most data, there is data error problem. In the final character recognition, if these data are taken into account, the resulting character and the actual character will have a certain error, in order to minimize the error, the data need to be pre-processed. Therefore, it is necessary to remove 5% of the invalid

data before recognizing the characters to achieve the preprocessing of the optical character data set.

(2).BP neural network model

Through the establishment of BP neural network model, the arrays in the range of variable fluctuation array are screened out and imported into matlab, 70% of the data are trained to get a curve, and then tested with 30% of the data, another curve is fitted, and the error between the prediction results of neural network and the actual results is obtained by comparing the two results. Change. As shown in Figure 3:

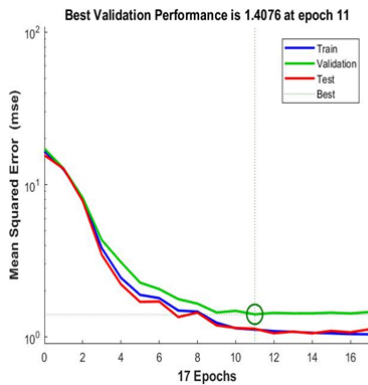


Fig. 3 error variation between neural network prediction and actual results

Then click Error histogram to see the error distribution between the predicted results and the actual results and the fitting situation.

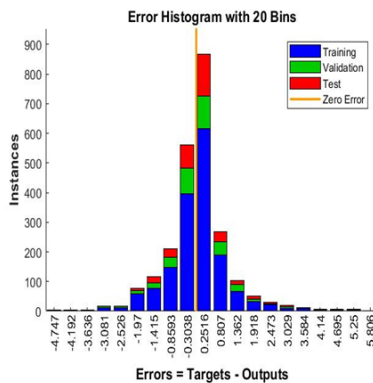


Fig. 4 error distribution between neural network prediction and actual results

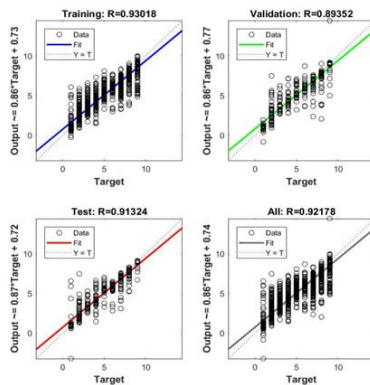


Fig. 5 fitting degree between neural network prediction results and actual results

According to the results, we found that the smaller the value of MSE, the closer the R value to 1, the better the training effect, the closer the fitting graph R to 1, the better the model fitting effect. After training multiple data, one of the best fitting degree was selected, and the correct rate of prediction was 93.018%.

The prediction accuracy based on BP neural network model shows that there are still some problems in the model. It is necessary to optimize the model to improve the overall performance of the whole scheme, so that the prediction accuracy is higher. In the principal component analysis model based on Pearson correlation coefficient, we can select the first ten characteristic variables of correlation degree ranking, and then enlarge the number of arrays, so that the random arrays can be better fitted in the wave array corresponding to the characters, so as to accurately get the specific characters.

In the evaluation model based on AHP, we can further refine the solution of the weight vector, because the weight vector is used to verify the accuracy of the contrast matrix, and the accuracy of the contrast matrix will directly affect the optimal evaluation of the regression model based on curve fitting linear least squares method.

3. EVALUATION AND IMPROVEMENT OF THE MODEL.

(1) evaluation of models

Firstly, the P-P diagram of normal frequency graph is used to test the rationality of normal distribution curve, and the weight vector is used to make the model more accurate and get the optimal evaluation of the model. Secondly, the BP neural network model is used to verify the fitting in matlab, and the accuracy is improved again. After three tests, the reliability of the final result is greatly improved.

(2) improvement of model

When verifying the accuracy of the contrast matrix, it needs to be applied to the calculation of the weight vector. However, the calculation steps of this part are more complicated and difficult to understand. It needs to simplify the complex data through application programming.

REFERENCES

[1]Ng Man Tat, Cheng Lizhi, et al. Mathematical modeling course [M] 2011 higher education press Changsha
 [2]Wang Zhihua. Recognition of Concatenated Character Verification Codes Based on Generalized Hough Transform [J].Journal of Jimei University (Natural Science Edition), 2018,23 (01): 75-80.
 [3]Fan Wang, Han Jungang, Gou Fan, Li Shuai.Convolutional Neural Network Recognition Chinese Character Verification Code [J].Computer Engineering and Applications, 2018,54(03): 160-165.
 [4]Wu Jiansheng, Zu Xuliang, Xue Hanjin.Text image orientation determination based on feature

- recognition[J].*Computer Engineering and Design*, 2015,36(08): 2260-2263+2296.
- [5]Wang Yang, Xu Yingqiu, Peng Yanbing. Identification of Intranet Verification Codes Based on KNN Technology [J].*Computer and Modernization*, 2017 (02): 93-97.
- [6]Gao Liang. Handwritten English alphabet recognition based on BP neural network [D]. North Central University, 2009.
- [7]Liu Li. Design and research of key algorithms in optical character recognition system [D]. University of Electronic Science and technology, 2011.
- [8]Xiao Lei Lei. Research and implementation of optical character recognition based on Android [D]. Wuhan University of Technology, 2013.
- [9]Jingtao, Wang Zhong. Optical character recognition technology and Prospect [J]. *Computer Engineering*, 2003 (02): 1-2+80.
- [10] Liu Li. Design and research of key algorithms in optical character recognition system [D]. University of Electronic Science and technology, 2011.
- [11]Nan Shuping, Zhang Bo, Wang Feng. Application of optical character recognition technology in handwritten character recognition [J].*Journal of Changchun Normal University*, 2015, 34 (12): 39-42.
- [12]Wang Rong Feng. Research on optical handwritten numeral character recognition technology [D]. Guangxi Normal University, 2014.
- [13]Lu Jun Yi. Research on optical character recognition of license documents [D]. Harbin Institute of Technology, 2016.

Clothing Design for High Temperature Operation

Zhuo Li^{1,2}, Yue Ma^{1,2}, Yitao Liu^{1,2}, Aimin Yang^{3,*}

¹North China university of technology by rising innovation education base, tangshan, hebei 063210

²Mathematical Modeling Innovation Lab, North China University of Science and Technology, tangshan, hebei 063210

³School of Science, North China University of Science and Technology, Tangshan 063210, China

*E-mail: 43698059@qq.com

Abstract: High temperature operation is an extremely dangerous task for the construction personnel. In order to ensure the safety of the construction personnel under high temperature, it is necessary for the workers to wear special clothes to weaken the influence of high temperature on the body. Therefore, it is common for enterprises to develop a high quality and low cost professional high temperature clothing. A matter of concern.

The heat conductivity, temperature, thickness and working time are substituted into Fourier equation to obtain the heat conduction rate of each layer of clothing fabric, and the temperature stratified distribution model is established with the heat conduction rate as the parameter. The temperature variation of each layer in unit time is solved, and the temperature distribution of each layer is simulated. Finally, the simulated temperature data of the outer skin of the dummy were compared with the actual measured data. The standard deviation was 2.502, which indicated that the data were in agreement with the actual model and that the model was correct.

Key words: high temperature operation special clothing Fourier law

1. MODEL ASSUMPTION

Assuming that under high temperature conditions, the air humidity around the dummy does not affect the temperature distribution. Suppose that all the heat transferred from the high temperature environment of the dummy to the high temperature work clothes is absorbed by each layer of the work clothes. No loss of energy occurred. Assuming that the high-temperature work clothes have strong radiation protection ability, the radiation to the human body is very little and can be ignored. Suppose that the basic parameters of the dummy can represent the basic parameters of all people.

2. THE ESTABLISH AND SOLUTION OF THE MODEL

(1)Temperature stratified distribution model based on Fourier law

Based on the Fourier's law, the model can calculate

the heat conduction rate of multi-layer material. The heat loss of each layer can be obtained by multiplying the heat conduction rate of each layer by the unit time. According to the law of conservation of energy, each layer is lost. Heat is equal to the heat absorbed by each layer. The heat conduction rate of each layer and the change rate of corresponding temperature in unit time are obtained. Among them, the stratification of high temperature work clothes is shown in Figure 1.

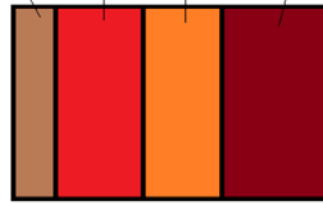


Fig. 1 stratification of work clothes

By calculating the temperature change rate per unit time of each layer, we can get the temperature distribution of each layer in the clothing under the condition of persistent high temperature in 90 minutes.

(2)Solution Of Model

Firstly, we can obtain the relation of the heat conduction rate of a single layer material by the integral transformation of both sides of Fourier law.

$$v = -\lambda A \frac{dt}{dx} \quad (1)$$

$$v = \frac{t_1 - t_2}{\frac{b}{\lambda A}} = \frac{\Delta t}{R} \quad (2)$$

Then, by further transformation, the equation for calculating the heat conduction rate of each layer for multi-layer material is obtained.

$$v = \frac{\Delta t_1 + \Delta t_2 + \Delta t_3 + \Delta t_4}{R_1 + R_2 + R_3 + R_4} = \frac{\sum \Delta t}{\sum R} \quad (3)$$

$$v = \frac{t_1 - t_{n+1}}{\sum_{i=1}^n \frac{b_i}{\lambda_i A}} \quad (4)$$

Because the heat from the outside environment is absorbed by the work clothes through heat transfer, the heat dissipated by the outside environment is equal to the sum of the heat absorbed by each layer of the work clothes according to the law of conservation of energy.

Solution of temperature change rate per unit time for IV layer.

$$v = \frac{\Delta t_1 + \Delta t_2 + \Delta t_3 + \Delta t_4}{\frac{b_1}{\lambda_1 A} + \frac{b_2}{\lambda_2 A} + \frac{b_3}{\lambda_3 A} + \frac{b_4}{\lambda_4 A}} \quad (5)$$

$$v = cm\Delta t = c\rho bA\Delta t \quad (6)$$

And because the I, II and III layers are in accordance with the following relations:

$$v = \frac{\Delta t_1}{R_1} = \frac{\Delta t_2}{R_2} = \frac{\Delta t_3}{R_3} \quad (7)$$

$$\Delta t_1 : \Delta t_2 : \Delta t_3 = R_1 : R_2 : R_3 \quad (8)$$

b is the thickness of the plane wall.

Δt is a temperature difference between two sides of a plane wall.

R is thermal conduction resistance.

A is the heat transfer area.

The thermal conductivity of lambda is thermal conductivity.

C is the fourth layer specific heat.

The density of Rho is fourth layers.

m is fourth tier quality.

It can be seen that the temperature drop of each layer is directly proportional to the thermal resistance. Then we can get the temperature drop of each layer and then calculate the temperature of each layer corresponding to the unit time.

(3) Verification of Model

When the ambient temperature is 75 C, the thickness of layer II is 6 mm, the thickness of layer IV is 5 mm, and the working time is 90 minutes, we can get the change of the outer skin temperature with time theoretically. Then, given the actual changes in Annex 2, we import the theoretical values and the actual values into the MATLAB in turn to simulate the data, and get the simulation curve as shown in Figure 2.

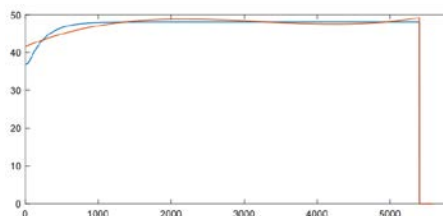


Fig. 2 curves of temperature versus time

Through the fitting of the two curves, it is easy to find that the theoretical curve and the actual curve gradually coincide and smooth transition over time. The simulation results show that the difference between theoretical value and actual value is

relatively small.

At the same time, the standard deviation between the theoretical data and the actual data is solved, and the similarity between the data is obtained. The standard deviation is 2.502, which shows that the data obtained by the model is accurate, in line with the actual results, and the model is applied correctly.

3.MODEL EVALUATION

Firstly, the temperature stratified distribution model based on Fourier's law is established. Since most of the materials used in high-temperature work are radiation-proof materials, the radiation heat transfer is neglected here and only the heat conduction is considered. By combining the multi-layer plane wall formula deduced by Fourier's law with the heat formula, we can get the increase value of temperature in unit time. Because the temperature of inner air layer changes all the time, the increase value of temperature in unit time decreases gradually, and the temperature tends to be gentle gradually, so the model is more accurate. It is true.

REFERENCES

- [1] Ng Man Tat, Cheng Lizhi, et al. Mathematical modeling course [M] 2011 higher education press Changsha
- [2] Yang Jie, Weng Wenguo. Prediction of physiological parameters based on high temperature human thermal response model. Journal of Tsinghua University (Natural Science Edition), 2014, 54 (11): 1422-1427.
- [3] Miao Miao, Lu Hong, Cheng Mengqi. Changes of body surface temperature and subjective thermal sensation evaluation before and after exercise [J]. Journal of Textiles, 2018, 39 (04): 116-122.
- [4] Shao Kaili, Fu Caiyuan, Zhang Zhenshuai, Xie Zhenzhen. Design of Intelligent Garment System Based on STC89C52 SCM. Wool Technology, 2018 (09): 61-65.
- [5] Shi Ze. Realization of Finite Difference Method of Heat Conduction Equation by MATLAB. Journal of Xianyang Normal University, 2009, 24(04): 27-29+36.
- [6] Xue Qiong, Xiao Xiaofeng. MATLAB Implementation of Finite Volume Method for Two-dimensional Heat Conduction Equation. Computer Engineering and Applications, 2012, 48(24): 197-200+221.
- [7] Feng Aifen, Zhang Yongyong. Dummy system for testing thermal insulation and fire protection performance of clothing. China Personal Protection Equipment, 2004 (02): 24-26.
- [8] Pan Bin. Mathematical modeling of heat transfer in thermal protective clothing and inverse problem of parameter determination [D]. Zhejiang Sci-Tech University, 2017.
- [9] Fu Ming, Weng Wenguo, Han Xuefeng. Thermal and humidity resistance of protective clothing under

high temperature. *Journal of Tsinghua University (Natural Science Edition)*, 2017, 57(03): 281-285+292.

[10] Yang Jie, Weng Wenguo. Prediction of physiological parameters based on high temperature human thermal response model. *Journal of Tsinghua University (Natural Science Edition)*, 2014, 54 (11): 1422-1427.

[11] Yang Jie. *Simulation and Experimental Study of Human Thermal Response to High Temperature Based on Human Body-Clothing-Environment [D]*. Tsinghua University, 2016.

[12] Huangpu Xiaodong. *Study on the protective performance of flame retardant and fire resistant clothing [D]*. Donghua University, 2014.

Analysis based on Color and Substance Concentration Identification

Rongping Ma^{1,2}, Jialin Wang^{1,2}, Yuehan Wang^{1,2}, Aimin Yang^{3,*}

¹Mathematical Modeling Innovation Lab, North China University of Science and Technology, Tangshan 063210, China

²North China University of Science and Technology, Tangshan 063210, China

³School of Science, North China University of Science and Technology, Tangshan 063210, China

*E-mail: 43698059@qq.com

Abstract: according to the data of five kinds of color readings and concentrations of matter in different concentrations, draw the scattered plot of color and concentration, we can know that there is a linear relationship between color reading and substance concentration. A multivariate linear regression model was established to determine the relationship between color degree and substance concentration. After data processing, the linear relationship between material concentration and color reading was obtained. According to the number of experimental data and the average standard deviation of color reading at different concentrations, the data were evaluated, namely potassium bromate > histamine > aluminum potassium sulfate > urea > industrial alkali in milk. According to the experimental data, the mathematical model of color reading and substance concentration is established. The cubic function is used to realize the model by principal component analysis. The significance is 0.022. The results meet the requirements, and the error analysis is made according to the fitting value and the actual value. The error is within the allowable range.

Keywords: multivariate linear fitting of compressive strength; principal component analysis; color reading; substance concentration

1. INTRODUCTION

Data processing of color readings in different concentrations of matter can be used to obtain scattered plot. It is found that there is a linear relationship between color reading and substance concentration [1]. The functional expression is obtained to determine the functional relationship between the color reading and the concentration of matter [2,3]. The quality of the samples is evaluated by the number of the experimental data and the average standard deviation of the color readings at different concentrations [4]. According to the mathematical model of color reading and substance concentration established by the attached document, the dimensionality reduction of many kinds of data is first carried out, and the main component analysis

method is used to select several color reading indexes which have the greatest influence on the concentration, and the function model is fitted out. And estimate its standard error.

2. MODEL OF COLOR READING

2.1 Determining the relationship between color readings and substance concentrations

According to the data of five kinds of color reading and concentration at different concentrations according to the group substances, we can determine the linear relationship between color reading and substance concentration [5-7]. Using multivariate linear fitting to obtain the function expression, the relation between color reading and substance concentration can be obtained.

Spss was used to fit the functional expression between the color reading and the concentration of matter. The following functional expressions for the color readings and concentration of the five groups of substances are obtained [8]:

2.2 Evaluation of data

The first is to count the number of the observed samples at the same concentration. The more the number of experiments, the closer the results are to the real values. Second, considering the average standard deviation of color readings at different concentrations, the deviation between the measured data and the mean value can be accurately reflected. [9] The method of calculation is to first calculate the standard deviation of each color reading at the same concentration with known data, and then calculate the average standard deviation of all color readings of the substance according to these standard deviation data except for the number of experiments, the smaller the average standard difference, It is proved that the more close the deviation between the data and the mean is, the better the data is. The results of the average standard deviations for each group are as follows:

According to the data of the above table, the order of arrangement of available data from superior to inferior is: potassium bicarbonate > histamine > potassium sulfate > milk , urea > industrial base .

3. RESULTS AND DISCUSSIONS

3.1 Analysis of principal components

The mathematical model of color reading and substance concentration is established. Firstly, the dimensionality reduction of many kinds of data is carried out. By using principal component analysis, several color reading indexes which have the greatest influence on the concentration are selected, and the function model is fitted with spss:

(1) The covariance matrix of the sample data calculated by the covariance matrix:

(2) The eigenvalue and the corresponding orthogonal zed unit eigenvector are obtained, where the first m eigenvalues of Σ are the coefficients of the main component corresponding to the unit eigenvector corresponding to the first m principal components. Then the itch principal component of the original variable is:

(3) Selection of principal components

Select the value of m according to the cumulative contribution rate of variance, and finally select several principal components:

When the cumulative contribution rate is greater than 85, we think that the value can reflect the information of the original variable sufficiently, and the corresponding m is the first m principal component of the extraction.

(4) Calculation of principal component loads

Principal component load is reflection of the correlation between principal component and the original variable X, and the load 1 of the original variable on the principal component.

(5) Calculating the principal component score and calculating the score of the sample on m principal components:

3.2 Linear regression

The linear regression equation can be written as, and the coefficient a and b in the linear regression equation satisfies:

In this paper, the dimension is understood as the number of factors that can determine the color reading, and the dimension is reduced from five groups of color readings to three dimensions to study fitting features. Use spss to fit images corresponding to functions of different degrees:

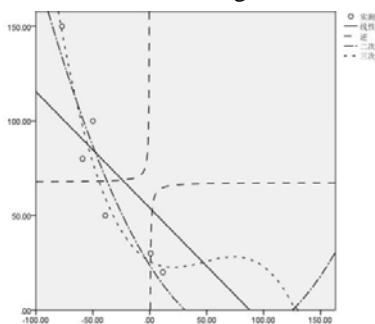


Figure.1 Image corresponding to times of fitting

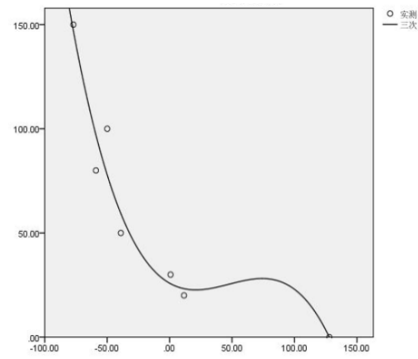


Figure.2 cubic image fitting

The relationship between color coefficient and substance concentration:

It can be seen that the fitting effect of the graph of cubic function for the actual data points is 0.022, and the fitting results meet the requirements when the significance value is less than 0.05.

REFERENCES:

[1] He Yuan-xiang, Shi Baoming. study on the identification model of color and substance concentration [J]. Journal of Lanzhou University of Arts and Sciences (Natural Science) 32 (03): 21-28.

[2] Tian Ruhui. Color and substance concentration Identification Modeling based on multiple regression Analysis [J]. Electronic Test. 2018 (07): 62-97.

[3] Wang Xueping. Mathematical Model of the relationship between the number of Color and the density of substance [J]. By means of mathematics, 35 (02): 105-110.

[4] Lin Qihong, Wu Huayao, Li Zihao, Yang Fangmei. Identification of color and substance concentration [J]. Application of regression Model of Journal of Heilongjiang Institute of Technology (Comprehensive Edition) .2018 (02)

[5] Xiao Yun. In colorimetric method [J]. Journal of Yang Ling Vocational and Technical College. 2018 (01) :11-22.

[6] Li Jianjun. The relationship between color and concentration identification based on principal component analysis [J]. Electronic Technology and Software Engineering .2018 (07):22-25.

[7] Bear wing. Study on Identification of Color and Mass concentration [J]. Journal of Chongqing Electric Power College .2018 (02).

[8] Li Wei, Ji Fei, Wang Hui, Wang Dongliang. Color and substance concentration Identification [J]. Computer products and Circulation. 2018 (01):34-37.

[9] Pavla Martinkova, Miroslav Pohanka. Colorimetric sensor based on bubblewrap and camera phone for glucose determination[J]. Journal of Applied Biomedicine, 2016, 14 (4).

Image Restoration Using Radon Transform

Yinduo Zhao^{1,2}, Jin Guan^{1,2}, Xueyong Jia^{1,2}, Cuihuan Ren^{3,*}

¹Engineering computing and simulation innovation, North China University of Science and Technology, Tangshan 063210, China

²North China University of Science and Technology, Tangshan 063210, China

³School of Science, North China University of Science and Technology, Tangshan 063210, China

*E-mail: 979624482@qq.com

Abstract: The Radon transform can well preserve the position information of the target and has a satisfactory performance in coaxial recognition and filtering. For the given transformation result, the original model can be obtained by the inverse transformation, and the position information of the original model is further calculated according to the transformation result, and the rotation center is further obtained.

Keywords: Image Restoration, Radon Transform, calculated according.

1. INTRODUCTION

Radon transform has a wide range of applications in CT image reconstruction, geological exploration and other fields. Due to the instability of the CT system, the center of rotation tends to deviate from the geometric center. There is also a certain error in the spacing of the detector, which directly affects the spatial characteristics of the reconstructed image and has an important impact on the model analysis. Therefore, the relevant parameters of the CT system are determined [1]. It is especially important. This paper proposes the calculation of the rotation angle, rotation center and detector spacing of the CT system by means of radon transformation and inverse transformation to correct the instability of the results due to industrial errors.

2. RADON TRANSFORM AND INVERSE TRANSFORM

The Austrian mathematician Radon proposed the basic mathematical theory of projection image reconstruction in 1917, and established the mathematical theory foundation for CT technology. The theory mathematically proves a two-dimensional distribution function of a physical parameter (such as the distribution of a slice attenuation coefficient) by which all line integrals in the domain are completely determined [2,3].

The angle between a straight line L and the axis X in the two-dimensional plane is ϕ , the distance from the origin to the perpendicular of L is s , and the point (x, y) on the line can be expressed as polar

coordinates.

Radon proved the following theorem:

If the function $f(x, y) = \hat{f}(r, \theta)$ is known to have an integral along the line L:

$$p = \int_L f(x, y) dl = \int_L \hat{f}(r, \theta) dl = \int_{-\infty}^{\infty} \hat{f}\left(\sqrt{s^2 + l^2}, \theta + \arctan \frac{l}{s}\right) dl \quad (1)$$

Then:

$$\hat{f}(r, \theta) = \frac{1}{2\pi} \int_0^{\pi} \int_{-\infty}^{+\infty} \frac{1}{r \cos(\theta - \phi) - s} \frac{\partial p}{\partial s} ds d\phi \quad (2)$$

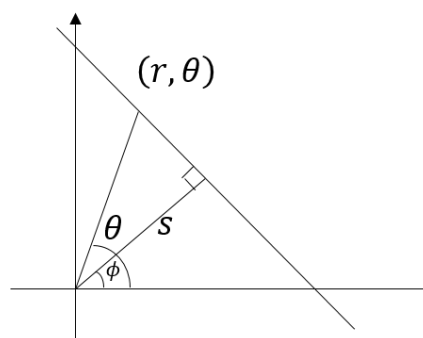


Figure 1 Radon transformation parameter diagram
Equation (1) is called Radon transform and refers to the line integral of a two-dimensional distribution function at a certain angle, that is, the actual ray projection. Equation (2) is called Radon inverse transform, and Radon inverse transform has important theoretical significance for CT reconstruction. It refers to the reconstruction of the tomographic image $\hat{f}(r, \theta)$ of the object by a certain amount of projection data p at the projection angle.

3. MODEL SOLVING

The scanner measures the radiant energy absorbed by the two-dimensional to-be-detected medium with fixed position on the detector with 512 equidistant elements for each X-ray direction, and obtains 180 sets of received information after processing by gain and the like [4]. The scan target is known as figure2.

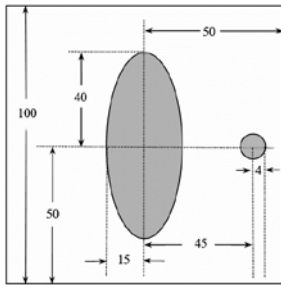


Figure 2 The scan target

From this, the long axis of the ellipse is 80 mm, the short axis is 40 mm, and the radius of the circle is 4 mm.

For the given data, MATLAB analysis can be obtained as figure3.

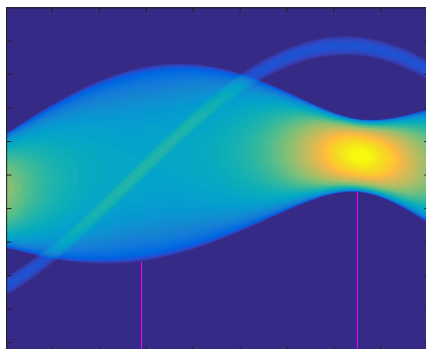


Figure 3 Attachment data visualization

Among them, the abscissa indicates 180 directions of scanning, and the ordinate indicates the number of detectors [5, 6]. According to the principle of random transform, the widest part of figure3 is when the CT system is perpendicular to the long axis of the ellipse, and the narrowest part is when the CT system is perpendicular to the short axis of the ellipse. The number of detectors covered by the widest area is known by the image $n_1=289$. The narrowest part covers the number of detectors $n_2=109$. From figure2, the long axis = 80mm, the short axis = 30mm, the detector spacing:

$$d = \left(\frac{n_1}{a} + \frac{n_2}{b}\right) / 2 \quad (3)$$

Calculated by calculation = 0.2768mm.

Since the angle between the long axis and the short axis is 90°, the widest part and the narrowest part are also 90°. According to the figure, the distance detection direction of the CT system at two locations is 150-58=92, and the number of non-zero detectors at each angle is counted to obtain figure 4:

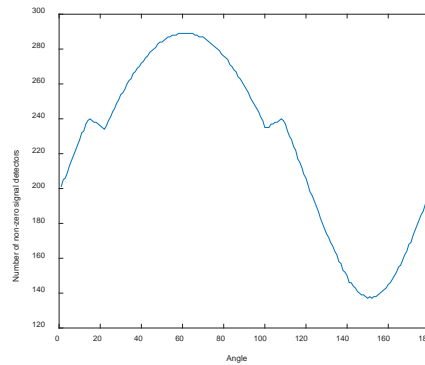


Figure 4 Number of detectors at different angles

It can be seen that the direction change is relatively uniform, and the rotation direction of the CT system can be described by the average value, and the angle of each rotation is about 1.0526°. From figure 4, we can also find that the initial angle of the CT system is about -29.7014°.

By combining the elliptical template and the circular template given in the title, the proportional transformation between the coordinate systems is carried out. By establishing the corresponding plane rectangular coordinate system, the ellipse center can be obtained separately, and the center of the circle is in the plane rectangular coordinate system. The coordinates are:

$P_1(273.6658, 291.6983)$ and $P_2(415.2547, 372.0849)$,

Assume the center of rotation $P_3(256.0000, 256.0000)$

The formula for the distance between two points in the plane: $d^2 = (X_i - X_j)^2 + (Y_i - Y_j)^2$, then:

$$\begin{aligned} d_{12} &= 162.8171 \\ d_{13} &= 39.8303 \\ d_{23} &= 197.0730 \end{aligned} \quad (4)$$

The equations for the coordinates of points P_1 and points P_2 are obtained by the equations of points P_1 and P_2 :

$$Y_1 = 0.5677X + 136.3382 \quad (5)$$

Let the point P_3 intersect the line Y_1 at the point P_4 , which is obtained by the vertical relationship between the plane lines: $P_4(244.9793, 275.4129)$. The straight line equation that can be obtained by P_3 and P_4 is

$$Y_2 = 1.7615X + 706.9440 \quad (6)$$

Therefore, the distance between the intersection point P_4 and the ellipse center PI and the rotation center P_3 is:

$$d_{14} = 31.7511 \quad (7)$$

$$d_{34} = 22,3230 \quad (8)$$

In the template diagram given in the title, another plane rectangular coordinate system with the ellipse center as the origin and the ellipse center and the circle center as the x-axis is established as follows:

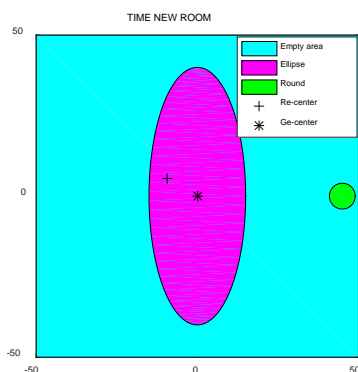


Figure 5 Square pallet plane rectangular coordinate system with the ellipse center as the origin In this plane, the ellipse center $Q_1(0,0)$, the center $Q_2(45,0)$ of the circle, and the distance $D_{12} = 45$ between the two can be obtained, there by obtaining the relative proportionality coefficient $\lambda = D_{12} / d_{12}$ between the two plane rectangular coordinate systems, and the center of rotation recorded in the coordinate system The coordinate is $Q_3(x_0, y_0)$, and the correspondence between the coordinate systems finds that Q_3 is located in the second quadrant. Its horizontal and vertical coordinates are:

$$x_0 = \lambda d_{14} \tag{9}$$

$$y_0 = \lambda d_{34} \tag{10}$$

Calculated $x_0 = -8.7755$, $y_0 = 6.1607$

The coordinates of the center of rotation of the CT system are: $Q_3(-8.7755, 6.1697)$, Very close to the true

value $Q_{re}(-9.2663, 6.2729)$.

4.CONCLUSION

In this paper, Radon transform and Radon inverse transform are used to process the data. According to the given conditions, the true rotation center of the CT system, the rotation direction of 180 rotations and the detector spacing are derived, which has important reference value for the correction of CT system.

REFERENCES

[1] Wang Yv, Huang Suhong, Cai Yu fang.Industrial CT image ring artifact correction[J]. Optical precision engineering,2010, 18(05): 1226-1233.
 [2]Liu Mingjin. Research on Positioning Method of Rotating Center of Industrial CT System[D].Chongqing University,2014
 [3]Time-Frequency Analysis of Power-Quality Disturbances via the Gabor-Wigner Transform. IEEE Transactions on Power Delivery Published: 2010.
 [4]Shi Yehao, Yu Yufeng, Cheng Xiaohong. Mathematics in CT scan-Radon transformation[J]. Journal of Capital Normal University (Natural Science Edition), 2013, 34(04):15-18.
 [5]Structural Light Weld Seam Tracking Image Processing Based on Radon Transform and Fuzzy Enhancement[J]. Welding Journal, 2017, 38(02):19-22+ 1-2.
 [6]Li Guoli, Zhu Weiyong, Luan Ming, "EDA and digital system design," China Machine PRESS, 2005.

Orbit Design and Control Strategy for Chang'e-3 Soft Landing

Yangyang Peng^{1,2}, Yinghao Zhu^{1,2}, Bing Tian¹, Lijing Feng^{3,*}

¹Mathematical Modeling Innovation Lab, North China University of Science and Technology, Tangshan 063210, China

²North China University of Science and Technology, Tangshan 063210, China

³School of Science, North China University of Science and Technology, Tangshan 063210, China

*E-mail:785926222@qq.com

Abstract: lunar exploration is a symbol of the development level of space technology and a manifestation of the comprehensive national strength of the country. China's "Chang'e-3" lunar probe successfully launched and landed on the lunar surface successfully, opening a new chapter in China's space. The soft landing process is divided into six stages. In order to ensure that Chang'e-3 can achieve a soft landing in the predetermined area accurately, the design of landing orbit and control strategy is very important. In order to meet the six stages of the soft landing process, the fuel consumption is minimized as much as possible.

Keywords: dynamic model; micro element method; spatial filtering; optimization model; spiral search method

1. INTRODUCTION

With the progress of society and the development of science and technology, space technology has become one of the manifestations of comprehensive national strength. Chang'e-3's successful soft landing on the moon highlights a major breakthrough in the field of space technology in China. There are six stages in the landing process of Chang'e-3, which are simulated as different ideal processes, and each process is decomposed into a direction to simplify the motion process. The minimum value of fuel consumption and the solution of the optimal landing point in six states are achieved [1].

2. NEAR POINT AND FAR MOON POINT

(1) Velocity solution of near point and far moon point

When Chang'e-3 moves in an elliptical orbit in space, the mechanical energy of the satellite is conserved, the sum of potential energy and kinetic energy is invariable,

$$E_j = \frac{1}{2}mv_1^2 - m\frac{GM}{r_1} \quad (1)$$

$$E_y = \frac{1}{2}mv_2^2 - m\frac{GM}{r_2} \quad (2)$$

$$E_j = E_y \quad (3)$$

G is a constant of gravity, r_1 is the distance from

perilunar point to lunar center, r_2 is the distance from perilunar point to lunar center, v_1 is perigee velocity, v_2 is apogee velocity. Also by Kepler's second law of planetary motion:

$$\frac{v_1}{v_2} = \frac{r_2}{r_1} \quad (4)$$

The simultaneous equations show that the perigee velocity v_1 is 1.67 km/s, the far-monthly velocity v_2 is 1.61 km/s, and the direction is along the tangent of the elliptical orbit [2].

(2) the solution of the location of near and far moon points

During the main deceleration phase, Chang'e-3 was only subjected to the gravity of the moon and the deceleration power provided by the main deceleration engine, regardless of other drag effects [3]. If gravity and deceleration power are all variable forces, there are many possibilities for their analysis. Assuming that the Moon's gravity to Chang'e-3 remains unchanged and the deceleration force makes it a constant value, the deceleration force can be decomposed into vertical force perpendicular to the moon's surface and horizontal force parallel to the moon's surface, so that the vertical velocity and horizontal velocity of Chang'e-3 both decrease [4].

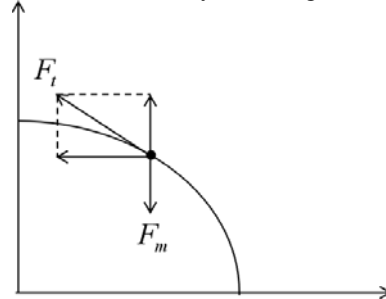


Figure 1 force decomposition diagram of Chang'e-3 main deceleration stage

The force distribution of Chang'e-3 in the horizontal and vertical directions during the main deceleration stage is analyzed and the dynamic knowledge in physics is combined to obtain:

$$ma\Delta H - F_s\Delta H = \frac{1}{2}m(v^2 - v_0^2) \quad (5)$$

$$ma - F_s = ma_s \tag{6}$$

$$\Delta H_s = \frac{1}{2} a_s t^2 \tag{7}$$

Simultaneous $F_s=3595.1\text{N}$, $t=421\text{s}$ can be obtained. The horizontal displacement of Chang'e-3 in the main deceleration stage is 357km.

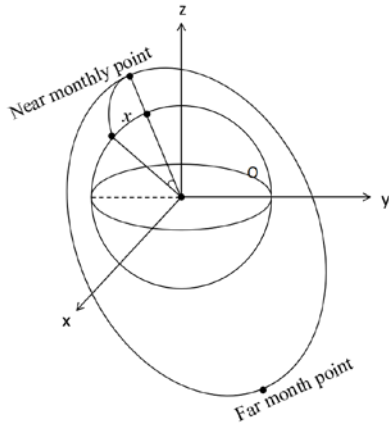


Figure 2 ellipse orbit and lunar 3D coordinate map
From the arc length formula, the degree of latitude corresponding to the displacement x can be obtained:

$$\Delta\alpha = \frac{x}{r_m} = 0.2055\text{rad} \tag{8}$$

Conversion angle is 11.78° . Considering the deviation of longitude caused by lunar rotation, the total time from soft landing to successful landing is 561.4s. Then, according to the lunar rotation speed of $2.662 \times 10^{-6} \text{rad/s}$, the total time of lunar landing in the six phases of Chang'e-3 is calculated [5]. The total rotation angle is about 0.856° , negligible. The position of the near moon is 15 kilometers above the point of longitude and latitude 19.51 W, 55.90 N, and the position of the far moon is 100 kilometers above the point of longitude and latitude 160.49 E, 55.90 N.

3. LANDING TRAJECTORY DESIGN

(1) Landing preparation track

Chang'e-3 travels in an elliptical orbit with the Moon's center as the focus. When it reaches the perilunar point, it enters the landing process from the perilunar point [6].

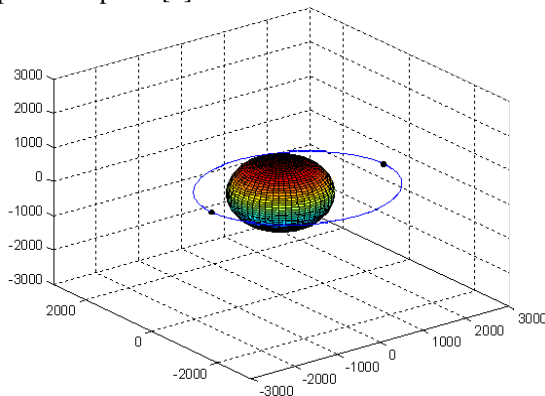


Figure 3 Chang'e-3 landing preparation orbit around the moon

(2) Main deceleration stage

The main deceleration stage is the main stage of the engine operation. Since most of the fuel on the lander is consumed in this stage, the optimal control of the main deceleration stage is to minimize the fuel consumption [7].

Chang'e-3 started the deceleration engine when it reached the near-lunar point. During its landing from 15000 m to 3000 m, Chang'e-3 was required to reach the expected landing coordinates above the prescribed high-altitude drop range, and its horizontal tangential velocity was 1.7 km/s at the near-lunar point. Therefore, the deceleration power provided by the main engine and the lunar-to-Chang'e-3 deceleration power were obtained. The gravitational force of Chang'e-3 should make Chang'e-3 decelerate to 0 in horizontal direction and reach the right speed in vertical direction. Taking the horizontal motion of Chang'e-3 as a uniform deceleration motion, the mass change caused by fuel consumption can be neglected. As for the vertical direction, the gravitational acceleration of the moon can be determined by the law of universal gravitation:

$$g_m = \frac{GM_m}{r^2} \tag{9}$$

r is the distance from Chang'e-3 to the moon's center. When Chang'e-3 descends gradually, although the distance from the moon's surface decreases gradually, it is relatively small for the average radius of 1737.013 km from the moon's surface to 15 km from the moon's surface to 3 km from the moon's surface, so the variation of R is very small. By calculating the gravitational acceleration of Chang'e-3 at the beginning and the end of the main deceleration phase, it can be concluded that only 0.02 m/s^2 has been increased in this process. So during the main deceleration phase, the motion in its vertical direction is viewed as free falling motion. The relationship between engine thrust and distance between Chang'e-3 and lunar center is analyzed. The relationship between fuel mass \bar{m} per unit time consumption and distance between Chang'e-3 and lunar center is obtained:

$$m = \frac{ma}{v_e} - \frac{GMm}{r^2 v_e} \tag{10}$$

The area under the curve is calculated by MATLAB, that is, the total fuel mass consumed in the process. The result is 1065.7 kg.

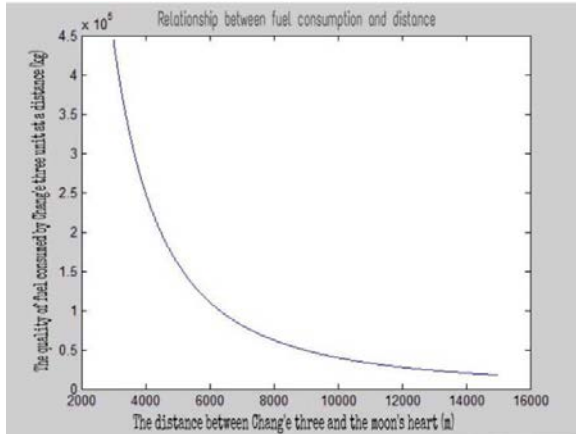


Figure 4 Relationship between fuel consumption and lunar core stance of Chang'e-3

Because the above solution process ignores the quality change of Chang'e-3 due to fuel consumption, a more accurate method is adopted to solve the minimum fuel consumption, and the mass change of Chang'e-3 is considered.

First, stress analysis is carried out for the main deceleration stage again. The deceleration power provided by the main deceleration engine is F , and the angle between the main engine and the horizontal line is β . In the main deceleration stage, the parabola is divided into numerous broken lines by the finite element method. The motion of each small segment can be regarded as the uniform deceleration movement in the horizontal direction and the uniform acceleration movement in the vertical direction [8].

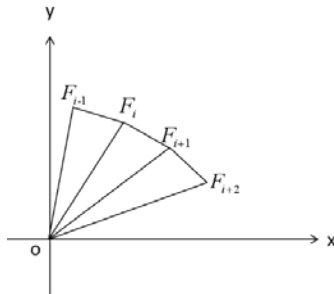


Figure 5 parabola piecewise graph

Chang'e-3 is the beginning of the next paragraph at the end of each paragraph:

$$v_p(i) = v_p(i-1) + a_p t \quad (11)$$

$$v_s(i) = v_s(i-1) + a_s t \quad (12)$$

$$m(i) = m(i-1) - \frac{F}{v_e} t \quad (13)$$

$$h_s(i) = h_s(i-1) - v_s(i-1)t - \frac{1}{2} a_s t^2 \quad (14)$$

$$h_p(i) = h_p(i-1) + v_p(i-1)t + \frac{1}{2} a_p t^2 \quad (15)$$

The specific impulse is 2940m/s. In MATLAB, the iterative solution satisfies the following constraints: thrust is greater than or equal to 1500N, less than or equal to 7500N; initial horizontal velocity v_p is 1.7km/s, v_s is 0; terminal horizontal velocity v_p is less

than or equal to 50m/s, vertical velocity v_s is 57m/s; angle between 90 degrees to 260 degrees, and the change angle is within 1 degree. The objective function is the main fuel consumption during the deceleration stage, and the quality of fuel consumption per unit time is:

$$\bar{m} = \frac{F}{v_e} \quad (16)$$

So the total fuel consumption in the main deceleration stage is:

$$m = \bar{m} t_0 \quad (17)$$

The result of minimizing the objective function in MATLAB is that the curve length of the main deceleration stage is 390.7 km, and the motion time t of the whole process is $t_0=430$ s.

$$y = 14.759 + 122.4x - 13670x^2 \quad (18)$$

The height of Y is km from the surface of the moon. In the main deceleration stage, the optimal strategy is as follows: the thrust value remains unchanged, always 7500N, and the direction changes. The angle between the horizontal lines changes with time.

$$\beta = 186.6 - 0.1t \quad (19)$$

The result shows that the beta angle of the main deceleration result is 143.6 degrees. According to the results, the horizontal speed and vertical speed of Chang'e-3 three are 34.83m/s and 44.9m/s respectively. The quality is reduced by 1096.9kg and time is 430s.

(3) Quick and justment section

During the rapid adjustment phase, Chang'e-3 reduced its horizontal velocity to 0 m/s from 3,000 m to 2,400 m from the lunar surface, causing the thrust of the main deceleration engine to be vertical downward. This process is simplified. It is considered that the thrust in the horizontal direction is invariable and the thrust direction is opposite to the horizontal velocity of Chang'e-3. In this process, Chang'e-3 is basically located above the landing point of the target, the horizontal displacement changes little, the speed decreases little, so the deceleration time is also small, the fuel consumption can be neglected, that is, the mass is approximately unchanged at this stage.

The last stage of the above stage is the initial state, and the horizontal direction is the uniform slow down process, and the equation is established:

$$\begin{cases} v_p = a_p t \\ v_s t - \frac{g t^2}{2} = 2400 - 100 \\ g = \frac{GM}{R^2} \end{cases} \quad (20)$$

The time required for adjustment is $t=7.2$ s, $a_p=4.83$ m/s, $F_i=6293.49$ N, and the quality of consumption is 18.2kg.

REFERENCES

[1] Yang Yu. Analysis of big data in the diagnosis and treatment of Diabetes Mellitus [J]. Computer

knowledge and Technology 2018 (20): 14-15.

[2] Zhao Yalin. Soft landing trajectory design and control strategy [J]. technology wind, 2015 (04): 71.

[3] Yang Jing. Attitude fault-tolerant control algorithm for flexible satellites during orbit control [D]. Harbin University of Technology, 2017.

[4] Lin Shengyong, Li Zhuji, and Hexing Lock. Optimization of Lunar Satellite Orbit Design [J]. Journal of Space Science, 2004 (05): 360-366.

[5] Li Feigao, Ren Fengxuan. A brief analysis of orbit design of Chang'e lunar exploration satellites [J]. Journal of Zhongzhou University, 2012, 29 (05):

122-124.

[6] Shao Zhujun. Study on configuration design and orbit transfer design of small thrust thruster based on GEO satellite [D]. Nanjing University of Aeronautics and Astronautics, 2016.

[7] Yang Yifei, Liao Liangcai. Optimization and Simulation of satellite orbit based on evolutionary algorithm [J]. Computer simulation, 2007 (06): 66-68.

[8] Zhang Yasheng, Feng Fei. Fast-response satellite orbit design method based on target motion characteristics [J]. Navigation and control, 2017, 16(04): 22-23.

Prediction of Coke Quality by Coal Rock Method

Wenchao Li^{1,2}, Kangkang Jin^{1,2}, Dao'an Li^{1,2}, Cuihuan Ren^{3,*}

¹ Engineering Computing and Simulation Innovation Lab, Tangshan, 063000, China

² North China University of Technology, Tangshan 063000, China

³ School of Science, North China University of Science and Technology, Tangshan 063210, China

*E-mail: 979624482@qq.com

Abstract: In order to predict coke quality with coal rock, a prediction model based on multiple linear regression was established. Correlation test was carried out on BJZZ, QZZ, JZZ, DZZ and KW data. It was judged that BJZZ was negatively correlated with M40, and the correlation was high. QZZ and M40 were negatively correlated, and the correlation was moderate. QZZ was negatively correlated with M10. It was highly correlated with KW, and the correlation was low. CRI was negatively correlated with JZZ and QZZ, and the correlation was moderate. CSR was negatively correlated with JZZ and BJZZ, and the correlation was moderate. In order to predict the relationship between variables and future development trends, multiple linear regression equations are used to regress M40, M10, CRI, CSR, and the regression degree of the curve is tested. According to the obtained regression curve, the corresponding correlation index can be found to be 0.97, 0.954, 0.96, and 0.998, indicating that the regression fit of this curve is better.

Keywords: Coal blending coking, Predictive model, Multiple linear regression, Coke quality.

1. INTRODUCTION

Under the current popularization of oxygen-enriched coal injection technology and the gradual maturity of coal injection technology, the role of coke in the blast furnace heat source, carburizing agent and reducing agent is gradually weakened, but the role of coke as a skeleton in the blast furnace column is still Unreplaceable, so the stability of coke quality in blast furnace smelting is very important.[1] Nowadays, science and technology are developing rapidly, and the application of coal and rock science is becoming more and more extensive. Among them, the method of using coal rock science to guide coal blending and predicting coke quality has become a coal blending method recognized by both domestic and foreign. By studying the variation characteristics of the components of coal rock in the coking process, we can understand the influence of coal with different components and different degrees of coalification on coking, so that the coking coal blending technology is

more mature. At the same time, the method of coal lithology can also predict the quality and properties of coke. At present, many advanced coking plants at home and abroad have used the viewpoint of coal lithology to establish an automated coal blending process. In the future, coal-rock methods will develop more rapidly and be more optimized. Based on the experimental data, the relationship between the average maximum reflectivity of the coal-rock components (the vitrinite group, the semi-vitrification group, the inerton group, the chitin group, and the minerals) and the vitrinite group was analyzed. SPSS software was used. Establish a coke quality prediction model to achieve the goal of optimizing coal blending, improving coke quality, reducing costs, and improving economic efficiency.[2]

2. COAL ROCK ANALYSIS

The operating conditions that affect the quality of coke are coal preparation sites for coking coal, coal blending schemes, and coke oven production processes. These operating conditions are mainly reflected in the coking coal particle size, coking coal moisture, coke oven quenching mode, coking coal packing density, coke oven temperature and coke oven coking time.[3] Although these conditions will affect the quality of coke, the decisive factor of coke quality is the inherent nature of coking coal. It not only affects the chemical composition of coke, such as sulfur and ash, but more importantly it basically determines the reaction of coke. Sex, post-reaction strength and crushing strength and wear resistance of coke. By optimizing the coal blending structure, the coke quality requirements for steelmaking blast furnaces are achieved, and on this basis, the cost of coking coal raw materials is reduced, and the use of high-quality coking coal is reduced.

2.1 COAL SAMPLE PREPARATION

According to GB474- -2008 "Preparation method of coal sample", coal such as fat coal, lean coal, coking coal and 1/3 coking coal is selected, and 278 coal samples are prepared according to the mass ratio, and each coal sample is not less than 100 kg put into a sealed bucket for use.

2.2 COKE QUALITY

The HXLJ_1 experimental coke oven was used to carry out coking experiments on 278 experimental coal samples under the same conditions. According to GB/T 4000--2008 "Coke reactivity and post-reaction strength determination method", coke reactivity CRI and post-reaction strength CSR; according to Table 1. Coal rock composition and coke quality

GB/T2006-2008 "Coke mechanical strength measurement method", determination The crushing strength of coke M40 and the wear resistance M10. The coal rock components and coke quality analysis results of 278 coking coal samples (intercepted in the text) are shown in Tab. 1.

JZZ	BJZZ	QZZ	DZZ	KW	M40	M10	CRI	CSR
51	0	0.2	15.5	0.1	91	5.1	20.8	71.1
52	0	0.2	17.2	0.1	90.8	5.7	21	71.1
51.2	0	1.8	17	0	90.9	5.1	19.7	72.1
51	0	0.5	15.1	0.1	91.1	5.8	20.7	71.9
53.8	0	0	11.2	0	90.9	5.7	20.1	73.2
52.1	0	0.1	17	0	90.9	5.7	20.8	72.1
52.5	0	0	17.5	0	90.9	5.7	20.5	72.1
55.2	0	0.8	12.3	1.8	89.1	5.8	19.9	72.7
53.2	0	1.2	13.8	1.8	89.1	5.1	19.5	72.3
51.5	0	0.1	12.3	2.1	89.5	5.1	19.1	72.8
51.5	0	0.1	11.2	1.8	89.1	5.1	19	72.5
53.2	0	0.1	15.1	0.8	89.1	5.8	20	72.8
53.9	0	0.8	13.7	1.1	89.2	5.8	19	72.1
55.8	1.2	1.1	38.1	3.2	89.1	5.1	19.9	72.1
51.5	0	0.5	13.1	2	89.1	5.8	19.1	72.5
55.3	0	0.1	12.3	2	89.1	5.7	19.9	72.1
51.5	0.9	0.7	12.1	1.5	89.2	5.8	19.7	72.5
53.8	0	0.1	12	2.8	89.7	5.7	19.7	72.7
51	0	0.1	12.1	3.1	89.2	5.8	19.9	72.7
51.0	0	1.1	12.1	3.1	89.1	5.8	20.1	72.5
52.9	0	1	13.2	3	89.1	5.7	20.9	72.5

3. SPECIFIC FORECASTING PROCESS

CSR and JZZ, BJZZ, QZZ, DZZ, and KW.

3.1 CORRELATION TEST

When sig < 0.01, there is a correlation between the two variables. The specific criteria for the correlation size are shown in Tab.2.

The spearman rank correlation was used to determine the correlation between M40, M10, CRI,

Table 2. A standard for judging correlation based on correlation coefficient

	$ r < 0.3$	$0.3 \leq r < 0.5$	$0.5 \leq r < 0.8$	$ r \geq 0.8$	$ r > 0.95$
Correlation	irrelevant	Low correlation	Moderate correlation	Highly correlated	Significant correlation

The correlation coefficient of M40 is shown in Tab.3.

Table 3. Correlation coefficient of M40

Cooperating with coal	Correlation coefficient	M40
JZZ	Correlation coefficient	0.054
	Sig	0.384
BJZZ	Correlation coefficient	-0.847
	Sig	0.002
QZZ	Correlation coefficient	-0.690
	Sig	0.002
DZZ	Correlation coefficient	-0.057
	Sig	0.358
KW	Correlation coefficient	0.066
	Sig	0.293

According to Tab.3, the sig values of M40 and BJZZ and QZZ are both 0.002, so BJZZ and QZZ

are related. The correlation coefficient of BJZZ is -0.847, which is negatively correlated with M40

and has a high correlation. The QZZ correlation coefficient is -0.690, which is negatively correlated

with M40, and the correlation is moderate. The M10 correlation coefficient is shown in Tab.4.

Table 4. Correlation coefficient of M10

Cooperating with coal	Correlation coefficient	M10
JZZ	Correlation coefficient	0.024
	Sig	0.701
BJZZ	Correlation coefficient	0.009
	Sig	0.881
QZZ	Correlation coefficient	0.841
	Sig	0.002
DZZ	Correlation coefficient	0.041
	Sig	0.508
KW	Correlation coefficient	-0.306
	Sig	0.001

According to Tab.4, the sigs of M10 and QZZ, KW are 0.002 and 0.001, respectively, and the correlation coefficients show high correlation and

low correlation, respectively. Therefore, M10 is related to QZZ and KW. The CRI correlation coefficient is shown in Tab.5.

Table 5. Correlation coefficient of CRI

Cooperating with coal	Correlation coefficient	CRI
JZZ	Correlation coefficient	-0.580
	Sig	0.0002
BJZZ	Correlation coefficient	0.071
	Sig	0.254
QZZ	Correlation coefficient	-0.703
	Sig	0.0008
DZZ	Correlation coefficient	0.017
	Sig	0.789
KW	Correlation coefficient	0.162
	Sig	0.09

As can be seen from Tab.5, the sigs of CRI and JZZ and QZZ are 0.0002 and 0.0008, respectively, and the correlation coefficients all show moderate

correlation. Therefore, CRI is related to JZZ and QZZ. The CSR correlation coefficient is shown in Tab.6.

Table 6. Correlation coefficient of CSR

Cooperating with coal	Correlation coefficient	CRI
JZZ	Correlation coefficient	-0.580
	Sig	0.0002
BJZZ	Correlation coefficient	0.071
	Sig	0.254
QZZ	Correlation coefficient	-0.703
	Sig	0.0008
DZZ	Correlation coefficient	0.017
	Sig	0.789
KW	Correlation coefficient	0.162
	Sig	0.09

According to Tab.6, the sigs of CSR and JZZ and QZZ are 0.003 and 0.002, respectively. Correlation coefficients are shown to be moderately correlated. Therefore, CSR is related to JZZ and BJZZ.

3.2 MULTIPLE LINEAR REGRESSION PREDICTIAN

Because the quality of coal is affected by multiple variables, and the basic idea of multiple linear regression prediction is to determine the dependent variable and multiple independent variables and the relationship between them, this paper adopts multiple linear regression to set and establish the model. Reuse the correlation test to confirm and eliminate the variables. Through the correlation test

screening, the regression coefficient is established by selecting the factor with the largest partial regression and the contribution of the partial regression. If the influence factor passes the significance test, it is selected to establish the equation, otherwise it will not enter the regression equation, and the method of multiple linear regression is eliminated. The factors affecting the dependent variable reduce the difficulty of the analysis problem, improve the computational efficiency and the stability of the regression equation with better prediction accuracy.[4]

Multivariate linear regression was performed on M40, M10, CRI and CSR by SPSS, and the

multiple linear regression equations of M40, M10, CRI and CSR were obtained respectively.

3.3 MODEL CHECKING

The merits of the curve regression can be measured by the sum of the squares of the errors.[5] Assume that the actual measured value is Y , the average value is Y_1 , and the theoretical value obtained from the fitting curve is Y_2 , then the sum of the squared errors is $\sum(Y-Y_2)^2$ and the mean square error is $\sum(Y-Y_1)^2$, if the ratio of the sum of squared error to the mean square error is smaller, the closer the actual observed value is to the estimated value, the better the curve fit.

In this case, based on the data given and the regression curve obtained above, the correlation indices of M40, M10, CRI and CSR can be found as: 0.97, 0.954, 0.96, 0.998.

It shows that the regression fit of this curve is better, which is basically consistent with the original data, and finally determines the multiple regression equation of coke quality.

4. CONCLUSIONS

In order to predict coke quality by coal rock method, we use multiple linear regression method to analyze the effects of coke quality M40, M10, CRI and CSR on JZZ, BJZZ, QZZ, DZZ and KW. The main influencing factors affecting M40 are BJZZ and QZZ, the main factors affecting M10 are QZZ and KW. The main factors affecting CRI are JZZ and QZZ. The main factors affecting CSR are JZZ and BJZZ, and the M40 regression equation is $y=-1.115 \times BJZZ-0.123 \times QZZ+91.314$. The M10 regression

equation $y=0.05 \times QZZ-0.024 \times KW+5.494$, the CIR regression equation $y=-0.106 \times QZZ-0.036 \times JZZ+21.516$, and the CSR regression equation $y=0.107 \times BJZZ-0.006 \times JZZ+72.846$. In order to verify the feasibility of the model, the correlation index R2 test, M40, M10, CRI, CSR correlation index: 0.97, 0.954, 0.96, 0.998, so the model is acceptable.

In order to improve the quality of coal, we propose the following suggestions: Minimize the content of coal vitrinite, Semi-mirror group, chitin, Inertial group, and minerals.

REFERENCES

- [1]Huang Qihua. "Analysis of coking coal properties and coke quality prediction in Laiwu Steel" [D]. Anhui University of Technology, 2016.
- [2]Bai YunQi, Bai QingZi, Zhao XianDe. "Coke quality prediction model based on the reflectance of coal and vitrinite components". Journal of heilongjiang university of science and technology, 2008,28(03):249-252.
- [3]Zhang YongLi. "Application study of coal petrology in coking coal blending" [D]. Tianjin university,2014.
- [4]Ye DaoMin, Xiao WenZhao, Luo JunWen. "Research on coal petrology blending and coke strength prediction". Coal field geology and exploration,1998(S1):5-8.
- [5]Liu Jingjuan. "Test Method for Multiple Linear Regression Model". Journal of Hunan Tax College,2005(05):49-50+60.

Analysis and Application of Network Hot Video Service Characteristics based on Big Data

Yang Fan

New Media College, Communication University of Zhejiang, Hangzhou, Zhejiang, 310018, the People's Republic of China

*E-mail: yangfan@cuz.edu.cn

Abstract: "Big data" is mentioned by more and more people in the contemporary Internet information technology industry and it is used to describe and define the mass of information that is constantly generated in the development of information. In today's information explosion era, data are being innovatively mined every day and data generated by economies of scale and scope can predict the direction of enterprise development and the flow of goods prices in the market.

Keywords: Big data era; Network hot video; Characteristic analysis

1. INTRODUCTION

In this era, data are booming and data formats are becoming more and more diversified. Many industries generate data, such as Internet, vehicle networking, GPS, finance and so on. The data units are sorted from small to large in order as Byte, KB, MB, GB, TB, PB, EB, ZB, YB, DB, NB and the margin between adjacent units is 1024, but in our daily life only the first five large data units are often used from TB. From 2006 to the present, the data has evolved from TB to ZB. We must understand the basic characteristics of large data if we want to control such huge data.

The first is large body size. According to statistics, the Internet produces 168 million DVDs a day, 294 billion emails and 2 million posts a day. Through these large amounts of data, we understand that social networks, e-commerce and mobile communications have brought mankind into a new era based on "PB" and PB has become a more normal situation. "Big" in large data expresses two concepts, one is mass and the other is global. The second feature is diversity. Today's data types have different formats than previous single text formats, and orders, logs, audio and other factors put forward higher requirements for people's ability to process data. There are three kinds of structured, semi-structured and unstructured data in which unstructured data is growing at a high rate. The third is high value. The Internet generates a lot of irrelevant information every day. Unprocessed raw materials are low-value, low-density data that requires

people to pan for gold in the sand. For example, a video with a playback time of two hours can be monitored continuously for only a second or two. How to "purify" data more quickly through powerful machine algorithms is a difficult problem in the current large data background. The fourth is speed. Big data is produced very quickly, such as stocks, news and other aspects of information at any time and anywhere in the transmission. Because of the timeliness of data, we need to process data quickly and get results. For example, for some e-commerce data, today's information can not produce effective results without processing, which will affect today's capture of a lot of business decisions, so the life of the enterprise is the processing efficiency of massive data.

2. THE DIFFERENCE IN VALUE BETWEEN BIG DATA AND TRADITIONAL DATA

Business transaction information data within an enterprise is mass transaction data, which mainly consists of two parts: online transaction data and online analysis data. Moreover, this kind of data is structured as static historical data managed and accessed through relational database rather than real-time data. These data do not let us predict what will happen in the future, but they do let us know what has happened before. Social media data produces a huge amount of interactive data and includes call details recording CDR, device and sensor information, GPS and geolocation mapping data, mass image files transmitted through Manage File Transfer protocol, Web text and click stream data, scientific information, e-mail, and so on. Compare the previous We find that through these data, we can predict what will happen in the future. Massive data processing can effectively process complex and massive data, and the emergence of large data has spawned architectures designed for data-intensive processing. For example, software with open source running in commodity hardware presents a challenge in accessing data quickly and reliably in a cost-effective manner.

Some people think that big data is the end and substitution of traditional data, but this view is not

generally accepted by scholars, compared with traditional data in the value of big data and processing methods are indeed very different. On purpose, traditional data processing follows that curing business is superior to efficient and efficient than discovery business. Big data processing reverses the order of traditional methods as a whole, first discovering business, then efficient and finally solidifying business. Traditionally, the data is generally faced with the internal data of the enterprise and the data volume is not more than 1 billion magnitude. However, the large data processing is a variety of data. In terms of technical means, the traditional data processing method uses the open source RDBMS of business intelligence. Big data processing methods use more open source technology, pay more attention to the data itself and use a variety of technologies to solve business problems. In the scenario, traditional data mainly deal with real-time, transactional, online business while large data will deal with a large number of batch data and a small number of online real-time data. In short, the traditional data is business-centric large data is data-centric data for business services.

3. THE ANALYSIS OF USER BEHAVIOR OF

(1) The development of contemporary Chinese network hot video. According to the report "The 33rd Statistical Report on Internet Development in China" published by the China Internet Network Information Center, the number of hot video users in China will reach 428 million by December 2013, an increase of 56.37 million and a growth rate of 15.2% compared with the end of the year. The usage rate of hot video on the Internet is 69.3%, which is 3.4 percentage points higher than that at the end of last year, and the scale is still showing a steady increase. At present, the mainstream network hot video media are mainly 10 Youku video, potato video, Sohu video, PPS network television, Thunderbolt look, Aiqi art, Le Video, Cool 6, Tencent video and some sites have a high degree of user overlap.

(2) The way of viewing the users of China's network hot video. According to the survey, access to video sites through search engines is still the most important way for current users to watch videos, such users have not yet formed loyalty to specific video sites. 96% of users watch videos online from PCs, and 49.4% use mobile devices (mobile phones, tablets) to watch videos online at the same time. With the improvement of mobile device performance and video client quality, mobile network hot video is gradually accepted by people.

(3) The monitoring mode of user behavior in China's network hot video. Among the emerging new services in the Internet field, network hot video service is undoubtedly the most concerned service, but it is also one of the largest bandwidth requirements in the network. Monitoring users' network behavior is the key to the successful development and promotion of

network hot video. By monitoring and understanding users' search, viewing and feedback behavior, reflecting the real video quality, we can accurately analyze the highlights and problems in video services and improve the quality of user experience.

(4) The evaluation index of China's network hot video user behavior. The significance of data acquisition lies in the adjustment and formulation of the data evaluation to guide the future strategy. These evaluation indicators include the following: exposure, click-through, click-through, exposure, click-through rate, UV click-through rate. Four more important indicators are eyeball coefficient, network cost per thousand, interaction number and hop loss rate. Eye coefficient refers to the ability index of each point to attract the viewer's eyes, which is calculated by measuring the attraction time and attraction time of infrared eye movement meter. The cost per thousand people refers to the cost of each video exposure per target audience of 1000. Interactive number refers to the number of people who participate in interactive activities such as visiting content pages, uploading and downloading, reviewing, sharing, games, etc. What is the percentage of people who leave the page without clicking on it?

4. APPLICATION OF NETWORK HOTSPOT VIDEO SERVICE

In the era of big data, network hotspot video services are mostly used in security monitoring and various live broadcasting platforms. It can be said that the live broadcast industry is created by big data video. Live broadcasting industry is not only limited to entertainment in education also has an indelible importance, and live broadcasting and sub-conference live, entertainment live, education live and production technology live broadcasting and so on, so that the network hotspot video business is affecting people's lives all the time.

5. CONCLUSION

Big data technology has been closely related to audio-visual media industry and will gradually change the concept and format of China's audio-visual industry, as well as the way of investigation and management. Big data can change everything to a certain extent, but it is absolutely no substitute for anything, no occasion, no time can use big data. Therefore, when recognizing and using big data, audiovisual industry or enterprise must fully realize its limitations and discard its advantages and disadvantages. Do not follow the trend of speculation, let alone its superstition.

ACKNOWLEDGE

Supported by Zhejiang province public welfare Technology Application Research Project, granted by Science Technology Department of Zhejiang Province, P.R.China(Grant No.2016C31086)

REFERENCE:

[1]Week. Research on the [J]. transmission power of Internet video user behavior from the perspective of

big data, 2018,2 (03): 129-130.

[2]Wu Guanfeng, patriarchal authority. Research on the status quo and security issues of network hot video surveillance [J].Network security technology and application, 2016 (12): 22 + 24.

[3]Lu Jianing, Wei Fang.User Behavior Analysis of

Network Hot Video under Big Data [J].Journalist, 2014 (07): 38-40.

[4]Editorial Department of this magazine. Embracing Video Cross-screen Marketing in the Age of Big Data [J]. Sound Screen World Advertiser, 2013 (06): 132.